Investigation of Palladium-NHC Catalysts to Probe the Mechanistic Action and Direct Site-Selectivity in Cross-Coupling Reactions

James Williams

Submitted in accordance with the requirements for the degree of
Doctor of Philosophy

The University of Leeds
School of Chemistry

August 2023

The candidate confirms that the work submitted is his own and that appropriate credit has been given where reference has been made to the work of others.

Acknowledgments

Firstly, I would like to thank my supervisor Dr Charlotte Willans for the unwavering support and guidance throughout my PhD. I whole heartedly believe that I couldn't have asked for a better supervisor, who helped me feel welcomed into a new city and university which was key in getting my PhD off to a great start. You went above and beyond to make sure that I and the rest of the group remained sane and looked after during the pandemic which I will be forever grateful for, even if you did make me do my least favourite thing in the world, writing! I hope for all the best in your future works, and I look forward to reading about the excellent chemistry from the Willans group.

I would also like to thank Prof. Ian Fairlamb from the University of York for the input and help on my project. The meetings we had were an endless wealth of knowledge, even if I had to Google a few things afterwards. Also, Dr Neda Jeddi, thank you for making time in your busy schedule to help me out with the mercury drop tests and making me feel welcome in York. Prof. Paddy McGowan, thank you for stepping in at the end of my project to take over as PI for a while and for the useful advice given throughout my PhD; your stories of your youthful academic experiences over drinks at the pub were both entertaining and unforgettable. Also, a thank you to Prof. Michaele Hardie for the help and support over the years.

Dr Chris Pask, not only are you quite possibly the most important person in the department, but you have also been a massive help during my PhD and I can't thank you enough! Regardless of whether it's chats about the weather, my frustrations with equipment, crystallography advice or just general chat, you've always lent an ear and offered sage advice, although I had best state that Leeds is in the north and nothing you say can ever change that! Nothing! To all your future endeavours, Chris, good luck. I can't forget to mention Dr Mark Howard, your help with all things NMR was invaluable and, unfortunately, you've instilled upon me a certain degree of NMR snobbery that I fear I won't be able to shake off any time soon.

The 1.32 office has really felt like home during my PhD, I couldn't have asked for a more friendly, supportive and all-round lovely group of people to share my time in Leeds with. Abi, you were the first person I met from Leeds and ever since that truly underwhelming tour of the department on my interview day, you have offered me nothing but support, kindness, and encouragement. You made lockdown more than bearable and I'm so very glad that you didn't get into medicine –in the nicest possible way! Jon (Matt) you made my PhD so enjoyable, and I learnt so much from you about pretty much everything, considering you know so much about pretty much everything. Although I'm still not entirely sure you aren't a Russian spy… I will miss

all of the geoguessing, crosswording, sporcleing, chatting, eating, drinking, and basically everything else that wasn't doing work, which we did so much of. Tom (T.O.M), despite initial trepidations, you quickly became an irreplaceable part of my PhD and I'm so glad you came into the group. Your philosophy of 'just don't get stressed' is very hard in practice but I will keep working on it. Your upbeat energy is infectious, and I will miss all the random day to day quotes. Will we ever find out what the air speed velocity of an unladen swallow is? Hamish, where would I be without you! You calmly suffered through being fumehood neighbours with grace and quiet decorum, which is at the very least highly commendable, whilst also having a positive impact on my skills as a chemist, I learned so much from you and I'm so grateful. Megan, our conversations/debates/arguments on interesting and relevant topics were genuinely stimulating but I'm afraid we will probably continue to disagree on most things except the importance of a nice cold pint down at the pub after a long day. Ellis Jamie Smith, how the hell you managed to complete a PhD whilst mastering chess and ironman-ing RuneScape is beyond me. It was great when you moved over into the office, you made it just that little bit more enjoyable. Ed, thank you so much for helping balance out the personalities in the office when I arrived, it was so unfortunate that certain pesky pandemical circumstances meant you were unceremoniously ripped away from us so abruptly, there was so many sporcles left unsporcled. Chrissi, you taught me a valuable lesson in the cost of my own time, I still have your mustard glass by the way. Belinda, even though you were part of the organic lot (ew!), you were still there for me throughout my PhD and I'm so glad we were friends and that's not only because of the biscoff millionaires shortbread!

A quick general thank you to a whole host of people that made my time in Leeds memorable and enjoyable, in no particular order: Rachel B, Tom D, Tom M, Tom N, Namrah S, Sarah B, Alex M, Alison M, Pablo C M and Bence S, I wish I could write more about each of you but I've just finished writing a thesis and my fingers feel like they're about to drop off! On the other hand, a very big special thanks goes to Apple air pods, I can confirm the noise cancelling works wonders on Tom (T.O.M), and that's really saying something! Also Fried, Pickard's, Lievitoo, Bakery 164 and Noodlesta.

Last and by no means least I would like to thank my family and friends for putting up with me for so very, very long and supporting me throughout. Jamie, Liam and Ben, you've kept my spirits high throughout this ordeal so thank you, and you'll finally be pleased to know that I've finished school. Mum and Dad, your love and encouragement over the years has played no small part to getting me to where I am now, all I can say is thank you for everything.

Abstract

This thesis examines the abnormal site-selectivity seen in the Suzuki-Miyaura cross-coupling reaction between 2,4-dibromopyridine and an arylboronic acid using palladium *N*-heterocyclic carbene (NHC) complexes as precatalysts. A range of NHC ligands were chosen to explore the effect of ligand sterics and electronics on catalytic activity and site-selectivity. A robust protocol was established for the catalytic studies with product yields determined though the use of quantitative ^{19}F NMR spectroscopy, utilising a fluorine handle on the arylboronic acid coupling partner (*p*-fluorophenylboronic acid).

Screening of the Pd-NHC complexes showed that the sterics of the NHC ligand did affect the site-selectivity of the reaction, whereby very bulky Pd-NHC complexes gave almost exclusive selectivity for the diarylated product (2,4-Ar) and the non-bulky Pd-NHC complexes gave selectivity for the abnormal product (4-Ar) over the normal product (2-Ar) and 2,4-Ar. It was found that the product selectivity when using the bulky Pd-NHC complexes was temperature dependent and at lower temperatures, product ratios more closely resemble the selectivity seen when using the non-bulky Pd-NHC complexes. The NHC ligand was shown to remain bound to the active species in the reaction and catalyst poisoning reactions indicated that the active species formed from the Pd-NHC complexes was homogeneous in nature. A mechanistic rationale was proposed for the observed 4-Ar selectivity when using the non-bulky Pd-NHC complexes and 2,4-Ar generation in both the bulky and non-bulky Pd-NHC complexes, the latter proceeding though a concerted mechanism.

Aspects of the catalysis were examined further with the use of stoichiometric studies. Activation of the complexes was found to proceed through the accepted route when subjected to appropriate conditions and substrate equivalents However, partial activation reactions conducted on a non-bulky Pd-NHC complex resulted in the generation of a *cis*-Pd-NHC_2 complex in significant quantities. The rationale for the formation of this complex was proposed. Multiple interesting species were also observed when conducting high-resolution mass spectrometry studies on the catalytic reaction mixtures, including several reductively eliminated C2 functionalised imidazolium salts and mass spectrometry fragments associated with the expected active species in the reaction.

The rationale for the concerted formation of 2,4-Ar was probed in greater detail by conducting investigations on 2,4-Ar generation from partially arylated substrates (2-Ar and 4-Ar), and the data was found to favour the proposed concerted 2,4-Ar formation mechanism. The mechanisms for the formation of 2,4-Ar from 2-Ar and 4-Ar were proposed, notably with the

involvement of unstable high order palladium species when using 2-Ar as the partially arylated substrate. Potential catalytic side-reaction/deactivation products were found when refining and examining the residues of multiple completed catalytic reaction mixtures. The structures found were unexpected and a mechanistic rationale for their formation was proposed.

The future work stemming from these investigations have been detailed and some initial studies were conducted. The involvement of palladium nanoparticles (PdNPs) in the catalytic reaction was examined though the synthesis and screening of imidazolium salt and NHC stabilised PdNPs. The data from this indicated that both classes of PdNPs result in the abnormal selectivity in the catalytic reaction of interest. The precursors to these PdNPs, imidazolium palladate salts were also identified as good candidates for further investigation considering the catalytic activity and apparent structure-activity relationship involved.

The effect of palladium complexes featuring chelating and asymmetrical NHC ligands and Pd-NHC_2 complexes was preliminarily examined also, through tracking product formation over time. The inclusion of palladium-bound halide ligands were shown to be necessary for precatalyst activation. NHC ligands featuring allyl *N*-substituents gave an unexpected and abrupt loss of activity and was suspected to occur through C-H activation forming a catalytically inactive palladacycle.

The findings of these initial additional investigations and the main body of this thesis appropriately aid in the achievement of the aims outlined for this project, including gaining a deeper understanding of the processes involved in the catalytic reaction and informing smart catalyst design to have tailored selectivity.

Table of Contents

List of Figures

List of Schemes

List of Tables

List of Equations

Table of Abbreviations

$\%V_{bur}$	Percent buried volume
°C	Degrees Celsius
$^{13}C\{^{1}H\}$	Proton-decoupled carbon (NMR)
2,4-Ar	2,4-Bis(*p*-fluorophenyl)pyridine
2-Ar	2-(*p*-Fluorophenyl)-4-bromopyridine
4-Ar	2-Bromo-4-(*p*-fluorophenyl)pyridine
Å	Angstroms (1×10^{-10} m)
API	Active pharmaceutical ingredient
d	Doublet multiplicity (NMR)
DCM	Dichloromethane
DFT	Density functional theory
Depp	Diisopropylphenyl
DMSO	Dimethyl sulphoxide
dppf	1,1′-Bis(diphenylphosphino)ferrocene
ESI	Electrospray ionisation
eV	Electron volts
FDMB	1-Fluoro-3,5-dimethoxybenzene
GC	Gas chromatography
HOMO	Highest occupied molecular orbital
HRMS	High resolution mass spectrometry
Hz	Hertz
IMes	1,3-Di(adamantly)imidazole-2-ylidene
IPr	1,3-Bismesityl-imidazol-2-ylidene
IPS	Imidazolium palladate salt
J	Coupling constant (NMR)
L	Ligand
LC-MS	Liquid chromatography mass spectrometry
LUMO	Lowest unoccupied molecular orbital
m	Multiplet multiplicity (NMR)
m/z	Mass to charge ratio
Mes	Mesityl
MHz	Megahertz
NHC	*N*-heterocyclic carbene

NMR	Nuclear magnetic resonance
NP	Nanoparticle
OA	Oxidative addition
PdNP	Palladium nanoparticle
PEPPSI	Pyridine-enhanced precatalyst, preparation, stabilisation and initiation
ppm	Parts per million
PVPy	Polyvinylpyridine
pyr	Pyridine
RE	Reductive elimination
RT	Room temperature
s	Singlet multiplicity (NMR)
SC-XRD	Single-crystal X-ray diffractometry
SMCC	Suzuki-Miyaura cross-coupling
t	Triplet multiplicity (NMR)
T_1	Spin-lattice relaxation time
TBAH	Tetrabutylammonium hydroxide
TEP	Tolman electronic parameter
THF	Tetrahydrofuran
TM	Transmetalation
TMB	Trimethoxybenzene
TON	Turn over number

Chapter 1

Introduction

1.1 Suzuki-Miyaura cross-coupling

Since its discovery in 1979,[1] the Suzuki-Miyaura reaction (or Suzuki cross-coupling) has become one of the most important and widely used chemical transformations in organic synthesis.[2] This and similar reactions such as the Heck, Stille, and Negishi coupling reactions, to name but a few, make up a class of reactions known as carbon-carbon cross-couplings. The formation of new carbon-carbon bonds are key in the construction of complex bio-active molecules and agrochemicals, making this class of reactions indispensable in the pharmaceutical sector, with Suzuki coupling alone accounting for *ca.* 20% of all cross-coupling reactions performed in small molecule synthesis.[3]

Specifically, the Suzuki-Miyaura cross-coupling (SMCC) is the catalytic C–C bond formation between aryl, alkenyl or alkynyl organoboranes (boronic acids or boronic esters) and, typically, aryl halides in the presence of a base (Scheme 1.1). Palladium is often used as the catalyst (either homo or heterogeneously) and is very well studied for this application, though other transitions metal catalysts, such as nickel, can be used.[4] The reaction is extremely tolerant with regard the coupling partners; electron-rich and -poor, highly functionalised and sterically hindered substrates are all able to undergo cross-coupling. This demonstrates the vast scope of the Suzuki-Miyaura cross-coupling reaction. Examples of coupling with aryl chlorides (a challenging substrate) have also been reported, even at very low catalyst loadings.[5]

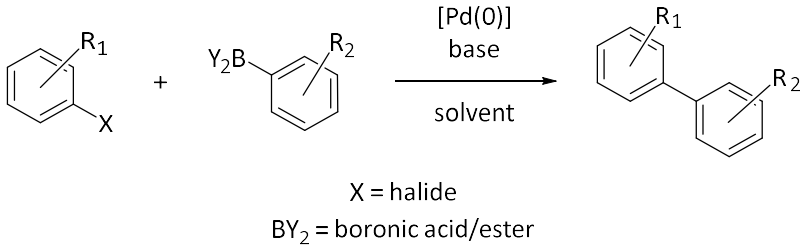

Scheme 1.1 – General reaction scheme of the SMCC reaction between arylhalide and an arylborane with palladium(0) catalyst.

The appeal of SMCC in comparison to other analogous reactions, namely the Heck reaction, is three-fold. Firstly, the reaction conditions are relatively mild, with coupling reactions usually occurring between 50 – 80 °C and many examples progressing at room temperature, whereas Heck classically requires reaction temperatures above 100 °C.[6-8] Secondly, the wide accessibility of both the organoboron and organohalide reagents, with many either commercially available

or easily synthesised, for example using the Miyaura borylation reaction (Scheme 1.2).[9] Furthermore, the straightforward removal of the boron containing side products makes purification of the final product relatively simple.[2]

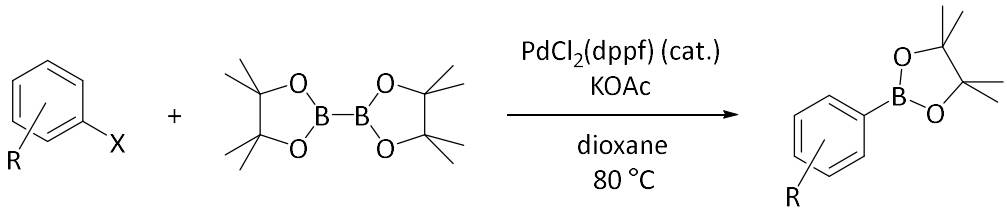

Scheme 1.2 – General reaction scheme of the Miyaura borylation reaction with an alkyl halide and bis(pinacolato)diboron forming the corresponding borylated species, using $PdCl_2$(dppf) as catalyst. (dppf = 1,1'-bis(diphenylphosphino)ferrocene).

Generally, homogeneous SMCC reactions proceeds *via* three fundamental steps: oxidative addition (OA), transmetalation (TM) and reductive elimination (RE) (Scheme 1.3).[10] Pd(0), either originating from the catalyst complex or generated *in situ* through reduction of a Pd(II) pre-catalyst, undergoes oxidative addition with the aryl halide species to form an aryl ligated palladium halide intermediate. Transmetalation occurs with the arylboronic acid/ester species to exchange the halide ligand with a second aryl ligand to form a bis-arylated palladium complex and boron containing side-products. Base is thought to be required for activation of the organoborane species to promote transmetalation.[11] The bis-arylated palladium complex is in *cis-trans* equilibrium; reductive elimination occurs from the *cis* form to give the cross-coupled product and regenerate the Pd(0) active catalyst species.[10]

A major challenge for SMCC is the instability of the catalytic species, particularly the propensity for degradation of carbon-phosphorus bonds at high temperatures, and acute air sensitivity of typical tertiary phosphine-based ligands. The inherent instability of these phosphine-based palladium catalysts necessitates rigorously inert, controlled reaction conditions and meticulous reagent handling to be observed. As a result, more stable palladium catalysts (and precatalysts) with non-phosphine ligand systems garner significant interest within the field.[12]

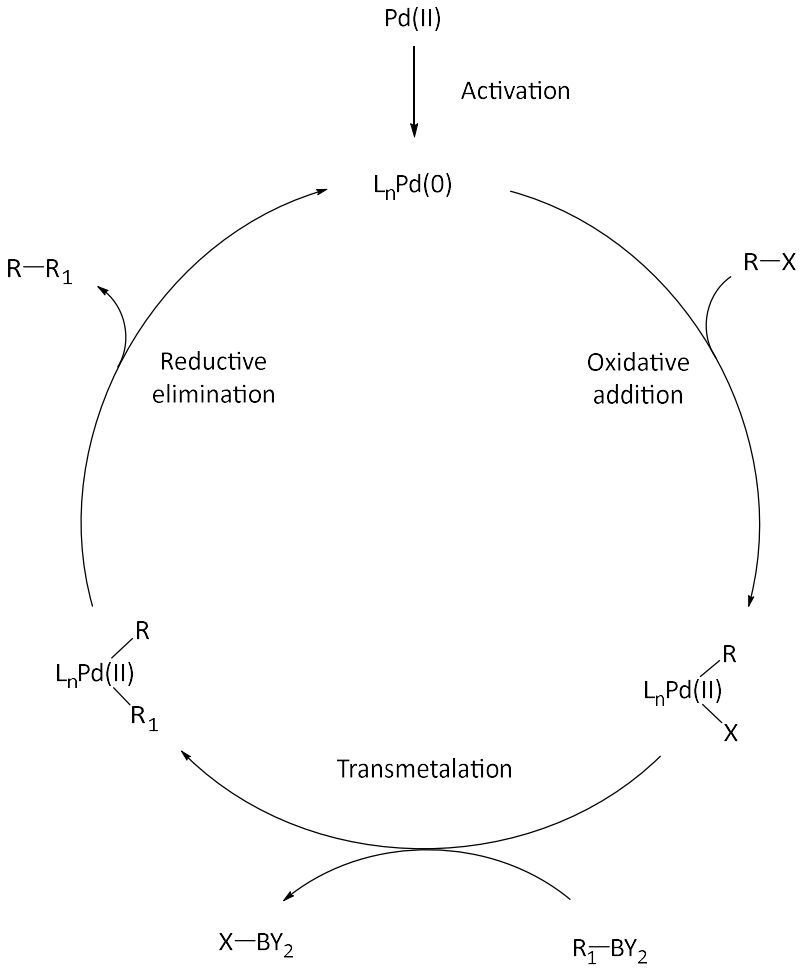

Scheme 1.3 – General mechanism for Suzuki-Miyaura reaction: 1 - catalyst activation, 2 - oxidative addition, 3 - transmetalation, 4 - reductive elimination to reform the catalytic active species.

1.2 Carbenes

Carbenes are a class of neutral compounds featuring a divalent carbon atom with six valence electrons.[13] Two of these valence electrons occupy non-bonding *p*-orbitals, while the others are used in bonding to the α-substituents. The central carbon atom can adopt either a linear or bent conformation, with each possessing a different degree of hybridisation. For linear geometries, the carbene has an *sp*-hybridised centre with two degenerate *p*-orbitals (p_x and p_y), the occupancy of the electrons in these orbitals affords triplet multiplicity (Figure 1.1).

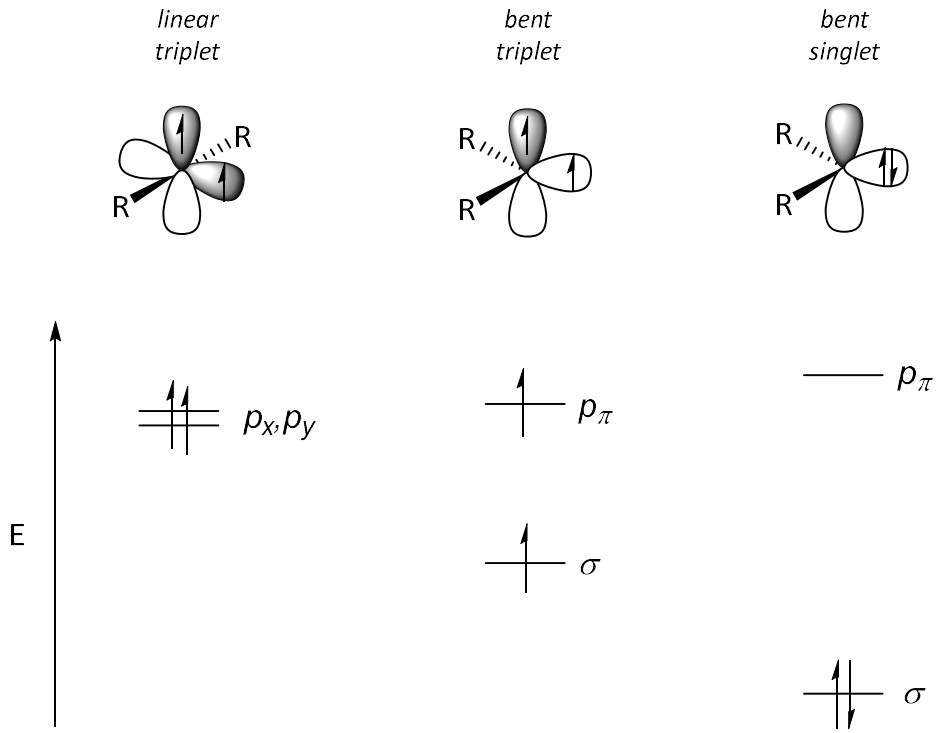

Figure 1.1 – Molecular orbitals and relative energies between p_π and σ orbitals for linear (triplet), bent (triplet) and bent (singlet) carbenes.

The vast majority of carbenes have a bent geometry; the degeneracy of the *p*-orbitals is broken and the carbon atom adopts sp^2-hybridisation. The p_y-orbital remains essentially unchanged (p_π-orbital), while the p_x-orbital becomes stabilised through gaining *s*-character (*σ*-orbital), thus the occupancy of the orbitals can change to yield either triplet or singlet state multiplicity (Figure 1.1).[13] The α-substituents on the carbon centre influence the ground state multiplicity of the carbene greatly, with heteroatom substituents generally forming singlet ground states, through large *σ*- and p_π-orbital energy differences (>2 eV).[14]

Complexes formed between a carbene and a metal centre are classified as either Fischer- or Schrock-type carbenes, depending on the interaction between the atomic orbitals.[15] Fischer-type carbenes are complexes formed through the interaction between a singlet state carbene (usually with at least one heteroatom α-substituent) and a singlet state metal centre. The dominant bonding interactions arise from carbene to metal σ-donation and metal to carbene π back-donation, as seen in Figure 1.2. The metals in Fischer-type carbenes are typically mid to late in the transition series, with a low oxidation state. These carbenes are usually electrophilic and susceptible to nucleophilic attack.[15, 16]

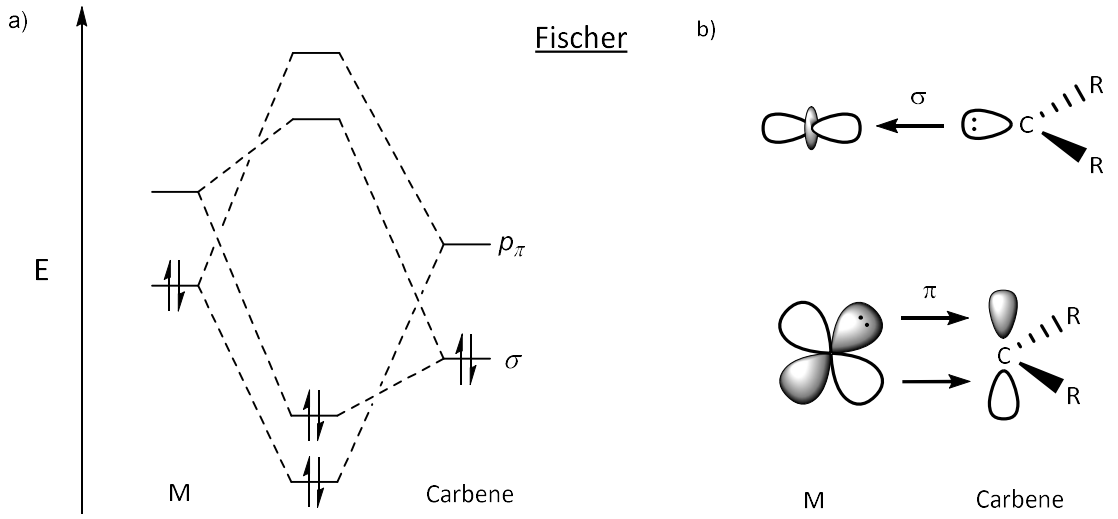

Figure 1.2 – a) Molecular orbital diagram displaying the interactions of a Fischer-type carbene and a singlet state metal centre. b) Illustration of orbital interactions of a Fischer-type carbene and a singlet state metal centre.

Schrock-type carbene complexes are formed through the interaction of a triplet ground state carbene (typically without π-stabilising α-substituents) and a triplet state metal centre. Bonding in Schrock carbenes has covalent character, with sharing of valence electrons between the atomic orbitals being the dominant bonding interaction, forming an equal distribution of electrons over the metal carbene bond, as seen in Figure 1.3. Unlike Fischer-type carbenes, there is no back-donation from the metal centre and the metal involved is usually in a high oxidation state. The metal carbene bond has nucleophilic character and is prone to electrophilic attack.[15,16]

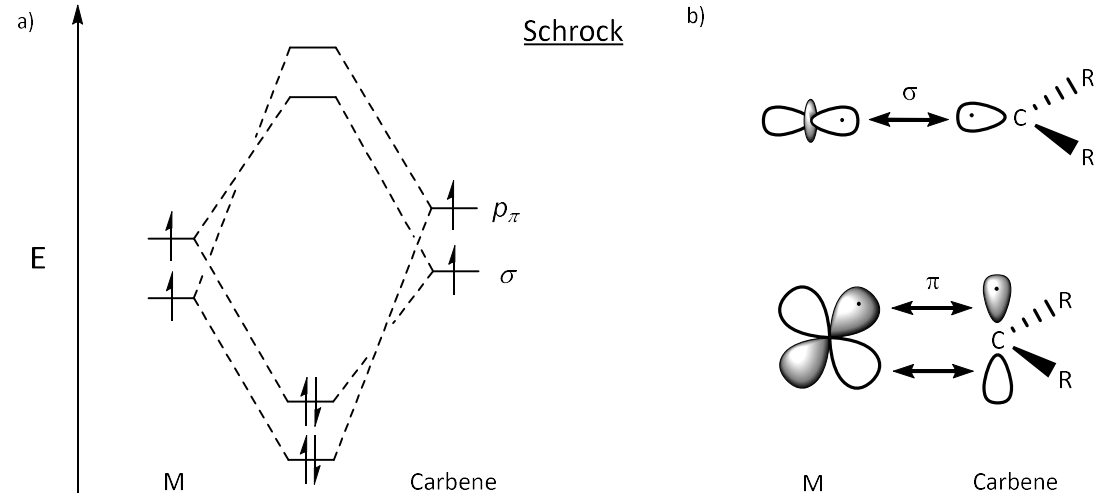

Figure 1.3 – a) Molecular orbital diagram displaying the interactions of a Schrock-type carbene and a triplet state metal centre. b) Illustration of orbital interactions of a Schrock-type carbene and a triplet state metal centre.

1.2.1 *N*-heterocyclic carbenes (NHCs)

Fischer-type carbenes afford many subsets of carbenes based on their structure and bonding, one such sub-class is *N*-heterocyclic carbenes (NHCs). NHCs are defined as singlet carbenes, in which a carbenic centre is connected to at least one nitrogen atom within a heterocycle (Figure 1.4).[13, 17] Unlike other traditional carbenes, NHCs are extremely durable and can readily exist as persistent free carbenes, due in part to the electronic stabilisation. This is due to the adjacent σ-electron withdrawing and π-electron donating nitrogen atoms, granting both inductive and mesomeric stabilisation respectively (Figure 1.5). Both these effects, in conjunction with a ring configuration locking the carbene in a bent geometry, ensure that a singlet ground state is maintained. Moreover, the architecture of the backbone is significant, providing both electronic stabilisation through partial aromaticity and tunability of the electronic structure, *via* variation of the backbone substituents.[18, 19]

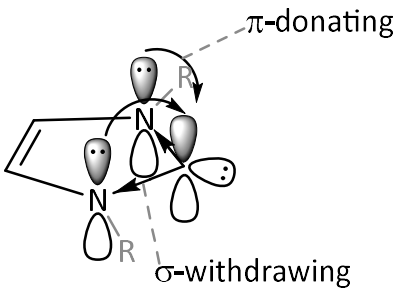

Figure 1.4 – a) General structure of an NHC. b) Illustration showing the orbital stabilisation mechanisms present in the NHC structure.

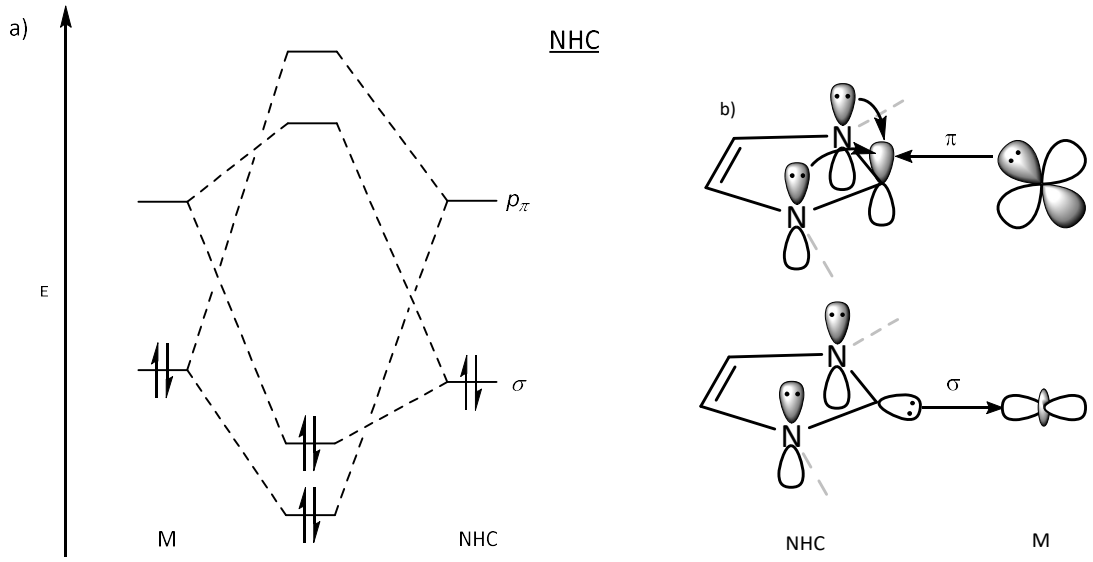

Figure 1.5 – a) Molecular orbital diagram displaying the interactions of an NHC and a singlet state metal centre. b) Illustration of orbital interactions of an NHC and a singlet state metal centre.

The first reported instance of a stable, free NHC came about in 1991, with the isolation of 1,3-di(adamantly)imidazole-2-ylidene (***1***, Figure 1.6).[20] As with ***1***, NHCs generally feature very bulky *N*-substituents to provide kinetic stability, disfavouring dimerisation (the Wanzlick equilibrium).[19, 21] However, due to the aforementioned stabilisation mechanisms, particularly for partially aromatic NHCs, there is less demand for proximal steric bulk to stabilise NHC-metal complexes.[22, 23]

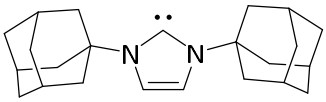

1

*Figure 1.6 – Structure of the free-NHC form of di(adamantly)imidazole-2-ylidene (**1**).*

The most commonly utilised precursors for NHC ligands are azolium salts, due to the extensive structural variation possible with simplistic synthetic routes.[24, 25] Formation of metal complexed NHC ligands typically occurs through the deprotonation of the azolium ion at the C2 position with a base to from the free carbene which can then undergo *in-situ* complexation to a metal centre (Scheme 1.4). Other strategies for free and ligated NHC formation include small molecule elimination from an NHC precursor, oxidative addition of C2 functionalised heterocycles and electrochemical generation of NHCs.[26-28] The transmetalation of silver(I)-NHC complexes is also a widely used strategy to generate transition metal-NHC complexes.[29]

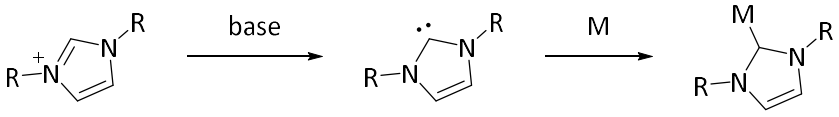

Scheme 1.4 – General reaction for metal assisted formation of metal-NHC complexes from azolium salt ligand precursors.

Typically, the sterics of an NHC are altered through modification of the *N*-substituents, which is usually implemented in the synthesis of the NHC precursor azolium salt. Other aspects can influence the sterics of NHCs such as the heterocycle ring size and degree of saturation. The electronics of the NHC are modified by utilising different backbone architectures, such as the incorporation of an aromatic ring in benzimidazolium, or through functionalisation of the backbone with electron-donating or withdrawing groups. The *N*-substituents also have some effect on the electronics of the NHC but to a lesser extent than the backbone.

A relatively simplistic measure of NHC sterics is the 'buried volume' parameter (%V_{bur}) as shown in Figure 1.7 and displays the steric influence of the ligand on the metal centre.[30] The parameter is defined as the percentage of a sphere centred on the metal (radius of 3.5 Å) occupied by the NHC ligand based on standardised atomic radii. This can therefore be used to quantify the steric profile of a range of NHC architecture and is not limited to symmetrical ligands.[31] Steric maps can also be used to graphically display the steric profile of the NHC ligand.[31]

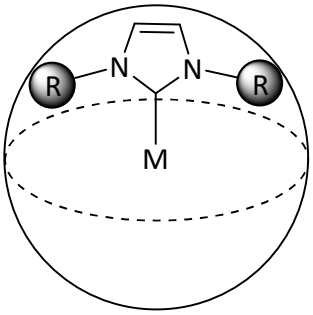

Figure 1.7 – Illustration of the buried volume parameter (%V_{bur}) used for measuring the steric bulk of NHCs, relating the percentage of a sphere of radius 3.5 Å taken up by the steric bulk of the coordinating ligand.[30]

The electronic properties of an NHC ligand are measured using the Tolman electronic parameter (TEP). The TEP uses the shift in the A_1 C–O vibrational mode in [L-Ni(CO)$_3$] is used to infer and measure the electron donating/withdrawing ability of a given ligand (L) (Figure 1.8).

Electron donating L
Weaker CO bond
Decreased ν(CO)

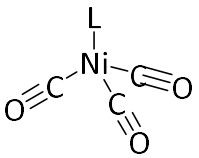

Electron withdrawing L
Stronger CO bond
Increased ν(CO)

Figure 1.8 – NiL(CO)$_3$ complex used to determine the Tolman electronic parameter (degree of electron donation/withdrawing ability) for a given ligand (L).

Metal-NHC complexes present more accessible, flexible and applicable electronic and steric tunability compared to analogous phosphine containing complexes. This has led to NHCs being used in a considerable number of applications. One such application is the use of metal-NHC complexes in catalysis.

1.3 Palladium-NHC complexes in catalysis

The first reported catalytically relevant NHC complex was for the Heck reaction in 1995.[32] Herrmann and co-workers presented two similar palladium-NHC complexes formed from [Pd(OAc)$_2$] with 1,3-dimethylimidazolium iodide and 3,3'-dimethyl-1,1'-methylenediimidazolium diiodide, ***2*** and ***3*** respectively (Figure 1.9). Both complexes catalysed the Heck olefination of chloro- and bromoarenes. Better activity was observed for complex ***2***,

the higher thermal stability over time for the active catalytic species of ***2*** resulted in higher turnover numbers (TONs) for the complex, even when compared to other well established palladium catalysts for this reaction.[32] This pioneering report sparked great intrigue in the field and, as such, NHCs have been utilised in a multitude of catalytic reactions.[12]

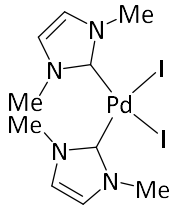

2

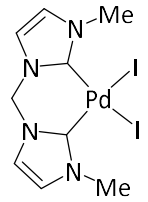

3

Figure 1.9 – Structures of Herrmann's palladium-NHC complexes: Bis(1,3-dihydro-1,3-dimethyl-2H-imidazol-2-ylidene)diiodo -palladium (left) and diiodo(methylenebis(3-methyl-1H-imidazol-1-yl-2(3H)-ylidene))-palladium (right).

Palladium complexes featuring bulky NHC ligands are amongst the most extensively applied, with the use of 1,3-bis(2,6-diisopropylphenyl)-imidazol-2-ylidene (IPr, ***4***) and 1,3-bismesityl-imidazol-2-ylidene (IMes, ***5***) (Figure 1.10) particularly widespread and commonplace. However in recent years, through the work of Glorius and co-workers with the IBiox series (***6***, Figure 1.11),[33, 34] the importance of flexible steric bulk has led to its implementation into the design of IPr, affording the ITent series (***7,*** Figure 1.11). The conformational flexibility within these systems allows the active species to adopt different steric requirements within a catalytic cycle, thus increasing the stability of the catalyst without affecting its productivity negatively. This new class of catalysts shows excellent activity for the synthesis of tetra-*ortho*-substituted biaryls under mild reaction conditions. This example demonstrates perfectly the versatility and the remarkable tunability of palladium-NHC complexes, all while performing under mild conditions.[34]

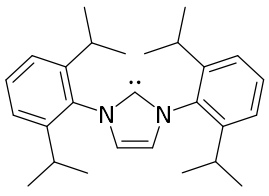

4

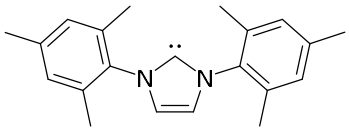

5

*Figure 1.10 – Structures of 1,3-bis(2,6-diisopropylphenyl)-imidazol-2-ylidene (IPr) (**4**) and 1,3-bismesityl-imidazol-2-ylidene (IMes) (**5**).*

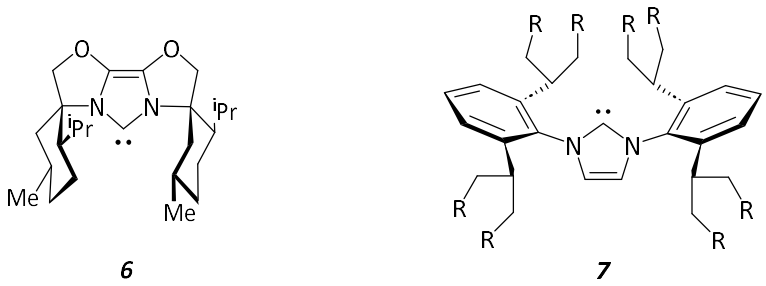

6 *7*

*Figure 1.11 – General structure of IBiox (**6**) and ITent (**7**) NHCs featuring flexible steric bulk, allowing for dynamic conformational flexibility during catalytic cycles (R= Me, Et, ^{i}Pr).*

Pyridine-enhanced precatalyst, preparation, stabilisation and initiation or PEPPSI is a term coined by Organ and co-workers in 2006, to describe a novel class of air and moisture stable palladium precatalysts for use in cross-coupling reactions.[6] The general structure of these compounds features a Pd(II) species, furnished with an NHC ligand, two anionic ligands (*e.g*. Cl, Br, OAc) and a fourth suitably substituted pyridine ligand (***8***, Figure 1.12). The enhanced catalytic activity of these complexes is attributed to the rapid dissociation of the "throw away" pyridine ligand leading to activation of the catalytic species. The initial findings were very promising with high stability of the complex and good catalytic activity.

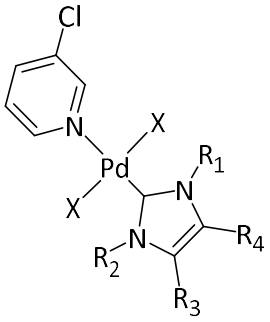

8

Figure 1.12 – General structure of Pyridine Enhanced Precatalyst Preparation, Stabilisation and Initiation (PEPPSI) palladium complexes. (X=Cl, Br, I, OAc etc.).

1.4 Palladium nanoparticles and clusters

Widely accepted mechanisms of palladium homogeneous catalysts for prominent cross-coupling reactions (Heck, Suzuki etc.) usually involve one or two palladium atoms in various oxidation states. Furthermore, mechanistic approaches involving direct or indirect heterogeneous palladium species along with the equilibrium between heterogeneous and homogeneous are often overlooked (Figure 1.13).[35] Many ubiquitous palladium catalysts can often display heterogeneous catalytic behaviour, typically through speciation to palladium clusters or nanoparticles.[36]

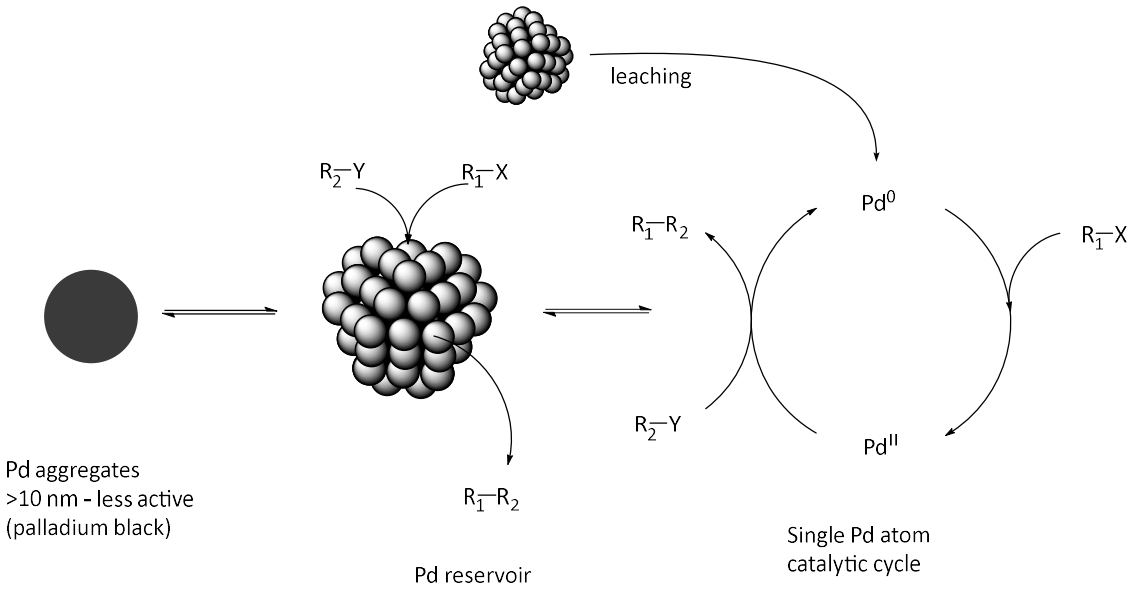

Figure 1.13 – A schematic representation of the aggregation of mononuclear homogeneous Pd catalysts into PdNPs, with leaching to reform mononucleic Pd. The formation of larger aggregates (palladium black) is also shown. (Figure adapted from reference [35]).

Both supported and solubilised palladium nanoparticles (PdNPs) have proven to be efficient catalysts for a wide variety of chemical transformations, including both the Heck and Suzuki cross-couplings.[12, 37-39] However, uncertainty of the active species in these transformations is a drawback, as greater catalytic activity and reduced precious metal waste could be achieved through better understanding.[40] Comprehensive investigations into the whole range of catalytic species is necessary, from mononuclear homogeneous catalysts to heterogeneous PdNPs.

An important criterion for the synthesis, stabilisation and function of disperse NPs is the choice of surface ligand.[41, 42] Minimisation of surface energy is key for the prevention of aggregation and retention of a narrow NP size distribution for colloidal systems. Many ligand types have demonstrated effective stabilisation of a range of metallic NPs, including thiols, amines, phosphines and isocyanides to name a few, with extensive investigations focussed on understanding the interactions and stabilisation mechanisms present.[41] As such, these surface ligands are now well understood and widely adopted as stabilisers in many NP applications including catalysis, sensing and biomedicine.[42]

The use of NHCs as metallic NP stabilising ligands is relatively new in comparison to more classically applied ligands, such as thiols. The first instances of intentional NHC use for stabilising Au and Pd systems were from the Fairlamb/Chechik and Tilley groups in 2009.[43, 44] Fairlamb and Chechik produced Au- and PdNPs featuring NHC surface ligands through exchange of dodecylsulfide-protected NPs with free carbene in solution (Figure 1.14).[43] These newly formed NPs were stable in the solid state for prolonged periods of time, however, they degraded quickly

in solution leading to aggregated NPs and production of mononuclear metal-NHC complexes. These interesting observations resulted from leaching of the mononuclear complexes from the NP surface, leading to aggregation and a deficit of stabilising ligands.

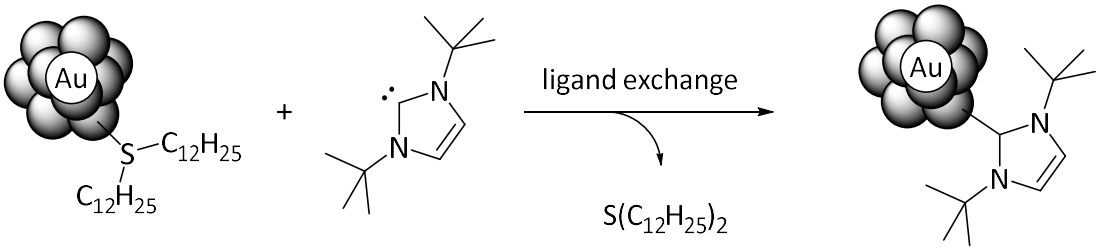

Figure 1.14 – Formation of AuNPs featuring NHC stabilising ligands through the substitution of dodecylsulfide ligands by Fairlamb and Chechik. [43]

Tilley and co-workers prepared AuNPs through reduction of mononuclear NHC-Au complexes.[44] They noted the importance of the NHC *N*-substituents for NP stability, demonstrating formation of small AuNPs using isopropyl *N*-substituents, but these were difficult to purify owing to the similarity in solubility to the parent complex. Successful synthesis of stable AuNPs was achieved however, with the use of NHCs featuring long chain alkyl *N*-substituents ($C_{14}H_{29}$), the corresponding AuNPs were stable for months in solution. Since these initial reports, there has been many studies investigating the effectiveness of NHCs, leading to NHCs becoming a well understood class of NP surface ligand, demonstrating high stability and functionality in colloidal systems. [45-50] This not only demonstrates the versatility of NHCs, but more appropriately provides a basis for deeper understanding of the complex relationship between hetero- and homogeneous catalytic systems.

The subtleties of this relationship could be expanded upon through investigation of the middle-ground between mononuclear and heterogeneous catalysis, however to date, little research has been conducted into smaller multinuclear palladium species as viable catalysts. Nevertheless, recent interest into stable palladium clusters, namely $[Pd_3(\mu\text{-Cl})(\mu\text{-PPh}_2)_2(PPh_3)_3]Cl$ (Coulson cluster (***9***), Figure 1.15) and its derivatives has identified them as viable novel catalytic species. Unique reactivity displayed by these clusters could help further understanding of the active species in catalytic systems as a whole. These species display high air and thermal stability. The catalytic activity of this cluster, alongside few analogous examples, was investigated using well established reactions showing very promising results.[51-53] Investigation and development of the activity of these clusters is sparse but the potential has been demonstrated and is auspicious.

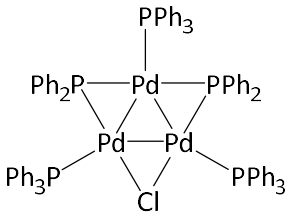

9

Figure 1.15 – Structure of the Coulson cluster, first reported in 1968.[54]

1.5 Sustainability

As mentioned previously, palladium-based complexes have almost exclusively been used as the catalyst for the SMCC which is used widely in industry. The use of palladium has several inherent downfalls, most notably in cost of the finite resource and the toxicity of the catalysts. Minimising the amount of toxic metal complexes in the desired products of drug synthesis strategies is paramount to prevent harmful side effects and unnecessary costs.[55] Efforts to reduce the residual toxic palladium levels in active pharmaceutical ingredients (APIs), to the accepted proportion of 10 ppm or less have proven successful, through the use of specialist scavenger molecules.[55-58] However, synthesis of such molecules is complex and can be applied more effectively by better understanding the mechanisms through which palladium becomes inactive and developing specific catalysts scavengers to maximise recovery of palladium.

The development of novel catalysts for SMCC using more economically viable and less toxic metals, such as iron and nickel, has become more prevalent, with numerous promising examples emerging in the past few years. However, nickel and iron-based catalysts that exhibit similar efficacy and adaptability to their well-established palladium counterparts, are still in the relatively early developmental stages. Therefore, parallel refinement of current palladium catalysts (particularly palladium-NHC catalysts) and reaction methods is a valid tactic for achieving improved sustainability. One avenue of research showing good promise would be the use of aforementioned palladium clusters, exhibiting novel reactivity and better processability than the mononucleic homogeneous counterparts.

1.6 Site-selectivity in SMCC

Site-selectivity or regiocontrol is a challenging aspect of cross-coupling catalysis. In SMCC, site-selectivity may be observed when employing an aryl halide substrate featuring multiple halide substituents, whereby reactivity bias results in the formation of a single regioisomer. Conventional site-selectivity, in the majority of cases, follows the expected route where reactivity is seen at the weakest bound halogen in the substrate.[59] For heteroarenes containing two or more halide substituents, selective coupling is usually observed at the reactive site closest to the heteroatom.[60] Examples of unconventional or abnormal site-selectivity have been reported through catalyst ligand control though, for the most part, the mechanisms that dictate the abnormal selectivity are not explored in rigourous detail.[61, 62]

Recent reports from Neufeldt and co-workers describe a departure from the normal site-selectivity of the SMCC reaction of 2,4-dichloropyridine with arylboronic acid when using Pd-NHC complexes.[60, 63, 64] The mechanism for the abnormal selectivity was explored experimentally and through DFT calculations of reactive intermediates. Interaction of the active catalytic species was found to favour a different mechanism of oxidative addition depending on the halide position (Figure 1.16). A concerted mechanism was found to be favourable at the 4-Cl position whereby the palladium would insert into the carbon-halide bond. A displacement mechanism was found to be favourable at the 2-Cl position where coordination of the pyridinyl carbon would facilitate the dissociation of the halide.

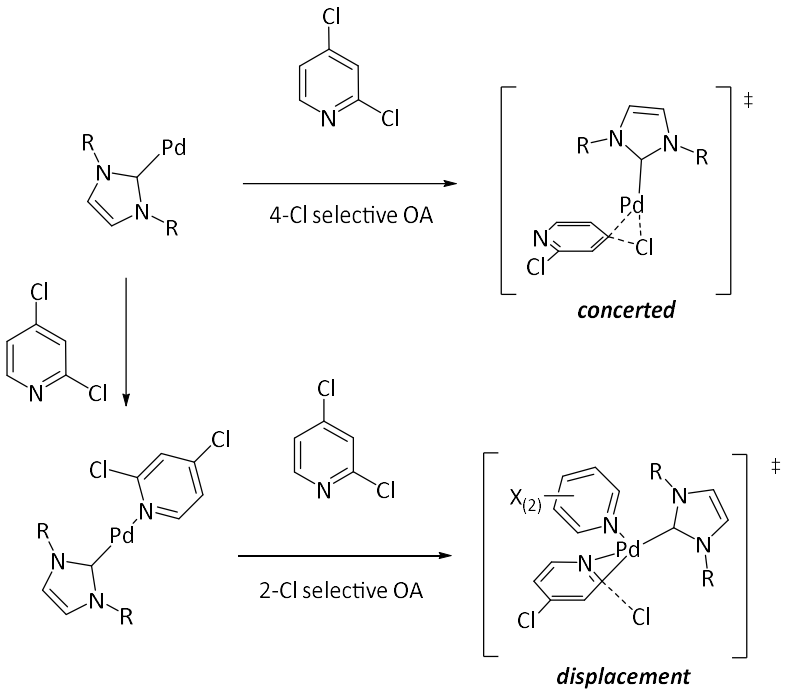

Figure 1.16 – Mechanistic rationale for site-selective oxidative addition of 2,4-dichloropyridine with Pd-NHC active catalytic species through either concerted (4-Cl selective) or displacement (2-Cl) reaction intermediates.

The NHC ligand architecture of the active palladium species was found to influence the site-selectivity of the reaction by preferential undergoing one of these mechanisms. Palladium active species with a sterically bulky NHC (Dipp *N*-substituents) were shown to undergo reactivity at the 4-Cl position through the concerted mechanism. Palladium active species featuring a 'less bulky' NHC ligand (Mes *N*-substituents) were shown to first undergo complexation of a pyridine to form a bis-ligated palladium(0) active species which would preferentially react *via* the displacement mechanism at the 2-Cl position. The difference in NHC ligand steric bulk for the complexes tested by Neufeldt is minimal, with many consider both Mes and Dipp NHC *N*-substituents to be bulky, highlighting the subtle nature of the catalyst interactions in the 2,4-dichloropyridine system. The implications of this have applications in rationale ligand design for abnormal site-selective catalysts.

Work conducted by Fairlamb and co-workers highlights the importance of a complete understanding of the mechanisms behind abnormal site-selectivity. When employing a $Pd(OAc)_2$:*n*PPh_3 catalyst system to the cross-coupling reaction of 2,4-dibromopyridine and arylboronic acid, a switch in site-selectivity was observed to preferentially form the abnormal 4-arylated pyridine product, observed when using <2 equivalents of PPh_3 (Scheme 1.5, Figure 1.17).[65]

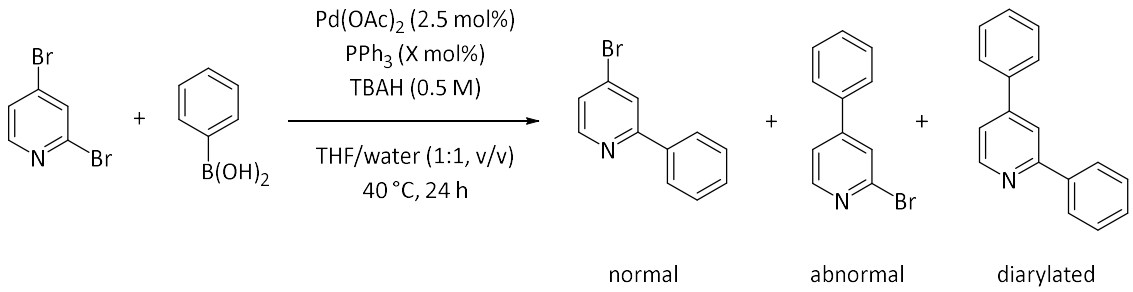

*Scheme 1.5 – Reaction between 2,4-dibromopyridine and phenylboronic acid using $Pd(OAc)_2$ at 2.5 mol% and PPh_3 at X mol% (where X = 0, 0.5, 1, 1.5, 2, 2.5, 3 and 4) as the catalyst system in a 1:1 THF:water solvent system at 40 °C. Tetrabutylammonium hydroxide was used as the base. *recreated from literature.* [65]

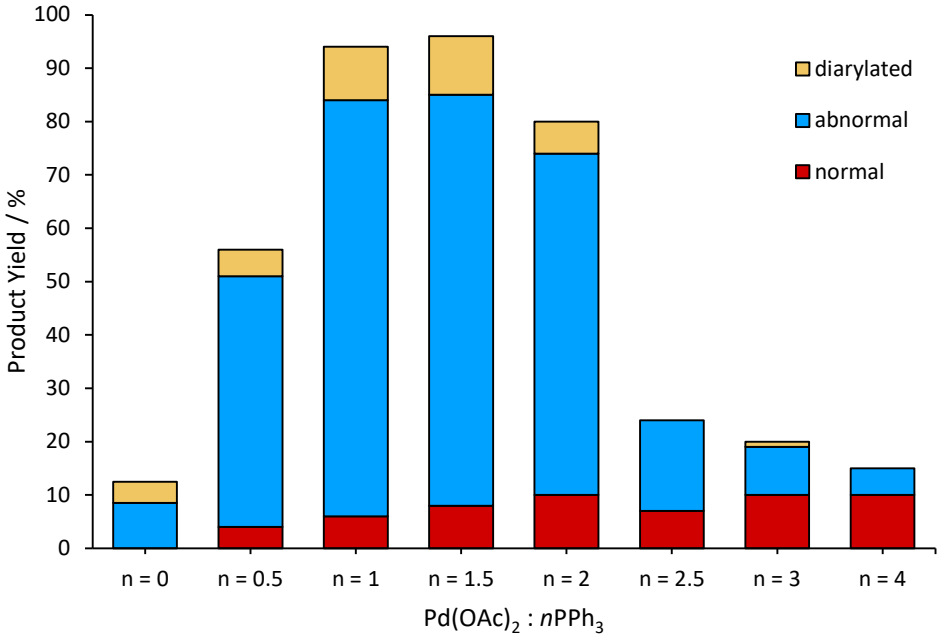

*Figure 1.17 – Reported results from the reaction of 2,4-dibromopyridine and p-fluorophenylboronic acid in the presence of different $Pd(OAc)_2$:nPPh_3 ratios (where n = 0, 0.5, 1, 1.5, 2, 2.5, 3 and 4) giving different product selectivity with a change in n. *Recreated from literature.* [65]

It was found that catalyst speciation dominated the selectivity of this reaction at low equivalents of PPh_3 with respect to palladium, whereby higher order palladium species would form and implement a change in mechanism of the coupling reaction (Figure 1.8). Instead of proceeding though the accepted mono nuclear SMCC mechanism with initial oxidative addition, transmetalation was shown to be the first step in the catalytic cycle, followed by oxidative addition. The inclusion of a nanoparticle stabilising salt species to the reaction resulted in enhanced 4-arylated pyridine formation indicating that higher order palladium species also share this abnormal selectivity and are present in the reaction also. This work demonstrates that catalyst speciation may be present in seemingly well understood homogeneous palladium catalyst systems and may be prevalent in reactions yielding abnormal site-selectivity.

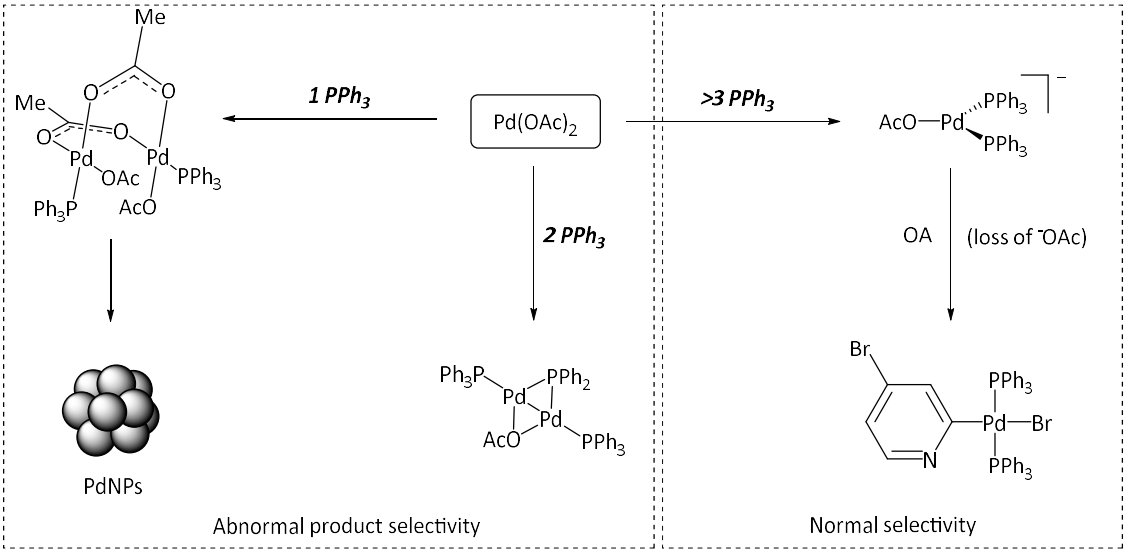

*Figure 1.18 – Rationale for the site selectivity observed in the reaction of 2,4-dibromopyridine and p-fluorophenylboronic acid with $Pd(OAc)_2$ / $nPPh_3$ catalyst system. *recreated from literature.* [65]

Work conducted by Willans and co-workers showed similar abnormal site selectivity in the reaction of 2,4-dibromopyridine with arylboronic acid (Scheme 1.6), when using Pd-NHC complexes, ***10–13*** as precatalysts (Figure 1.19, Figure 1.20).[66] Unlike the work by Neufeldt, the abnormal selectivity was seen for relatively non-bulky NHC complexes, which suggests that either a different mono-nuclear mechanism is in operation or that, like Fairlamb's work suggests, a higher order palladium active species may be in operation and dictating the selectivity of the reaction. However, a significant quantity of the diarylated pyridine product was also seen in the reaction, which departs from Fairlamb's rationale where very little 'over-arylation' was seen with high order palladium species. The abnormal site-selectivity in this reaction therefore requires rigorous investigation to elucidate the mechanisms involved and progress general understanding of how abnormal site-selectivity may occur in palladium catalysis.

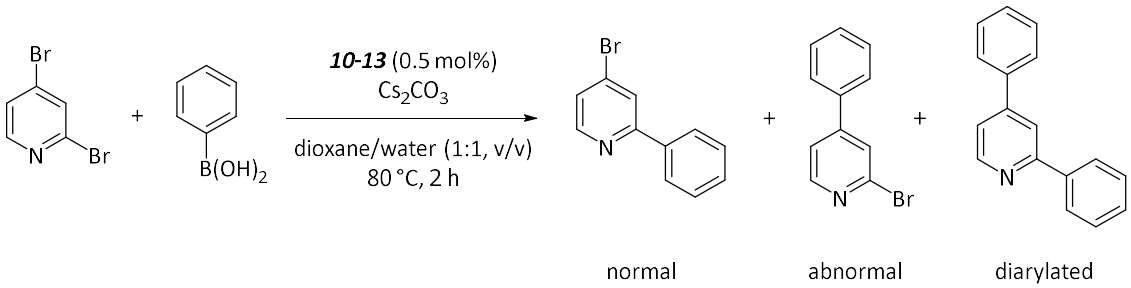

*Scheme 1.6 – Reaction between 2,4-dibromopyridine and phenylboronic acid using Pd-NHC complexes **10-13** as precatalysts at 0.5 mol% 1:1 dioxane:water solvent system at 80 °C. Caesium carbonate was used as the base. *Recreated from literature.*[66]

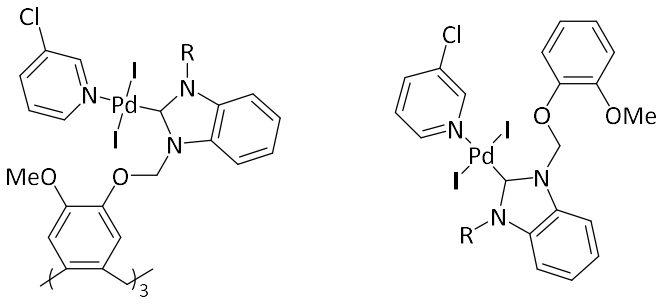

10 R = Me
11 R = Bn

12 R = Me
13 R = Bn

*Figure 1.19 – Structures of Pd-NHC complexes **10**–**13** used for the cross-coupling reaction of 2,4-dibromopyridine and phenylboronic acid. [66]*

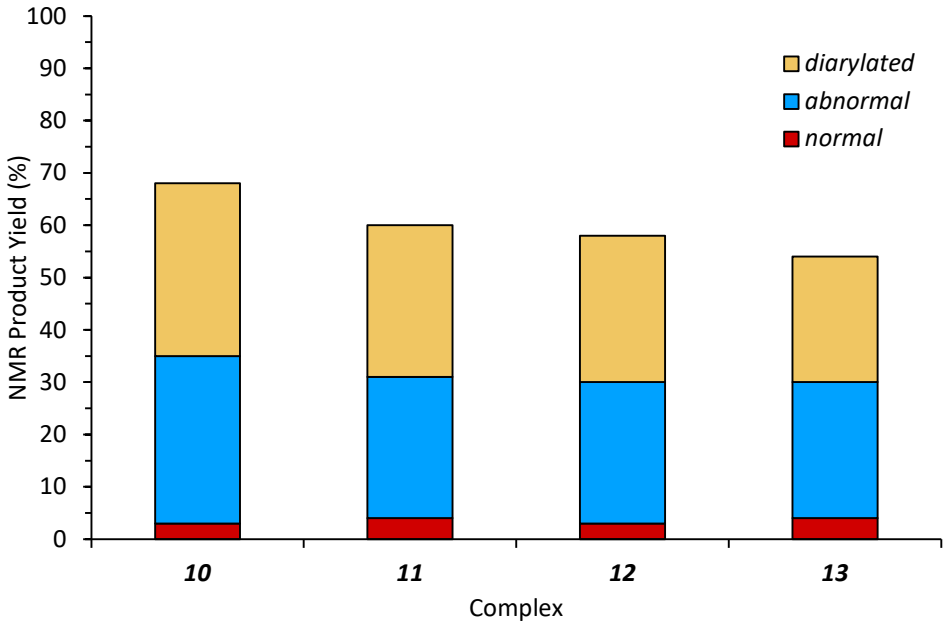

*Figure 1.20 – Reported results from the reaction of 2,4-dibromopyridine and p-fluorophenylboronic acid in the presence of Pd-NHC complexes **10**–**13** giving abnormal product selectivity. *Recreated from literature.[66]*

1.7 Project Outline

The main goal of this project is to investigate the abnormal site-selectivity for the reaction of 2,4-dibromopyridine with *p*-fluorophenylboronic acid when using Pd-NHC complexes, as a direct extension of the work by Willans and co-workers. Specifically, this project aims to gain a rigorous mechanistic understanding of the product formation in this reaction, with a view to using the findings to inform smart catalyst design for tailored site-selectivity. A deeper understanding of palladium catalysis and smarter catalyst design will lead to the more efficient use of palladium in the future. Additionally, catalyst deactivation will remain a focus of this work. The deactivation pathways of homogeneous palladium catalyst are relatively less well explored than would be expected for such an important and well used class of catalysts.[67] Therefore, where possible, the deactivation of the Pd-NHC catalysts in the SMCC under investigation will be considered and explored. This work will align with the recent literature findings and outlook, with strong reference to the work by Fairlamb on catalyst speciation and that of Neufeldt.[51, 60, 63-65]

1.8 References

1. N. Miyaura, K. Yamada and A. Suzuki, *Tetrahedron Lett.*, 1979, **20**, 3437-3440.
2. S. G. Gujal, S. Khatri and P. Riyal, *IGJPS*, 2012, **2**, 351-367.
3. J. S. Carey, D. Laffan, C. Thomson and M. T. Williams, *Org. Biomol. Chem.*, 2006, **4**, 2337-2347.
4. F. S. Han, *Chem. Soc. Rev.*, 2013, **42**, 5270-5298.
5. T. E. Barder, S. D. Walker, J. R. Martinelli and S. L. Buchwald, *J. Am. Chem. Soc.*, 2005, **127**, 4685-4696.
6. C. J. O'Brien, E. A. Kantchev, C. Valente, N. Hadei, G. A. Chass, A. Lough, A. C. Hopkinson and M. G. Organ, *Chemistry (Easton)*, 2006, **12**, 4743-4748.
7. C. Sicre, J. L. Alonso-Gomez and M. M. Cid, *Tetrahedron*, 2006, **62**, 11063-11072.
8. P. Y. Choy, X. He and F. Y. Kwong, in *Palladacycles*, Elsevier, 2019, pp. 21-173.
9. A. J. Lennox and G. C. Lloyd-Jones, *Chem. Soc. Rev.*, 2014, **43**, 412-443.
10. C. Len, S. Bruniaux, F. Delbecq and V. S. Parmar, *Catalysts*, 2017, **7**.
11. C. Amatore, A. Jutand and G. Le Duc, *Chemistry (Easton)*, 2011, **17**, 2492-2503.
12. S. Díez-González and S. P. Nolan, in *N-Heterocyclic Carbenes in Transition Metal Catalysis*, Springer, 2006, pp. 47-82.
13. D. Bourissou, O. Guerret, F. P. Gabbai and G. Bertrand, *Chem. Rev.*, 2000, **100**, 39-92.
14. R. Hoffmann, *J. Am. Chem. Soc.*, 2002, **90**, 1475-1485.
15. G. Frenking, M. Sola and S. F. Vyboishchikov, *J. Organomet. Chem.*, 2005, **690**, 6178-6204.
16. D. J. Cardin, Cetinkay.B and M. F. Lappert, *Chem. Rev.*, 1972, **72**, 545.
17. Y. Canac, M. Soleilhavoup, S. Conejero and G. Bertrand, *J. Organomet. Chem.*, 2004, **689**, 3857-3865.
18. L. Benhamou, E. Chardon, G. Lavigne, S. Bellemin-Laponnaz and V. Cesar, *Chem. Rev.*, 2011, **111**, 2705-2733.
19. M. N. Hopkinson, C. Richter, M. Schedler and F. Glorius, *Nature*, 2014, **510**, 485-496.
20. A. J. Arduengo, R. L. Harlow and M. Kline, *J. Am. Chem. Soc.*, 1991, **113**, 361-363.
21. H. W. Wanzlick and E. Schikora, *Angew. Chem.*, 1960, **72**, 494-494.
22. M. G. Gardiner, C. C. Ho, F. M. Mackay, D. S. McGuinness and M. Tucker, *Dalton Trans.*, 2013, **42**, 7447-7457.
23. P. J. Rayner, P. Norcott, K. M. Appleby, W. Iali, R. O. John, S. J. Hart, A. C. Whitwood and S. B. Duckett, *Nat. Commun.*, 2018, **9**, 4251.
24. A. A. Gridnev and I. M. Mihaltseva, *Synth. Commun.*, 1994, **24**, 1547-1555.
25. I. Nieto, F. Cervantes-Lee and J. M. Smith, *Chem. Commun.*, 2005, 3811-3813.

26. B. Liu, Y. Zhang, D. Xu and W. Chen, *Chem. Commun.*, 2011, **47**, 2883-2885.
27. T. M. Trnka, J. P. Morgan, M. S. Sanford, T. E. Wilhelm, M. Scholl, T. L. Choi, S. Ding, M. W. Day and R. H. Grubbs, *J. Am. Chem. Soc.*, 2003, **125**, 2546-2558.
28. T. Kosterke, T. Pape and F. E. Hahn, *J. Am. Chem. Soc.*, 2011, **133**, 2112-2115.
29. H. M. J. Wang and I. J. B. Lin, *Organometallics*, 1998, **17**, 972-975.
30. H. Clavier and S. P. Nolan, *Chem. Commun.*, 2010, **46**, 841-861.
31. A. Gomez-Suarez, D. J. Nelson and S. P. Nolan, *Chem. Commun.*, 2017, **53**, 2650-2660.
32. W. A. Herrmann, M. Elison, J. Fischer, C. Kocher and G. R. J. Artus, *Angew. Chem. Int. Ed. Engl.*, 1995, **34**, 2371-2374.
33. G. Altenhoff, R. Goddard, C. W. Lehmann and F. Glorius, *J. Am. Chem. Soc.*, 2004, **126**, 15195-15201.
34. S. M. P. Vanden Broeck, F. Nahra and C. S. J. Cazin, *Inorganics*, 2019, **7**.
35. A. J. Reay and I. J. Fairlamb, *Chem. Commun.*, 2015, **51**, 16289-16307.
36. A. J. Reay, L. K. Neumann and I. J. S. Fairlamb, *Synlett*, 2016, **27**, 1211-1216.
37. Y. Li, X. M. Hong, D. M. Collard and M. A. El-Sayed, *Org. Lett.*, 2000, **2**, 2385-2388.
38. S. Klingelhofer, W. Heitz, A. Greiner, S. Oestreich, S. Forster and M. Antonietti, *J. Am. Chem. Soc.*, 1997, **119**, 10116-10120.
39. M. T. Reetz, R. Breinbauer and K. Wanninger, *Tetrahedron Lett.*, 1996, **37**, 4499-4502.
40. P. J. Ellis, I. J. Fairlamb, S. F. Hackett, K. Wilson and A. F. Lee, *Angew. Chem. Int. Ed. Engl.*, 2010, **49**, 1820-1824.
41. C. A. Smith, M. R. Narouz, P. A. Lummis, I. Singh, A. Nazemi, C. H. Li and C. M. Crudden, *Chem. Rev.*, 2019, **119**, 4986-5056.
42. A. Heuer-Jungemann, N. Feliu, I. Bakaimi, M. Hamaly, A. Alkilany, I. Chakraborty, A. Masood, M. F. Casula, A. Kostopoulou, E. Oh, K. Susumu, M. H. Stewart, I. L. Medintz, E. Stratakis, W. J. Parak and A. G. Kanaras, *Chem. Rev.*, 2019, **119**, 4819-4880.
43. E. C. Hurst, K. Wilson, I. J. S. Fairlamb and V. Chechik, *New J. Chem.*, 2009, **33**, 1837-1840.
44. J. Vignolle and T. D. Tilley, *Chem. Commun.*, 2009, 7230-7232.
45. M. Planellas, R. Pleixats and A. Shafir, *Adv. Synth. Catal.*, 2012, **354**, 651-662.
46. P. Tegeder, M. Marelli, M. Freitag, L. Polito, S. Lamping, R. Psaro, F. Glorius, B. J. Ravoo and C. Evangelisti, *Dalton Trans.*, 2018, **47**, 12647-12651.
47. A. Ruhling, K. Schaepe, L. Rakers, B. Vonhoren, P. Tegeder, B. J. Ravoo and F. Glorius, *Angew. Chem. Int. Ed. Engl.*, 2016, **55**, 5856-5860.
48. P. Tegeder, M. Freitag, K. M. Chepiga, S. Muratsugu, N. Moller, S. Lamping, M. Tada, F. Glorius and B. J. Ravoo, *Chemistry (Easton)*, 2018, **24**, 18682-18688.

49. A. Ferry, K. Schaepe, P. Tegeder, C. Richter, K. M. Chepiga, B. J. Ravoo and F. Glorius, *ACS Catal.*, 2015, **5**, 5414-5420.
50. Z. Zhou, M. Li, G. Liu, G. Xu and J. Xue, *Appl. Organomet. Chem.*, 2019, **33**.
51. N. W. J. Scott, M. J. Ford, C. Schotes, R. R. Parker, A. C. Whitwood and I. J. S. Fairlamb, *Chem. Sci.*, 2019, **10**, 7898-7906.
52. F. Fu, J. Xiang, H. Cheng, L. Cheng, H. Chong, S. Wang, P. Li, S. Wei, M. Zhu and Y. Li, *ACS Catal.*, 2017, **7**, 1860-1867.
53. C. J. Diehl, T. Scattolin, U. Englert and F. Schoenebeck, *Angew. Chem. Int. Ed. Engl.*, 2019, **58**, 211-215.
54. D. R. Coulson, *Chem. Commun.*, 1968, 1530-&.
55. B. W. Cue and J. Zhang, *Green Chem. Lett. Rev.*, 2009, **2**, 193-211.
56. E. J. Flahive, B. L. Ewanicki, N. W. Sach, S. A. O'Neill-Slawecki, N. S. Stankovic, S. Yu, S. M. Guinness and J. Dunn, *Org. Process Res. Dev.*, 2008, **12**, 637-645.
57. S. Phillips, D. Holdsworth, P. Kauppinen and C. Mac Namara, *Johnson Matthey Technol. Rev.*, 2016, **60**, 277-286.
58. P. Slavik, D. W. Kurka and D. K. Smith, *Chem. Sci.*, 2018, **9**, 8673-8681.
59. Y. Garcia, F. Schoenebeck, C. Y. Legault, C. A. Merlic and K. N. Houk, *J. Am. Chem. Soc.*, 2009, **131**, 6632-6639.
60. J. P. Norman and S. R. Neufeldt, *ACS Catal.*, 2022, **12**, 12014-12026.
61. I. J. Fairlamb, *Chem. Soc. Rev.*, 2007, **36**, 1036-1045.
62. J. Almond-Thynne, D. C. Blakemore, D. C. Pryde and A. C. Spivey, *Chem. Sci.*, 2017, **8**, 40-62.
63. J. P. Norman, N. G. Larson, E. D. Entz and S. R. Neufeldt, *J. Org. Chem.*, 2022, **87**, 7414-7421.
64. J. P. Norman, N. G. Larson and S. R. Neufeldt, *ACS Catal.*, 2022, **12**, 8822-8828.
65. N. W. J. Scott, M. J. Ford, N. Jeddi, A. Eyles, L. Simon, A. C. Whitwood, T. Tanner, C. E. Willans and I. J. S. Fairlamb, *J. Am. Chem. Soc.*, 2021, **143**, 9682-9693.
66. J. M. Fowler, E. Britton, C. M. Pask, C. E. Willans and M. J. Hardie, *Dalton Trans.*, 2019, **48**, 14687-14695.
67. R. H. Crabtree, *Chem. Rev.*, 2015, **115**, 127-150.

Chapter 2

Synthesis of Palladium *N*-Heterocyclic Carbene Complexes

NHC ligands are typically formed through the deprotonation of an imidazolium salt to form a free carbene which can then ligate to a metal centre. Modification of the steric and electronic properties of imidazolium salts, and therefore subsequent NHCs, can be achieved in several ways, including altering the ring size and ring saturation, extending the ring system, and introducing different heteroatoms or backbiting side chains.[1] However, the simplest and most common ways to change the sterics and electronics are to alter the imidazolium salt's *N*-substituents and backbone substituents, respectively (Figure 2.1). To probe the effects of NHC ligands on the unusual product selectivity for the Suzuki-Miyaura cross-coupling (SMCC) of 2,4-dibromopyridine and arylboronic acid, a library of NHC ligands with different steric and electronic properties were investigated.

Figure 2.1 – Generic NHC showing the variability in N-substituent (red), backbone substituents (blue), ring size (pink) and degree of saturation (green).

2.1 NHC Electronics

The electronics of an NHC are typically quantified using the Tolman electronic parameter (TEP), discussed in more detail in the introduction (Chapter 1.2.1). Many factors have been shown to affect the TEP of NHC ligands bound to a metal centre. For example, increasing the steric bulk of the *N*-substituent for NHCs with the same base heterocycle typically indirectly decreases their TEP values.[2, 3] A low TEP value corresponds to a more electron donating NHC ligand.

Five-membered unsaturated heterocyclic rings (imidazole-based) were chosen as the basic ring architecture of the NHC ligands investigated. An increase in ring size would decrease the angle between the NHC *N*-substituent and the metal carbene bond, increasing the proximity of the *N*-substituent and the metal centre (Figure 2.2). Including NHC ligands with different ring sizes would have caused alterations to both the steric and electronic parameters of the ligand which may have been difficult to quantify. Similarly, the use of saturated ring architectures would remove the planarity of the NHC ligand to different degrees depending on the *N*-substituent,

causing different effects on the proximal steric bulk with respect to the metal centre and overall ligand binding strength.[1]

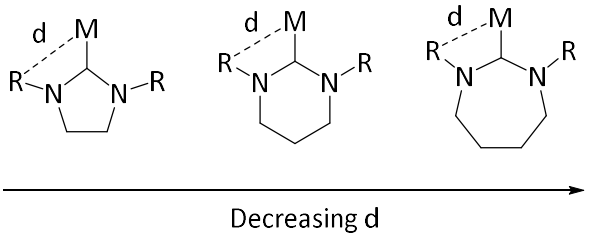

Figure 2.2 – Illustration showing how increasing the NHC ring size decreases the proximity of the N-substituent and the metal centre (d).

Typically, the simplest way to vary the TEP value significantly for an NHC of fixed heterocycle architecture is to vary the backbone substituents, a strategy that was applied in this work. A set of backbone substituents chosen to vary the electron donating characteristics of the NHC ligand were incorporated into the NHC precursors to examine the electronic effects of the NHC on catalyst selectivity. Compared with unsubstituted imidazole, 4,5-chloroimidazole and benzimidazole were chosen as less electron donating architectures and 4,5-methylimidazole as a more electron donating architecture, based on experimentally and computationally calculated TEP values (Figure 2.3).[2]

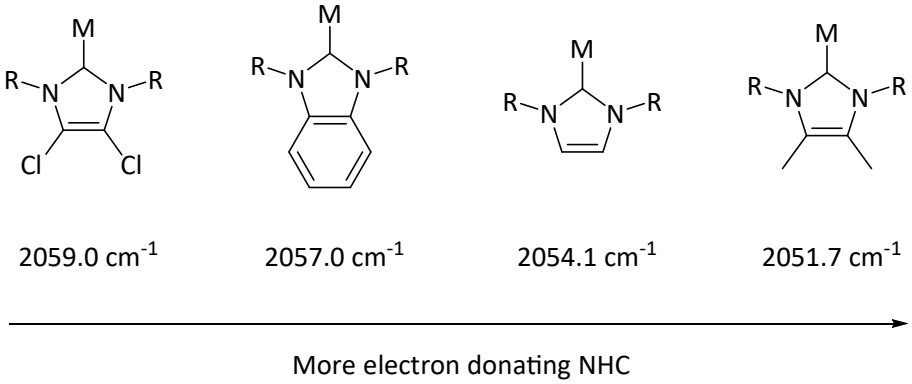

Figure 2.3 – Structures of metal-bound NHC ligands featuring 4,5-dichloroimidazole, benzimidazole, imidazole and 4,5-dimethylimidazole ring architectures to show the relationship between structure and TEP value (units: cm^{-1}). TEP values shown are for CO stretching frequency (ν_{CO}) in Ni-NHC-$(CO)_3$ (R = Me).[2]

NMR spectroscopy of NHC ligand precursors highlights the change in electronics of the ligand precursors which feature the same *N*-substituent and counterion but different backbone architectures, specifically when examining the proton signal at the 2-position of the ring (Figure 2.4). The shift in this proton signal denotes the degree of shielding this proton experiences. The imidazolium with the most electron-donating architecture by TEP value, 4,5-dimethylimidazolium, shows the greatest degree of proton shielding and, conversely, the benzimidazolium and 4,5-dichloroimidazolium show the least proton shielding. The proton shifts

of the 4,5-chloroimidazolium and benzimidazolium are reversed from what would be expected when considering the TEP data. The reason for this is unknown, however possible explanations include the change in *N*-substituent from methyl (literature data) to 2-phenylethyl (NMR data) or the metal-ligand interactions in the literature data.[2] Nevertheless, the ligand architectures were ordered in terms of NHC electron donation with respect to the NMR spectroscopic data collected for this investigation, such that 4,5-dimethylimidazolium was the most electron donating heterocycle and benzimidazolium the least.

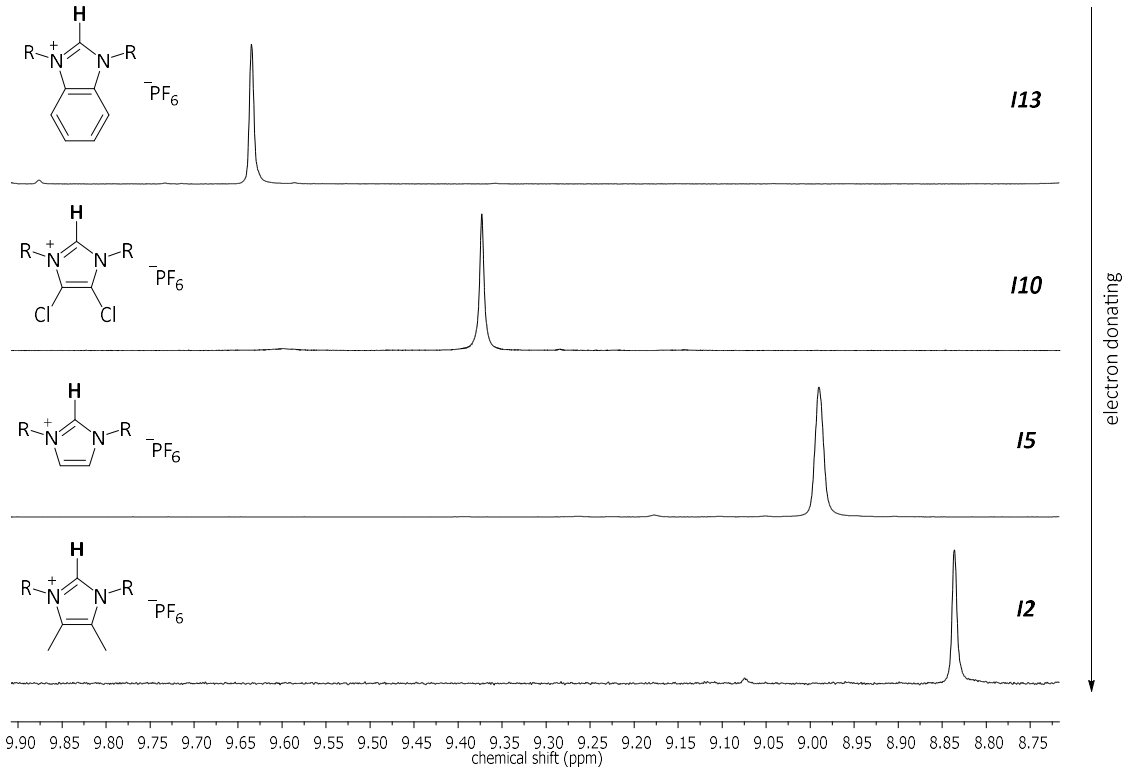

*Figure 2.4 – Stacked ^{1}H NMR spectrum (DMSO-d6, 400 MHz) showing the chemical shifts for the C2 (NC**H**N) proton in **I2**, **I5**, **I10** and **I13**. (R = 2-phenylethyl).*

2.2 NHC Sterics

The steric effects of NHC ligands are typically varied through alterations to the NHC *N*-substituents. Subtle changes to the *N*-substituent can have significant changes to the overall ligand properties.[4-6] The NHC ligand *N*-substituents were chosen with consideration of the ligand sterics of the Pd-NHC complex originally shown to exhibit abnormal selectivity in the SMCC reaction investigated here (***NHC1*** and ***NHC2***, Figure 2.5). Despite the *N*-substituents of ***NHC1*** and ***NHC2*** being unsymmetrical, all the ligand architectures used in this study were symmetrical as introducing asymmetry would have complicated the variations in steric parameters.

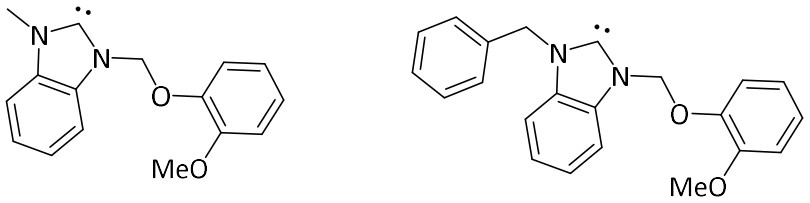

NHC1 ***NHC2***

Figure 2.5 – Structure of the mononuclear Pd-NHC ligands used in the initial work conducted by Willans and co-workers, ***NHC1*** *and* ***NHC2****.*[7]

A set of *N*-substituents were chosen to implement into the NHC ligand design that would display a range of NHC steric bulk, from very bulky to non-bulky, and with variations in side chain flexibility. The 2-phenylethyl *N*-substituent was chosen to closely resemble the (2-methoxyphenoxy)methyl *N*-substituent of ***NHC1*** and ***NHC2*** (Figure 2.6). The flexibility of the 2-phenylethyl and (2-methoxyphenoxy)methyl *N*-substituents are similar due to the same chain length between the nitrogen atom and the major site of steric bulk for both. As a result, introducing 2-phenylethyl *N*-substituents onto a benzimidazole architecture would represent a close analogue of the original ligand, assuming the main meaningful difference would be the asymmetry in ***NHC1*** and ***NHC2***. Benzyl *N*-substituents were chosen to reduce the flexibility and increase proximal steric bulk compared with the 2-phenylethyl *N*-substituents. On the other hand, *n*-propyl *N*-substituents were used to reduce the overall steric bulk of the ligand. Finally, diisopropylphenyl (Dipp) and mesityl (Mes) *N*-substituents were chosen to investigate large NHC ligand steric bulk. Both Dipp and Mes *N*-substituent NHCs are used extensively in catalysis.[6, 8-10]

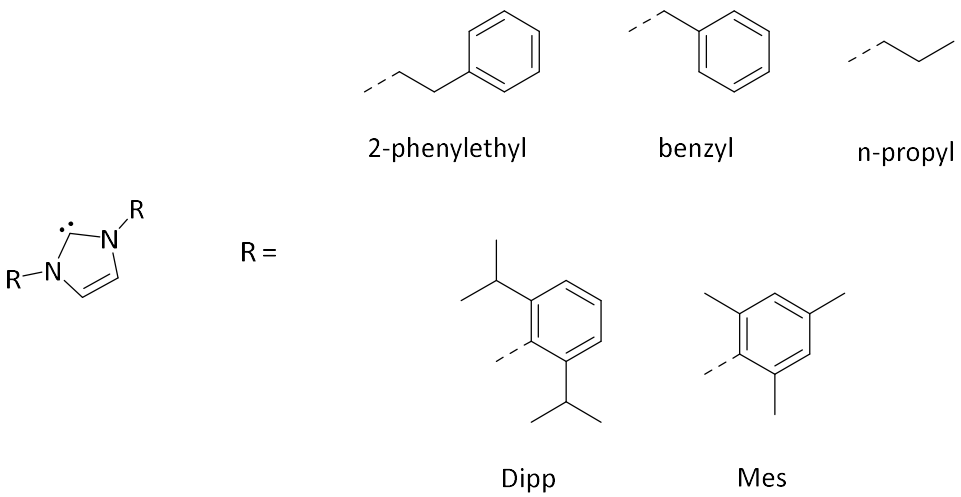

Figure 2.6 – Structure of the NHC N-substituents used in this investigation of abnormal SMCC site-selectivity. Dipp = diisopropylphenyl and Mes = mesityl.

Variation of both the *N*-substituent and the ring architecture resulted in a library of 14 NHC ligand precursors from which the corresponding palladium-NHC complexes were synthesised (Figure 2.7). This NHC library accounted for a range of steric and electronic parameters which were used to identify trends when considering catalytic data for the palladium-NHC complexes. Due to limited synthetic scope, electronic variation of the ligands featuring Dipp and Mes *N*-substituents were not performed and as such these ligands were only available for comparison against the imidazole-based NHC ligands.

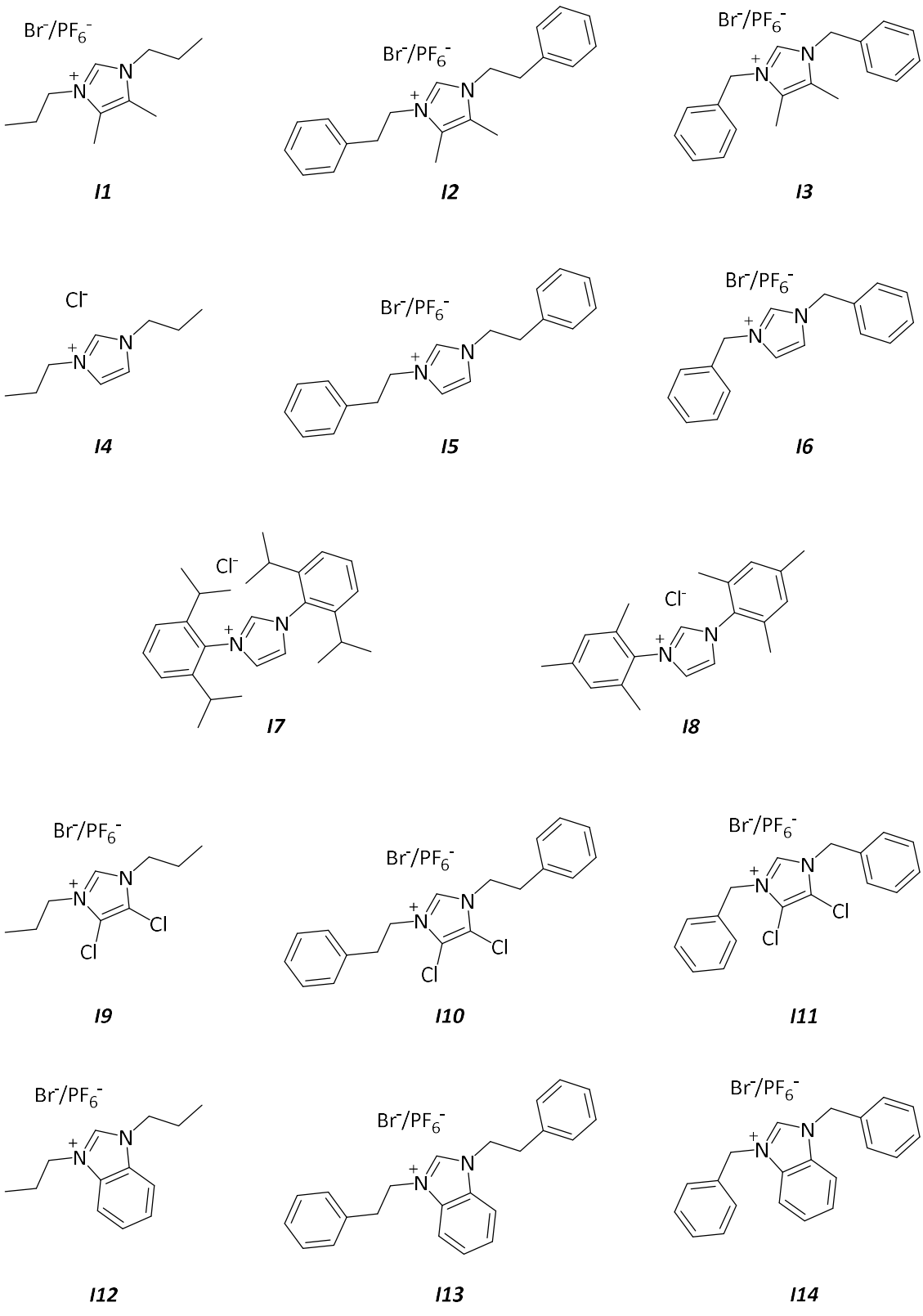

*Figure 2.7 – NHC ligand precursor library showing the structures of **I1–I14.***

2.3 NHC Ligand Precursor Synthesis

The synthesis of the NHC precursor imidazolium salts ***I1–14*** (Figure 2.7) was achieved through one of two routes: the first method, adapted from Nolan and co-workers, involved reaction of the amine derivative of the desired imidazolium *N*-substituent with glyoxal in the presence of an acid catalyst to initially form an *N*-functionalised diimine (Step 1, Scheme 2.1).[11] A ring closing reaction was then performed under acidic conditions, using hydrochloric acid, to form the desired imidazolium as the chloride salt (Step 2, Scheme 2.1).[12] This route is widely applied to synthesise unsaturated imidazolium salts,[13-16] and was employed in the synthesis of ligand precursors ***I4, I7*** *and* ***I8***.[17]

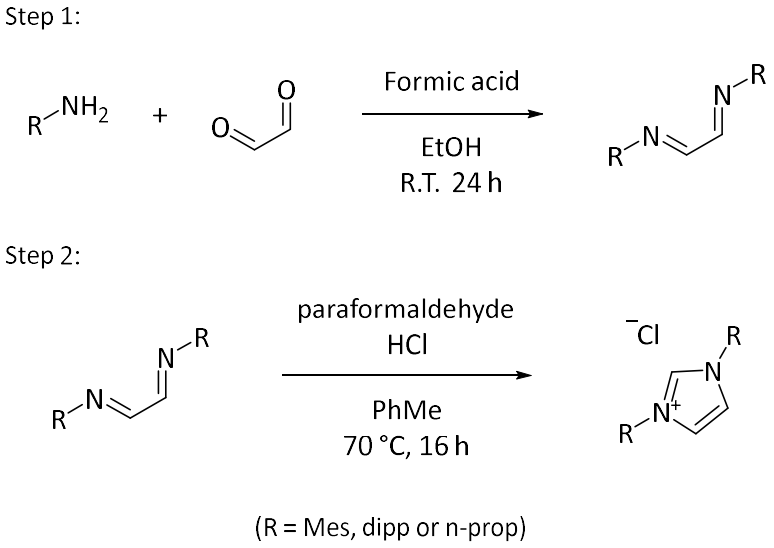

*Scheme 2.1 – General reaction pathway for the formation of imidazolium salts (**I4, I7** and **I8**). Formation of the N-functionalised diimine followed by ring closing.[11, 12]*

The remaining ligand precursors were all synthesised by an alternative route, through the direct functionalisation of either 4,5-dimethylimidazole (***I1–I3***), imidazole (***I5*** and ***I6***), 4,5-dichloroimidazole (***I9–I11***) or benzimidazole (***I10–I14***) *via* nucleophilic attack by the corresponding bromoalkyl species (Scheme 2.2).[18] The imidazolium salt was formed as a bromide salt when utilising this methodology. To prevent mono-substitution of the ligand precursors, the bromoalkyl species was used in large excess (4–5 eq.).

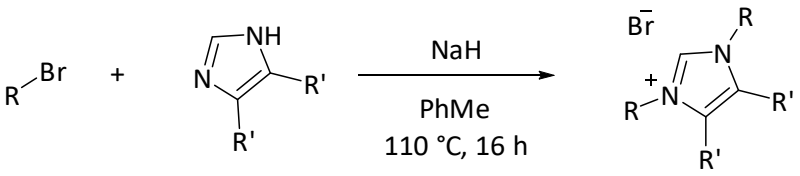

R = n-propyl, benzyl or phenylethyl
R' = Me, H, Cl or (benzimidazole)

Scheme 2.2 – General reaction scheme for the direct functionalisation of the nitrogen atoms on imidazole using bromoalkyl under basic conditions.[18]

All NHC ligand precursors ***I1–14*** were characterised using ^{1}H and ^{13}C NMR spectroscopy and high-resolution mass spectrometry (HRMS). The characterisation data was compared to literature data, where possible.[10, 19-25] ***I1–I3***, ***I9*** and ***I10*** were found to be novel imidazolium salts.

The characteristic C2 proton signal (NC***H***N) in the ^{1}H NMR spectra for ***I1–I14*** was identified; in each case, a chemical shift between 8.5 and 12.0 ppm was observed. Figure 2.8 shows an example ^{1}H NMR spectrum. The C2 signal (N***C***N) for ***I1–I14*** in the ^{13}C NMR spectra typically had a chemical shift between 135 and 145 ppm.

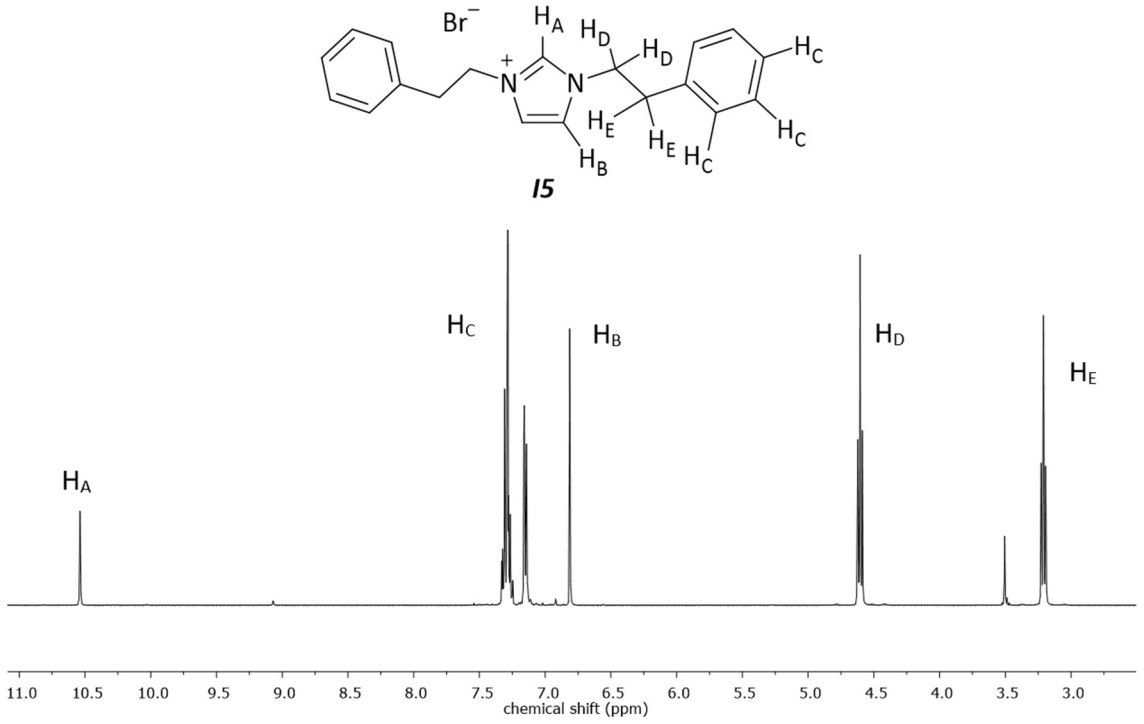

*Figure 2.8 – ^{1}H NMR spectrum (chloroform-d, 500 MHz) of **I5**, illustrating the characteristic C2 proton (H_A, 10.5 ppm) and backbone protons (H_B, 6.97 ppm) of imidazolium salts (H_C, 7.1-7.3 ppm, H_D, 4.6 ppm and H_E, 3.2 ppm).*

HRMS was used to identify the imidazolium cations for ***I1***–***I14*** which were compared to the calculated values. Any incomplete reaction products or other impurities could also be identified. Figure 2.9 shows an example mass spectrum for ***I5***.

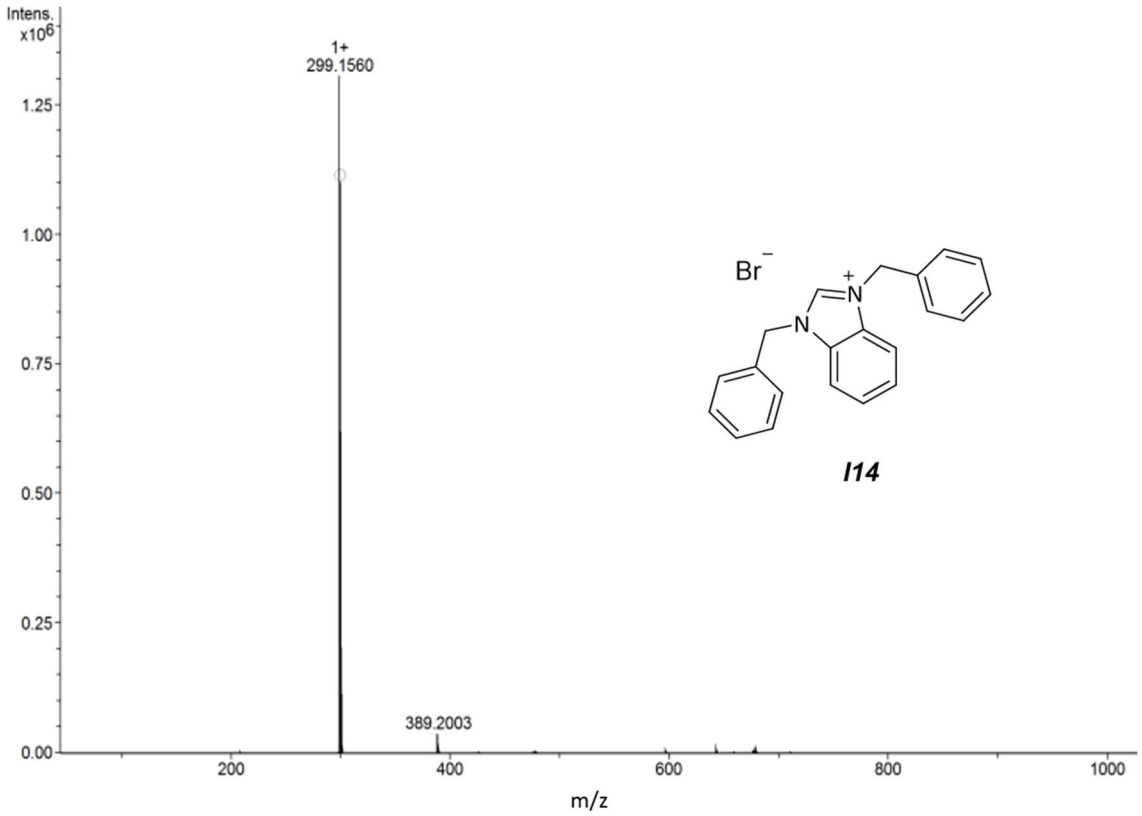

*Figure 2.9 – HRMS (ESI+) of imidazolium salt **I14** (X = Br) to illustrate successful synthesis of the ligand (calculated value for m/z = 299.1543 $[M\text{-}Br]^+$). The small peak at 389.2003 is 2-benzyl-**I14**.*

2.4 Synthesis of Palladium-NHC Complexes

Pd-NHC complexes ***C1***–***C14*** (Figure 2.10) were synthesised using the method outlined by Organ and co-workers.[10] Deprotonation of the imidazolium salt (***I1***–***I14***) by potassium carbonate in neat 3-chloropydidine generated the free NHC species. The free NHC and 3-chloropyridine then coordinated to palladium chloride, generating the corresponding Pd-NHC complex (Scheme 2.3). The activity of PEPPSI catalysts is dependent on the 'throw away' pyridine ligand architecture as it alters activation of the catalyst and changes the rate of association/dissociation to palladium in solution.[26] 3-Chloropyridine is typically used as the optimal pyridine ligand to use in catalysis.[27]

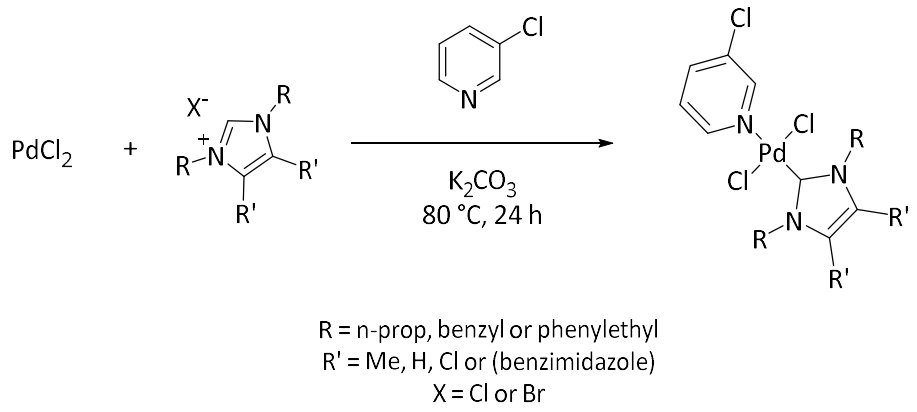

Scheme 2.3 – General reaction scheme for the synthesis of the Pd-NHC complexes to be used in this study. 3-chloropyridine acted as both solvent and reactant.

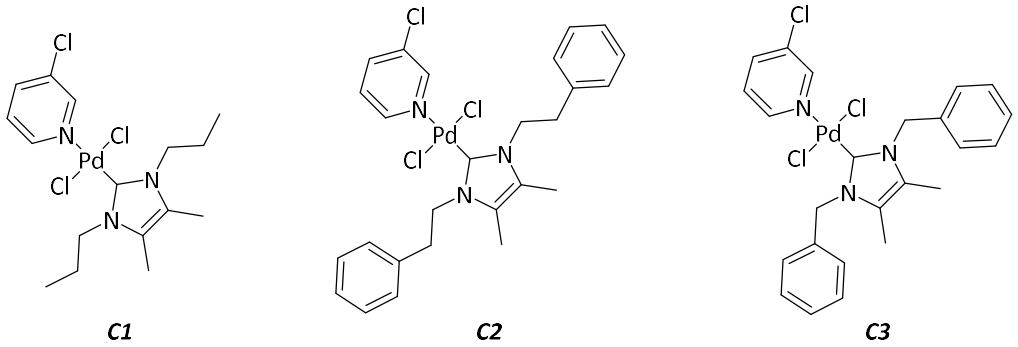

C1 ***C2*** ***C3***

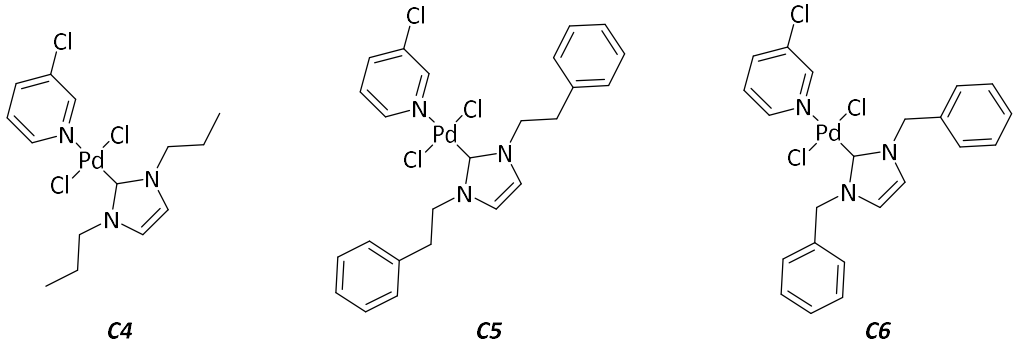

C4 ***C5*** ***C6***

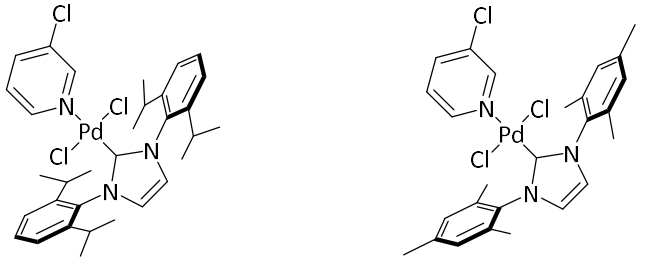

C7 ***C8***

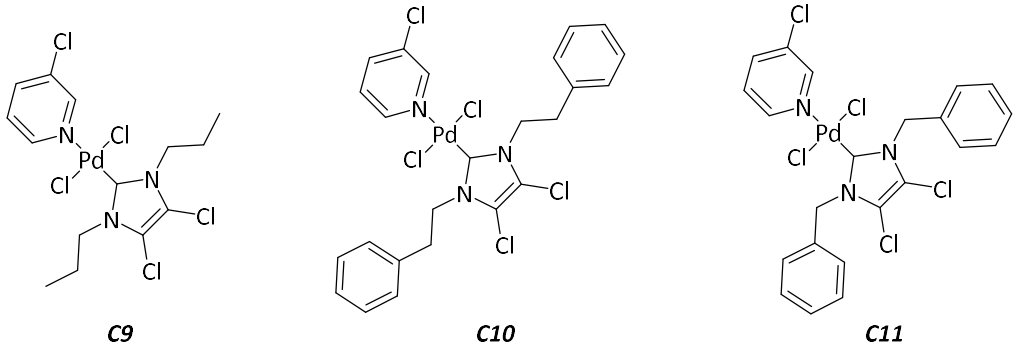

C9 ***C10*** ***C11***

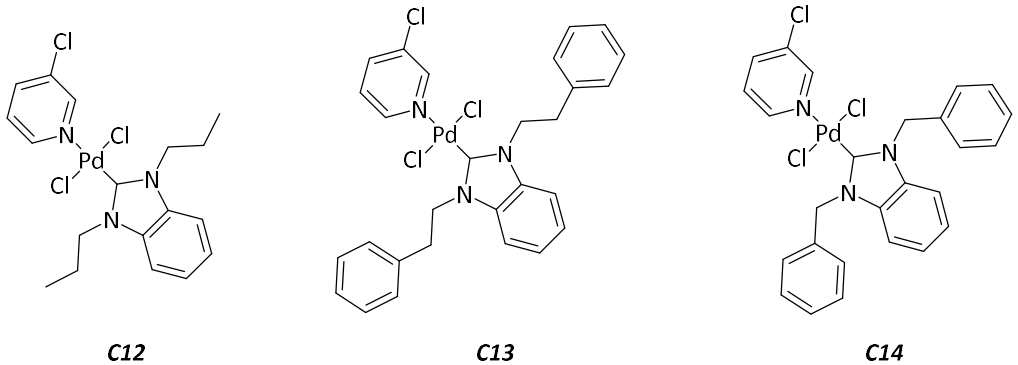

C12 ***C13*** ***C14***

*Figure 2.10 – Chemical structures of the Pd-NHC complexes (**C1**–**C14**) generated using the methods described by Organ and co-workers.* [10]

This method was used initially to synthesise ***C4***–***C8***. The imidazolium salts with chloride counterions formed the corresponding complexes as expected. However, when using the NHC precursors with a bromide counterion (***I5*** and ***I6***), it was noticed that there was possible mixing of the halide ligands on the complex. All signals in the ^{1}H NMR spectra for ***C5*** and ***C6*** were in triplicate, consistent with the three possible complexes formed with mixed halides, as shown in Figure 2.11. Direct comparison of ^{1}H NMR spectroscopic data of ***C5*** and ***C6*** to literature values of these complexes featuring either bromide or chloride ligands is not possible as they are novel, however, the small 0.5 ppm shift in ligand environment signals observed is consistent with analogous complexes when a change in halide ligand has occurred.[28, 29] In addition, crystallographic data collected for ***C6***, synthesised using an imidazolium featuring a bromide counterion, agrees with the mixed halide hypothesis. Modelling the halide positions as a near 1:1 mixture of chlorides and bromides gave best agreement with the experimentally collected crystallographic data. It has been shown that altering the palladium bound halide can affect the catalytic activity of the complexes and as such the halide needed to be fixed for valid comparisons. [28]

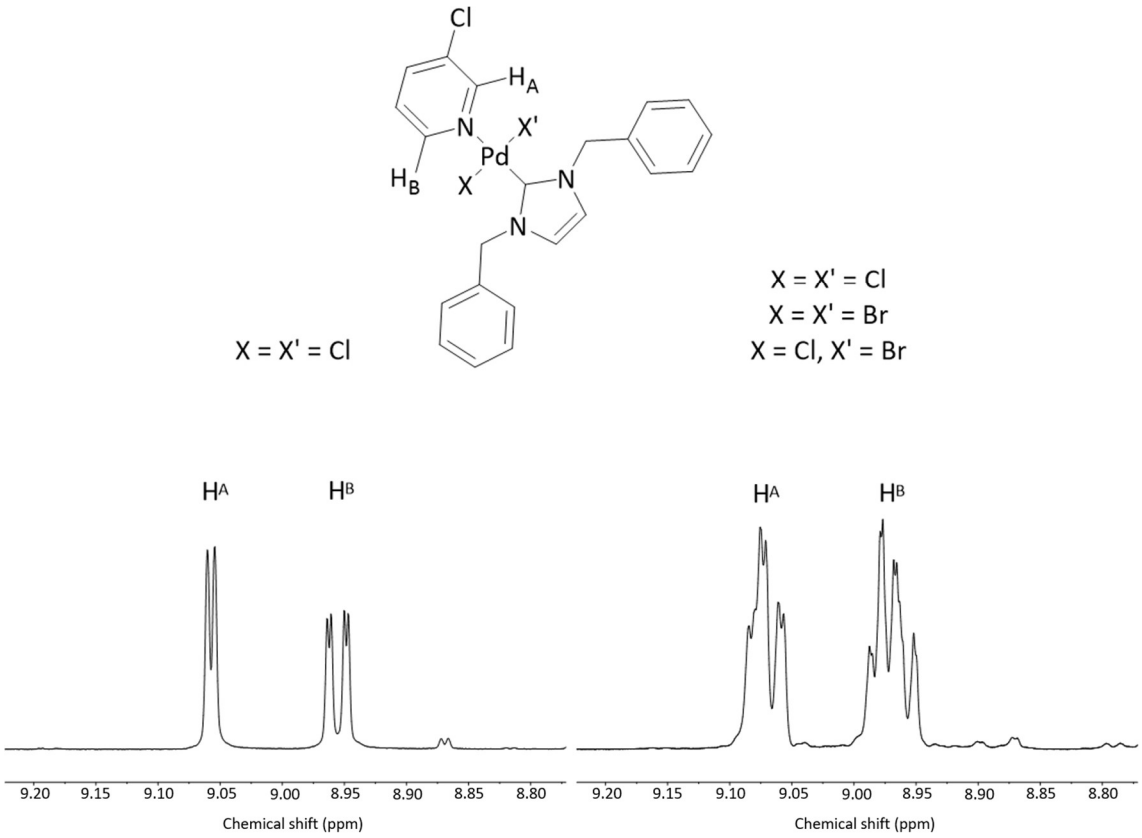

*Figure 2.11 – ^{1}H NMR spectrum (chloroform-d, 500 MHz) of the Pd-NHC complex **C6**, showing the pyridine protons occupying three different environments, suggesting the presence of mixed halides.*

In order to minimise the halide mixing, a reaction was conducted with a potassium chloride additive to saturate the reaction mixture with chloride ions with the aim of forming the chloride

complex exclusively. However, this did not work, and triplicate signals were once again observed in the ^{1}H NMR spectroscopic analysis. In literature, complexes of the PEPPSI architecture have been successfully synthesised using imidazolium salts with non-coordinating counterions.[30, 31] This approach to the synthesis would remove the possibility of forming mixed halide complexes and the halide ligands on the resulting complex would originate from the palladium source, in this case palladium chloride. A counterion exchange was therefore performed on the two NHC ligand precursors (***I5*** and ***I6***) to replace the bromide ion with a non-coordinating hexafluorophosphate counterion (Scheme 2.4). Successful counterion switches were characterised by the shift of signals in ^{1}H and ^{13}C NMR spectroscopy and purity determined with HRMS. The use of these hexafluorophosphate salts in the complexation reaction resulted in the synthesis of the expected product and as such this strategy was applied to the synthesis of all the remaining complexes (Scheme 2.5). Reasonable yields were observed for most complexes synthesised from both the ligand precursors featuring a hexafluorophosphate counterion (48 % – 81 %) and a chloride counterion (41% – 53%), falling withing the range of yields for synthesis of similar complexes reported in literature. [10, 27, 30-32] Lower yields of 17% and 29% were observed for ***C2*** and ***C11*** respectively, the cause of which is unknown but may be due to side reactions taking place during the synthesis.

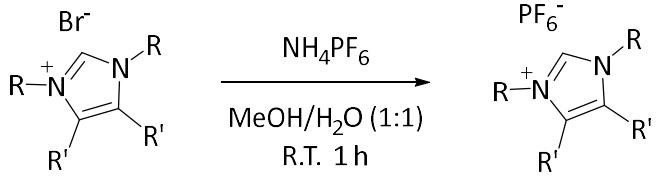

R = n-propyl, benzyl or phenylethyl
R' = Me, H, Cl or (benzimidazole)

Scheme 2.4 – General reaction scheme for the conversion of imidazolium counterion from bromide to hexafluorophosphate for complexing to Pd, preventing the formation of a mixed halide complex.

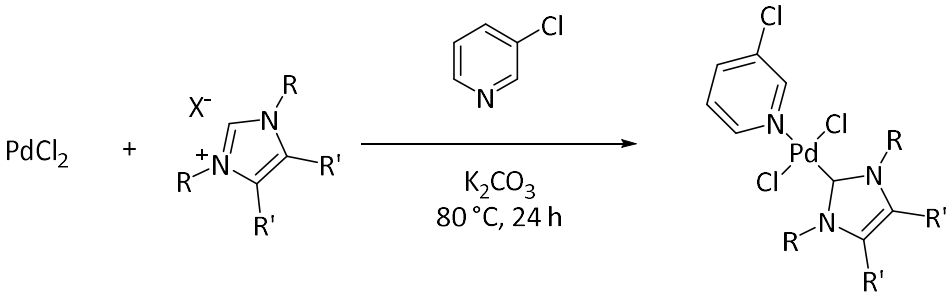

R = n-propyl, benzyl or phenylethyl
R' = Me, H, Cl or (benzimidazole)
X = Cl or PF_6

Scheme 2.5 – General reaction scheme for the synthesis of the Pd-NHC complexes to be used in this study using PF_6^- salts instead of bromide salts. 3-Chloropyridine acted as both solvent and reactant.

The successful synthesis of the palladium-NHC complexes (***C1***–***C14***) was verified by ^{1}H and ^{13}C NMR spectroscopy, mass spectrometry and, in some cases, single-crystal X-ray diffractometry (SC-XRD). The successful formation and complexation of the NHC ligand was characterised by the loss of the imidazolium salt C2 proton signal (H_A) and a shift in the backbone protons (H_B) in the ^{1}H NMR spectrum of the corresponding complex (Figure 2.12). Coordination of 3-chloropyridine can also be seen with four characteristic peaks in the ^{1}H NMR spectrum (H_F, H_G, H_H, H_I, Figure 2.12). The analytical data for ***C7***, ***C8*** and ***C14*** was found to be consistent with literature data.[10, 32] The remaining complexes, ***C1***–***C6*** and ***C9***–***C13*** are novel.

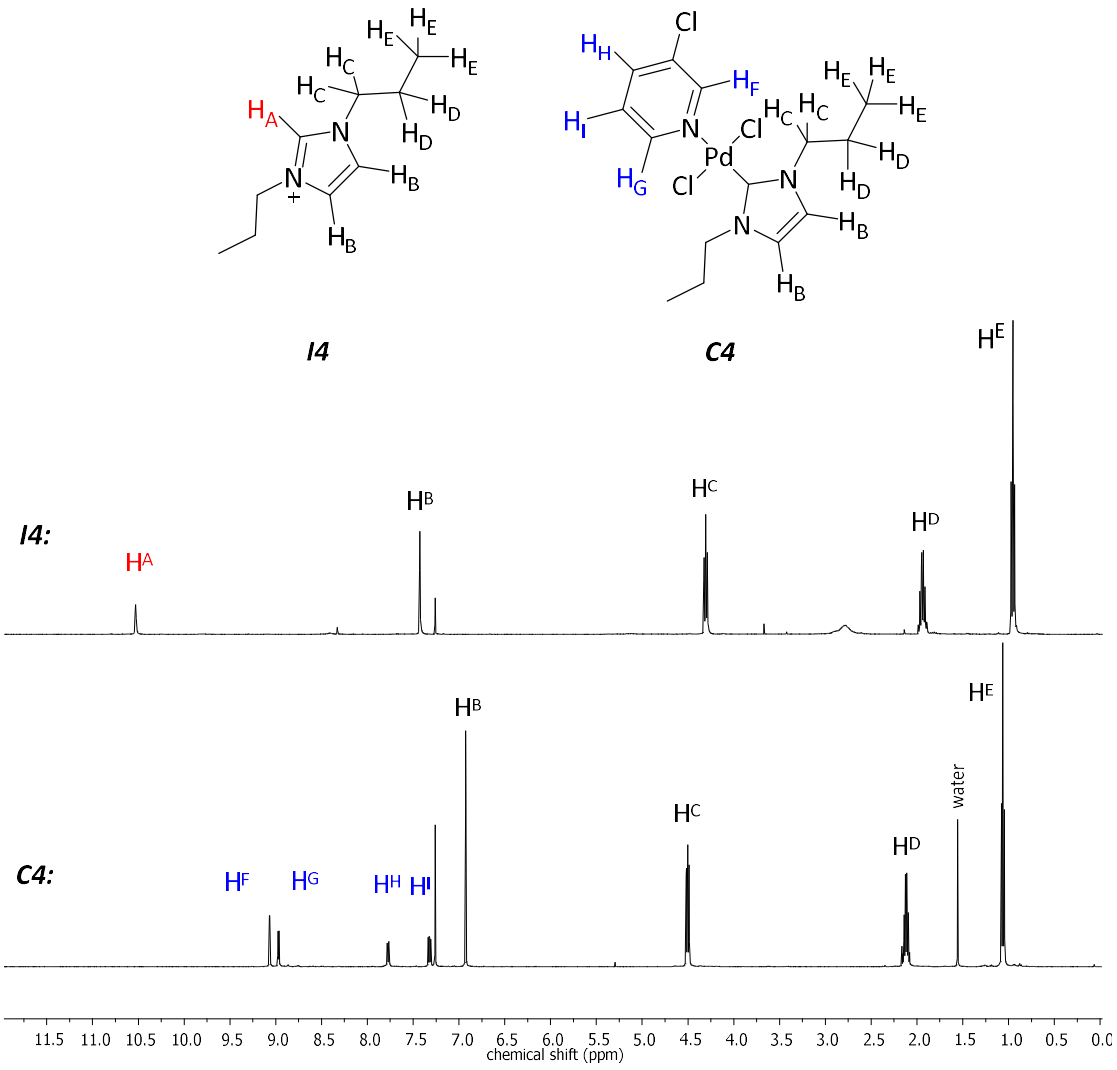

*Figure 2.12 – Stacked ^{1}H NMR spectra (chloroform-d, 500 MHz) of **I4** (top) and **C4** (bottom) showing the disappearance of the C2 proton (H_A, red), shift of the backbone protons (H_B) and the appearance of the coordinated 3-chloropyridine signals (H_F-H_I, blue).*

HRMS analysis of the palladium-NHC complexes (***C1***–***C14***) highlighted a large degree of fragmentation (Figure 2.13). The abundance of peaks was not due to product impurity as HRMS analysis on single-crystal samples of the complexes revealed very similar fragmentation patterns to the bulk solid following isolation. Unfortunately, the structures relating to many of these

fragmentation signals could not be identified. Signals corresponding to identifiable fragments were checked against calculated values for that structure. The isotope patterns for the identified fragment were also compared to simulated isotope patterns, an example with ***C7*** can be seen in Figure 2.14.

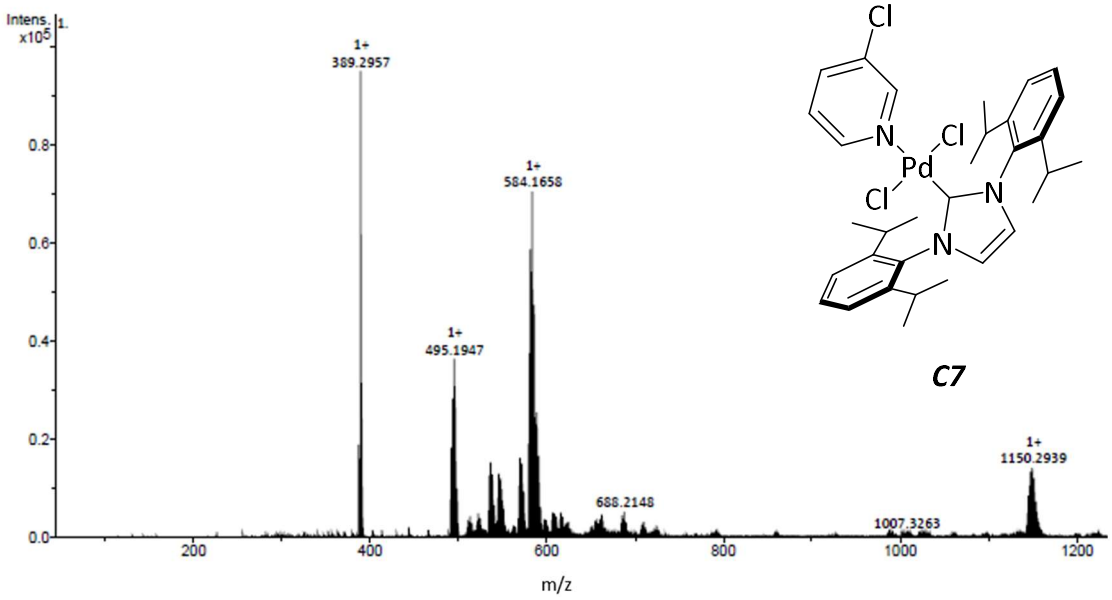

*Figure 2.13 – HRMS (ESI+) for crystalline **C7** as an example of the large degree of fragmentation for the Pd-NHC complexes.*

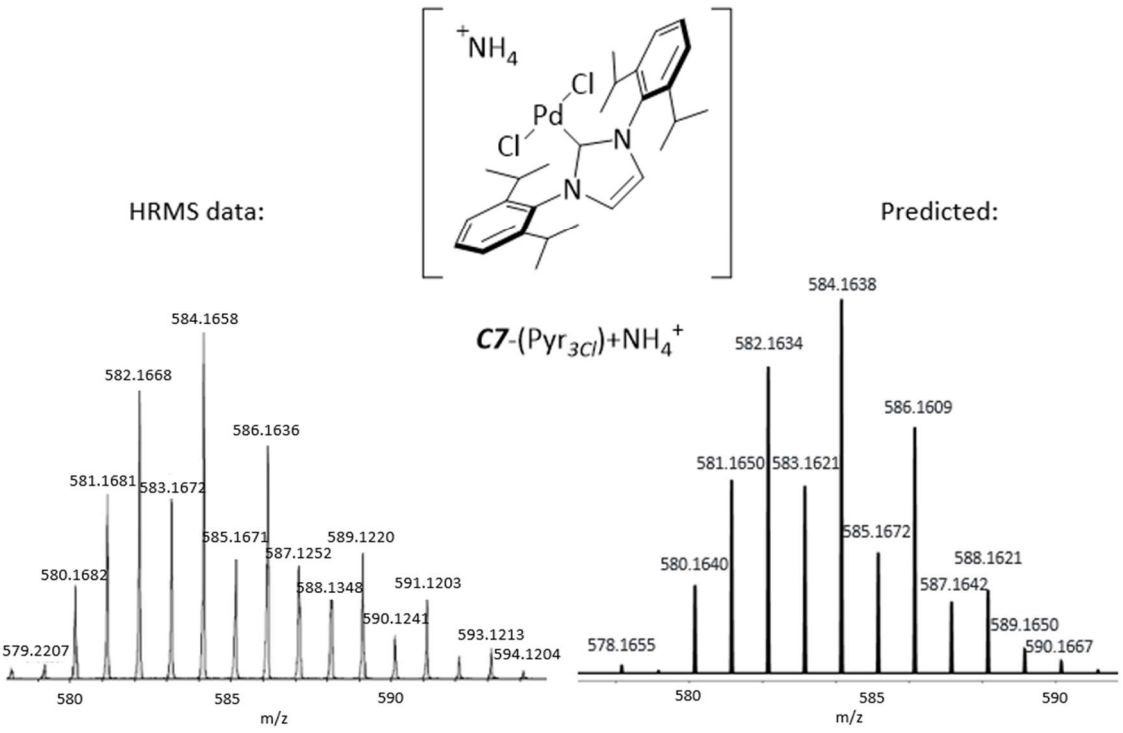

Figure 2.14 *– The zoomed HRMS (ESI+) spectrum for **C7** to show the signal associated with the mass-fragment [**C7**-(Pyr$_{3Cl}$)+NH$_4^+$] 584.1658 AMU (calc = 584.1638 AMU) (left) and the simulated isotope pattern (right).*

Where possible, single-crystals of the palladium-NHC complexes were grown through slow vapour diffusion (hexane into DCM). SC-XRD was then used to collect empirical structural data for ***C2***, ***C4***–***C8***, ***C11*** and ***C13***. Figure 2.15 shows the structure of ***C11*** determined by SC-XRD. The complexes were found to adopt a square planar geometry. The Pd-NHC bond distances were found to be between 1.945 Å and 1.968 Å and the Pd-(3-chloropyridine) bond distances between 2.081 Å and 2.118 Å (Table 2.1), both within the expected range for palladium binding.[26, 33-35] The symmetry planes associated with the NHC-heterocycle, 3-chloropyridine and the square planar palladium were all twisted with respect to each other, presumably due to steric hinderance.

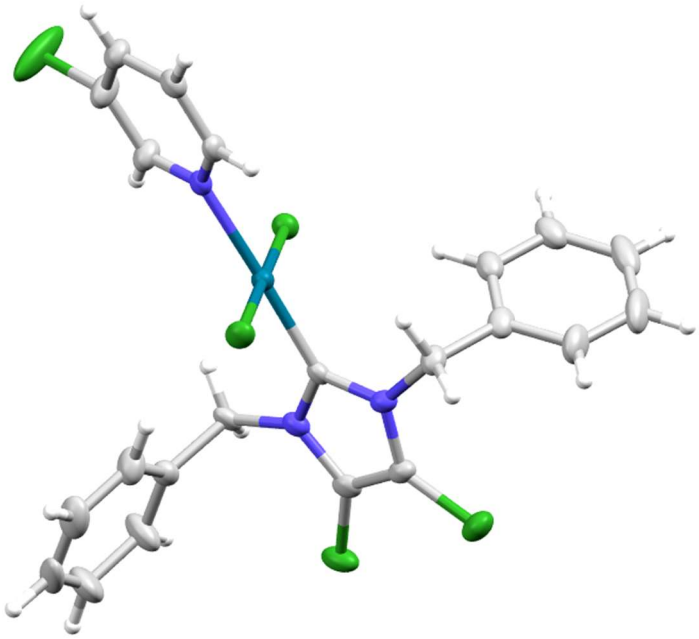

*Figure 2.15 – Structure of **C11** as determined by SC-XRD. Thermal ellipsoids are at 50% probability level.*

*Table 2.1 – Showing the Pd-C (NHC) and Pd-N (Pyr) bond distances for **C2**, **C4**–**C8**, **C11** and **C13**, determined by SC-XRD.*

Pd-NHC complex	Pd–C distance / Å	Pd–N distance / Å
C2	1.962 (8)	2.121 (5)
C4	1.961 (8)	2.116 (6)
C5	1.946 (7)	2.113 (5)
C6	1.945 (8)	2.093 (5)
C7	1.962 (10)	2.081 (6)
C8	1.968 (8)	2.118 (6)
C11	1.966 (7)	2.086 (5)
C13	1.964 (9)	2.114 (6)

2.5 Summary

14 imidazolium salts and Pd-NHC complexes were prepared and fully characterised using ^{1}H and ^{13}C NMR spectroscopy, mass spectrometry and, in some cases, SC-XRD. Imidazolium salts ***I1***–***I3***, ***I9*** and ***I10,*** and Pd-NHC complexes ***C1***–***6*** and ***C9***–***C13*** are novel. Mixed halide Pd-NHC complexes were observed when using imidazolium bromide salts as $PdCl_2$ was used as the palladium source. Hence imidazolium hexafluorophosphate salts were generated and successfully used as precursors to Pd-NHC complexes containing only chloride ligands.

2.6 References

1. D. Bourissou, O. Guerret, F. P. Gabbai and G. Bertrand, *Chem. Rev.*, 2000, **100**, 39-92.
2. D. G. Gusev, *Organometallics*, 2009, **28**, 6458-6461.
3. S. Leuthausser, D. Schwarz and H. Plenio, *Chemistry (Easton)*, 2007, **13**, 7195-7203.
4. W. A. Herrmann, *Angew. Chem. Int. Ed. Engl.*, 2002, **41**, 1290-1309.
5. G. Altenhoff, R. Goddard, C. W. Lehmann and F. Glorius, *J. Am. Chem. Soc.*, 2004, **126**, 15195-15201.
6. M. N. Hopkinson, C. Richter, M. Schedler and F. Glorius, *Nature*, 2014, **510**, 485-496.
7. J. M. Fowler, E. Britton, C. M. Pask, C. E. Willans and M. J. Hardie, *Dalton Trans.*, 2019, **48**, 14687-14695.
8. S. Díez-González and S. P. Nolan, in *N-Heterocyclic Carbenes in Transition Metal Catalysis*, Springer, 2006, pp. 47-82.
9. C. J. O'Brien, E. A. Kantchev, C. Valente, N. Hadei, G. A. Chass, A. Lough, A. C. Hopkinson and M. G. Organ, *Chemistry (Easton)*, 2006, **12**, 4743-4748.
10. M. G. Organ, G. A. Chass, D. C. Fang, A. C. Hopkinson and C. Valente, *Synthesis-Stuttgart*, 2008, 2776-2797.
11. G. A. Grasa, M. S. Viciu, J. Huang and S. P. Nolan, *J. Org. Chem.*, 2001, **66**, 7729-7737.
12. X. Bantreil and S. P. Nolan, *Nat. Protoc.*, 2011, **6**, 69-77.
13. L. Benhamou, E. Chardon, G. Lavigne, S. Bellemin-Laponnaz and V. Cesar, *Chem. Rev.*, 2011, **111**, 2705-2733.
14. C. J. Serpell, J. Cookson, A. L. Thompson, C. M. Brown and P. D. Beer, *Dalton Trans.*, 2013, **42**, 1385-1393.
15. T. Schaub and U. Radius, *Chemistry (Easton)*, 2005, **11**, 5024-5030.
16. *N-Heterocyclic Carbenes*, The Royal Society of Chemistry, 2016.
17. S. Burling, B. M. Paine, D. Nama, V. S. Brown, M. F. Mahon, T. J. Prior, P. S. Pregosin, M. K. Whittlesey and J. M. Williams, *J. Am. Chem. Soc.*, 2007, **129**, 1987-1995.
18. C. Hirtenlehner, C. Krims, J. Holbling, M. List, M. Zabel, M. Fleck, R. J. Berger, W. Schoefberger and U. Monkowius, *Dalton Trans.*, 2011, **40**, 9899-9910.
19. İ. Özdemir, S. Demir, Y. Gök, E. Çetinkaya and B. Çetinkaya, *J. Mol. Catal. A: Chem.*, 2004, **222**, 97-102.
20. T. Schaub, M. Backes and U. Radius, *Organometallics*, 2006, **25**, 4196-4206.
21. A. Bittermann, P. Harter, E. Herdtweck, S. D. Hoffmann and W. A. Herrmann, *J. Organomet. Chem.*, 2008, **693**, 2079-2090.
22. V. Amendola, G. Bergamaschi, M. Boiocchi, L. Fabbrizzi and N. Fusco, *Dalton Trans.*, 2011, **40**, 8367-8376.

23. M. C. Cassani, M. A. Brucka, C. Femoni, M. Mancinelli, A. Mazzanti, R. Mazzoni and G. Solinas, *New J. Chem.*, 2014, **38**, 1768-1779.
24. O. V. Khazipov, M. A. Shevchenko, A. Y. Chernenko, A. V. Astakhov, D. V. Pasyukov, D. B. Eremin, Y. V. Zubavichus, V. N. Khrustalev, V. M. Chernyshev and V. P. Ananikov, *Organometallics*, 2018, **37**, 1483-1492.
25. A. Titi, S. M. Almutairi, A. F. Alrefaei, S. Manoharadas, B. A. Alqurashy, P. K. Sahu, B. Hammouti, R. Touzani, M. Messali and I. Ali, *J. Mol. Liq.*, 2020, **315**.
26. J. Nasielski, N. Hadei, G. Achonduh, E. A. Kantchev, C. J. O'Brien, A. Lough and M. G. Organ, *Chemistry (Easton)*, 2010, **16**, 10844-10853.
27. G. C. Fortman and S. P. Nolan, *Chem. Soc. Rev.*, 2011, **40**, 5151-5169.
28. A. V. Astakhov, O. V. Khazipov, A. Y. Chernenko, D. V. Pasyukov, A. S. Kashin, E. G. Gordeev, V. N. Khrustalev, V. M. Chernyshev and V. P. Ananikov, *Organometallics*, 2017, **36**, 1981-1992.
29. Y. Shi, Z. Cai, Y. Peng, Z. Shi and G. Pang, *Journal of Chemical Research*, 2011, **35**, 161-162.
30. Y. Ye, Z. Liu, Y. Wang, Y. Zhang, F. Yin, Q. He, J. Peng, K. Tan and Y. Shen, *Tetrahedron Lett.*, 2022, **107**.
31. M. A. Topchiy, M. A. Zotova, S. M. Masoud, A. K. Mailyan, I. V. Ananyev, S. E. Nefedov, A. F. Asachenko and S. N. Osipov, *Chemistry (Easton)*, 2017, **23**, 6663-6674.
32. S. Akkoç and Y. Gök, *Inorg. Chim. Acta*, 2015, **429**, 34-38.
33. A. Zeiler, M. Rudolph, F. Rominger and A. S. Hashmi, *Chemistry (Easton)*, 2015, **21**, 11065-11071.
34. M. Osińska, A. Gniewek and A. M. Trzeciak, *J. Mol. Catal. A: Chem.*, 2016, **418-419**, 9-18.
35. F. W. Han, Y. Xu, R. J. Zhu, G. Y. Liu, C. Chen and J. H. Wang, *New J. Chem.*, 2018, **42**, 7422-7427.

Chapter 3

Catalytic Protocol and Conditions Refinement for Pd-NHC Complexes

With the library of Pd-NHC complexes synthesised (Chapter 2.4) a reliable and robust catalytic protocol had to be determined in order to effectively evaluate the catalytic activity and selectivity in the Suzuki-Miyaura cross-coupling (SMCC) reaction of interest. The conditions in which to perform the catalytic investigation reactions also needed to be addressed prior to further investigations. The work by Fairlamb and Willans give a strong foundation from which the most ideal catalytic protocol and conditions could be determined. [1, 2]

3.1 Catalytic Protocol Development

3.1.1 Isolation and Characterisation of Catalytic Products

Fairlamb and co-workers showed that the abnormal selectivity in the cross-coupling of 2,4-dibromopyrine and arylboronic acid using the palladium acetate / triphenylphosphine catalyst system could be achieved with multiple different functionalised arylboronic acid coupling partners. As such *p*-fluorophenylboronic acid was chosen as the coupling partner for this investigation (Scheme 3.1); the inclusion of fluorine in the product molecules allowed for the catalysis product yields to be calculated using ^{19}F NMR spectroscopy. ^{1}H NMR spectroscopy could also be used, however the signals associated with each of the products would be much clearer with ^{19}F NMR and influenced less by any unexpected impurities.

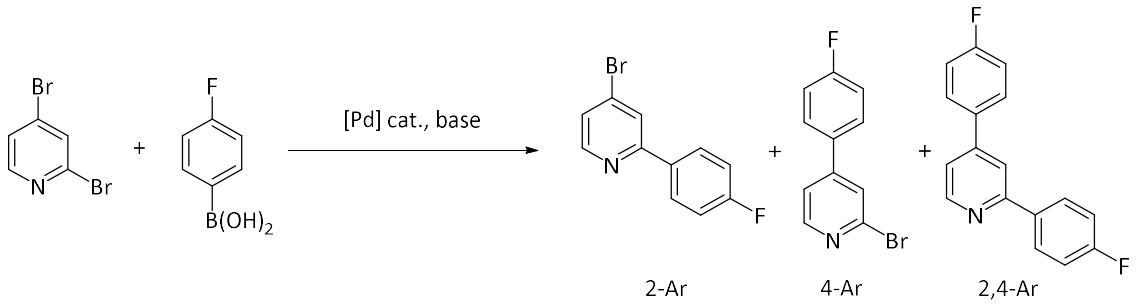

Scheme 3.1 – General reaction of palladium catalysed SMCC of 2,4-dibromopyridine and p-fluorophenylboronic acid to yield 2-bromo-4-(p-fluorophenyl)pyridine (4-Ar), 2-(p-fluorophenyl)-4-bromo-pyridine (2-Ar) and 2,4-bis(p-fluorophenyl)pyridine (2,4-Ar).

The three products, 2-(*p*-fluorophenyl)-4-bromopyridine (2-Ar), 2-bromo-4-(*p*-fluorophenyl)pyridine (4-Ar) and 2,4-bis(*p*-fluorophenyl)pyridine (2,4-Ar), were first isolated using column chromatography and fully characterised with ^{1}H, ^{13}C and ^{19}F NMR spectroscopy

and mass spectrometry. This allowed for the ^{19}F NMR signals for each product to be determined accurately for later use in determining product yields. The ^{19}F NMR chemical shifts were found to be -111.29 and -111.87 ppm for 4-Ar and 2-Ar respectively and 2,4-Ar showed two signals of -112.46 and -112.84 ppm (Figure 3.1). The corresponding ^{1}H NMR spectroscopic data was consistent with the literature values for each product.[2]

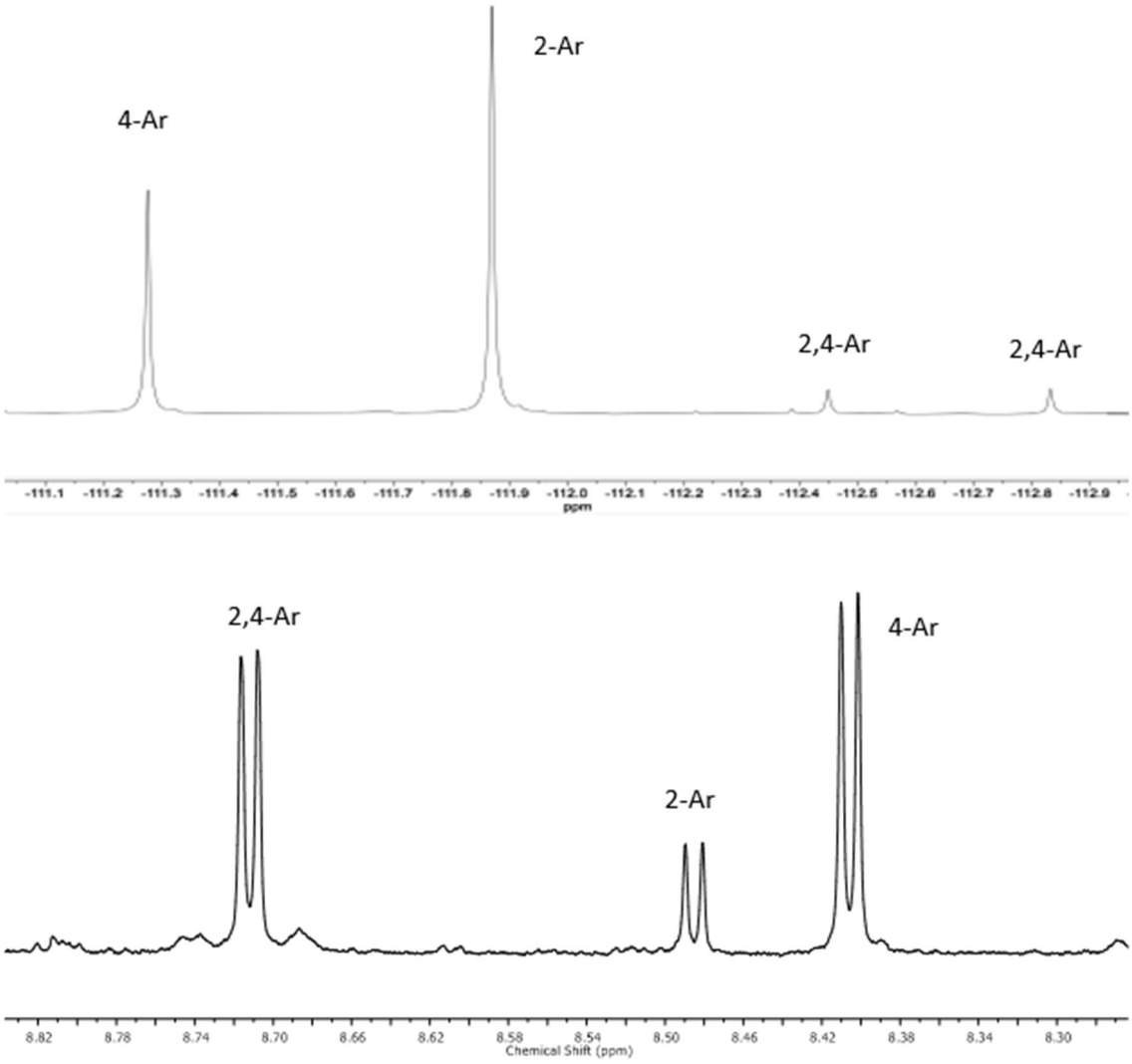

Figure 3.1 – top - ^{19}F NMR spectrum (chloroform-d, 500 MHz) of catalysis products, 2,Ar, 4-Ar and 2,4-Ar (internal reference of 1-fluoro-3,5-dimethoxy benzene at -111.0 ppm – not shown on spectrum). bottom - ^{1}H NMR spectrum (chloroform-d, 500 MHz) of catalysis products 2,Ar, 4-Ar and 2,4-Ar showing protons on the 6-position of each pyridine.

Spin-lattice relaxation times (T_1) were determined for the individual ^{19}F NMR signals for each product such that a suitable quantitative ^{19}F NMR experiment could be generated. The T_1 relaxation time of ^{19}F atoms can vary depending on the environment occupied in the molecule. All fluorine nuclei in the sample need to fully relax between pulses so all environments are accurately accounted for. The standard acquisition time in quantitative NMR spectroscopy is five times the longest T_1 relaxation time in the sample, thus ensuring all (>99.9%) appropriate

environments are fully relaxed between scans and signal intensities are determined accurately.[3] The ^{19}F T_1 relaxation times for each product were determined and a quantitative NMR experiment was generated for analysis of the product yields and ratios going forward.

3.1.2 Choice of Internal Standard

An internal standard was used to calculate product yields from ^{1}H and ^{19}F NMR spectroscopic data. An internal standard must be inert in the reaction to prevent side reactions skewing results, and fully soluble so accurate yield calculations can be performed. Trimethoxy benzene (TMB) is a common inert internal NMR standard and was used by Willans and co-workers in their investigations.[2] Replacement of a methoxy group on TMB with fluorine, giving 1-fluoro-3,5-dimethoxybenzene (FDMB, Figure 3.2), retains the desirable inertness and provides a reference signal in ^{19}F NMR spectroscopy allowing for product yield calculations by signal integration comparison. FDMB is a liquid at room temperature and therefore solubility was not an issue.

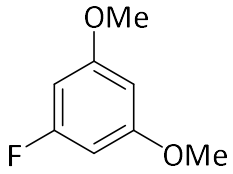

Figure 3.2 – Structure of 1-fluoro-3,5-dimethoxybenzene (FDMB) uses as the internal standard for catalytic yield determination.

To test the accuracy of the quantitative NMR spectroscopy experiment, NMR samples of a known amount of both the internal standard (FDMB) and the catalytic products (2-Ar, 4-Ar and 2,4-Ar) were prepared and analysed. The results from these tests showed very good agreement of the actual catalytic product quantity with respect to the internal standard in both ^{1}H and ^{19}F NMR spectroscopy.

3.1.3 Choice of Reaction Vessel

Palladium catalysed SMCC reactions are widely accepted to be air sensitive. The choice of reaction vessel must therefore be able to maintain an inert atmosphere over prolonged periods of time and allow for multiple samples to be taken and give reproducible product yield data at any given timepoint. Two suitable reaction vessels were considered; a Young's ampoule equipped with a Suba seal, and a smaller volume reaction vial with a silicone septum and argon inlet needle (Figure 3.3). Several factors were considered when making this choice, in particularly the ability for the reaction vessel to maintain an inert atmosphere for the duration of the catalytic reaction (24 h). Other factors include ease of sampling, maintaining constant heating and good mixing and ability to perform multiple catalytic reactions simultaneously.

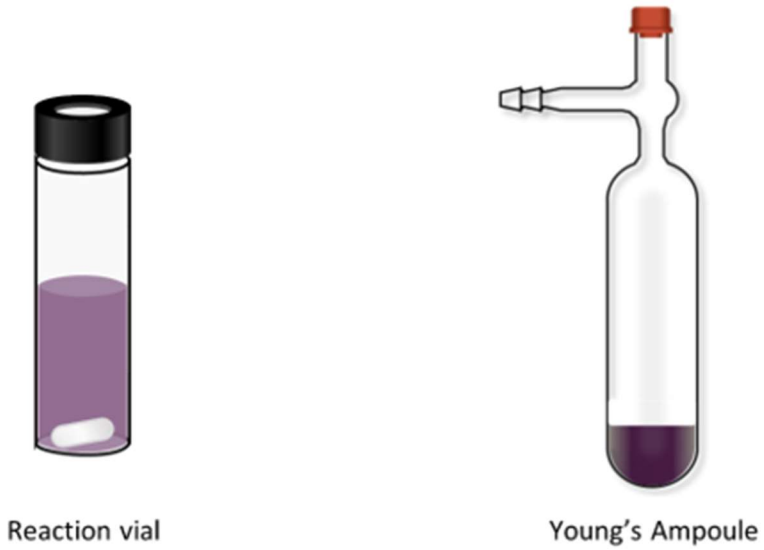

Figure 3.3 – Illustration of the vial and the ampoule for use in the catalytic studies. An inert atmosphere was provided by an Ar inlet needle for the vial, and an Ar line attached to the side inlet for the ampoule.

The viability of the two reaction vessels was assessed by performing a catalytic reaction (outlined in Scheme 3.1) using tetrakis triphenylphosphine palladium(0) as the catalyst and stock solutions of base and reagents to minimise variability. The ability of the vial to maintain an inert atmosphere was determined by the product yield comparisons of the vial to the ampoule, the latter being specifically designed to maintain an inert atmosphere. Multiple samples were taken over time and there was no significant variation in product yields between the vessels. This confirms that the reaction vial maintained the inert atmosphere throughout the reaction.

For good comparison of data between multiple catalytic runs and minimisation of error, reaction conditions must be kept constant, *i.e*. heating must be maintained throughout the course of the reaction. This proved to be a problem for the ampoule, as sampling necessitates the removal of the ampoule from the heat source (in this case an oil bath) and partial inversion so a sample of the reaction mixture can be collected (*via* micro syringe). For the vial, however, samples can be collected with ease and removal of the reaction vessel from the heat source is not necessary. Several parallel reactions can be run simultaneously with vials, as an aluminium block with the capacity for 16 vials mounted on a stirrer hotplate is used as the heat source. Running more than two parallel reactions in ampoules with an oil bath as a heat source would be impractical and unsafe. Overall, with the confirmation that the vials can hold an inert atmosphere throughout the duration of the reaction and the multiple logistical advantages they have over ampoules, the catalytic reactions moving forward will be conducted with vials as the reaction vessel.

3.1.4 Catalytic Work-up

The same sample work up procedure used by Willans and co-workers was adopted for these investigations.[2] A 100 µL sample was taken from the reaction mixture and quenched by rapid dissolution in DCM (1 mL), this sample solution was then passed over a Celite® filter to remove any insoluble deposits then concentrated to dryness under reduced pressure to leave a residue. This residue was dissolved in the NMR solvent (deacidified deuterated chloroform). Aspects of this workup were investigated further to determine that this was the optimum workup procedure.

3.1.4.1 Choice of Filter Type

Filtration of catalytic samples over Celite® can remove any aggregated palladium, potentially formed during the reaction,[1] and unreacted arylboronic acid, though the latter is not well discussed in the literature. The removal of arylboronic acid from a sample is desirable to reduce the potential for continued reactivity following the workup procedure. Removal of the arylboronic acid, however, has implications for kinetic analysis, whereby accurate arylboronic acid concentrations in the reaction mixture cannot be calculated from the sample analysis.

To determine the extent of the arylboronic acid removal by the filtration step of the workup, a series of filters were tested and the boronic acid retention of the sample determined (Figure 3.4). The standard filter for the workup procedure consists of a cotton wool plug supporting a short depth (*ca.* 1 cm) of Celite® in a glass pipette (Short Celite®, Figure 3.4). As points of comparison, an unfiltered sample, a sample filtered through cotton wool and a Celite® filter with a greater depth (*ca.* 3 cm) of Celite® were tested. The results clearly show that the Celite® filters removed a significant amount of the arylboronic acid. A small amount of boronic acid was also removed by the cotton wool.

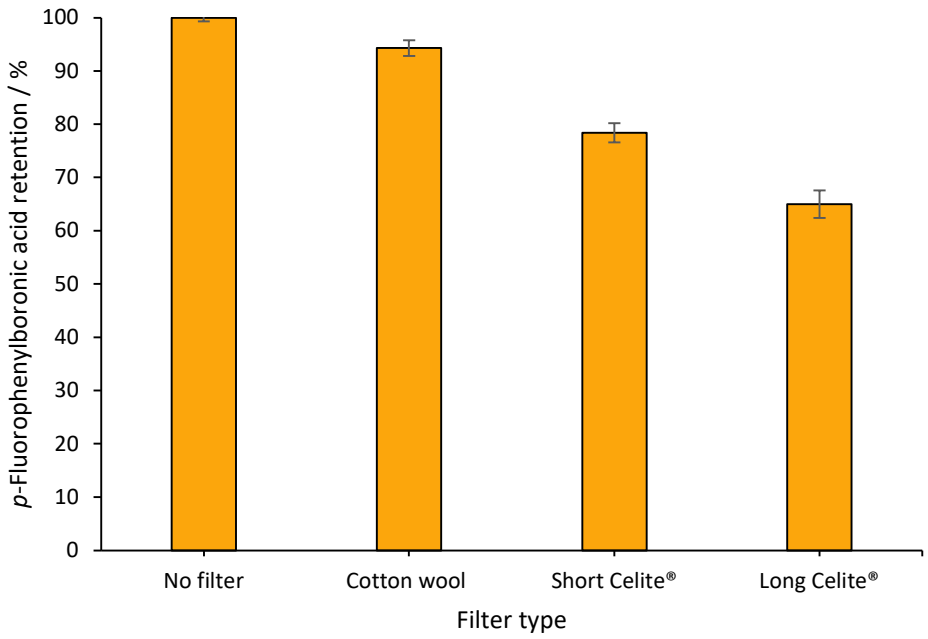

Figure 3.4 – Percentage retention of p-fluorophenylboronic acid in a mock reaction sample passed over different filters: no filter, cotton wool and Celite® (short and long). Retention calculated with respect to FDMB. Percentage retentions are an average of two experiments and error bars represent standard deviation.

3.1.4.2 Investigation of Reagent Sublimation

Again, with respect to gathering usable kinetic data over time, the retention of 2,4-dibromopyridine by the sample solution was investigated. It was found that 2,4-dibromopyridine slowly sublimes under standard atmospheric pressure and temperature. Any workup procedure for this reaction would involve removal of the sample solvent under reduced pressure, and hence the likely removal of the 2,4-dibromopyridine.

The 2,4-dibromopyridine retention was therefore tested with a range of rotary evaporator times to observe the extent of sublimation. First reduced pressure was applied until the sample was visually observed to be dry, then with continued reduced pressure for 2 and 30 mins (Figure 3.5). The results show that there were minimal losses (<3%) with the shorter rotary evaporation times (dryness and dryness + 2 mins at <100 mbar pressure) and greater losses at the extended reduced pressure datapoint (dryness + 30 mins at <100 mbar pressure), confirming that the 2,4-dibromopyridine does indeed sublime from the sample under the conditions used for the workup. As with the arylboronic acid, the sublimation of 2,4-dibromopyridne limits the kinetic analysis available for this reaction.

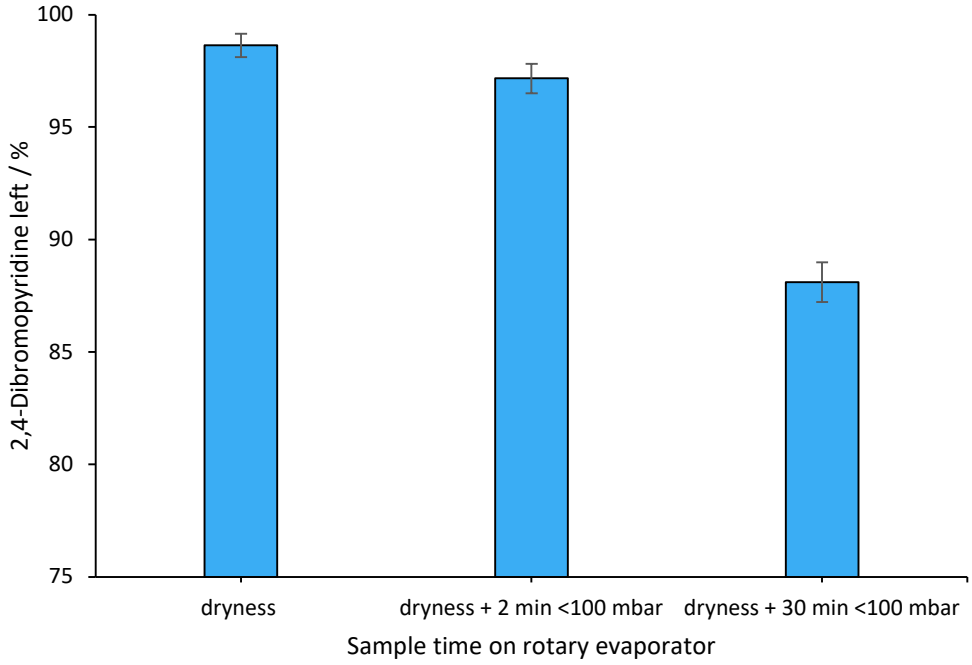

Figure 3.5 – Percentage retention of 2,4-dibromopyridine in a mock reaction sample dried under reduced pressure until dry and with 2 and 30 mins extra drying time. Retention calculated with respect to FDMB. Percentage retentions are an average of two experiments and error bars represent standard deviation.

The catalytic products (2-Ar, 4-Ar and 2,4-Ar) were subjected to the same treatment and were found not to be affected by the conditions used for the workup. Therefore, the product concentrations or yields calculated from the ^{1}H or ^{19}F NMR spectroscopic analysis of the samples are representative of that of the reaction mixture.

3.1.4.3 Assessment of Sample Stability

A stability test was conducted on the NMR samples to ensure that the signals associated with the catalytic products do not change in intensity over time. An increase in relative signal intensity would indicate continued reactivity of the sample following the workup, a decreased relative intensity would indicate product degradation. Over a 72-hour period the NMR sample was tested periodically and showed no change in product peak integrations. This allows for multiple samples to be prepared and queued for analysis, during time course reaction for example, without the risk of sample degradation before analysis.

3.1.5 Assessment of Protocol Robustness with a Benchmark Reaction

With the reaction vessel and means for reliable product analysis in hand, the catalytic protocol could now be tested against results reported in the literature to determine robustness. Replication of the results reported by Fairlamb, and co-workers was attempted (Scheme 3.2, Figure 3.6).[1] Fairlamb reports upon the ratios of palladium acetate and triphenylphosphine ($Pd(OAc)_2$:*n*PPh_3) used in the catalyst system and the resulting catalytic product yields. With

higher equivalents of triphenylphosphine (n = 3 – 4), there is selectivity for the 2-arylated (normal) product and low overall product yield. At lower equivalents of triphenylphosphine (n = 0.5 – 2.5), selectivity for the 4-arylated (abnormal) product is observed and typically a much greater overall product yield. These reactions were conducted in a 1:1 THF and water solvent mixture at 40 °C with tetrabutylammonium hydroxide (TBAH) as the base (Scheme 3.2).

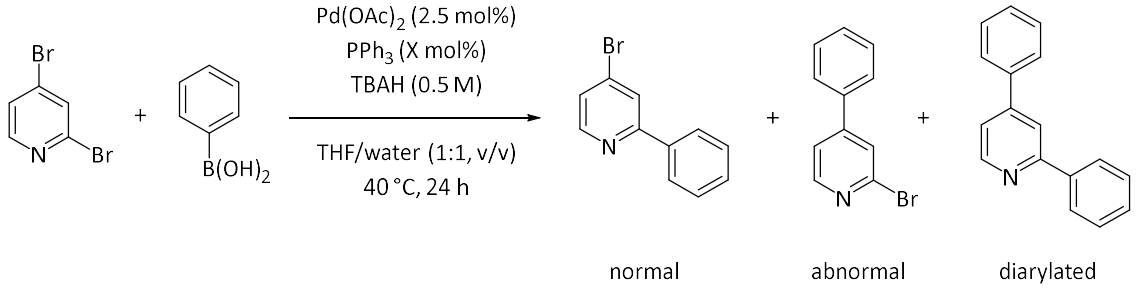

*Scheme 3.2 – Reaction between 2,4-dibromopyridine and phenylboronic acid using $Pd(OAc)_2$ at 2.5 mol% and PPh_3 at X mol% (where X = 0, 0.5, 1, 1.5, 2, 2.5, 3 and 4) as the catalyst system in a 1:1 THF:water solvent system at 40 °C. Tetrabutylammonium hydroxide (TBAH) was used as the base. *Recreated from literature.[1]*

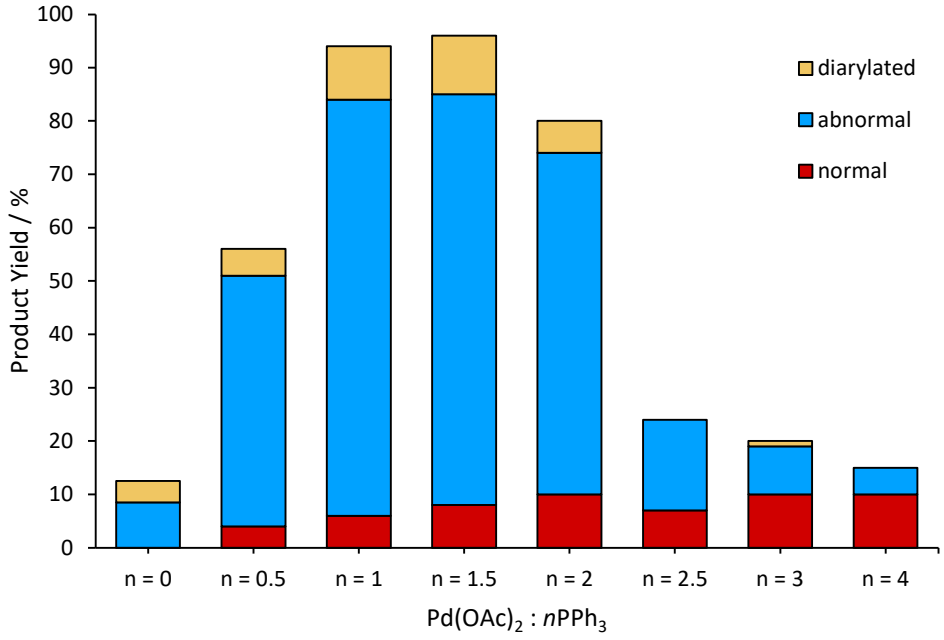

*Figure 3.6 – Reported results from the reaction of 2,4-dibromopyridine and phenylboronic acid using different $Pd(OAc)_2$:nPPh_3 ratios (where n = 0, 0.5, 1, 1.5, 2, 2.5, 3 and 4) giving different product selectivity with a change in n. *Recreated from literature. [1]*

The data points for 2 and 4 equivalents of triphenylphosphine to palladium acetate were chosen to replicate using the catalytic protocol developed in this work, as the significant difference in yield and switch in product selectivity between the $Pd(OAc)_2$:$n$$PPh_3$ ratios would be a strong indicator of procedure robustness. Fairlamb and co-workers report that fluorinated boronic acid coupling partners show a slightly lower product yield but similar product selectivity to

unfunctionalized phenylboronic acid.[1] Therefore, the data collected for the different $Pd(OAc)_2$:PPh_3 ratios with *p*-fluorophenylboronic acid was expected to show slight deviations from the compared data but still show the same switch in selectivity.

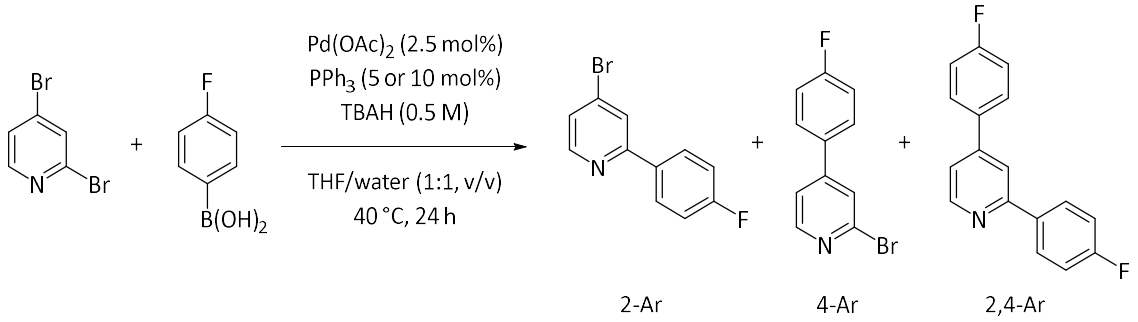

Scheme 3.3 – Benchmark reaction of 2,4-dibromopyridine and p-fluorophenylboronic acid using $Pd(OAc)_2$:nPPh_3 (where n = 2 and 4) as the catalyst system in a 1:1 THF:water solvent system at 40 °C. Tetrabutylammonium hydroxide (TBAH) was used as the base.

The data collected from this initial control reaction showed no product formation. Since the protocol, reaction sampling and sample work-up was rigorously tested, the source of this inactivity likely originated from a starting material impurity.

3.1.5.1 Purification of Catalysis Reagents

It has been reported in the literature that the performance of SMCC reactions can be strongly affected by the purity of the starting materials, in particular the phenylboronic acid.[4] To examine if the starting material purity was a cause for the apparent catalytic poisoning, all reagents were purified. The *p*-fluorophenylboronic acid was recrystallised from chloroform to give white needle-like crystals.[4] ^{1}H NMR spectroscopic analysis and single-crystal X-ray diffractometry of the recrystalised *p*-fluorophenylboronic acid indicated the sample was predominantly composed of tri(*p*-fluorophenyl)boroxine (Figure 3.7) with a small amount of *p*-fluorophenylboronic acid.

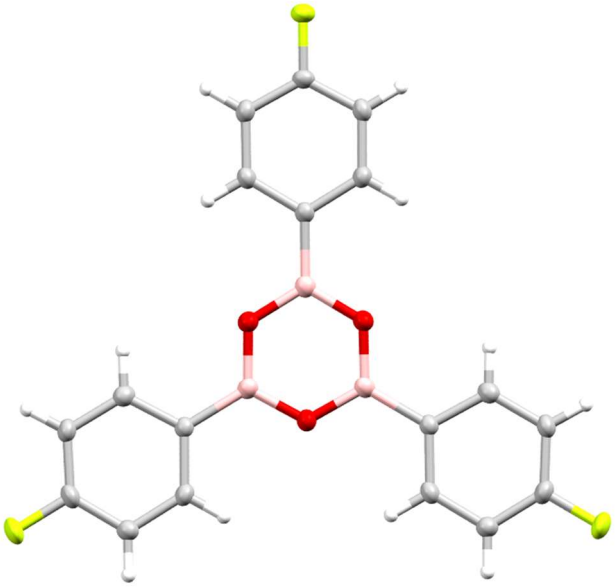

Figure 3.7 – Structure of tri(p-fluorophenyl)boroxine found from the recrystallisation of p-fluorophenylboronic acid in chloroform. Structure determined using single-crystal X-ray diffractometry (SC-XRD). Ellipsoids are at 50% probability level. Bond lengths and angles are consistent with previously reported structural data. [5]

This triarylboroxine species is formed through reversible dehydration of the corresponding boronic acid. When used in a SMCC reaction where water is present, the triarylboroxine species acts as a source of arylboronic acid through complete hydrolysis of the boroxine ring (Scheme 3.4).[6] It has been shown that even residual water from a boroxine sample and from an organic reaction solvent can facilitate the complete hydrolysis and form the corresponding boronic acid in solution.[7] The proportions of tri(*p*-fluorophenyl)boroxine and *p*-fluorophenylboronic acid in recrystalised batches of commercial *p*-fluorophenylboronic acid were calculated before usage through the use of ^{1}H NMR spectroscopy and found to be consistent between batches at a molar ratio of 4:1 respectively. Assuming complete hydrolysis of tri(*p*-fluorophenyl)boroxine under catalytic reactions, the actual equivalents of *p*-fluorophenylboronic acid in the catalytic reactions used in this study was 1.36 with respect to 2,4-dibromopyridine.

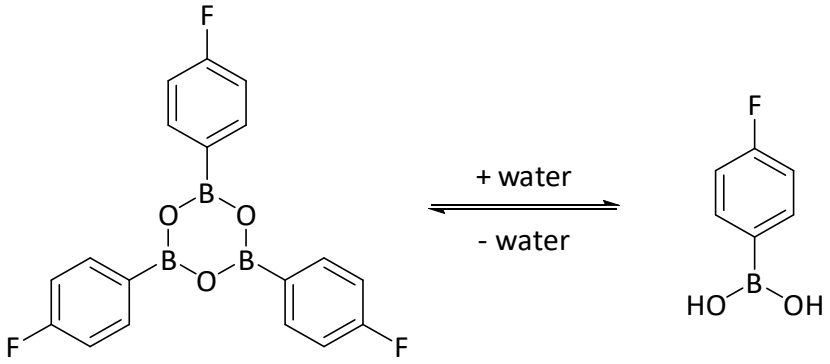

Scheme 3.4 – The reversible dehydration of p-fluorophenylboronic acid to form tri(p-fluorophenyl)boroxine.

2,4-Dibromopyridine was purified from any salt by-products present from the manufacturing process by dissolving it in chloroform and filtering over Celite®; the solvent was then removed from the filtrate to leave an off-white solid. Triphenylphosphine was purified from any triphenylphosphine oxide which may have formed over time using a literature method.[8] The purity of these reagents was confirmed using ^{1}H NMR spectroscopy and LC-MS. The THF solvent used in the catalysis was obtained from a Grubbs solvent purification system and was degassed and stored under argon prior to use.

3.1.5.2 Benchmark Reaction with Purified Reagents

The benchmark catalytic reaction (with $Pd(OAc)_2$:*n*PPh_3 catalyst system) was performed again using the same conditions outlined previously with the purified reagents (Scheme 3.3, Figure 3.8). Reactivity is seen when using purified reagents indicating that one or more reagent impurities was poisoning the catalysis initially. The switch in selectivity from 2-Ar to 4-Ar when lower equivalents of triphenylphosphine are used (from *n* = 4 to *n* = 2) in the catalyst mixture is clearly displayed in these data. Also observed is the higher overall reaction yield using fewer triphenylphosphine equivalents (*n* = 2). There was a higher proportion of 2,4-Ar observed when using *n* = 2 triphenylphosphine equivalents in this data collection compared to the literature data, 19.5% and 6% respectively, however discrepancies in product yield were expected therefore replication of the literature data was deemed to be satisfactory.

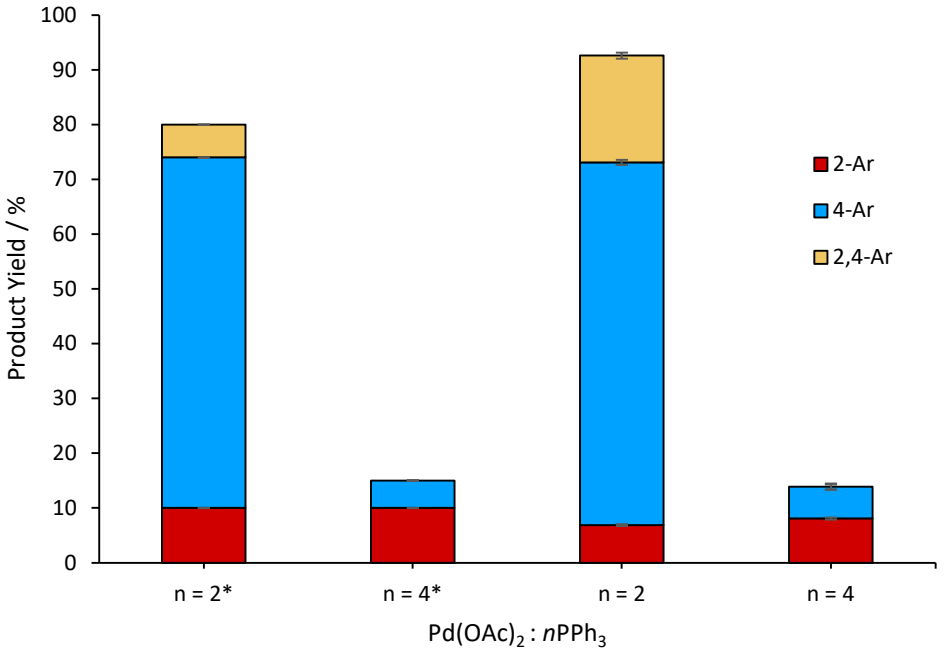

*Figure 3.8 – Product yields of 2-Ar, 4-Ar and 2,4-Ar for the reaction between purified 2,4-dibromopyridine and p-fluorophenylboronic acid in the presence of different $Pd(OAc)_2$:nPPh_3 ratios (n = 2 and 4) giving different product selectivity with a change in n. Product yields are determined using ^{19}F NMR spectroscopy with respect to FDMB internal standard. Error bars represent standard error. *Literature data from Fairlamb.[1]*

3.1.6 Test Catalytic Screen of Pd-NHC Complexes 1

Having shown that the catalytic reaction protocol and sample work-up was successful for the Pd(OAc):*n*PPh_3 catalyst system and could sufficiently replicate literature trends in product selectivity, the methodology could then be applied for the Pd-NHC complexes under investigation, ***C1***–***C14***. The reaction conditions used for the benchmark reactions were utilised for a test screening reaction (Scheme 3.5) on a small selection of the Pd-NHC complexes, namely ***C2***, ***C5***, ***C6***, ***C11*** and ***C13*** (Figure 3.9). The complexes in the test screen were used at a 2.5 mol% precatalyst loading.

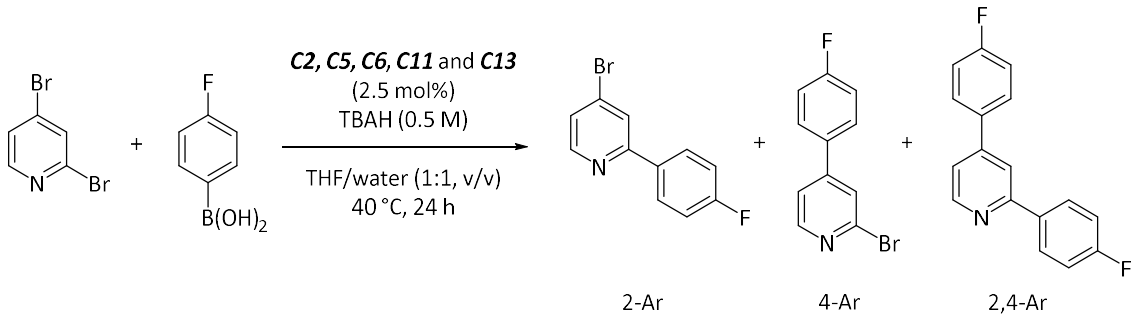

Scheme 3.5 – Catalytic reaction between 2,4-dibromopyridine and p-fluorophenylboronic acid under benchmark conditions. ***C2, C5, C6, C11*** *and* ***C13*** *were used as precatalyst with a loading of 2.5 mol%.*

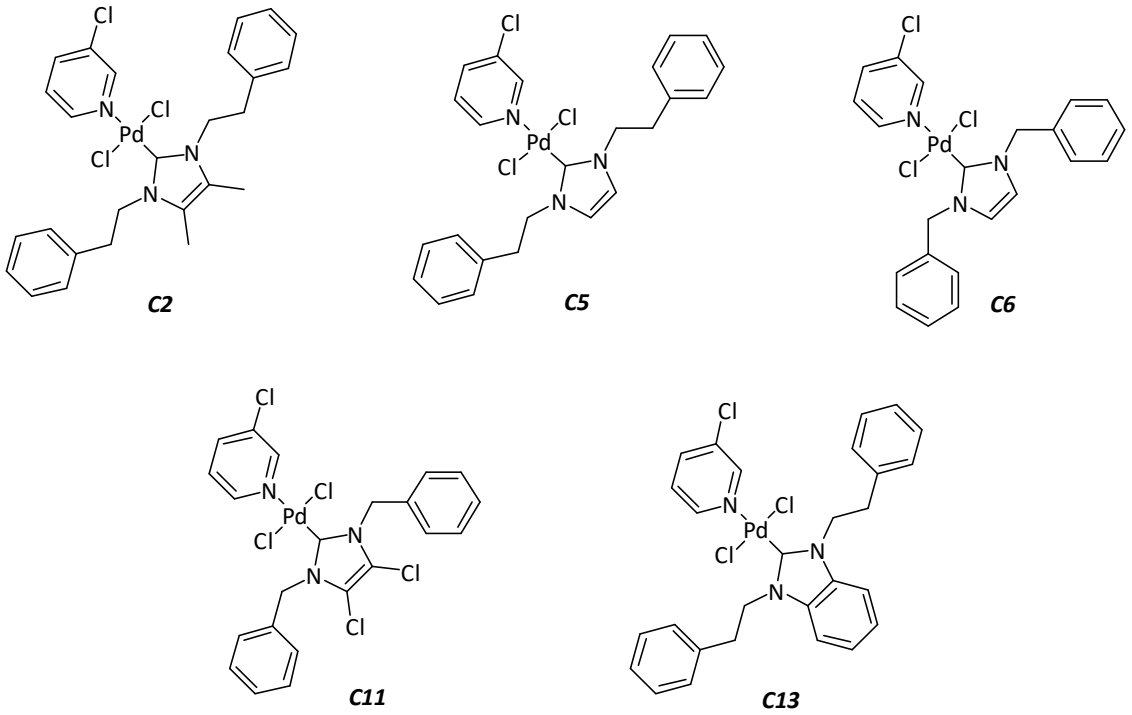

Figure 3.9 – Complexes used in test catalytic screen ***C2***, ***C5***, ***C6***, ***C11*** *and* ***C13***.

All five complexes were found to have poor activity, with all showing similar overall product yields between 6 – 7% (Figure 3.10). The unusual selectivity for 4-Ar was observed, but at such low product yields the conditions used for the benchmark reaction were not suitable for further catalytic studies. The reaction temperature, solvent and base were identified as the most likely parameters that could catalyst performance and as such were investigated further.

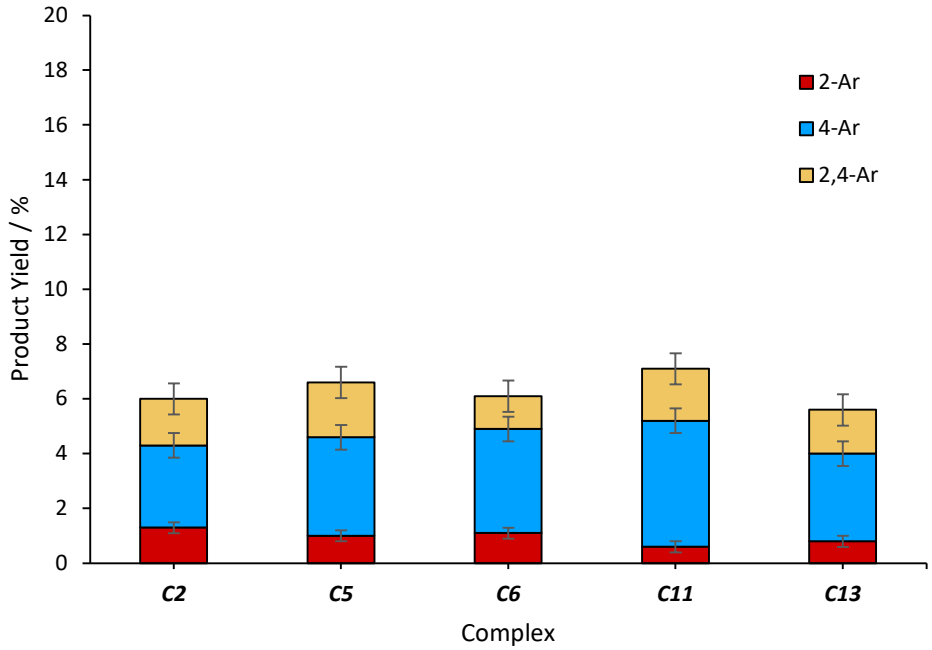

Figure 3.10 – First test catalytic screen data showing product yields of 2-Ar, 4-Ar and 2,4-Ar for the reaction between 2,4-dibromopyridine and p-fluorophenylboronic acid under benchmark reaction conditions. ***C2****,* ***C5****,* ***C6****,* ***C11*** *and* ***C13*** *were used as precatalyst with a loading of 2.5 mol%. Product yields are determined by* ^{19}*F NMR spectroscopy with respect to FDMB internal standard. Error bars represent standard error.*

3.2 Catalytic Conditions Refinement

3.2.1 Temperature Variation

It was thought that the 40 °C reaction temperature used may have been too low to allow full precatalyst activation in the case of the Pd-NHCs. The catalytic cross-coupling of 2,4-dibromopyridine and arylboronic acid reported by Willans and co-workers was conducted under different conditions, including at a much higher reaction temperature of 80 °C culminating in a reasonable overall product yield of 58%.[2] This does suggest that a higher temperature is needed for activation of the palladium-NHC complexes compared to the $Pd(OAc)_2$:*n*PPh_3 catalyst system used by Fairlamb and co-workers.

The catalytic reaction was therefore performed at elevated temperatures of 60, 70 and 80 °C and the product yields determined after 24 hours reaction time (Scheme 3.6). Only ***C13*** was used during this investigation (Figure 3.9). ***C13*** was expected to display a similar overall catalytic

reaction yield to the complex used by Willans and co-workers, ***Pd-NHC1*** due to the similarity in the complexes' NHC structure (Figure 3.11) (discussed previously in Chapter 2.2).

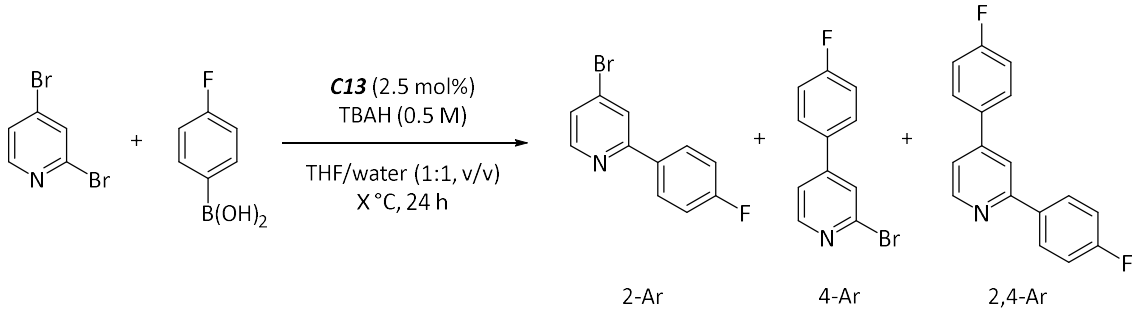

Scheme 3.6 – Catalytic reaction between 2,4-dibromopyridine and p-fluorophenylboronic acid under benchmark conditions at different temperatures, 60, 70 and 80 °C. ***C13*** *was used as the precatalyst with a loading of 2.5 mol%.*

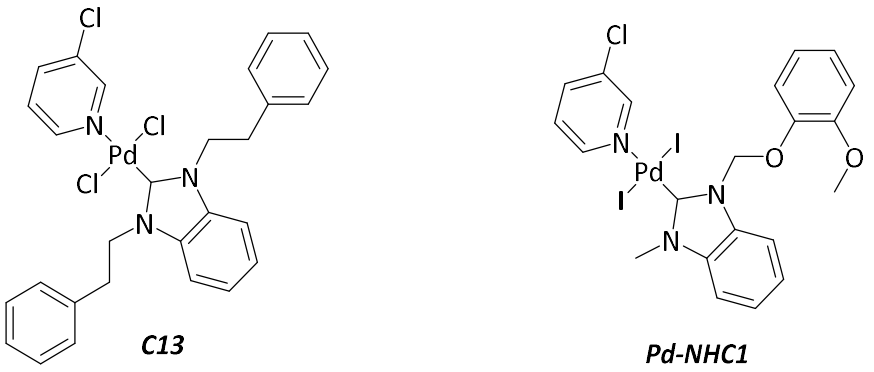

Figure 3.11 – Structure of ***C13*** *used in the temperature variation experiments (Scheme 3.6) in comparison to* ***Pd-NHC1,*** *used by Willans and co-workers.* [2]

There was a slight increase to the overall reaction yield as a result of the higher temperatures, from 6% at 40 °C to 8% at 80 °C (Figure 3.12). This increase in product yield, however is negligible and suggests that the low activity for the screened complexes under the reaction conditions used by Fairlamb and co-workers (Scheme 3.5), could be due to catalyst poisoning rather than incomplete precatalyst activation.

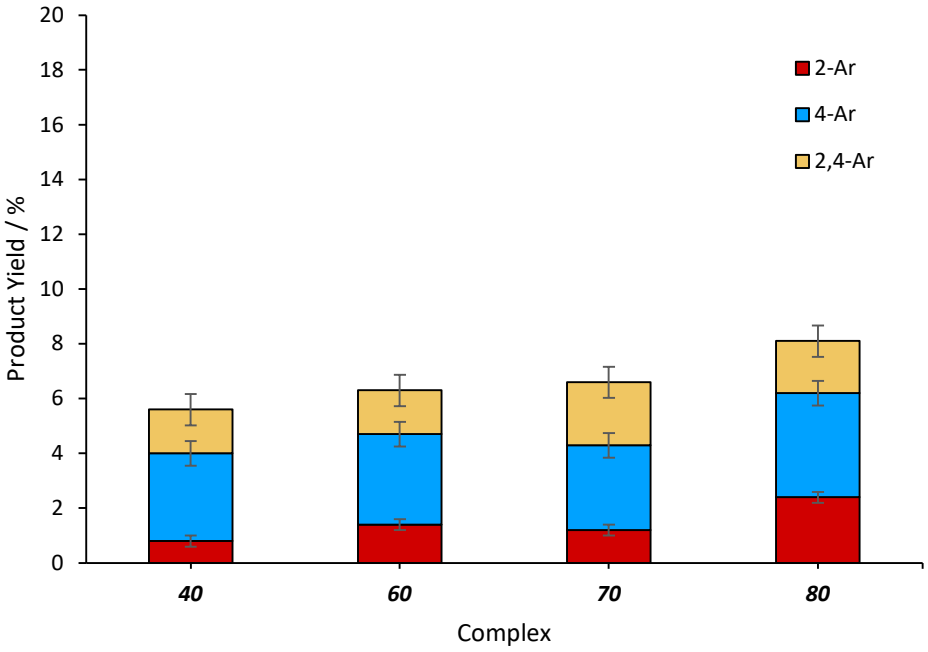

*Figure 3.12 – Product yields of 2-Ar, 4-Ar and 2,4-Ar for the reaction between 2,4-dibromopyridine and p-fluorophenylboronic acid using **C13** as the precatalyst using conditions outlined in Scheme 3.6 at different temperatures (40, 60, 70 and 80 °C) to promote precatalyst activation. Product yields are determined by ^{19}F NMR spectroscopy with respect to FDMB internal standard. Error bars represent standard error.*

3.2.2 Base Variation

The selection of the base in the catalytic reaction was then explored. Tetrabutylammonium hydroxide (TBAH) was shown by Fairlamb and co-workers to enhance the abnormal product selectivity when using the $Pd(OAc)_2$:*n*PPh_3 catalyst system. The conditions reported by Willans and co-workers include the use of caesium carbonate as the base for the catalytic reaction. It was thought that TBAH may have a negative effect on the catalytic product yield when using the Pd-NHC complexes as precatalysts. To test this a reaction was conducted using caesium carbonate instead of TBAH as the base and the same solvent mixture and temperature as the screening reaction, *i.e*. THF and water (1:1, v:v) and 40 °C respectively (Scheme 3.7). Again, this reaction was carried out using ***C13***.

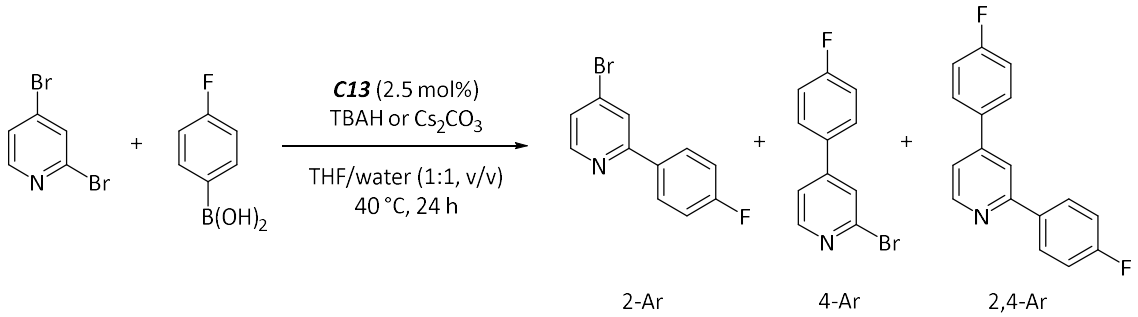

Scheme 3.7 – Catalytic reaction between 2,4-dibromopyridine and p-fluorophenylboronic acid under benchmark conditions with either caesium carbonate or tetrabutylammonium hydroxide as the base. ***C13*** *was used as the precatalyst with a loading of 2.5 mol%.*

The change in base from TBAH to caesium carbonate resulted in a three-fold increase to the overall product yield, 6% with TBAH and 17% with caesium carbonate (Figure 3.13). The abnormal selectivity was also retained with the change in base. This increase in yield was encouraging and indicated that to some extent the reaction catalysed by the complexes investigated here is base sensitive.

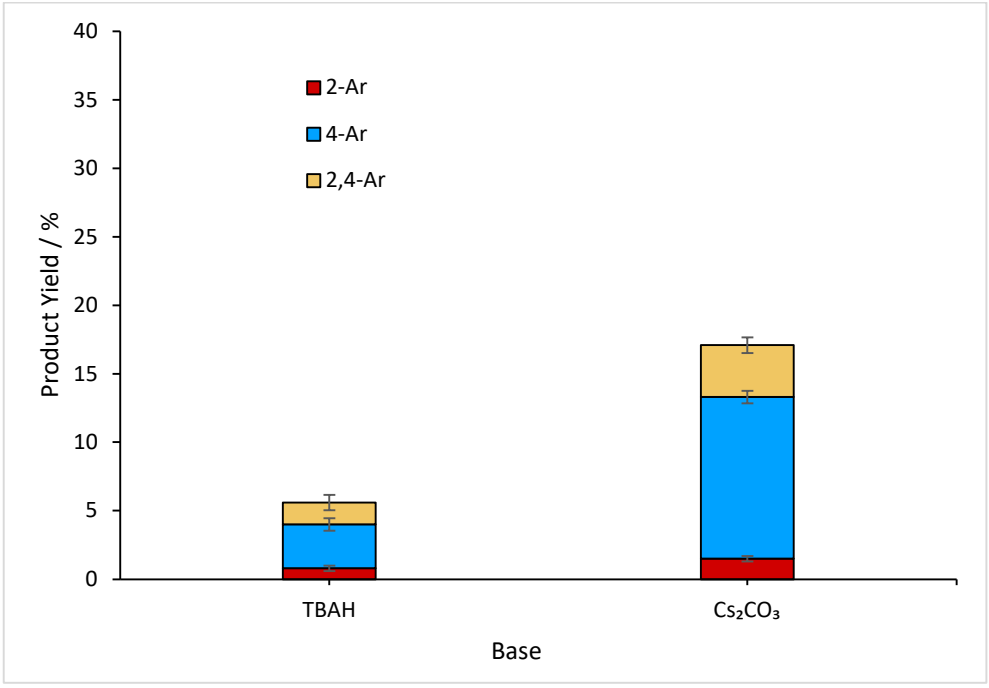

Figure 3.13 – Product yields of 2-Ar, 4-Ar and 2,4-Ar for the reaction of 2,4-dibromopyridine and p-fluorophenylboronic acid using ***C13*** *as the precatalyst using conditions outlined in Scheme 3.7 with different bases. Product yields are determined by ^{19}F NMR spectroscopy with respect to FDMB internal standard. Error bars represent standard error.*

3.2.3 Solvent Variation

Finally, the solvent mixture was examined to evaluate its effect on the catalytic activity of the complexes used in the initial screening reaction. The solvent used for SMCC reactions has been shown to influence site-selectivity with dihaloarenes as coupling partners.[9, 10]

As with the investigations into the reaction temperature and base, the reaction was conducted with the same overall conditions as the test screen, except for modification of the solvent (Scheme 3.8). Willans and co-workers used 1,4-dioxane and water (1:1, v:v) in the reactions demonstrating abnormal product selectivity.[2] This solvent system was adopted here to compare to the THF and water (1:1, v:v) solvent system used in the test screen and by Fairlamb and co-workers. Like the THF and water solvent system used for the previous reactions, the dioxane and water solvent mixture was degassed with argon prior to use.

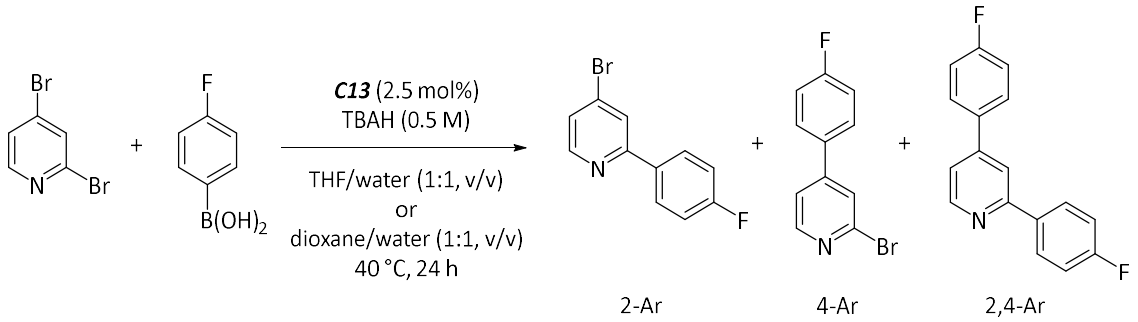

Scheme 3.8 – Catalytic reaction between 2,4-dibromopyridine and p-fluorophenylboronic acid under benchmark conditions with either THF or dioxane and water (1:1) as the solvent. ***C13*** *was used as the precatalyst with a loading of 2.5 mol%.*

The change in solvent had the largest effect on the overall catalytic product yield in this set of investigations (Figure 3.14). The overall product yield increased from 6% with THF and water to 34% with dioxane and water. The abnormal selectivity was still observed with the solvent change and there was also a significant increase in the yield of 2,4-Ar. These results clearly indicated that the THF and water solvent system was the main cause of reduced catalytic activity shown in the test screening reactions.

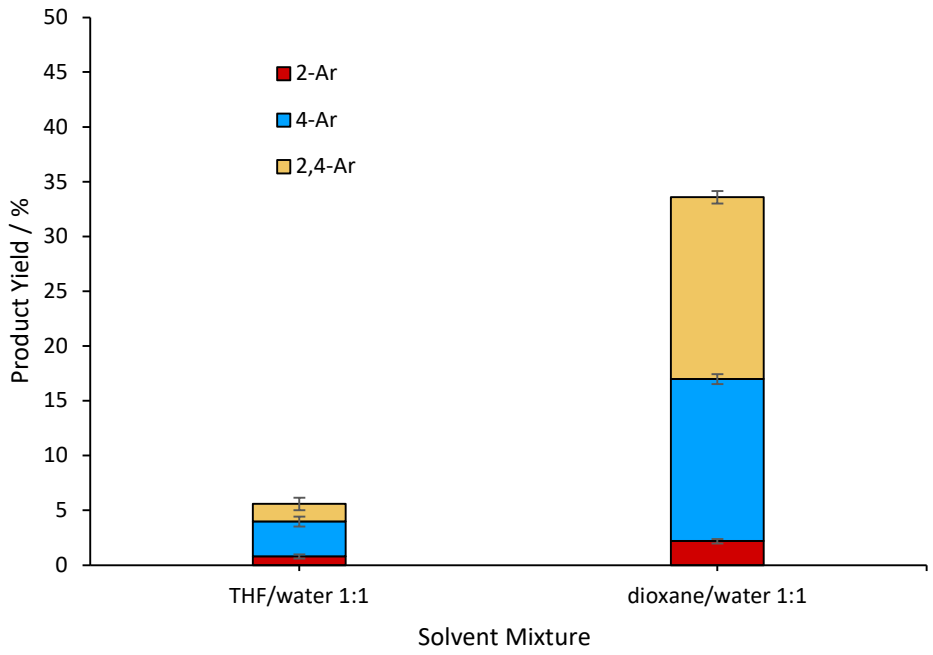

*Figure 3.14 – Product yields of 2-Ar, 4-Ar and 2,4-Ar for the reaction of 2,4-dibromopyridine and p-fluorophenylboronic acid using **C13** as the precatalyst using conditions outlined in Scheme 3.8 at different solvent mixtures. Product yields are determined by ^{19}F NMR spectroscopy with respect to FDMB internal standard. Error bars represent standard error.*

The independent evaluation of the reaction condition variables has shown that when using a Pd-NHC complex as the precatalyst optimal catalyst activity was achieved when using the conditions outlined by Willans and co-workers. Therefore, going forward, any further catalytic reactions were conducted using caesium carbonate as the base, a 1,4-dioxane and water (1:1, v:v) solvent mixture and 80 °C reaction temperature, and will be referred to as 'the standard catalytic conditions', unless otherwise stated.

3.2.3.1 Solvent Variation Revisited

The cause for the decreased catalytic activity when using the THF and water solvent system was revisited again later to gain a deeper understanding for why the solvent may affect the yield so much. A series of reactions were carried out with ***C14*** as the precatalyst where the solvent mixture was varied with different proportions of THF and dioxane. Water was kept constant at 1:1 with respect to the total volume of organic solvents. The series consisted of organic solvent ratios of dioxane/THF: 1:0, 0.8:0.2, 0.6:0.4, 0.4:0.6, 0.2:0.8 and 0:1 (Scheme 3.9). The reaction was carried out using the standard catalytic conditions previously established (with caesium carbonate and 80 °C reaction temperature) with the expectation that increasing THF would have a noticeable effect on product yields.

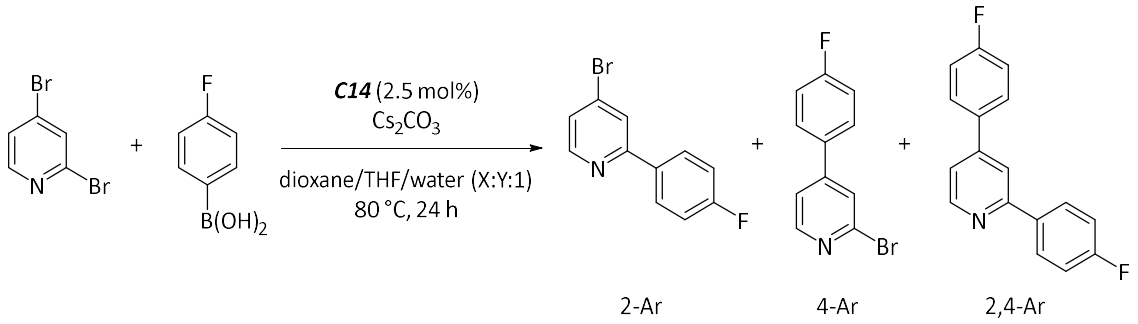

Scheme 3.9 – Catalytic reaction between 2,4-dibromopyridine and p-fluorophenylboronic acid under standard conditions with THF, dioxane and water (X:Y:1) as the solvent where X = 1, 0.8, 0.6, 0.4, 0.2, 0 and Y = 0, 0.2, 0.4, 0.6, 0.8 and 1 and X + Y = 1. ***C14*** *was used as the precatalyst with a loading of 2.5 mol%.*

The results from this further investigation were unexpected (Figure 3.15). The reactions all exhibit similar behaviour with yields of 42 – 53%, and no decrease in activity upon increasing the amount of THF. Earlier studies found much lower yields when using THF and water, indicating that the THF solvent used in the earlier experiments was contaminated in some way.

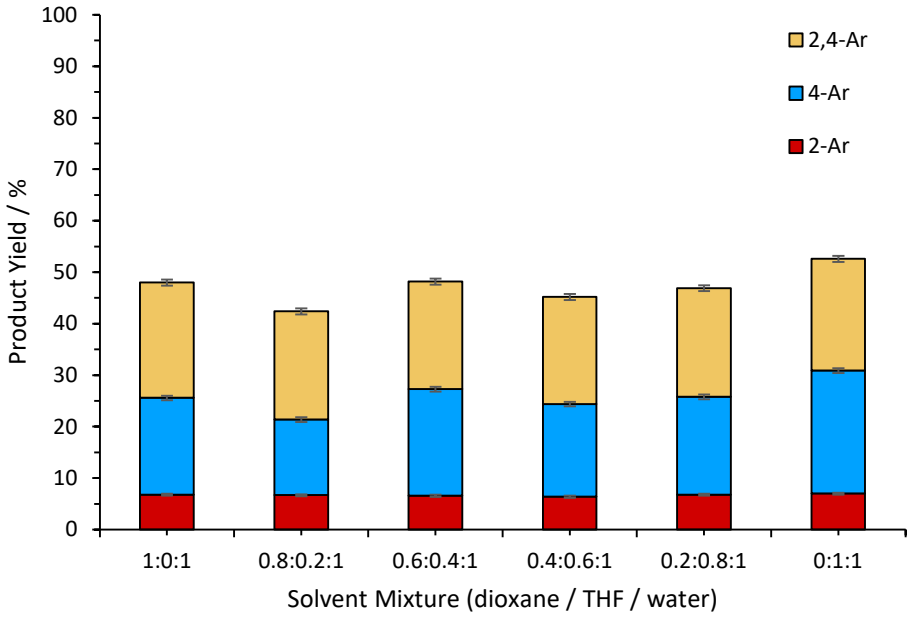

Figure 3.15 – Product yields of 2-Ar, 4-Ar and 2,4-Ar for the reaction of 2,4-dibromopyridine and p-fluorophenylboronic acid using ***C14*** *as the precatalyst using conditions outlined in Scheme 3.9 at different solvent ratios. Product yields are determined by ^{19}F NMR spectroscopy with respect to FDMB internal standard. Error bars represent standard error.*

The THF used in all cases was collected from a Grubbs solvent purification system and thoughroughly degassed with argon. THF is known to form peroxide species when stored without a stabilising agent.[11] Peroxide species are known to bind to palladium and may alter the catalytic activity.[12, 13] The THF used in the first test catalyst screen (Scheme 3.5) and following

investigations into temperature, base and solvent variation was stored prior to use, whereas the THF used for the reactions shown in Scheme 3.9 was used fresh. Therefore, the buildup of peroxides in the THF over time is thought to be the major cause of the reduced actvity in the test screen reaction (Figure 3.10).

3.2.4 Test Catalytic Screen of Pd-NHC Complexes 2

A second test catalyst screening reaction was performed using the standard catalytic conditions (Scheme 3.10) and the same selection of five complexes as for the first test screen reaction, ***C2***, ***C5***, ***C6***, ***C11*** and ***C13*** (Figure 3.9).

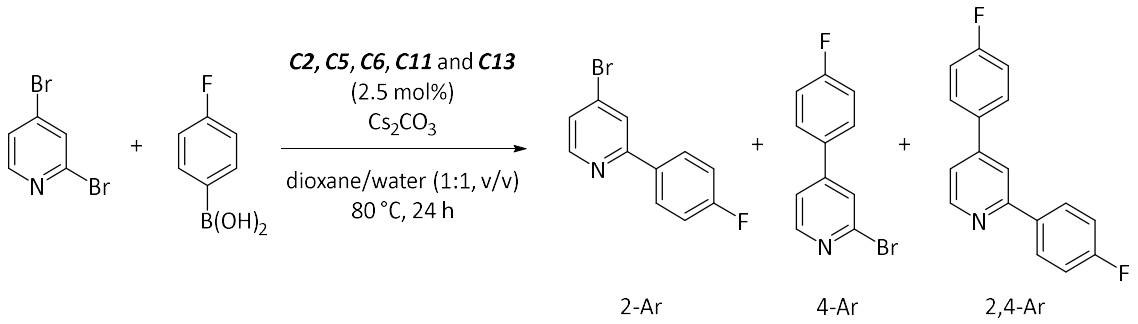

Scheme 3.10 – Catalytic reaction between 2,4-dibromopyridine and p-fluorophenylboronic acid under standard conditions. ***C2, C5, C6, C11*** *and* ***C13*** *were used as precatalyst with a loading of 2.5 mol%.*

The data collected from this second test catalyst screen shows a much greater catalytic activity for the complexes than in the first test catalyst screen (Figure *3.16*). All of the complexes displayed reasonable product yields, hence the conditions were taken forward to a full complex screen (***C1***–***C14***) and further investigations. The relationship between NHC ligand sterics and electronics, and the corresponding complexes catalytic activity will not be discussed for this small screen but will be expanded upon later with reference to the full complex screen. With all necessary rection condition variables and logistical factors explored, the further catalytic studies could be carried out with full confidence in the data and results.

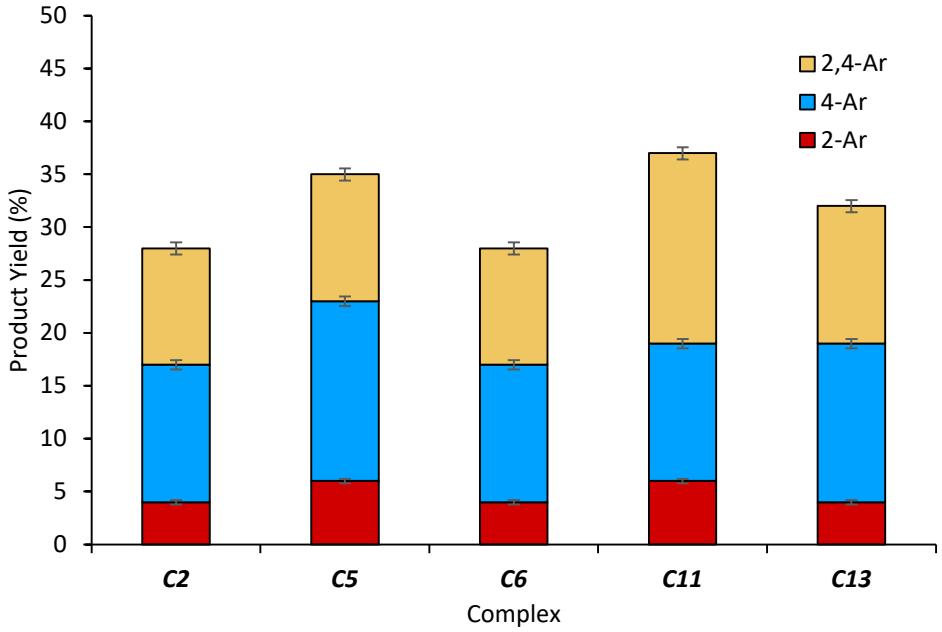

Figure 3.16 – *Second test catalytic screen data showing product yields of 2-Ar, 4-Ar and 2,4-Ar for the reaction of 2,4-dibromopyridine and p-fluorophenylboronic acid using* ***C2***, ***C5, C6, C11*** *and* ***C13*** *as precatalyst a loading of 2.5 mol% under standard reaction conditions (Scheme 3.10). Product yields are determined by* ^{19}*F NMR spectroscopy with respect to FDMB internal standard. Error bars represent standard error.*

3.2.5 Benchmark Reaction with New Catalytic Reaction Conditions

The benchmark reaction utilising the $Pd(OAc)_2$:*n*PPh_3 catalyst system (where *n* = 2 and 4) was conducted again using the standard catalytic conditions shown to work for the Pd-NHC complexes (Scheme 3.11). Though the exact ratios of the three products are not expected to be reproduced, since the change in conditions would likely affect each yield independently, the switch in selectivity from the normal (2-Ar) to abnormal (4-Ar) product when using less equivalents of triphenylphosphine should be observable.

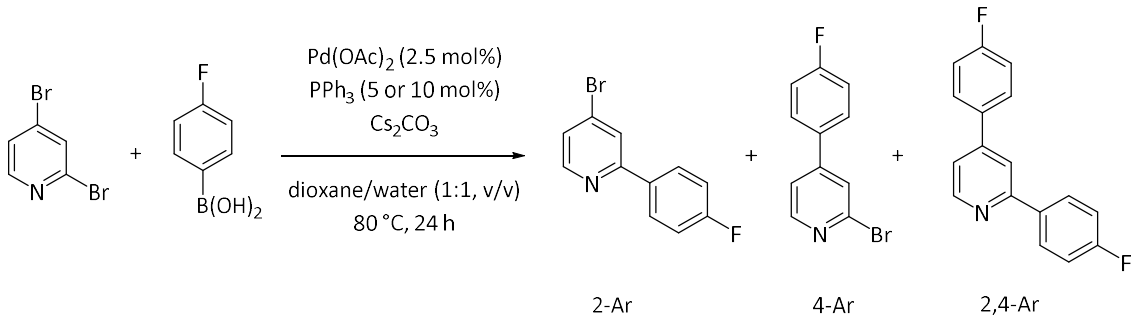

Scheme 3.11 – Benchmark reaction of 2,4-dibromopyridine and p-fluorophenylboronic acid using $Pd(OAc)_2$*:n*PPh_3 *(where n = 2 and 4) as the catalyst system in a 1:1 dioxane:water solvent system at 80 °C. Caesium carbonate was used as the base.*

Indeed, the results did show a significant difference in overall yield for the reactions (Figure 3.17). The *n* = 4 datapoint had a significantly increased overall yield compared to literature data, likely caused by the increase in reaction temperature from 40 °C in the Fairlamb data to 80 °C in the standard catalytic conditions used here. More 2,4-Ar is also seen when using the standard conditions. Fairlamb and co-workers report the consumption of the mono-arylated products to form 2,4-Ar. The increased temperature used here could therefore enhance the formation of 2,4-Ar and resulting increased yield. The increased reaction time used in the standard conditions may also cause this increased 2,4-Ar yield. The switch from 2-Ar selectivity to 4-Ar selectivity with reduced triphenylphosphine equivalents is still observed in this data which supports the literature findings, giving further validation that the standard catalytic conditions are viable for further use in this investigation.[1]

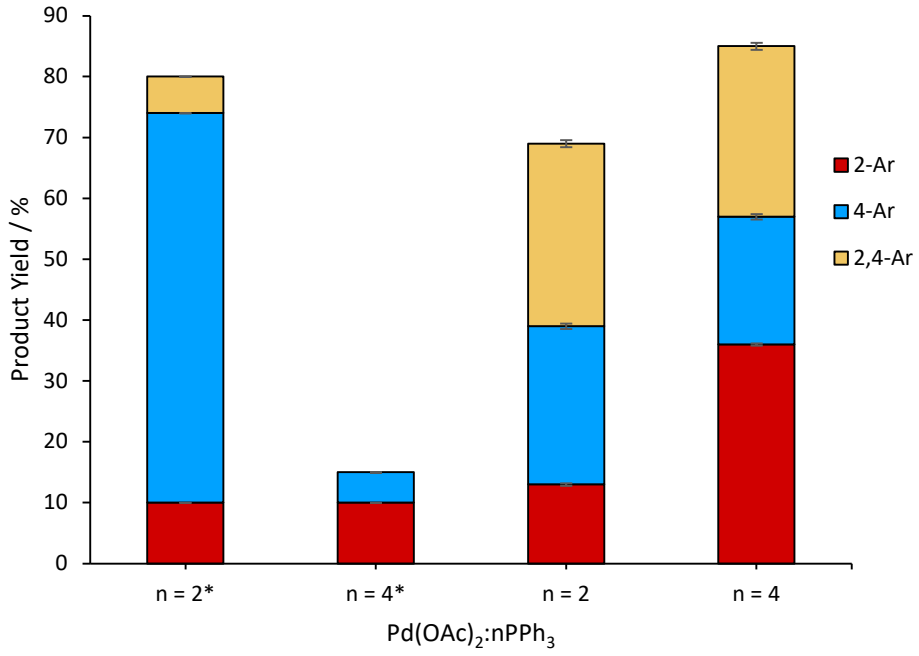

*Figure 3.17 – Product yields of 2-Ar, 4-Ar and 2,4-Ar for the reaction of 2,4-dibromopyridine and p-fluorophenylboronic acid using different $Pd(OAc)_2$:$nPPh_3$ ratios (n = 2 and 4) giving different product selectivity with a change in n. Product yields are determined by ^{19}F NMR spectroscopy with respect to FDMB internal standard. Error bars represent standard error. *Literature data from Scott.[1]*

3.3 Summary

The catalytic protocol and reaction conditions for the SMCC of 2,4-dibromopyridine and *p*-fluorophenylboronic were scrutinised in detail to allow for the generation of accurate and reproducible data for the investigation of Pd-NHC complexes. The use of a fluorinated reagent allowed for the analysis of product yields by ^{19}F NMR spectroscopy and, as such, a quantitative NMR experiment was developed using spin-lattice relaxation times of the isolated products. It was found that 2,4-dibromopyridine sublimation and boronic acid removal on Celite® occurred during the work-up procedure, limiting the amount of kinetic analysis available for the catalytic reaction. The robustness of the protocol was verified by the successful replication of literature yields for a similar reaction.

However, when applying the Pd-NHC complexes as precatalysts in this benchmark reaction, very poor activity was observed. The conditions of the reaction were therefore systematically scrutinised to identify any cause for the catalytic inactivity. The temperature, base and solvent were all varied and it was found that the solvent had the largest impact on catalyst activity, however, it was later found that peroxide formation in the solvent was a likely cause for the reduced catalytic activity. The base used in this reaction was also found to influence the catalysts performance. Through this systematic investigation, optimal reaction conditions were identified for use with Pd-NHC complexes, which could be used in the following investigations.

3.4 References

1. N. W. J. Scott, M. J. Ford, N. Jeddi, A. Eyles, L. Simon, A. C. Whitwood, T. Tanner, C. E. Willans and I. J. S. Fairlamb, *J. Am. Chem. Soc.*, 2021, **143**, 9682-9693.
2. J. M. Fowler, E. Britton, C. M. Pask, C. E. Willans and M. J. Hardie, *Dalton Trans.*, 2019, **48**, 14687-14695.
3. A. O. Mattes, D. Russell, E. Tishchenko, Y. Z. Liu, R. H. Cichewicz and S. J. Robinson, *Conc. Magn. Reson. A*, 2016, **45a**, e21422.
4. E. J. Flahive, B. L. Ewanicki, N. W. Sach, S. A. O'Neill-Slawecki, N. S. Stankovic, S. Yu, S. M. Guinness and J. Dunn, *Org. Process Res. Dev.*, 2008, **12**, 637-645.
5. Z. Chai, C. Wang, J. Wang, F. Liu, Y. Xie, Y. Z. Zhang, J. R. Li, Q. Li and Z. Li, *Chem. Sci.*, 2017, **8**, 8336-8344.
6. *United States of America Pat.,* US2004/171836, 2004.
7. P. Leszczyński, T. Hofman, E. Kaczorowska, A. Adamczyk-Woźniak and A. Sporzyński, *J. Organomet. Chem.*, 2021, **949**.
8. D. C. Batesky, M. J. Goldfogel and D. J. Weix, *J. Org. Chem.*, 2017, **82**, 9931-9936.
9. E. K. Reeves, O. R. Bauman, G. B. Mitchem and S. R. Neufeldt, *Isr. J. Chem.*, 2020, **60**, 406-409.
10. E. K. Elias, S. M. Rehbein and S. R. Neufeldt, *Chem. Sci.*, 2022, **13**, 1618-1628.
11. D. E. Clark, *Chem. Health Saf.*, 2001, **8**, 12-22.
12. A. Heumann, K.-J. Jens and M. Réglier, in *Prog. Inorg. Chem.*, 2007, pp. 483-576.
13. I. S. Cho and H. Alper, *J. Mol. Catal. A: Chem.*, 1996, **106**, 7-10.

Chapter 4

Proposal of Site-Selectivity Rationale through Catalytic Screening of Pd-NHC Complexes, Time Course and Poisoning Reactions

Following preliminary data showing the unusual site-selectivity using palladium-NHC complexes in a Suzuki-Miyaura cross-coupling (SMCC) reaction involving 2,4-dibromopyridine, several techniques were employed with the aim of gaining a deeper understanding of both the unusual site-selectivity of palladium-NHC complexes and the catalytic reaction as a whole. Product yields and selectivities were determined for reactions catalysed by each complex and trends in activity are discussed. The homo/heterogeneity was explored through poisoning reactions and the effects of temperature on product selectivity and reaction yield were probed. A proposed mechanistic profile is discussed using a combination of experimental data and literature evidence.

4.1 Full Catalyst Screen of Pd-NHC Complexes

Complexes ***C1***–***C14*** (Figure 4.1) were screened in the catalytic reaction of 2,4-dibromopyridine with *p*-fluorophenylboronic acid at a precatalyst loading of 2.5 mol% and under the standard catalytic conditions previously discussed (Scheme 4.1). The product yields for each reaction are shown in Figure 4.2. All complexes were catalytically active in this SMCC reaction. The screen data shows that the complexes featuring a bulky ligand architecture, ***C7*** and ***C8***, have a different product profile when compared to the other complexes featuring less bulky NHC ligands. The bulky Pd-NHC complexes formed predominantly the bis-arylated pyridine product (2,4-Ar) with some 4-Ar. The less bulky Pd-NHC complexes preferentially formed the 4-arylated product (4-Ar) over the 2-arylated product (2-Ar), the same abnormal selectivity described by Fairlamb when using the $Pd(OAc)_2$:*n*PPh_3 (where $n < 3$) catalyst system and by Willans when using the Pd-NHC complexes.[1, 2]

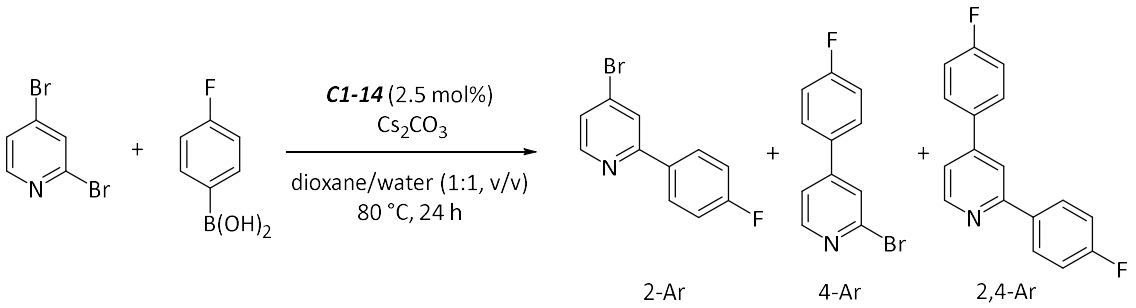

Scheme 4.1 – Screening reaction between 2,4-dibromopyridine and p-fluorophenylboronic acid to yield 2-bromo-4-(p-fluorophenyl)pyridine (4-Ar), 2-(p-fluorophenyl)-4-bromo-pyridine (2-Ar) and 2,4-bis(p-fluorophenyl)pyridine (2,4-Ar) using C1–C14 as precatalysts.

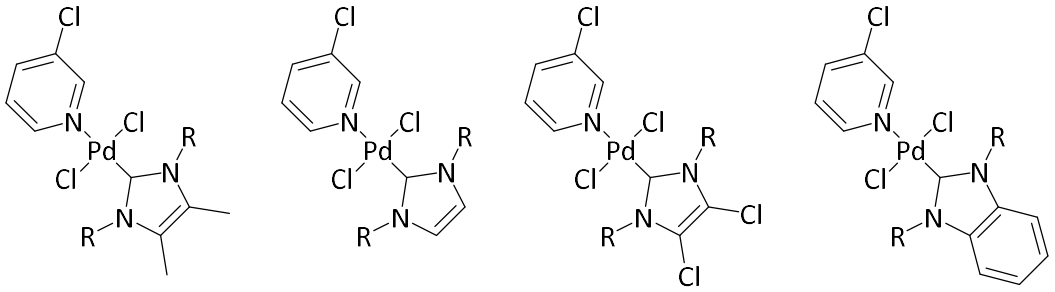

R =	^{n}Pr	(***C1***)	^{n}Pr	(***C4***)	^{n}Pr	(***C9***)	^{n}Pr	(***C12***)
	CH_2CH_2Ph	(***C2***)	CH_2CH_2Ph	(***C5***)	CH_2CH_2Ph	(***C10***)	CH_2CH_2Ph	(***C13***)
	CH_2Ph	(***C3***)	CH_2Ph	(***C6***)	CH_2Ph	(***C11***)	CH_2Ph	(***C14***)
			Dipp	(***C7***)				
			Mes	(***C8***)				

*Figure 4.1 – Structure of complexes **C1–C14** synthesised for catalytic screening. NHC backbone architectures are displayed, and N-substituents listed.*

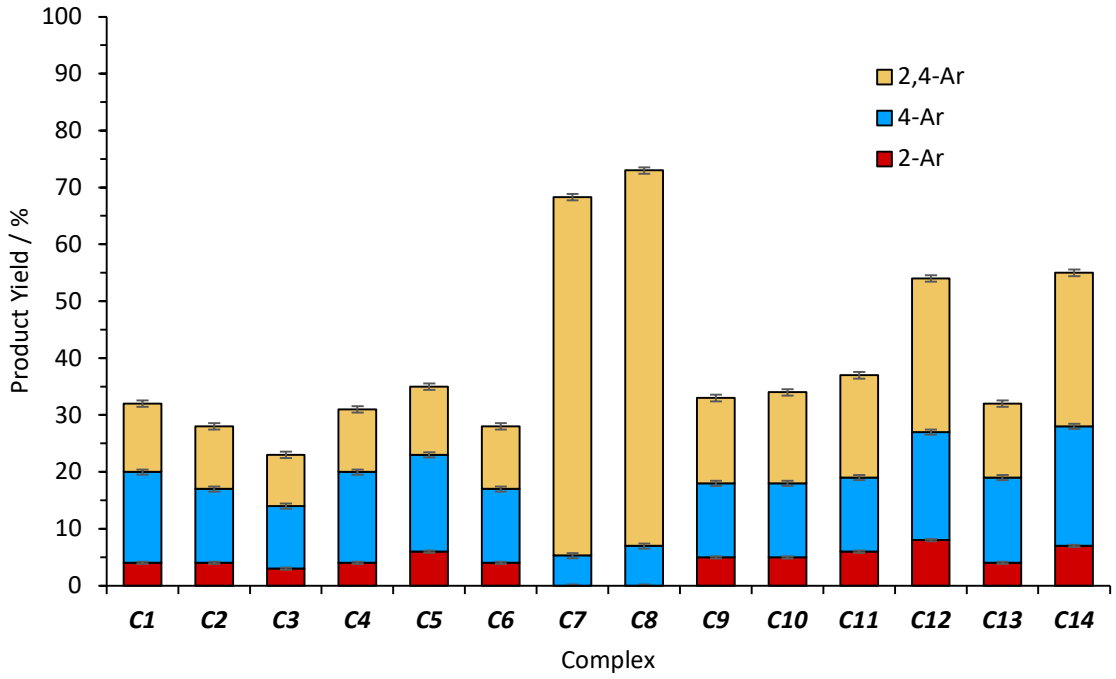

*Figure 4.2 – Product yields of 2-Ar, 4-Ar and 2,4-Ar for the reaction of 2,4-dibromopyridine and p-fluorophenylboronic acid using Pd-NHC complexes **C1**–**C14** as precatalysts under conditions shown in Scheme 4.1. Product yields are determined by ^{19}F NMR spectroscopy with respect to FDMB internal standard. Error bars represent standard error.*

The product yields in Figure 4.2 are calculated on the basis of 2,4-dibromopyridine being the rate limiting reagent, as 1.0 mmol was used with 1.2 mmol *p*-fluorophenylboronic acid. However, when 2,4-Ar is formed the *p*-fluorophenylboronic acid becomes the rate limiting reagent. Figure 4.3 shows the overall yield for each reaction when the boronic acid is treated as the rate-limiting reagent. The bulky Pd-NHC complexes, ***C7*** and ***C8***, result in overall product yields >90% showing that they are much more active than the non-bulky complexes and/or that they are more protected against deactivation. This can be probed using time course analysis which is described later (Chapter 4.2.2).

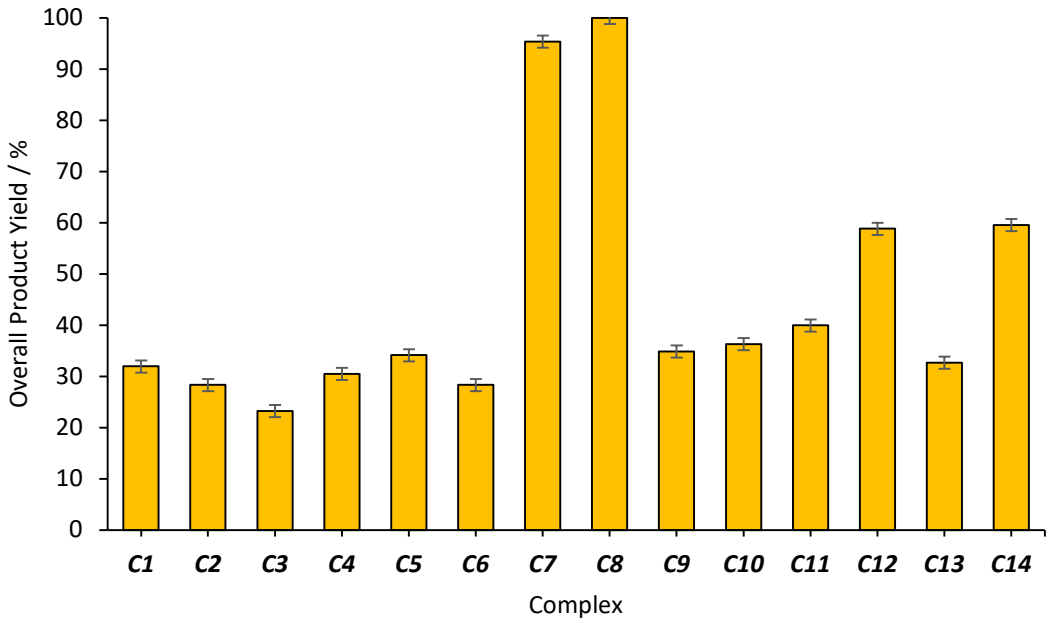

*Figure 4.3 – Combined product yields of 2-Ar, 4-Ar and 2,4-Ar for the reaction between 2,4-dibromopyridine and p-fluorophenylboronic acid (limiting reagent) using Pd-NHC complexes **C1**–**C14** as precatalysts under conditions shown in Scheme 4.1. Product yields are determined by ^{19}F NMR spectroscopy with respect to FDMB internal standard. Error bars represent standard error.*

Examination of the overall product yields with respect to the non-bulky NHC ligand backbone structure highlights a slight trend for increased activity with more electron withdrawing NHC architectures (Figure 4.4). The highest average activity is seen for complexes featuring a benzimidazole backbone structure. Typically in SMCC reactions, greater catalytic activity is seen with more electron donating ligands as the often rate limiting oxidative addition step is promoted by electron rich palladium. The overall product yield data collected for the non-bulky complexes therefore suggests either that oxidative addition is not the rate limiting step or that a more complicated mechanism is in effect.

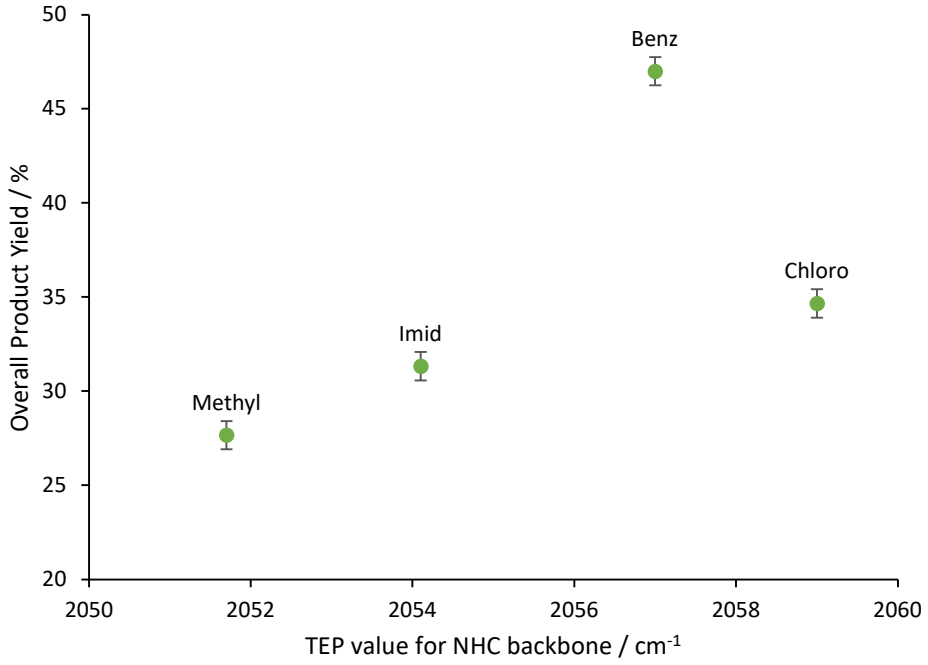

Figure 4.4 – Relationship between the overall product yield and backbone electronics in the SMCC reaction between 2,4-dibromopyridine and p-fluorophenylboronic acid using the non-bulky Pd-NHC complexes as precatalysts under conditions shown in Scheme 4.1. Product yields are determined by ^{19}F NMR spectroscopy with respect to FDMB as an internal standard. Datapoints are averages for the complexes featuring the same backbone architecture (labelled). Error bars represent standard error.

The ratio of the 4-arylated product (4-Ar) to the other products was also examined to determine if there are any trends in 4-Ar selectivity for the non-bulky complexes with respect to the NHC ligand electronics (Figure 4.5). It appears that the ligand electronics have a very small effect on the selectivity as more electron donating NHC backbones, such as 4,5-dimethylimidazole and imidazole, generally show slightly stronger selectivity for 4-Ar. This may be partly due to the relative catalytic activity associated with the backbones such that a greater catalytic activity for a complex would result in a greater proportion of 2,4-Ar thus lowering the overall selectivity for 4-Ar.

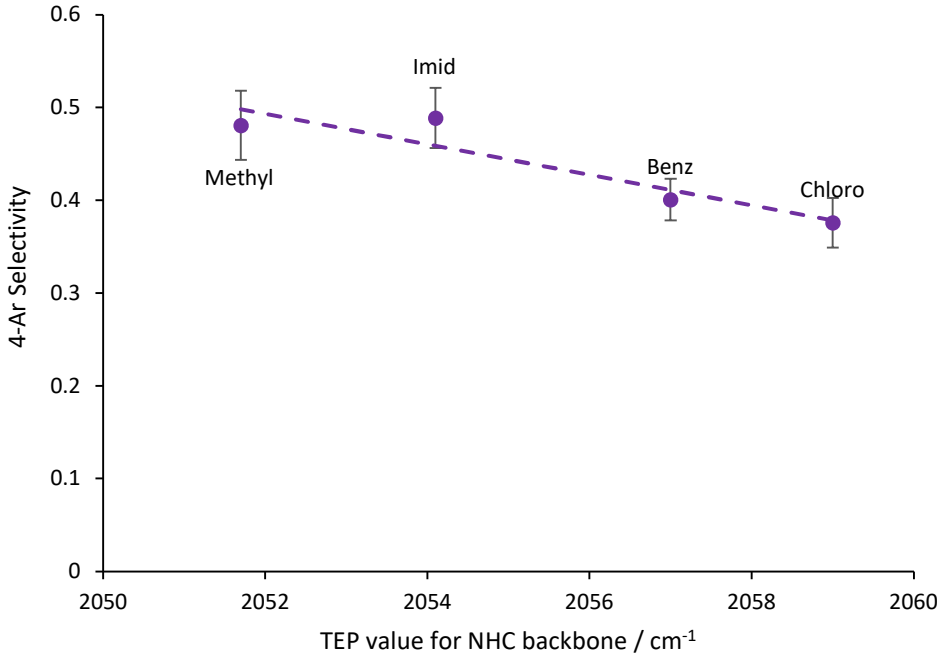

Figure 4.5 – 4-Ar selectivity against NHC ligand electronics (TEP) in the SMCC reaction between 2,4-dibromopyridine and p-fluorophenylboronic acid using the non-bulky Pd-NHC complexes as precatalysts under conditions shown in Scheme 4.1. Datapoints are averages for the complexes featuring the same backbone architecture (labelled). Error bars represent standard error.

There is no obvious trend in product selectivity when comparing the sterics of the non-bulky NHC *N*-substituents: *n*-propyl, benzyl and 2-phenylethyl. It is noted that the steric parameters (%V_{bur}) associated with the non-bulky *N*-substituents fall within a narrow range, so large changes to 4-Ar selectivity would not be expected. The data clearly shows no significant difference in the 4-Ar selectivity over this steric range. This is likely due to the flexibility of the *N*-substituents enabling any bulk to move away from the palladium centre, whilst more rigid steric bulk close to the palladium centre (for ***C7*** and ***C8***) has a dramatic effect on product selectivity/catalytic activity.

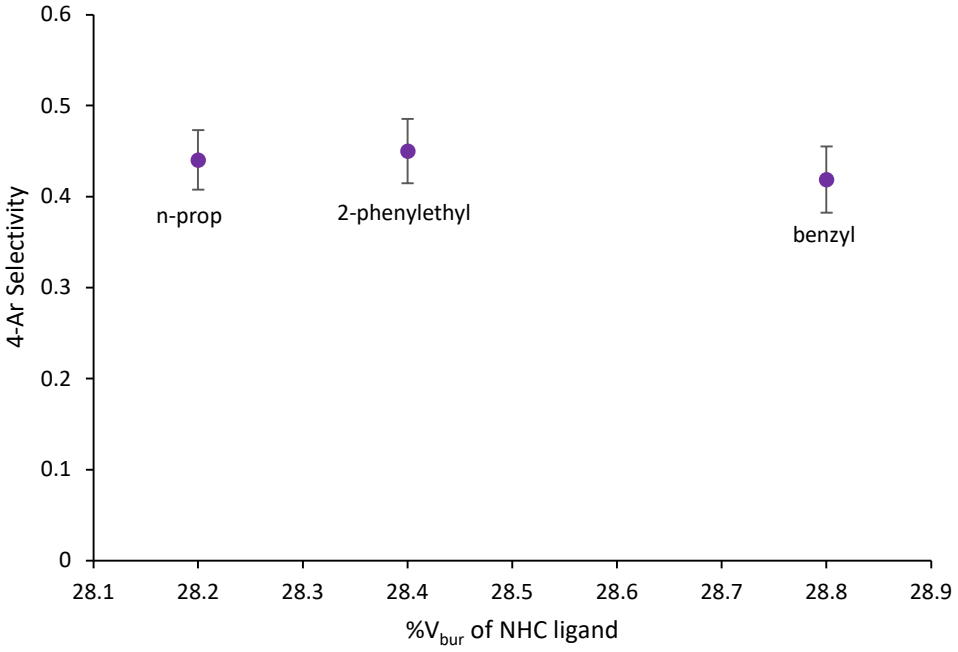

Figure 4.6 – 4-Ar selectivity against NHC ligand sterics (%V_{bur}) in the SMCC reaction between 2,4-dibromopyridine and p-fluorophenylboronic acid using the non-bulky Pd-NHC complexes as precatalysts under conditions shown in Scheme 4.1. Datapoints are averages for the complexes featuring the same NHC N-substituents (labelled). Error bars represent standard error.

Following the screen, three complexes, ***C4***, ***C7*** and ***C14*** (Figure 4.7), were chosen to investigate further. ***C7*** (bulky NHC complex) for the unusually high selectivity for the disubstituted product and ***C14*** (non-bulky NHC complex), as it gave the greatest overall product yield of reactions catalysed by the non-bulky complexes. ***C4*** was also selected as it has the simplest ligand environment of the non-bulky complexes to study using NMR spectroscopy.

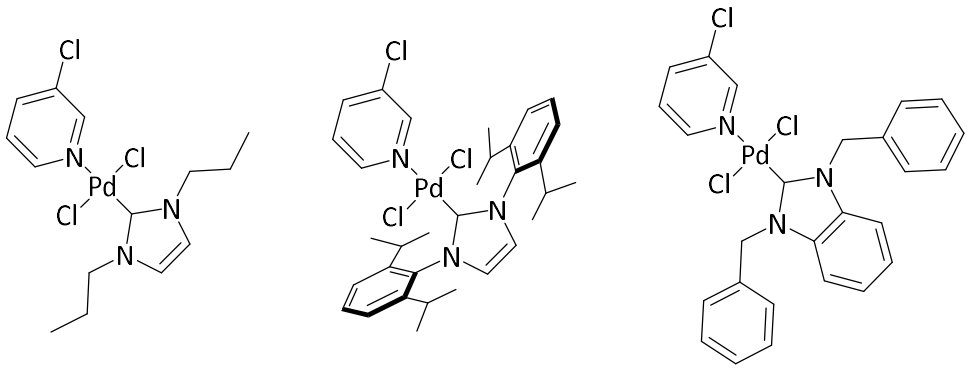

C4 ***C7*** ***C14***

*Figure 4.7 – Structures of complexes **C4**, **C7** and **C14** to be used in further investigations.*

4.1.1 Determination of NHC Prescence in the Active Catalytic Species

It has been shown in the screen data that the NHC ligand can have a large effect on catalyst performance. It is, however, unclear if the NHC remains bound to or is removed from the active

species during the catalysis. In the latter case, the presumably free NHC or imidazolium salt could still alter the product selectivity of the active species in some way. A simple test was conducted to aid in determining if the NHC ligand remains bound to the active species or not. This was achieved by comparing the product yields for reactions catalysed by one of the palladium-NHC complexes (***C7***), a palladium source (palladium chloride) with an imidazolium salt (***I7***), and the palladium source alone as a control, all under the same conditions used for the catalyst screen (Scheme 4.1). ***C7*** and its corresponding imidazolium salt, ***I7***, were chosen for this test as any discrepancy in outcome would be most apparent with this complex, due to its strong 2,4-Ar selectivity. The results show that palladium chloride with an imidazolium salt gave almost identical product yields to that of the palladium chloride alone (Figure 4.8), indicating that an effective NHC is not generated from the imidazolium in this reaction. The fact that the reaction outcome when catalysed by **C7** is so different suggests that the NHC ligand does indeed remain bound to the palladium during the catalysis and has an effect.

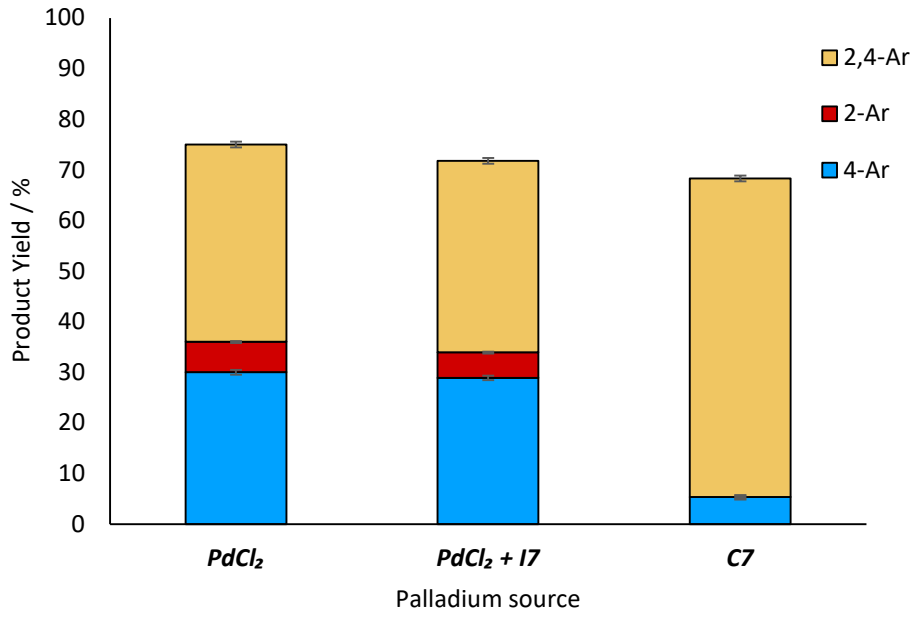

*Figure 4.8 – Product yields of 2-Ar, 4-Ar and 2,4-Ar for the SMCC reaction between 2,4-dibromopyridine and p-fluorophenylboronic acid using **C7**, $PdCl_2$ and combined $PdCl_2$ and **I7** as precatalysts under conditions shown in Scheme 4.1. Samples were taken at 24 hours reaction time. Product yields are determined by ^{19}F NMR spectroscopy with respect to FDMB internal standard. Error bars represent standard error.*

4.2 Examination of Product Formation over Time with Pd-NHC Complexes

The catalytic reaction was sampled over time employing both bulky and non-bulky complexes as precatalysts under standard reaction conditions (Scheme 4.2). Time course reactions can give valuable insight to how a catalyst behaves over the course of the reaction and can be used to provide mechanistic rationale. These time course reactions were also conducted to establish control reaction profiles which can be used to compare to catalyst poisoning reaction profiles (Chapter 4.3).

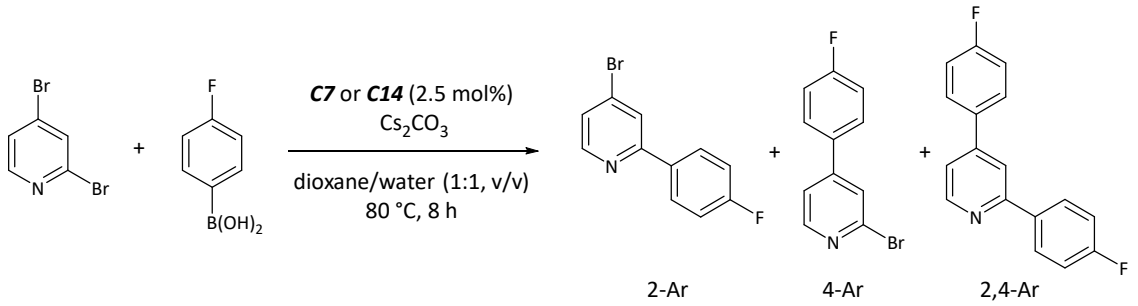

*Scheme 4.2 – Reaction between 2,4-dibromopyridine and p-fluorophenylboronic acid to yield 2-bromo-4-(p-fluorophenyl)pyridine (4-Ar), 2-(p-fluorophenyl)-4-bromo-pyridine (2-Ar) and 2,4-bis(p-fluorophenyl)pyridine (2,4-Ar) using **C7** and **C14** as precatalysts.*

4.2.1 Time Course Studies of the SMCC Reaction Using a Non-Bulky Pd-NHC Complex

When utilising the non-bulky complex, ***C14***, the two mono-arylated products (2-Ar and 4-Ar) are formed with similar reaction profiles, each being generated relatively quickly then plateauing after ~160 mins (Figure 4.9). More of 4-Ar is generated than 2-Ar (~3:1 ratio). 2,4-Ar displays a slightly elongated profile with respect to the mono-products, whereby it takes longer to reach a maximum yield. At 120 mins there is a switch from 4-Ar to 2,4-Ar being the major product.

These reaction profiles suggest that there may be a different mechanism, or an alternative active species present for the formation of the mono-arylated products and 2,4-Ar. Since the mono-arylated products reach a plateau before the maximum yield of 2,4-Ar is achieved and there is no apparent consumption of either mono-arylated product at any point in the reaction profile, then it is reasonable to suggest that 2,4-Ar is formed primarily *via* a concerted mechanism. A concerted mechanism would suggest that for a mononuclear active catalytic species, transmetalation is the rate determining step. This will be explored in more detail later (Chapter 4.4.3).

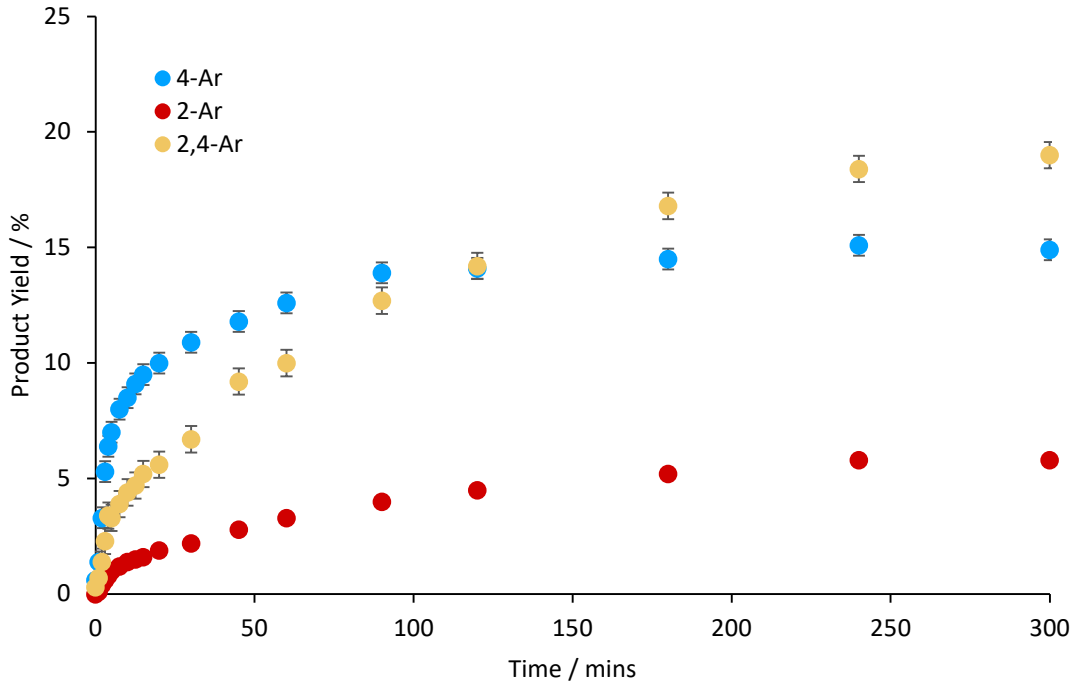

*Figure 4.9 – Time course data showing product yields of 2-Ar, 4-Ar and 2,4-Ar for the reaction between 2,4-dibromopyridine and p-fluorophenylboronic acid using **C14** as the precatalyst. Product yields are determined by ^{19}F NMR spectroscopy with respect to FDMB internal standard. Error bars represent standard error.*

4.2.1.1 Kinetic Analysis of Non-Bulky Pd-NHC Complex Time Course Data

Further analysis of the time course reaction data was conducted using Compunetics software. An algorithm uses a provided reaction model, initial reaction conditions and experimental data to optimise and fit a kinetic profile to the data and generate information on rate constants corresponding to the input model. Poor agreement of the experimental data and fitted data suggests that the model is not representative of the true nature of the reaction and refinement of the model is necessary. Good agreement suggests that the provided model is representative of the major processes in the physical reaction. The generated kinetic parameters can give valuable information into the rates of certain steps in the reaction, such as the rate of catalyst activation or deactivation. The software does, however, have some relevant limitations, for example the number of terms available in the input model constricts the complexity of the model so complicated systems may afford a poor kinetic fit.

For the time course data collected for the non-bulky complex, ***C14***, the most suitable model suggested terms relating to catalyst activation, formation of 2-Ar and 4-Ar, the formation of 2,4-Ar by a concerted mechanism and through consumption of 2-Ar and 4-Ar and finally catalyst deactivation (Table 4.1). Note this model is based upon the assumption that the reaction proceeds *via* a homogeneous pathway, the nature of the active catalytic species is explored in more detail later (Chapter 4.3). The fit of the kinetic profile to the experimental data is not

perfect, however, this model provided the best fit of all the reasonable models tested. The computed kinetic profile does share important features with the time course data such as the initially fast formation of the mono-arylated products followed by 2,4-Ar becoming the major product after some time (Figure 4.10). A more complex model is likely required to describe the reaction profile exactly, however, the model presented is reasonable considering the limitations of the Compunetics software.

*Table 4.1 – Compunetics model terms, their descriptions and calculated rate constants (k) for kinetic fitting to experimental data collected for the SMCC reaction between 2,4-dibromopyridine and p-fluorophenylboronic acid using **C14** as the precatalyst. Pyr = 2,4-dibromopyridine, BA = p-fluorophenylboronic acid, precat = **C14**, cat = active catalytic species and decat = deactivated catalyst.*

Model Term	Description	k value
precat + 2BA → cat	Precatalyst activation	59.6 M^2min^{-1}
Pyr + BA + cat → 4-Ar + cat	4-Ar formation	0.839 M^2min^{-1}
Pyr + BA + cat → 2-Ar + cat	2-Ar formation	0.148 M^2min^{-1}
Pyr + 2BA + 2cat → 2,4-Ar + 2cat	2,4-Ar formation (concerted)	16.18 M^4min^{-1}
4-Ar + BA + cat → 2,4-Ar + cat	2,4-Ar formation (4-Ar consumption)	3.19 M^2min^{-1}
2-Ar + BA + cat → 2,4-Ar + cat	2,4-Ar formation (2-Ar consumption)	0 M^2min^{-1}
cat → decat	Catalyst deactivation	0.0209 min^{-1}

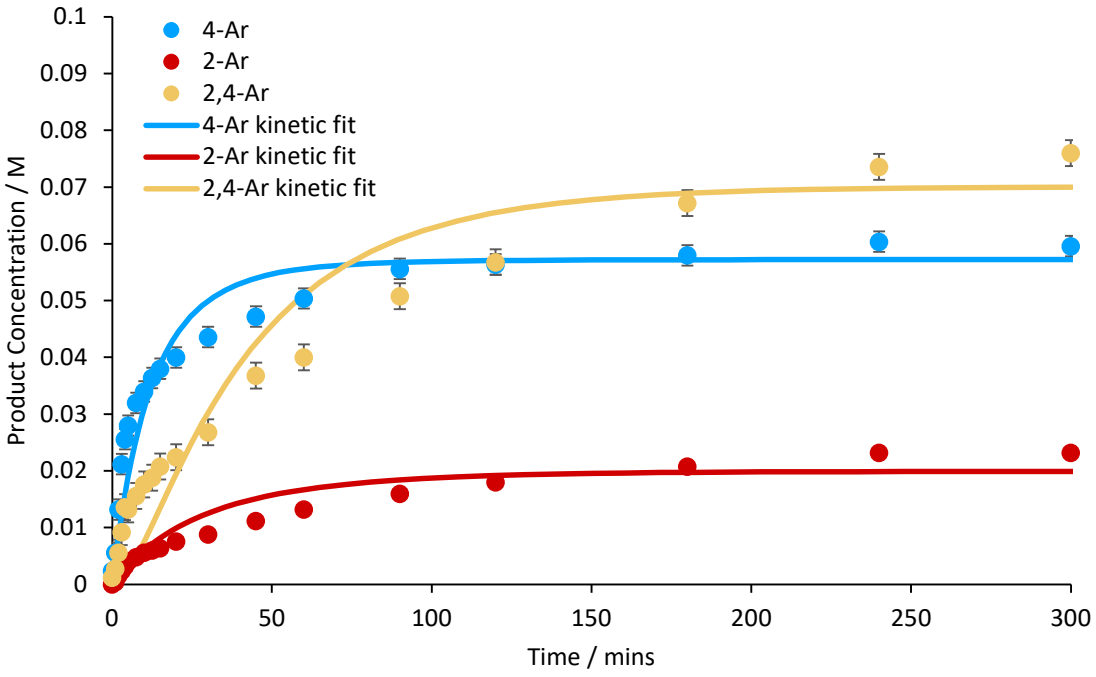

*Figure 4.10 – Time course data showing concentrations of 2-Ar, 4-Ar and 2,4-Ar for the reaction between 2,4-dibromopyridine and p-fluorophenylboronic acid using **C14** as the precatalyst. Error bars represent standard error. Kinetic fitting uses reaction model detailed in Table 4.1.*

The generated rate constants for each term (or reaction) in the model give an indication of the relative rate of these reactions used to form the optimal kinetic fit. The rate constant associated with the catalyst activation term, for example, is relatively large in comparison to the other terms suggesting that the catalyst activation occurs at a very fast rate in relation to the main catalytic reaction. This is reasonable considering the very short initiation period seen in the reaction profile (< 2 mins). As is expected, the formation of 4-Ar is associated with a greater rate constant than 2-Ar, 0.839 M^2min^{-1} and 0.148 M^2min^{-1} respectively, highlighting the preferential reactivity of the active catalytic species towards 4-Ar. Three individual terms were used in the model to describe the formation of 2,4-Ar, through a concerted mechanism and through consumption of 2-Ar and 4-Ar. The kinetic fitting suggests that 2,4-Ar is formed mainly through the concerted pathway and partially through the consumption of 4-Ar. There is no formation of 2,4-Ar from the consumption of 2-Ar, likely due to the relatively low concentration of 2-Ar in the reaction mixture. The deactivation of the active catalytic species is associated with a rate constant of 0.0209 min^{-1}, this accounts for the reaction not reaching full conversion. Though the catalyst deactivation is described as a spontaneous reaction in the kinetic model, in reality this term may account for multiple different reactions that result in loss of catalyst activity.

4.2.2 Time Course Studies of the SMCC Reaction using a Bulky Pd-NHC Complex

The initial time course data using ***C7*** as a precatalyst resulted in a more rapid reaction when compared to using ***C14***, where maximum yield was achieved in under 20 mins. Poisoning studies conducted on a reaction with such a fast rate would be both impractical and yield inaccurate results. The reaction temperature was therefore lowered to 60 °C from 80 °C, to slow down the reaction (Scheme 4.3).

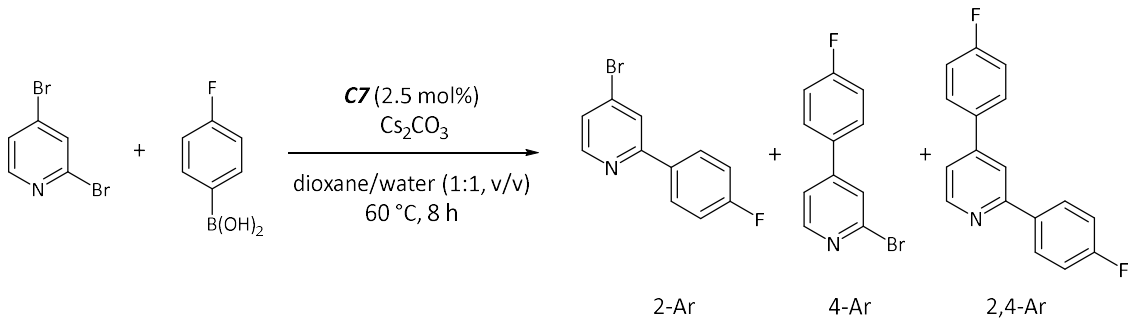

*Scheme 4.3 – Reaction between 2,4-dibromopyridine and p-fluorophenylboronic acid to yield 2-bromo-4-(p-fluorophenyl)pyridine (4-Ar), 2-(p-fluorophenyl)-4-bromo-pyridine (2-Ar) and 2,4-bis(p-fluorophenyl)pyridine (2,4-Ar) with **C7** as the precatalyst at lower reaction temperature (60 °C).*

The reaction profile when using the bulky complex, ***C7***, differs markedly from that of the non-bulky complex (Figure 4.11). The disubstituted product 2,4-Ar was the major product from the start of the reaction, with only a small amount of the mono-arylated products forming over time. Again, as with the non-bulky complex, there was seemingly no consumption of the mono-arylated products in the formation of the disubstituted product. Even at the reduced temperature of 60 °C the rate of reaction was still high, demonstrating that ***C7*** forms a highly active catalyst.

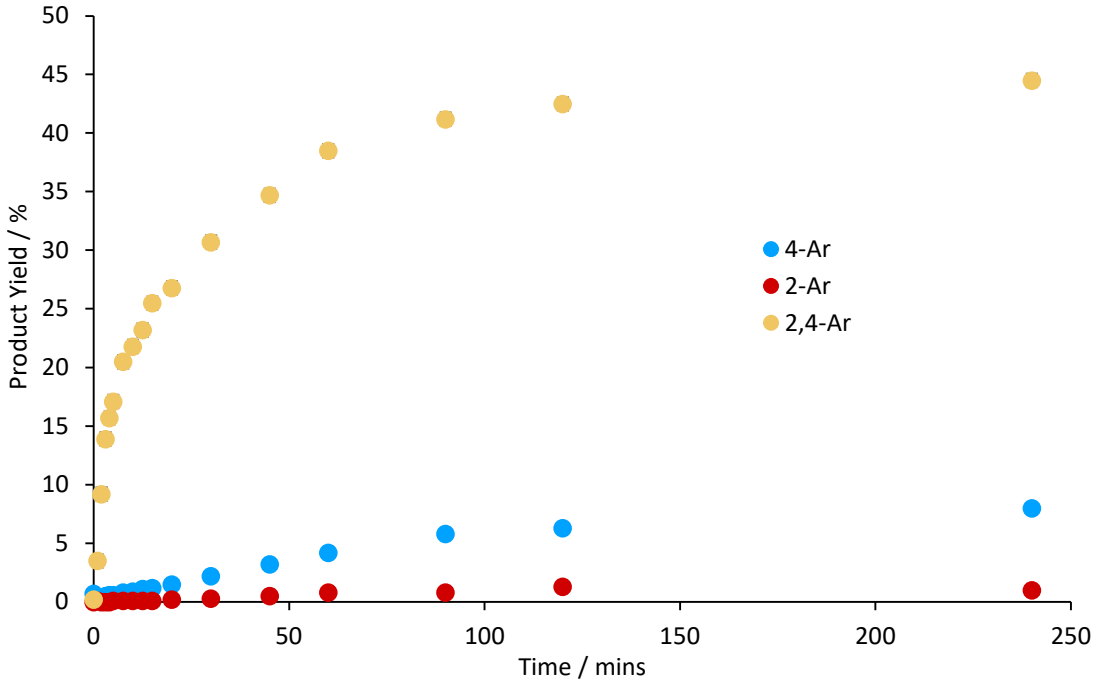

*Figure 4.11 – Time-course data showing product yields of 2-Ar, 4-Ar and 2,4-Ar for the reaction between 2,4-dibromopyridine and p-fluorophenylboronic acid using **C7** as the precatalyst. Product yields are determined by ^{19}F NMR spectroscopy with respect to FDMB internal standard. 60 °C reaction temperature. Error bars represent standard error.*

In comparison to the initial screening reaction with ***C7*** at 80 °C, further formation of the mono-arylated products were observed at 60 °C, which is not unexpected. This observation is due to a greater rate of formation of 2,4-Ar in the reaction at 80 °C, consuming the limiting reagents rapidly and preventing slower reactions from proceeding. Slowing the rate of 2,4-Ar formation would allow the slower mono-arylation reactions to progress more, thus a higher mono-arylated product yield is observed.

4.2.2.1 Kinetic Analysis of Bulky Pd-NHC Complex Time Course Data

For kinetic analysis of ***C7***, the model used to generate the optimal fit contained the same terms as the optimal model used for ***C14*** (Table 4.2). However, a better fit was achieved when using this model for the ***C7*** time course data (Figure 4.12).

*Table 4.2 – Compunetics model terms, their descriptions and calculated rate constants (k) for kinetic fitting to experimental data collected for the SMCC reaction between 2,4-dibromopyridine and p-fluorophenylboronic acid using **C7** as the precatalyst. Pyr = 2,4-dibromopyridine, BA = p-fluorophenylboronic acid, precat = **C7**, cat = active catalytic species and decat = deactivated catalyst.*

Model Term	Description	k value
precat + 2BA → cat	Precatalyst activation	269 M^2min^{-1}
Pyr + BA + cat → 4-Ar + cat	4-Ar formation	0.223 M^2min^{-1}
Pyr + BA + cat → 2-Ar + cat	2-Ar formation	0.0421 M^2min^{-1}
Pyr + 2BA + 2cat → 2,4-Ar + 2cat	2,4-Ar formation (concerted)	286 M^4min^{-1}
4-Ar + BA + cat → 2,4-Ar + cat	2,4-Ar formation (4-Ar consumption)	0 M^2min^{-1}
2-Ar + BA + cat → 2,4-Ar + cat	2,4-Ar formation (2-Ar consumption)	0 M^2min^{-1}
cat → decat	catalyst deactivation	0.00611 min^{-1}

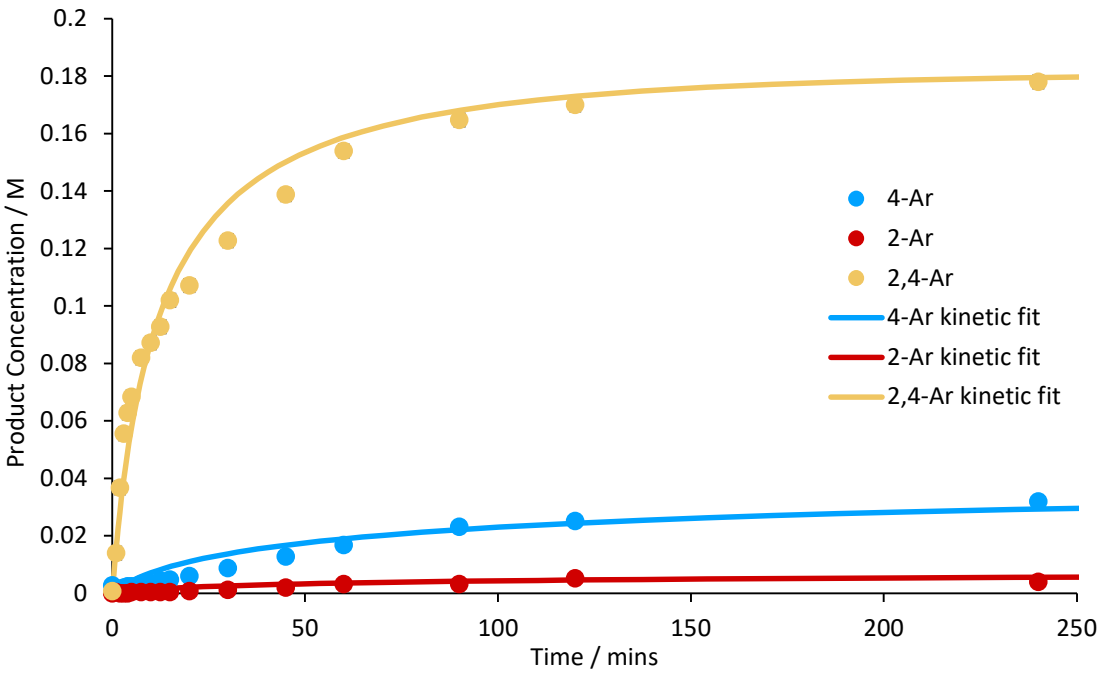

*Figure 4.12 – Time course data showing concentrations of 2-Ar, 4-Ar and 2,4-Ar for the reaction between 2,4-dibromopyridine and p-fluorophenylboronic acid using **C7** as the precatalyst. Error bars represent standard error. Kinetic fitting uses reaction model detailed in Table 4.2.*

Some key differences are observed in the rate constants associated with the terms of the kinetic model for ***C7*** and ***C14***. Firstly, the activation of ***C7*** is associated with a considerably larger rate constant when compared to ***C14***, 269 M^2min^{-1} and 59.6 M^2min^{-1} respectively. This is likely due to the larger sterics of the NHC ligand in ***C7*** facilitating the activation reaction more readily than in ***C14***. The specifics of this activation reaction are discussed in more detail in Chapter 5.1.1. The rate constants associated with the formation of the mono-arylated reaction products for ***C7***

share the same relationship as for ***C14***, with 4-Ar having a larger value and thus a higher rate of formation. Interestingly, the model suggests that there is no consumption of the mono-arylated products in the formation of 2,4-Ar and 2,4-Ar is formed through a concerted mechanism exclusively, with an associated rate constant of 286 M^4min^{-1}. Finally, the rate constants associated with the deactivation of the complexes is different, with ***C7*** having an almost 4-fold decrease with respect to ***C14***. This is likely due to the large sterics of the NHC ligand protecting ***C7*** from deactivation pathways more effectively than the comparatively small sterics of the NHC ligand in ***C14***.

4.2.2.2 Temperature Dependence

The screening reaction with ***C7*** at 80 °C showed a final 4-Ar yield of 4% (Figure 4.13), less than the 9% observed with the lowered reaction temperature of 60 °C, indicating that the selectivity of the bulky complex is somewhat temperature dependent, especially when selecting for 2,4-Ar. To investigate this further a reaction was conducted at a much lower temperature of 30 °C and product yields were measured over time. The reaction rate was much lower at 30 °C with completion achieved after 3 days, but the final product yields did indeed indicate temperature dependence (Figure 4.13). The reaction at 30 °C resulted in a final product yield of 17% for 4-Ar.

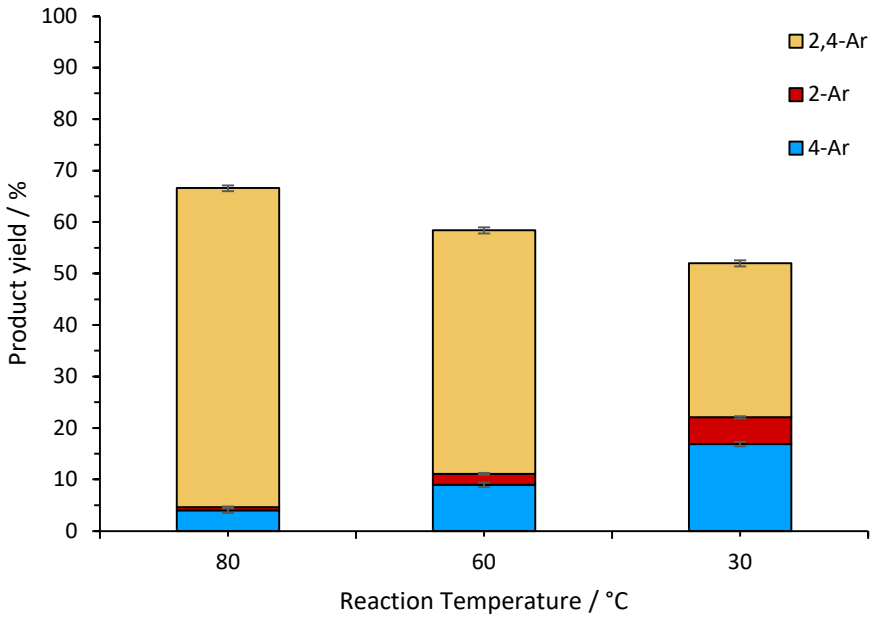

*Figure 4.13 – Product yields of 2-Ar, 4-Ar and 2,4-Ar for the reaction of 2,4-dibromopyridine and p-fluorophenylboronic acid using **C7** at reaction temperatures of 80 °C, 60 °C and 30 °C. Samples shown were taken upon reaction completion. Product yields are determined by ^{19}F NMR spectroscopy with respect to FDMB internal standard. Error bars represent standard error.*

This suggests that the general structure of the active catalytic species formed from the bulky and non-bulky complexes is similar. The enhanced 2,4-Ar selectivity for the bulky complexes could originate from an increased activity due to the NHC ligands steric bulk. Both bulky and non-bulky complexes were investigated further to build upon this hypothesis.

4.3 Determination of Catalyst Nature with Poisoning Reactions

4.3.1 Mercury Drop Test

The mercury drop test is widely used to probe whether a given transition metal-catalysed reaction proceeds *via* a homogeneous or heterogeneous route. Elemental mercury is added to a catalytic reaction in vast excess with respect to the catalyst and the reaction is sampled over time. A comparison of this reaction profile to a reaction without mercury can indicate the presence of a nanoparticle catalyst. The catalytic reaction will show a significant decrease in activity following the addition of elemental mercury in a heterogeneous system. This is due to the coating of any active metal nanoparticles in a layer of mercury atoms, which blocks active sites, thus, quenching reactivity (Figure 4.14). Alternatively, amalgamation of the nanoparticles into the bulk mercury would quench reactivity.[3]

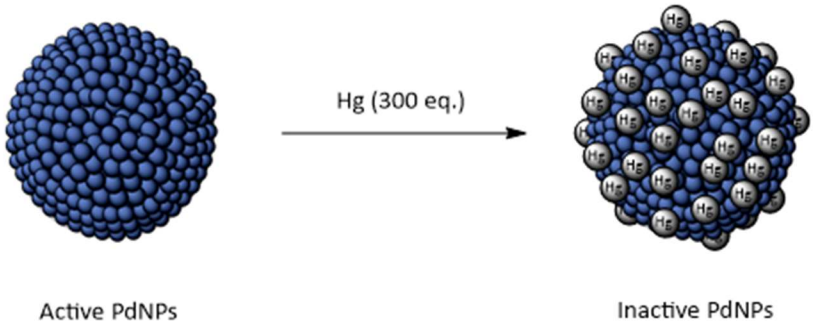

Figure 4.14 – Illustration showing the coating of an active palladium nanoparticle with elemental Hg during a mercury drop test resulting in an inactive palladium nanoparticle.

The mercury drop test is not infallible however, with recent work by Ananikov and co-workers suggesting that the test can provide false-positives for nanoparticle-catalysed reactions,[4] and generally provide inaccurate results for some homogeneous catalyst systems.[5] With this in mind, the mercury drop test was conducted on the SMCC of 2,4-dibromopyridine and *p*-fluorophenylboronic acid using the bulky and non-bulky complexes as precatalysts. The results from the mercury drop tests will not be used to determine the hetero/homogeneous nature of the reaction alone but will be used in combination with other tests to determine the catalytic nature. It is unclear with current understanding if the mercury drop test affects the activity of

cluster catalysts, such as the Coulson cluster (Figure 4.15).[2, 6, 7] Subsequently, the test will not be used to provide evidence for-or-against the involvement of clusters in the catalysis.

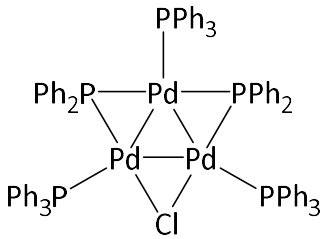

Figure 4.15 – Structure of the Coulson cluster.[6]

Using the time course reaction profiles above (Figure 4.9 and Figure 4.11), suitable times for addition of the mercury were determined for both ***C7*** and ***C14*** catalysed reactions, at 15 and 20 mins respectively. It is necessary for the reaction to proceed for a short time before adding the mercury to ensure the reaction is proceeding as expected and that the data following the mercury addition is reliable.

The profiles for the reactions catalysed by ***C14*** (Scheme 1.4) with and without mercury are shown on the same plot (top, Figure 4.16) and individually on smaller plots (bottom, Figure 4.16) for clarity. It was observed that the reactivity persists following the addition of the mercury to the reaction mixture as all product yields continued to rise. Additionally, the dominant product switched from being 4-Ar to 2,4-Ar, a feature that was observed in the absence of mercury, is evident even after the addition of mercury.

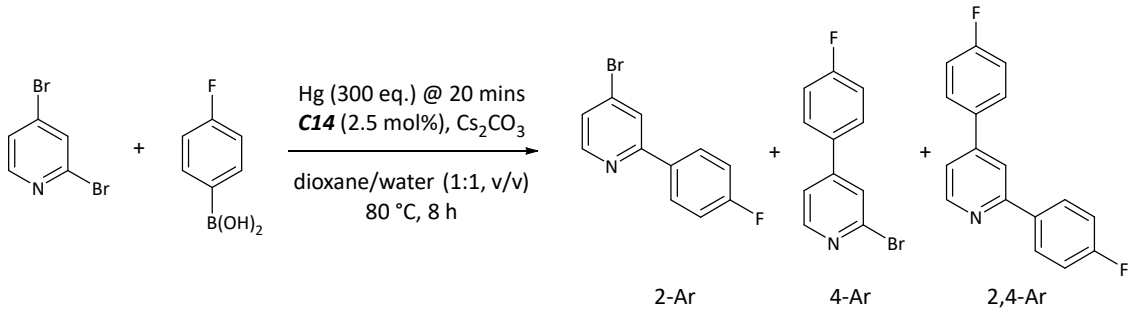

Scheme 4.4 *– Reaction between 2,4-dibromopyridine and p-fluorophenylboronic acid to yield 2-bromo-4-(p-fluorophenyl)pyridine (4-Ar), 2-(p-fluorophenyl)-4-bromo-pyridine (2-Ar) and 2,4-di(p-fluorophenyl)pyridine (2,4-Ar) with* ***C14*** *as the precatalyst. Hg was added after the reaction had proceeded for 20 mins.*

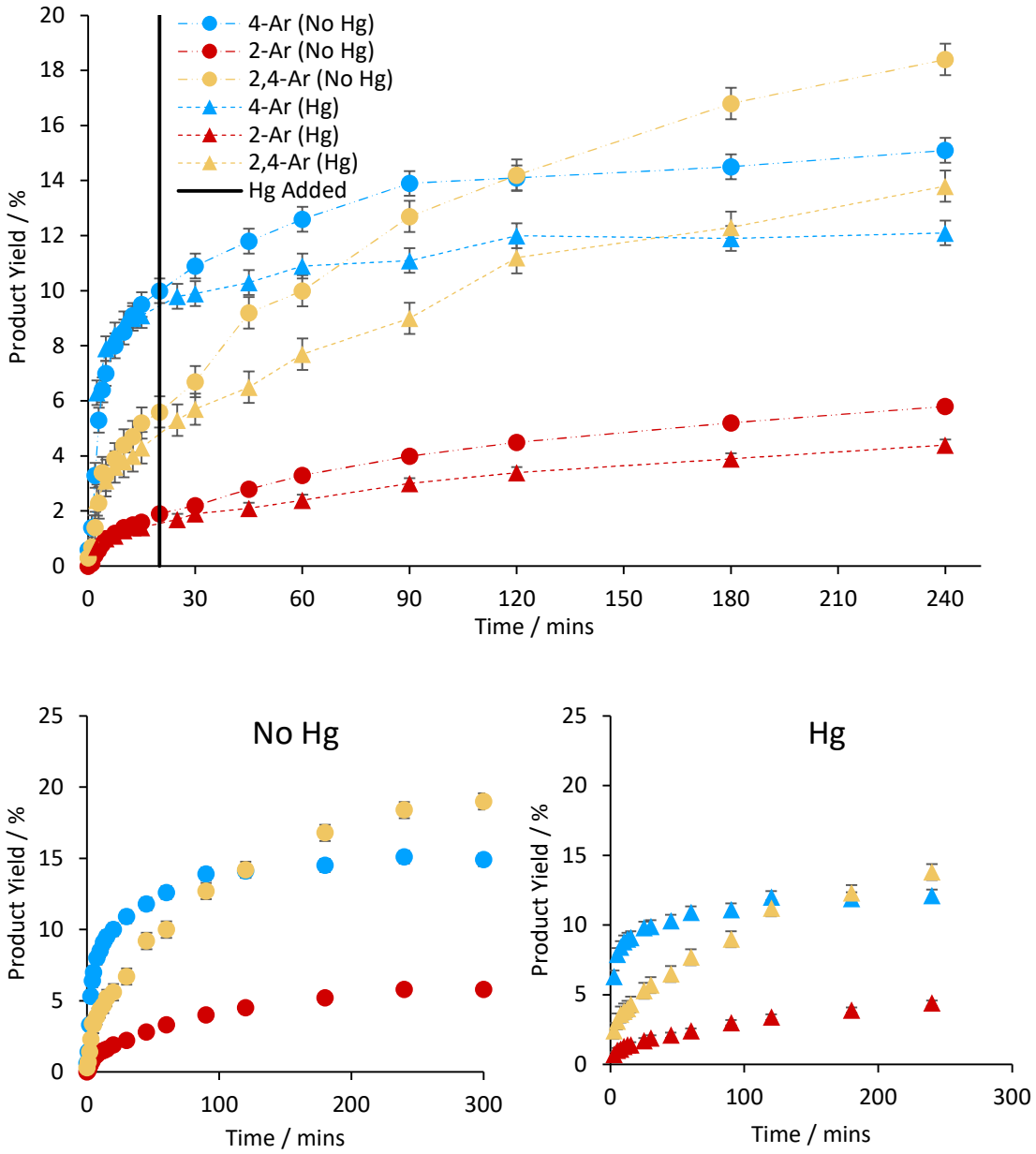

*Figure 4.16 – Mercury drop test data showing product yields of 2-Ar, 4-Ar and 2,4-Ar for the reaction between 2,4-dibromopyridine and p-fluorophenylboronic acid using **C14** as the precatalyst with and without mercury. Product yields are determined by ^{19}F NMR spectroscopy with respect to FDMB internal standard. Overlaid data (top) separate data without Hg (bottom left) and with Hg (bottom right). Error bars represent standard error. Dotted lines are for clarity of data and do not represent kinetic fitting.*

The two plots do not overlap however, this is likely due to the use of a larger volume Young's ampoule and higher rate of stirring of ca. 1250 rpm for the mercury drop test in comparison to the smaller reaction vial and ca. 750 rpm stirring rate for the other reactions. The rate of stirring is known in literature to have an effect on the product yield, especially when considering a biphasic reaction system.[8-10] Despite this, the overall product ratios (4-Ar:2-Ar:2,4-Ar) were similar in both reactions, 2.7:1.0:3.1 and 2.6:1.0:3.2, with and without mercury, respectively.

This may suggest that whilst using ***C14*** as the precatalyst, the reaction proceeds *via* a homogeneous pathway.

For the reaction catalysed by the bulky complex, ***C7***, the mercury was added after 15 mins (Scheme 4.5). Since 2,4-Ar is almost exclusively formed during this reaction, the other mono-arylated products are not shown in Figure 4.17. Similar to the reaction catalysed by the non-bulky complex, the catalytic activity is maintained following the addition of the mercury. Once again, the profiles do not overlay which was likely due to the aforementioned reasons. As with ***C14***, the results suggest that the reaction mechanism with ***C7*** involves a homogeneous pathway.

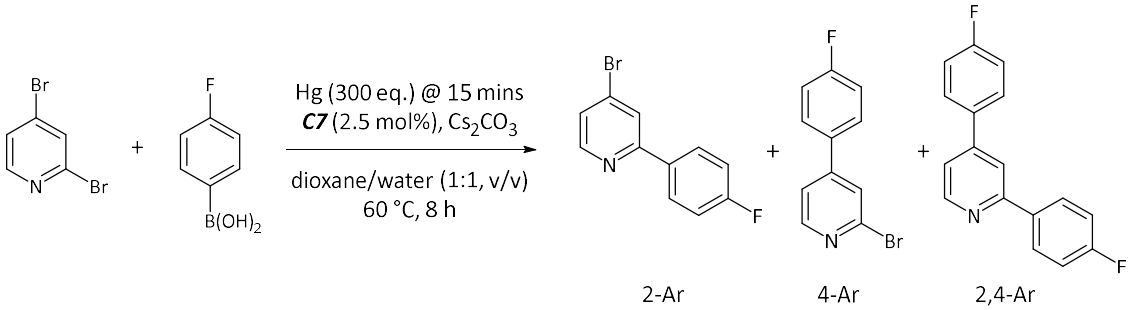

*Scheme 4.5 – Reaction between 2,4-dibromopyridine and p-fluorophenylboronic acid to yield 2-bromo-4-(p-fluorophenyl)pyridine (4-Ar), 2-(p-fluorophenyl)-4-bromo-pyridine (2-Ar) and 2,4-di(p-fluorophenyl)pyridine (2,4-Ar) with **C7** as the precatalyst. Hg was added after the reaction had proceeded for 15 mins.*

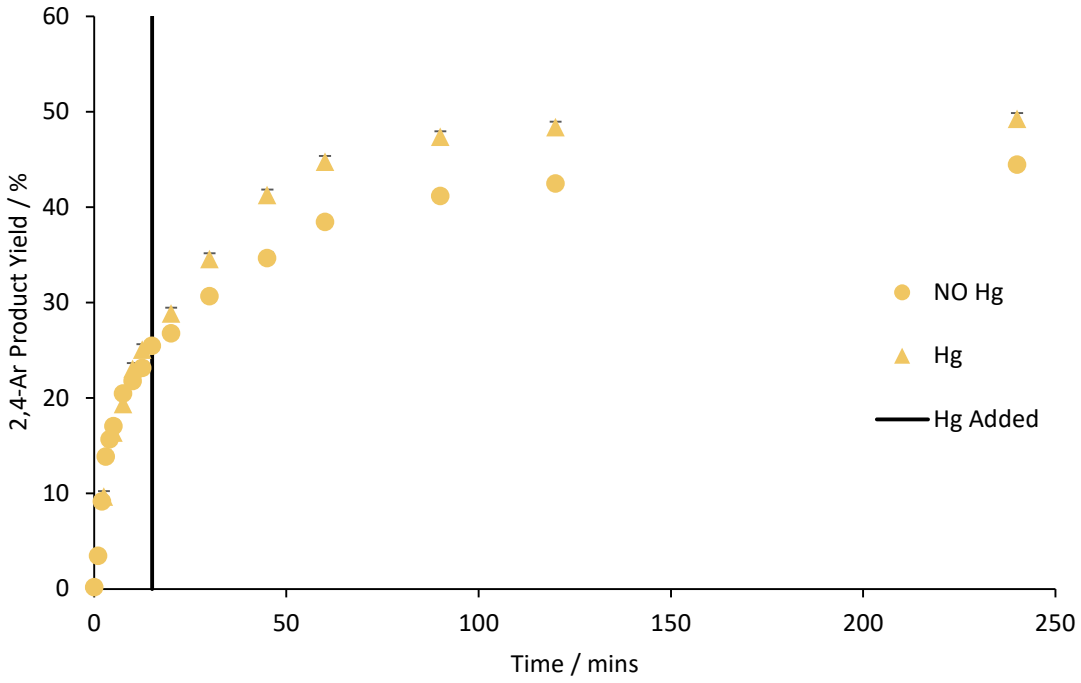

*Figure 4.17 – Mercury drop test data showing product yields of 2-Ar, 4-Ar and 2,4-Ar for the reaction between 2,4-dibromopyridine and p-fluorophenylboronic acid using **C7** as the precatalyst with and without mercury. Product yields are determined by ^{19}F NMR spectroscopy with respect to FDMB internal standard. 60 °C reaction temperature. Error bars represent standard error.*

4.3.2 Polyvinylpyridine (PVPy) Poisoning

Polyvinylpyridine (PVPy) is known to strongly bind to solubilised Pd(II) ions and, as a result, can poison a catalytic reaction that utilises Pd(II) ions during the catalytic cycle. PVPy poisoning has been used in conjunction with the mercury drop test in identifying if an active catalytic species is homo/heterogeneous in nature.[11-13] The PVPy is used in vast excess to the catalyst and acts as a multidentate ligand for any Pd(II) species in solution, occupying all vacant coordination sites and presumably replacing all labile ligands, thus rendering the palladium catalytically inactive (Figure 4.18).

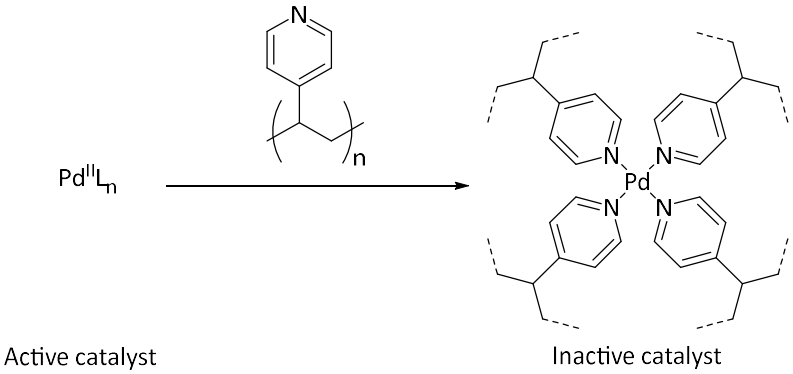

Figure 4.18 – Illustration showing the trapping of a Pd(II) species with polyvinyl pyridine (PVPy) during a PVPy poisoning reaction resulting in coordinatively saturated palladium.

As with the mercury drop test, it is necessary to ensure the catalytic reaction is proceeding normally before the addition of the PVPy. The PVPy (40 eq. WRT palladium) was therefore added after 20 mins for the reaction using the non-bulky complex, ***C14***, as the precatalyst (Scheme 4.6).

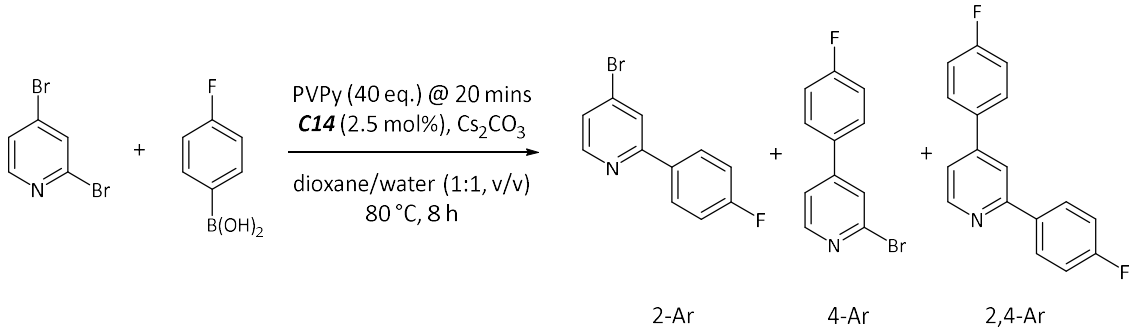

*Scheme 4.6 – Reaction between 2,4-dibromopyridine and p-fluorophenylboronic acid to yield 2-bromo-4-(p-fluorophenyl)pyridine (4-Ar), 2-(p-fluorophenyl)-4-bromo-pyridine (2-Ar) and 2,4-di(p-fluorophenyl)pyridine (2,4-Ar) with **C14** as the precatalyst. PVPy was added after the reaction had proceeded for 20 mins.*

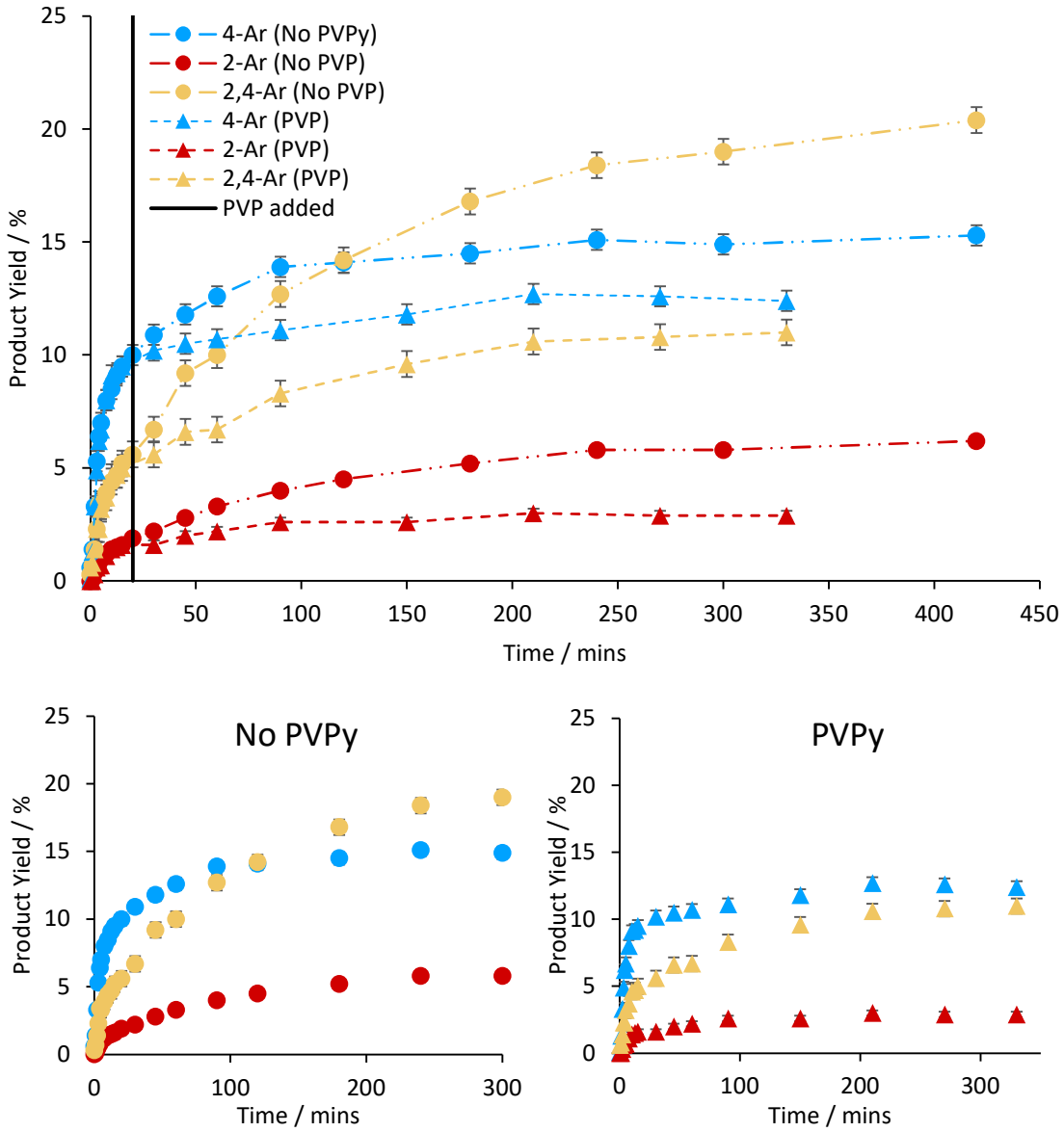

*Figure 4.19 – PVPy poisoning data showing product yields of 2-Ar, 4-Ar and 2,4-Ar for the reaction between 2,4-dibromopyridine and p-fluorophenylboronic acid using **C14** as the precatalyst with and without mercury. Product yields are determined by ^{19}F NMR spectroscopy with respect to FDMB internal standard. Overlaid data (top) separate data without PVPy (bottom left) and with PVPy (bottom right). Error bars represent standard error. Dotted lines are for clarity of data and do not represent kinetic fitting.*

The reaction profiles collected for the PVPy poisoning for the reaction catalysed by ***C14*** has several interesting features (Figure 4.19). As with the mercury drop test, the reaction profile before the addition of PVPy is almost identical to the control profile, signifying any discrepancies after the addition of PVPy are due to the PVPy. All the products had a reduced final yield, and their profiles begin to deviate from the control profile following the PVPy addition. It is also worth noting that a key feature of the control profile, namely the switch in dominant product from 4-Ar to 2,4-Ar, is not present in the reaction using PVPy (Figure 4.19, bottom). 2,4-Ar does continue to increase in yield following the PVPy addition but at a significantly slower rate than would be expected if no catalyst poisoning had occurred. All of this suggests that the active

catalytic species in the reaction has been poisoned to some extent and thus, for the reaction catalysed by the non-bulky complex (***C14***), the active species is homogeneous in nature.

Again, as with the mercury drop test, the PVPy was added after 15 mins to the reaction catalysed by the bulky complex, ***C7*** (Scheme 4.7). The reaction profile following the addition of the PVPy is different to the control profile, however, product is clearly still being formed (Figure 4.20). This could be due to the bulky nature of the NHC preventing full coordination to the PVPy and thus full deactivation of the active catalytic species. Alternatively, the formation of 2,4-Ar could be catalysed partially by palladium clusters as it is unclear from literature if PVPy causes deactivation of palladium clusters.

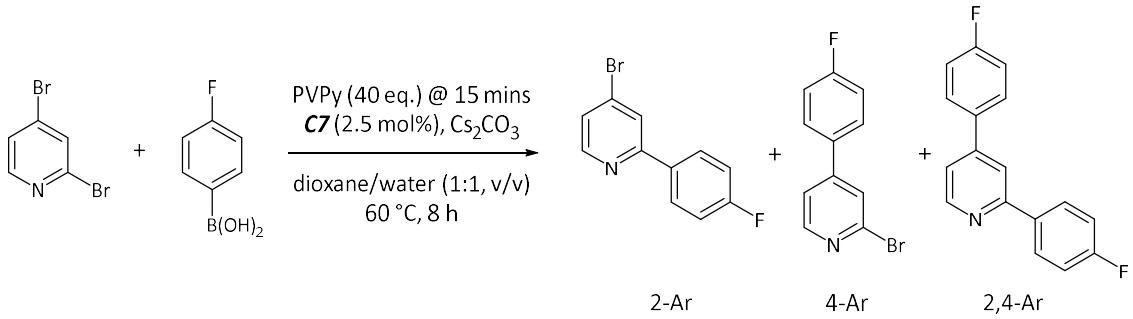

*Scheme 4.7 – Reaction between 2,4-dibromopyridine and p-fluorophenylboronic acid to yield 2-bromo-4-(p-fluorophenyl)pyridine (4-Ar), 2-(p-fluorophenyl)-4-bromo-pyridine (2-Ar) and 2,4-di(p-fluorophenyl)pyridine (2,4-Ar) with **C7** as the precatalyst. PVPy was added after the reaction had proceeded for 15 mins.*

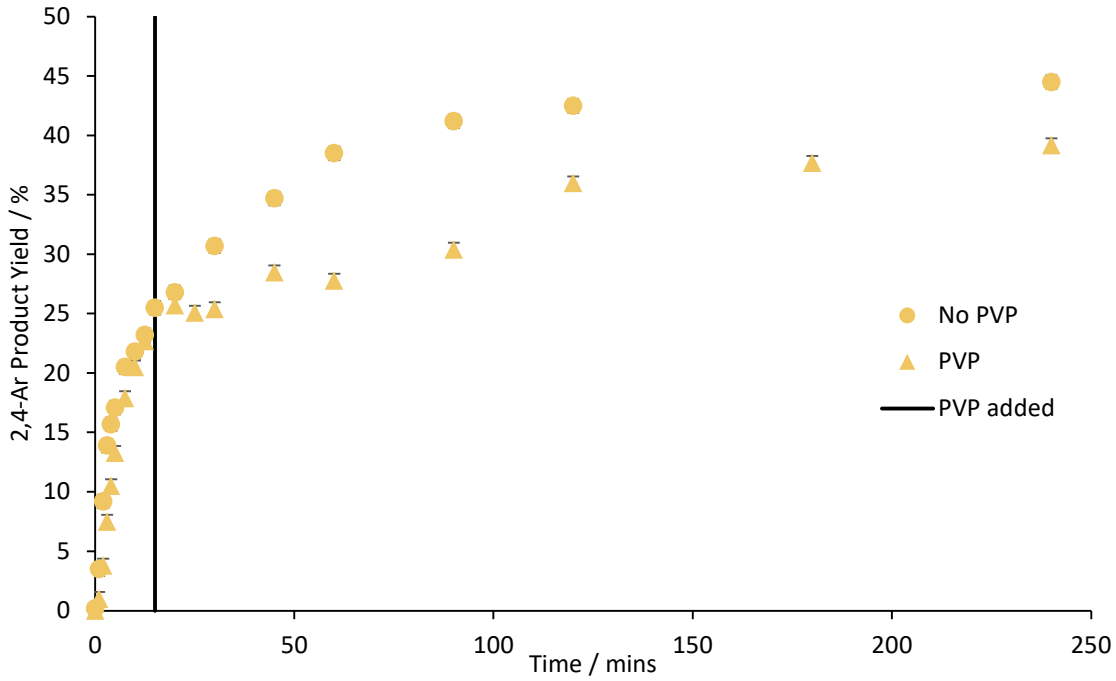

*Figure 4.20 – PVPy poisoning data showing product yields of 2-Ar, 4-Ar and 2,4-Ar for the reaction between 2,4-dibromopyridine and p-fluorophenylboronic acid using **C7** as the precatalyst with and without mercury. Product yields are determined by ^{19}F NMR spectroscopy with respect to FDMB internal standard. 60 °C reaction temperature. Error bars represent standard error.*

The data from both the mercury drop tests and PVPy poisoning reactions indicate that, when employing Pd-NHC complexes as precatalysts for the SMCC reaction of interest, the catalyst system is homogeneous in nature. Further methodologies could be employed to test this more thoroughly, such as the three-phase test where one coupling partner is immobilised on a porous support and the consumption of the other coupling partner would give evidence for homogeneity.[2] As discussed previously however (Chapter 3.1.4.1 and Chapter 3.1.4.2), the method for sample workup and analysis is not suitable to measure reagent consumption accurately and therefore the three-phase test is not applicable.

4.4 Mechanistic Reasoning for Site-Selectivity when using Pd-NHC Complexes

The evidence collected thus far on the site-selectivity of the SMCC reaction using complexes ***C1***–***C14***, and further investigations into the catalyst nature and behaviour under certain conditions, have given a strong basis from which a general mechanism can be proposed.

4.4.1 Related Literature Mechanism

Recent publications by Neufeldt and co-workers report the abnormal (4-Ar^{Cl}) selectivity in the SMCC reaction of 2,4-dichloropyridine with arylboronic acid when using complexes ***C7*** and ***C8*** (Scheme 4.8, Figure 4.21).[14-17] Other dihaloarene substrates exhibiting abnormal selectivity with palladium catalyst systems are also reported, including the abnormal 4-Ar selectivity when using 2,4-dibromopyridine as the substrate with ***C7***, though it is noted that a significant amount of 'over-arylation' occurs (2,4-Ar selectivity), mirroring the results reported in this investigation.[15] The focus of Neufeldt's work in these publications is to elucidate a mechanism for the abnormal selectivity in the 2,4-dichloropyridine system using DFT calculations on proposed reaction intermediates.[16, 17]

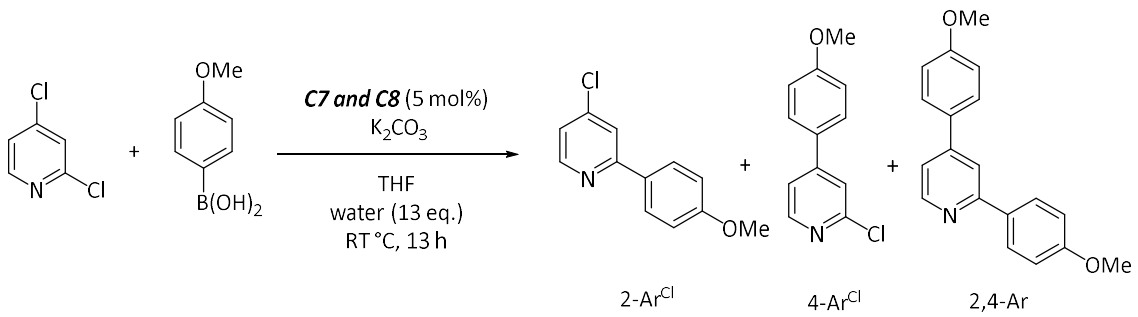

*Scheme 4.8 – Reaction between 2,4-dichloropyridine and p-methoxyphenylboronic acid to yield 2-bromo-4-(p-methoxyphenyl)pyridine (4-Ar), 2-(p-methoxyphenyl)-4-bromo-pyridine (2-Ar) and 2,4-bis(p-methoxyphenyl)pyridine (2,4-Ar) with **C7** and **C8** as precatalysts. Conditions from Neufeldt.[15-17]*

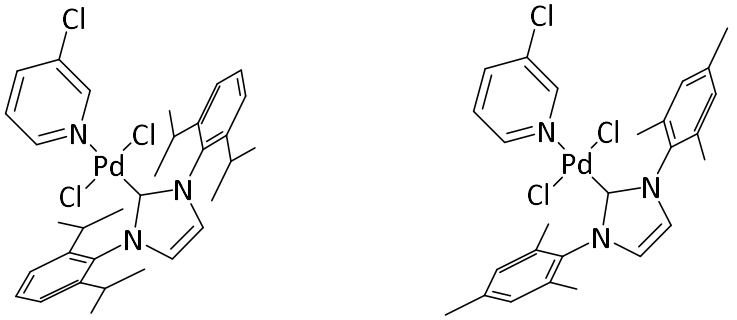

*Figure 4.21 – Structures of Pd-NHC complexes **C7** and **C8** used in Neufeldts work.*

The oxidative addition step of the reaction is the most important in determining product selectivity, *i.e*. oxidative addition of the 4-Cl bond onto palladium would result in formation of the 4-Ar^{Cl} product. It was found that mono-ligated Pd(0) ('***PdL***') and bis-ligated Pd(0) ('***PdL₂***') favoured oxidative addition at different sites of the substrate due to their respective HOMO symmetries.[16, 17] ***PdL*** is defined as Pd(0)-NHC and ***PdL₂*** as Pd-NHC-(substrate) where the substrate is nitrogen bound 2,4-dichloropyridine.

When employing an NHC with diisopropylphenyl *N*-substituents (***C7***), oxidative addition of the 4-Cl bond was energetically favourable over the 2-Cl bond and followed a 3-centred concerted mechanism with a ***PdL*** active species (Figure 4.22). The ***PdL₂*** system favoured oxidative addition of the 2-Cl bond and followed a displacement (or S_NAr type) intermediate pathway, however, this pathway was higher in energy than the ***PdL*** concerted oxidative addition pathway and thus explains their experimentally observed 4-Ar^{Cl} selectivity. The difference in energy between the ***PdL*** and ***PdL₂*** oxidative addition pathways is less pronounced when using an NHC ligand with mesityl *N*-substituents (***C8***), which was again consistent with their experimental data where weaker 4-Ar^{Cl} selectivity is observed.

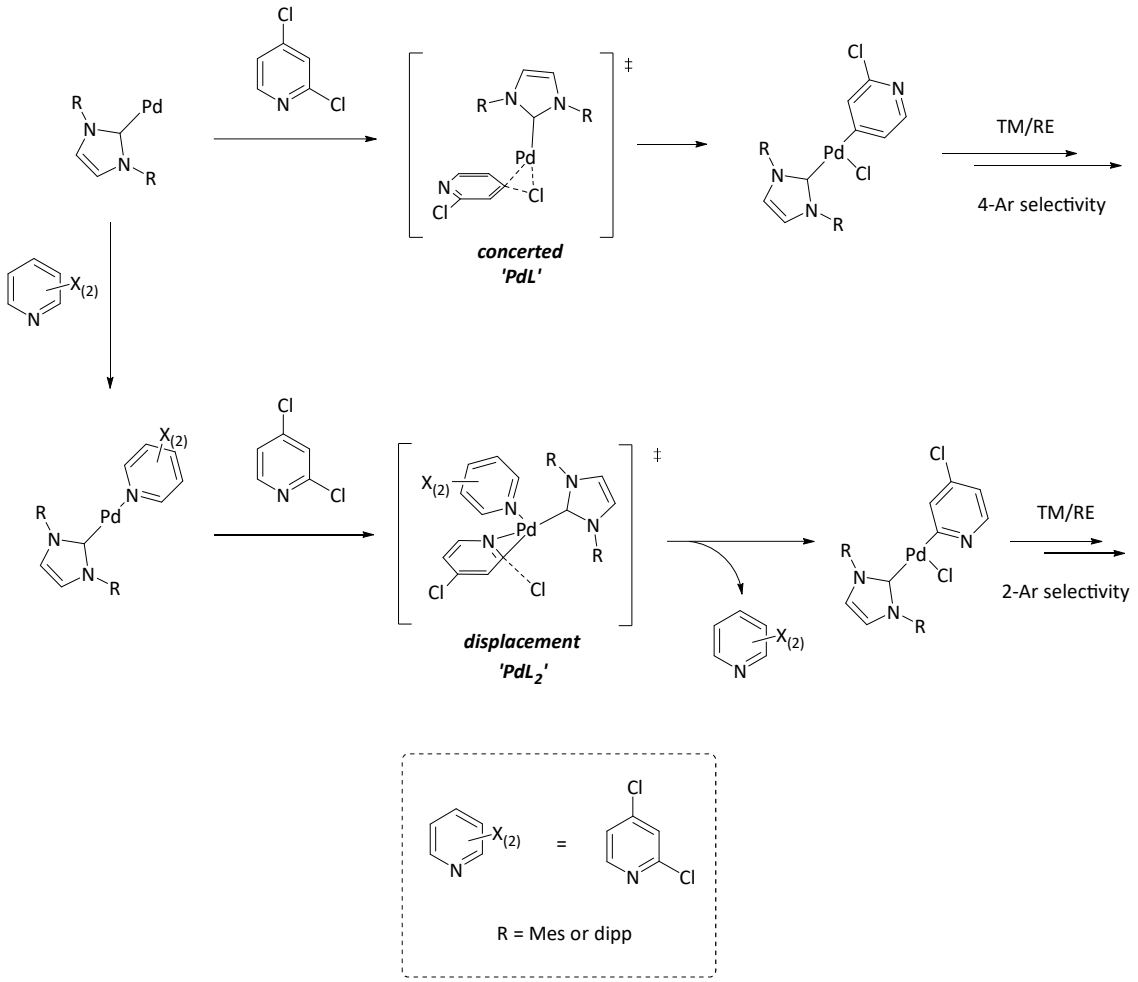

*Figure 4.22 – General mechanism determined by Neufeldt and co-workers for the oxidative addition of Pd-NHC (**PdL**) or Pd-NHC-pyridine (**PdL$_2$**) onto dichloropyridine at the 4-Cl or 2-Cl position respectively. Adapted from literature.[16]*

The authors report that some additional factors may somewhat influence the reaction selectivity, notably the coordination of the substrate pyridine to any acidic species present in solution (*e.g*. K^+ from the base, boron or water) could reduce the likelihood of PdL_2 formation and thus enhance 4-Ar^{Cl} selectivity.[16, 17] Conversely, an increased concentration of substrate with respect to the catalyst could promote PdL_2 formation and enhance 2-Ar^{Cl} selectivity.

4.4.2 Site-Selectivity in the 2,4-Dibromopyridine System

The findings of Neufeldt's investigations aid in understanding the product selectivity observed in the investigations conducted here.[16, 17] The relative bond dissociation energies for 2-Cl and 4-Cl in 2,4-dichloropyridine, and 2-Br and 4-Br in 2,4-dibromopyridine share a linear relationship and as such would be expected to share similar site-selectivities for a given catalyst system. Therefore, when applying the rationale of Neufeldt to the cross coupling of 2,4-dibromopyridine and arylboronic acid with Pd-NHC catalysts the same abnormal 4-Ar selectivity is expected. This is indeed observed for all of the non-bulky Pd-NHC complexes (***C1***–***C6***, ***C9***–***C14***), where 4-Ar is

formed predominantly over 2-Ar (Figure 4.2) and for the bulky Pd-NHC complexes (***C7*** and ***C8***) when used in reactions at lower temperatures (Figure 4.13).

For the formation of 4-Ar then, it is proposed that a catalytically active mono-ligated Pd-NHC species undergoes oxidative addition with the 4-Br bond (Figure 4.23), analogously to the concerted pathway described by Neufeldt (Figure 4.22). From this transmetalation and reductive elimination can ensue to generate 4-Ar. Again, assuming an analogous mechanism to Neufeldt, 2-Ar is proposed to form through oxidative addition with the 2-Br bond by the ***PdL₂*** or displacement mechanism followed by transmetalation and reductive elimination of 2-Ar. The identity of the second ligand in ***PdL₂*** (where NHC is the first) for the non-bulky complexes could either be a second NHC ligand (from a ligand exchange reaction for example) or one of multiple pyridine species in the reaction mixture. A second NHC ligand would likely remain bound following the oxidative addition whereas a pyridine would not. The large NHC steric environment of ***C7*** and ***C8*** make the formation Pd-NHC_2 very unlikely and as such the second ligand would be a pyridine species present in the reaction.[16]

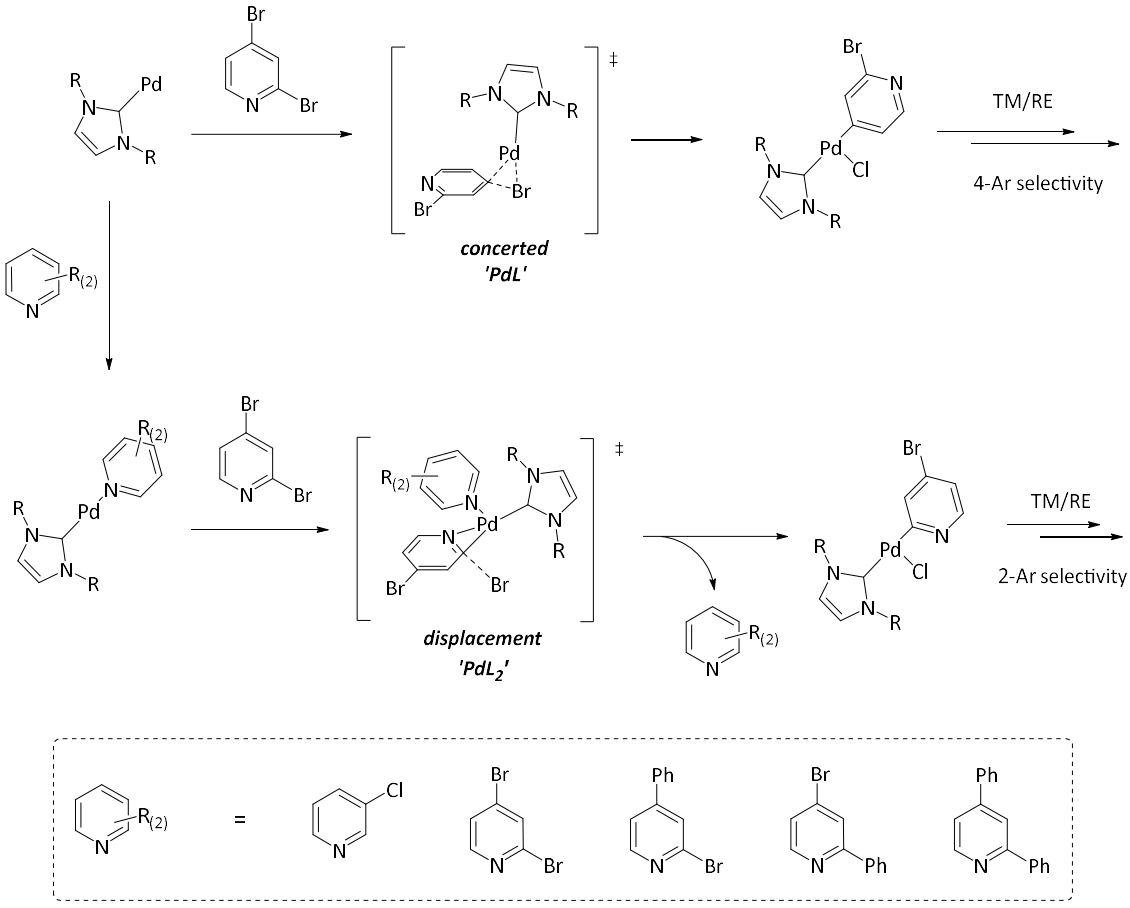

*Figure 4.23 – Proposed mechanism for 2-Ar and 4-Ar selectivity with complexes **C1–C14** in the reaction of interest. Mechanism was derived from experimental data and literature evidence.[16, 17]*

4.4.3 Rational for High Yields of 2,4-Ar when Using Bulky Pd-NHC complexes

Going further to predict how 2,4-Ar would form relies on experimental evidence that 2,4-Ar forms concertedly (Chapter 4.2.2) The most feasible formation of 2,4-Ar commences by coordination of the 4-Br oxidative addition product to a second Pd-NHC species through the exposed pyridinyl nitrogen (Pathway 2, Figure 4.24). The placement of this second palladium proximal to the 2-Br bond would facilitate the second oxidative addition step, either by the concerted or displacement mechanism. From here successive transmetalation and reductive elimination steps would generate 2,4-Ar.

Formation of the double oxidative addition product from the 2-Br oxidative addition product could also occur but it expected to be less favourable as pyridinyl coordination does not place the second palladium proximal to the 4-Br bond.

This rationale for 2,4-Ar formation with Pd-NHC complexes (***C1***–***C14***) could also offer an explanation as to why the bulky complexes form 2,4-Ar almost exclusively. It is proposed that the 4-Br oxidative addition product goes on to react in one of two ways, either through transmetalation and reductive elimination to form 4-Ar (Pathway 1, Figure 4.24) or by the second oxidative addition of Pd-NHC and resulting transmetalation and reductive elimination steps to form 2,4-Ar (Pathway 2, Figure 4.24). The relative rates of the transmetalation in pathway 1 and oxidative addition of pathway 2 would influence the selectivity of 4-Ar with respect to 2,4-Ar.

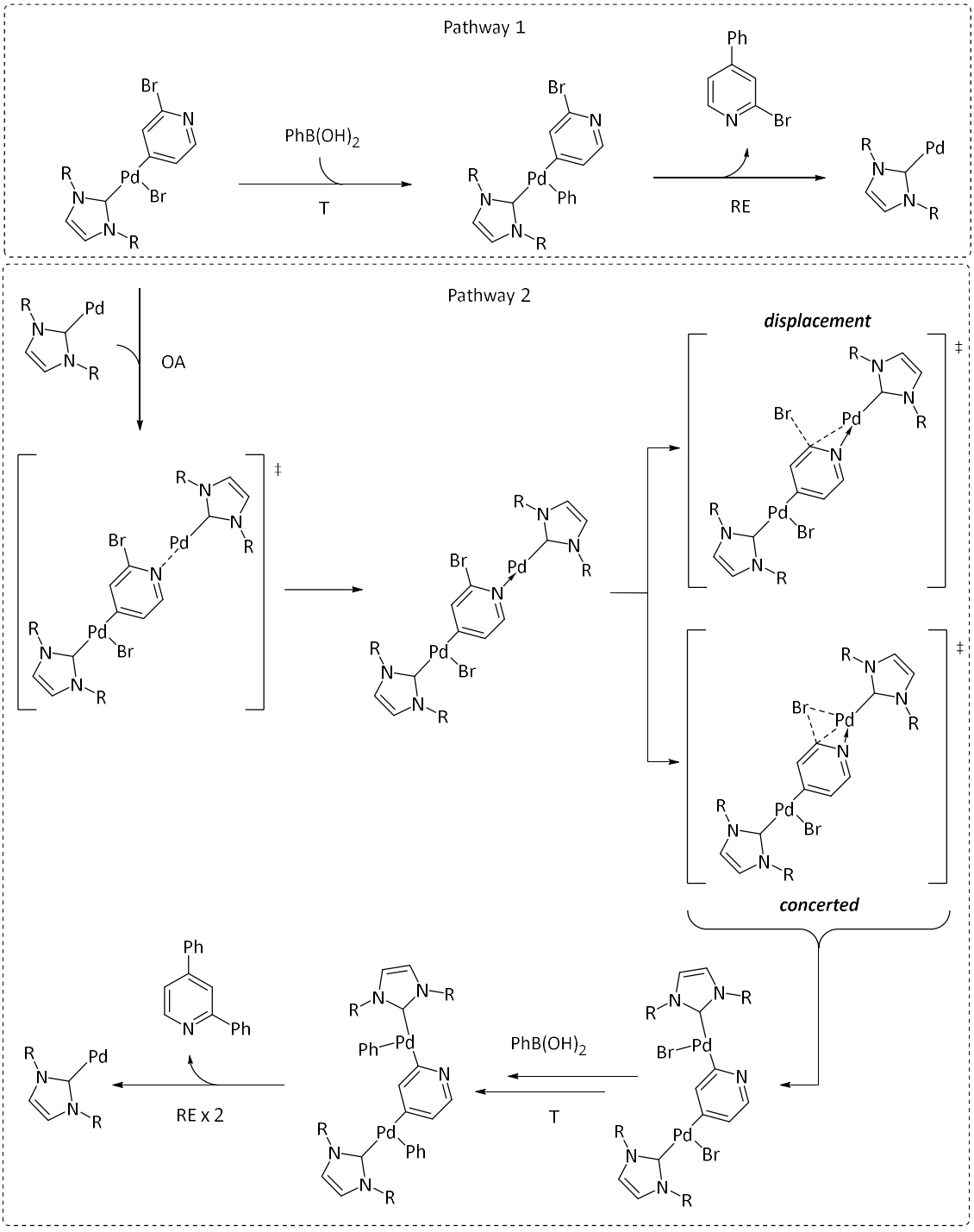

Figure 4.24 – Pathway 1 - from the oxidative addition product proposed from Figure 4.23, transmetalation (T) and reductive elimination (RE) occurs to form the mono-arylated catalytic products. Pathway 2 - concerted formation of 2,4-Ar through pyridine coordination of the oxidative addition product and oxidative addition to a second palladium, followed by successive transmetalation and reductive elimination reactions.

Considering the sterics of the bulky NHC ligands, the transmetalation step may be unfavourable due to introducing steric clashes between the ligand and coordinated phenyl group, thus reducing the rate of transmetalation (Figure 4.25). Ligand sterics have been shown to effect the rate of transmetalation with phosphine ligand environments.[18] Reducing the rate of transmetalation could therefore increase the propensity for the second oxidative addition step

and therefore 2,4-Ar would form more readily, as is observed experimentally in the complex screening reaction. Conversely, a less bulky NHC ligand environment would display more competitive relative rates of transmetalation and oxidative addition (Figure 4.25), therefore selecting more strongly for 4-Ar over 2,4-Ar, again this matches the screen data.

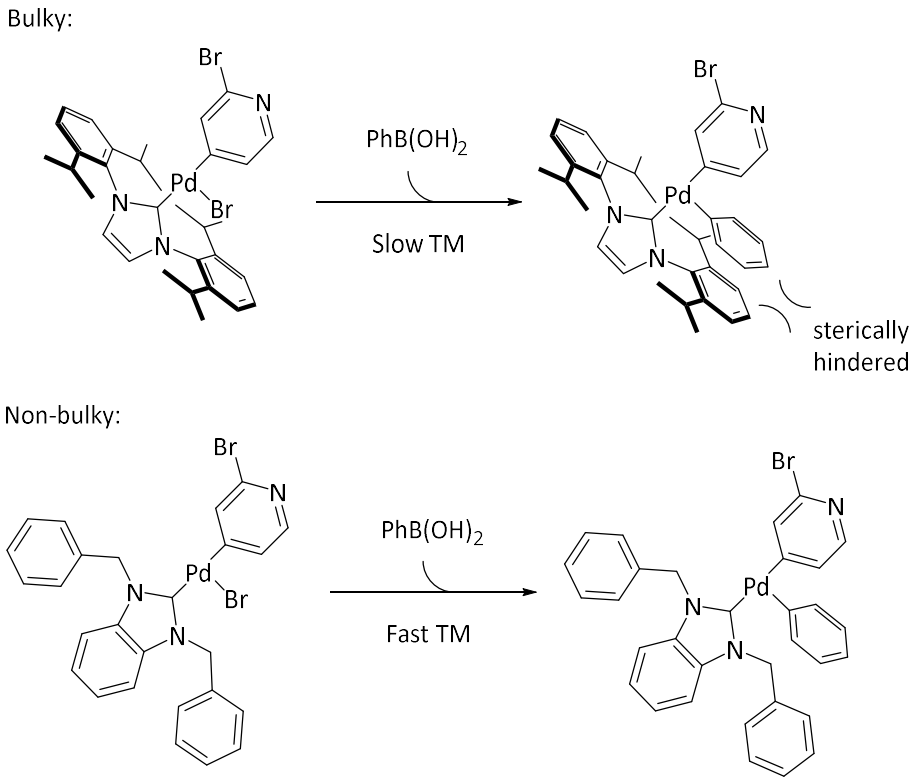

Figure 4.25 – General transmetalation (TM) reaction for the oxidative addition products of 2,4-dibromopyridine and Pd-NHC to show how large NHC ligand sterics may induce steric hinderance thus making the reaction less favourable.

A plot of idealised rate constants vs temperature was generated to show how the NHC ligand sterics alter the selectivity of 4-Ar over 2,4-Ar (Figure 4.26). The rate constants used here were calculated using the Arrhenius equation with a modification to include a steric factor (x) to the frequency coefficient for transmetalation (A) (Equation 4.1), a reasonable assumption considering larger steric environments will negatively influence interactions proximal to the palladium.[18] Idealised activation energies were used to illustrate the point more clearly.

$$k = (x)Ae^{\frac{-Ea}{RT}}$$

Equation 4.1 – Modified Arrhenius equation where: x is a steric factor of the NHC ligand (0 < x < 1), A is the frequency coefficient, E_a is activation energy, R is the ideal gas constant and T is temperature.

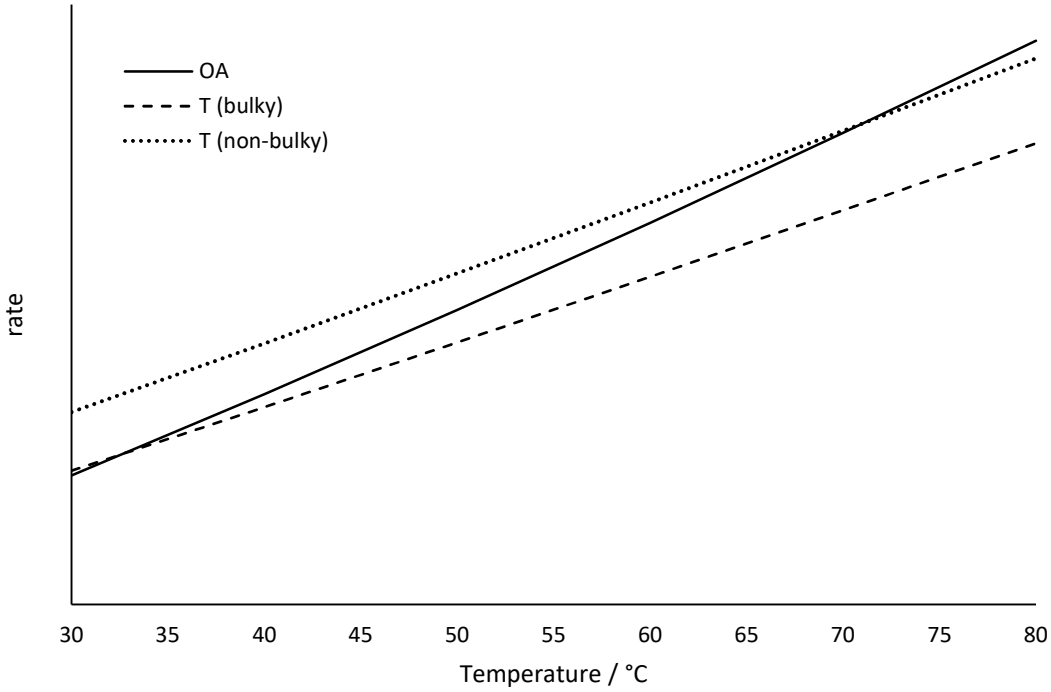

Figure 4.26 – Idealised plot of reaction rate constant over a temperature range (30 °C – 80 °C) for oxidative addition (OA) and transmetalation (T) for bulky and non-bulky NHC ligands.

This simplified model shows that for a bulky NHC (large steric factor) at low temperatures the rates of transmetalation and oxidative addition are similar and, as such, 4-Ar and 2,4-Ar would form competitively. At increased temperatures the rate of oxidative addition is greater than transmetalation and 2,4-Ar selectivity would be expected. This parallels the experimental results on the temperature dependence of the bulky complex discussed earlier. Decreasing the steric factor for less bulky NHC ligands increases the relative rate of transmetalation and therefore competitive selectivity is expected at higher temperatures, also observed experimentally.

4.5 Summary

The site-selectivity in the reaction of interest catalysed by Pd-NHC complexes ***C1***–***C14*** was probed through a screening reaction where all 14 complexes were found to be catalytically active and, for the most part, shared similar reaction outcomes. 4-Ar was formed predominantly over 2-Ar in all cases when using the non-bulky complexes but no obvious structure activity relationship was apparent. Bulky complexes, ***C7*** and ***C8***, induce a different selectivity to the other complexes tested, forming 2,4-Ar almost exclusively, and time course reactions show how the catalytic product yields change over the course of the reaction. The evidence gathered indicates that 2,4-Ar is formed concertedly under these reaction conditions and using Pd-NHC complexes as the precatalyst.

Poisoning reactions applied to reactions using the bulky and non-bulky complexes indicate that a homogeneous catalyst system is in operation, though it is noted that the NHC steric profile may cause some interference in the PVPy poisoning reaction. It was also shown that the bulky complex site-selectivity is temperature dependent, with 2,4-Ar more prominent at higher temperatures and selectivity more typical of the non-bulky complexes at lower temperatures.

With these observations, and the aid of literature mechanistic studies by Neufeldt and co-workers on a related catalytic system, a mechanism was proposed that accounts for the site-selectivity of the complexes and offers reasonable assumptions on how 2,4-Ar is generated in the reaction. Though this mechanism has not been tested quantitatively, through the use of DFT and specific kinetic investigations into individual proposed steps of the catalytic cycle, it is built upon reliable experimental evidence, reasonable assumptions drawn from applicable literature. Further investigations into this complex catalytic system have a solid platform to build upon.

4.6 References

1. J. M. Fowler, E. Britton, C. M. Pask, C. E. Willans and M. J. Hardie, *Dalton Trans.*, 2019, **48**, 14687-14695.
2. N. W. J. Scott, M. J. Ford, N. Jeddi, A. Eyles, L. Simon, A. C. Whitwood, T. Tanner, C. E. Willans and I. J. S. Fairlamb, *J. Am. Chem. Soc.*, 2021, **143**, 9682-9693.
3. J. A. Widegren and R. G. Finke, *J. Mol. Catal. A: Chem.*, 2003, **198**, 317-341.
4. V. M. Chernyshev, A. V. Astakhov, I. E. Chikunov, R. V. Tyurin, D. B. Eremin, G. S. Ranny, V. N. Khrustalev and V. P. Ananikov, *ACS Catal.*, 2019, **9**, 2984-2995.
5. O. N. Gorunova, I. M. Novitskiy, Y. K. Grishin, I. P. Gloriozov, V. A. Roznyatovsky, V. N. Khrustalev, K. A. Kochetkov and V. V. Dunina, *Organometallics*, 2018, **37**, 2842-2858.
6. F. Fu, J. Xiang, H. Cheng, L. Cheng, H. Chong, S. Wang, P. Li, S. Wei, M. Zhu and Y. Li, *ACS Catal.*, 2017, **7**, 1860-1867.
7. J. Campos, A. Nova, E. L. Kolychev and S. Aldridge, *Chemistry (Easton)*, 2017, **23**, 12655-12667.
8. E. Monti, A. Ventimiglia, C. A. Garcia Soto, F. Martelli, E. Rodríguez-Aguado, J. A. Cecilia, A. Sadier, F. Ospitali, T. Tabanelli, S. Albonetti, F. Cavani, R. Wojcieszak and N. Dimitratos, *Catalysts*, 2022, **12**.
9. M. Schrimpf, P. A. Graefe, A. Holl, A. J. Vorholt and W. Leitner, *ACS Catal.*, 2022, **12**, 7850-7861.
10. R. L. Jezorek, M. Enayati, R. B. Smail, J. Lejnieks, S. Grama, M. J. Monteiro and V. Percec, *Polymer Chemistry*, 2017, **8**, 3405-3424.
11. K. Yu, *J. Catal.*, 2004, **226**, 101-110.
12. K. Q. Yu, W. Sommer, J. M. Richardson, M. Weck and C. W. Jones, *Adv. Synth. Catal.*, 2005, **347**, 161-171.
13. A. J. Reay, L. A. Hammarback, J. T. W. Bray, T. Sheridan, D. Turnbull, A. C. Whitwood and I. J. S. Fairlamb, *ACS Catal.*, 2017, **7**, 5174-5179.
14. E. K. Reeves, E. D. Entz and S. R. Neufeldt, *Chemistry (Easton)*, 2021, **27**, 6161-6177.
15. J. P. Norman, N. G. Larson, E. D. Entz and S. R. Neufeldt, *J. Org. Chem.*, 2022, **87**, 7414-7421.
16. J. P. Norman, N. G. Larson and S. R. Neufeldt, *ACS Catal.*, 2022, **12**, 8822-8828.
17. J. P. Norman and S. R. Neufeldt, *ACS Catal.*, 2022, **12**, 12014-12026.
18. M. L. Clarke and M. Heydt, *Organometallics*, 2005, **24**, 6475-6478.

Chapter 5

Further Evaluation of the Mechanistic Rationale Through Stoichiometric reactions, Pre-Arylation Reactions and Side-Product Analysis

In the previous chapter (Chapter 4), the site-selectivity using complexes ***C1***–***C14*** in the SMCC reaction of 2,4-dibromopyridine and *p*-fluorophenylboronic acid was displayed and explored, resulting in a viable mechanistic rationale being proposed for the site-selectivity and the abundant formation of 2,4-Ar in reactions using the bulky complexes. To build upon this, further investigations were conducted to rigorously understand the processes involved in the catalytic reaction. The catalytic activation of the complexes was scrutinised with considerations of how the stabilisation of the generated active species may occur. HRMS studies were conducted to aid in the elucidation of any possible active species at various points during the reaction and to identify low-concentration by-products of catalyst speciation or deactivation. The hypothesis of the concerted formation of 2,4-Ar was also probed further, through the investigation of 2,4-Ar formation from 2-Ar and 4-Ar independently. General mechanisms for this were proposed using experimental data. Finally, the formation of an unusual palladium structure identified from catalyst waste collections was discussed. All of this was conducted to gain a greater breadth of understanding of the nuances of this reaction.

5.1 Stoichiometric Reactions of Studied using NMR Spectroscopy

One of the most valuable ways to investigate the nature of a catalyst for a particular reaction is to perform a stoichiometric study, which involves the reaction of an equivalent amount of catalyst/precatalyst with one of the starting materials for the reaction of interest. The starting material is selected on the assumption that it is the first species to interact with the catalytic/precatalytic species, mimicking the interactions taking place at the start of a catalytic cycle. Since there are no other reactants present to progress the cycle, the reaction is held in a semi-stable state where the nature of the first intermediate species may be investigated through spectroscopy. The technique provides a deep insight into the first stages of the catalysis and can aid in suggesting a rational mechanism for the reaction in question.

The complexes under investigation act as precatalysts for the coupling reaction of interest and, as such, the first interaction is that of the complex with aryl boronic acid to generate the assumed active catalytic species. The generally accepted route of activation for complexes featuring the PEPPSI architecture is with two consecutive transmetalation reactions of the

complex using arylboronic acid, replacing the chloride ligands with aryl groups (Figure 5.1).[1, 2] Reductive elimination of biphenyl from the palladium centre then occurs, leaving the palladium in a zero oxidation state (Figure 5.1), ready to begin the catalytic cycle by oxidative addition of the aryl halide. It is thought that the coordinated pyridine ligand readily dissociates during this process to form a Pd(0)L active species.

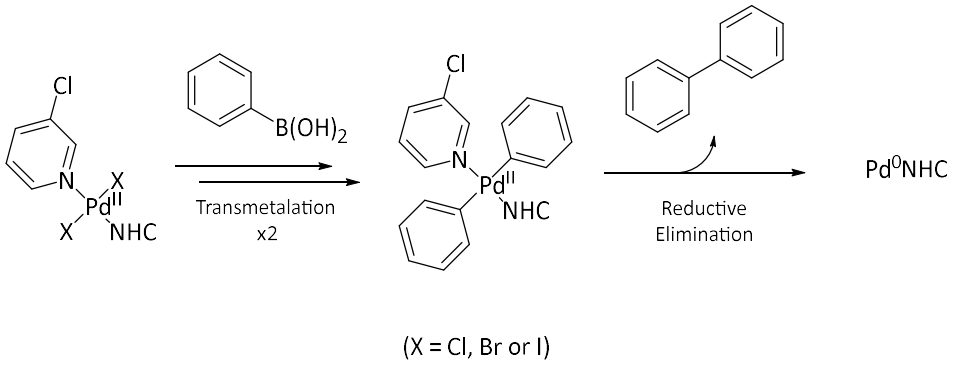

Figure 5.1 – Generally accepted activation route for PEPPSI precatalysts: Two successive transmetalation reactions followed by reductive elimination to form the catalytically active Pd(0) species.

Though the activation pathway for the complexes of interest in general SMCC reactions is known, these investigations are still important to determine if the catalytic activation differs from the expected pathway, and if any species can be identified to account for the abnormal selectivity in this SMCC reaction. Complex ***C4*** was used to investigate the activation considering the ligand environment of the NHC is the simplest of all the complexes synthesised (Figure 5.2). Analysis by ^{1}H NMR spectroscopy would clearly show any differences between the parent complex and any palladium ligand environment following the activation, as it was previously established that the NHC ligand remains bound to the palladium during catalysis (Chapter 4.1.1).

A control was established by adding ***C4*** to the catalysis solvent mixture (dioxane/water (1:1, v:v)) and subjecting it to reaction temperature (80 °C) for 1 hour, to ensure that auto-activation does not occur. There was no change to the colour of the solution or to the ^{1}H NMR spectroscopic data for the complex after this treatment, confirming that no auto-activation had occurred. This ^{1}H NMR spectrum was used as a benchmark to compare to those of later stoichiometric reactions.

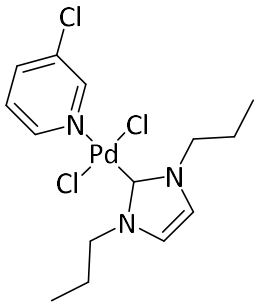

C4

*Figure 5.2 – Structure of **C4**, Pd-NHC complex with n-propyl N-substituents.*

5.1.1 Catalytic Activation of Non-Bulky Pd-NHC Complexes – 1:2 Study

The first stoichiometric study involved the reaction of ***C4*** and two equivalents of *p*-fluorophenylboronic acid (Scheme 5.1), in order to mimic the accepted activation mechanism discussed previously (Figure 5.1). Significant amounts of palladium black formed very soon after this reaction was initiated (Figure 5.3), suggesting that the palladium had been successfully reduced by *p*-fluorophenylboronic acid, but the Pd(0) species was not stable against agglomeration.

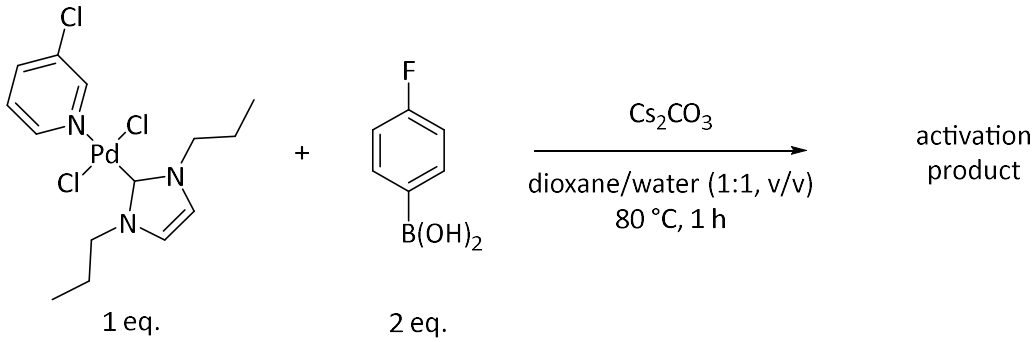

*Scheme 5.1 – 1:2 reaction between **C4** and p-fluorophenylboronic acid to determine the activation route and identify any activation products. Standard catalytic reaction conditions were used.*

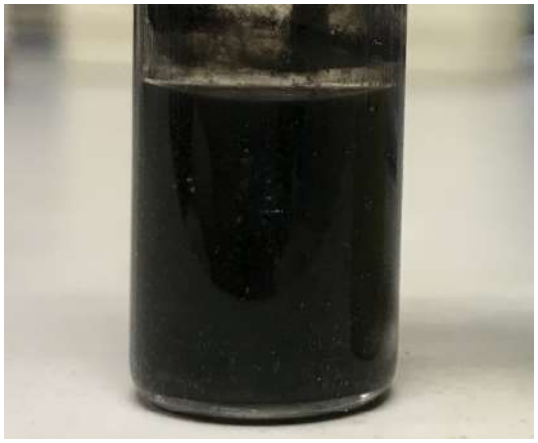

Figure 5.3 – Photograph of the reaction mixture outlined in Scheme 5.1. Significant palladium black generation has occurred.

The reaction mixture was filtered to remove the palladium deposits and then analysed by ^{1}H NMR spectroscopy (Figure 5.4). The signals associated with the coordinated 3-chloropyridine of the parent complex (***C4***, Figure 5.5) shifted significantly following the reaction and indicated ligand dissociation. The signals associated with the NHC ligand are no longer present after the reaction. The loss of these signals is not unexpected as the NHC ligand would likely have remained bound to the palladium after the activation of the precatalyst, and during the ensuing speciation to form the palladium black. This surface bound NHC would be removed from the reaction by filtration of the palladium black prior to the NMR analysis. Also observed in the NMR spectrum is 4,4'-difluorobiphenyl (Figure 5.5) in equal amounts to the dissociated 3-chloropyridine, indicating the activation proceeds *via* the expected route (Figure 5.1).

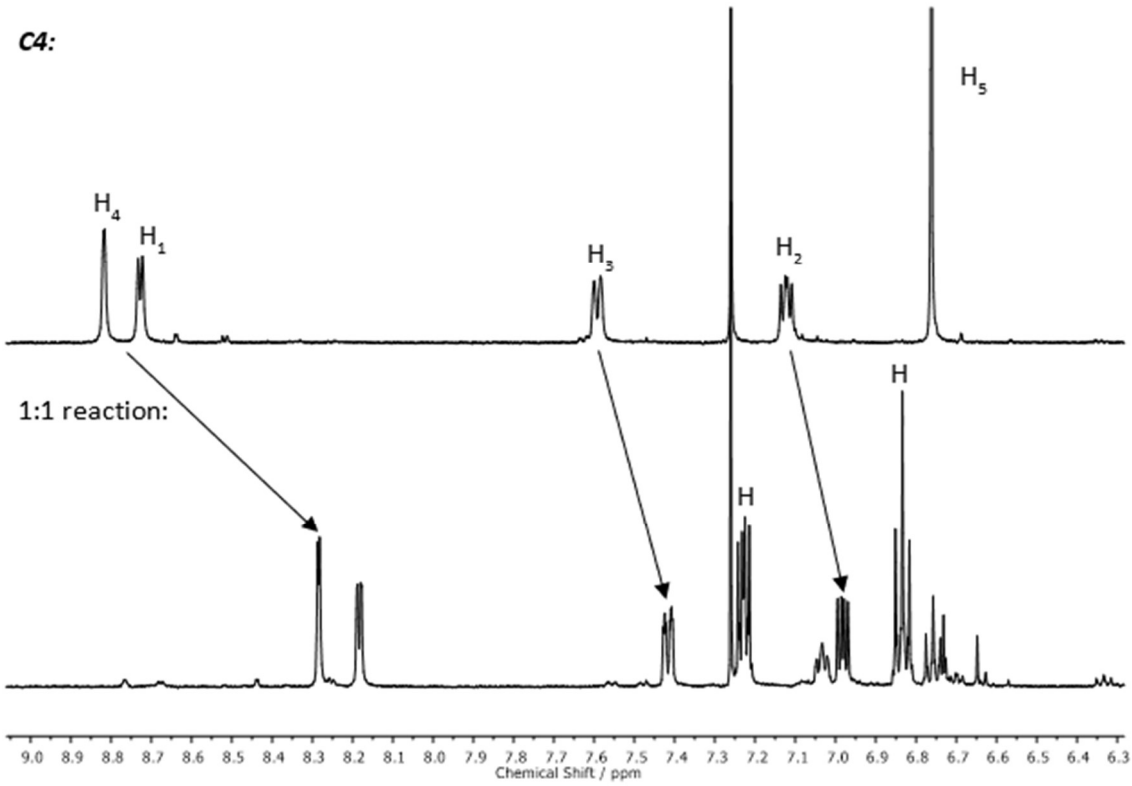

*Figure 5.4 – Stacked ^{1}H NMR spectra (500 MHz, chloroform-d) of **C4** and the reaction mixture outlined in Scheme 5.1. Shifted protons relating to dissociation of 3-chloropyridine (H_{1-4}), NHC backbone (H_5) disappearance and homocoupled 4,4'difluorobiphenyl (H_6 and H_7) appearance indicated.*

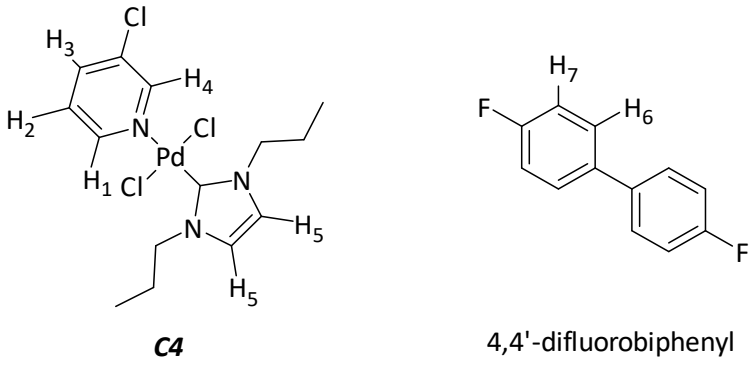

C4 4,4'-difluorobiphenyl

*Figure 5.5 – Structures of **C4** and 4,4'difluorobiphenyl with relevant protons for ^{1}H NMR spectroscopic analysis indicated.*

5.1.2 Partial Catalytic Activation of Non-Bulky Pd-NHC Complexes – 1:1 Study

A second analogous reaction was performed with ***C4*** and one equivalent of *p*-fluorophenylboronic acid to investigate the effect of incomplete/partial activation of the complex (Scheme 5.2). As in the previous reaction, a considerable amount of palladium black was observed, once again indicating the activation of the precatalyst and subsequent speciation to form insoluble palladium deposits.

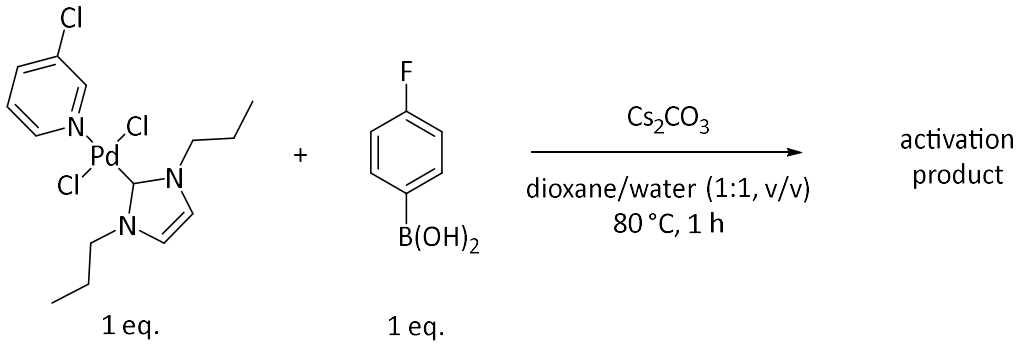

*Scheme 5.2 – 1:1 reaction between **C4** and p-fluorophenylboronic acid to determine the activation route and identify any activation products. Standard catalytic reaction conditions were used.*

It was thought that the ^{1}H NMR spectrum following the reaction would be very similar to that of the first stoichiometric reaction, differing only with the inclusion of signals from unreacted ***C4***, however this was not observed. The *n*-propyl *N*-substituents of the NHC ligand had seemingly become rotationally locked into position, removing proton degeneracy, and resulting in much more complicated splitting patterns for the non-terminal protons (Figure 5.6).

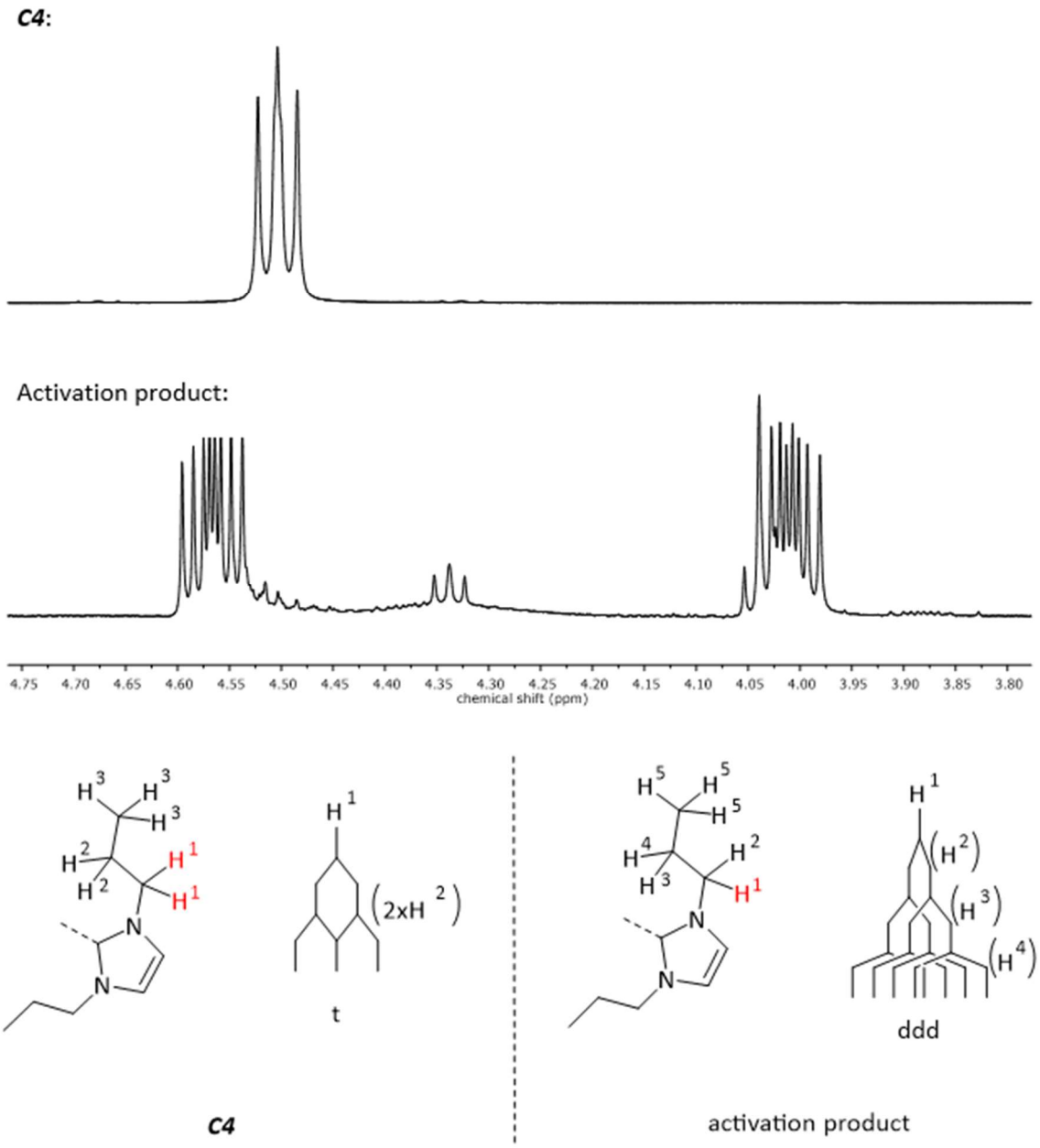

*Figure 5.6 – Stacked ^{1}H NMR spectra (500 MHz, chloroform-d) of **C4** and the reaction mixture outlined in Scheme 5.2, showing the clear difference in the NHC N-substituent N**CH$_2$**C protons. The splitting pattern for the specific protons in C4 and the activation product are shown.*

Fortunately, this product could be crystallised from the NMR sample and single-crystal X-ray diffractometry (SC-XRD) showed that the product of this reaction was a *cis*-NHC palladium complex, ***C15*** (Figure 5.7). The NHC *N*-substituent signal locking in the ^{1}H NMR spectrum is likely due to the proximity of the two NHC ligands on the palladium, preventing rotation and removing proton degeneracy (Table 5.1). Similar structures have previously been reported through the isomerisation of a *trans*-NHC$_2$ palladium complex or by directed synthesis, and corresponding ^{1}H NMR spectroscopic data shows similar *N*-substituent rotational locking.[3, 4] The instantaneous

formation of this *cis*-NHC_2 palladium complex under catalytic conditions is seemingly unreported in literature.

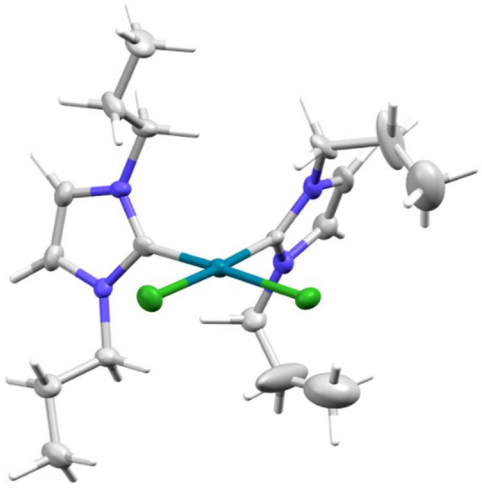

Figure 5.7 – Structure (left) and SC-XRD image (right) of the activation product, ***C15****, of the (1:1) reaction outlined in Scheme 5.2. Note $CHCl_3$ solvent structure removed from SC-XRD structure for clarity. Thermal ellipsoids are at 50% probability level.*

Table 5.1 – Showing the Pd-C (NHC) and Pd-Cl bond distances and C-Pd-C and Cl-Pd-Cl bond angles for ***C15****, determined by SC-XRD.*

Pd–C distance / Å	Pd–Cl distance / Å	C–Pd–C angle / deg	Cl–Pd–Cl angle / deg
1.990 (10)	2.363 (3)	90.9 (4)	92.33 (10)
1.966 (10)	2.348 (3)		

The reaction to form this complex only differs from the previous reaction by having one less equivalent of *p*-fluorophenylboronic acid. The same reaction pathway likely proceeds here to initially form the activated palladium intermediate (Pd(0)-NHC), which could then undergo some ligand exchange process with the unreacted parent complex present in solution to yield the *cis*-NHC_2 Pd(II) complex and Pd(0) (Scheme 5.3). Interestingly however, the ^{1}H NMR spectra from this reaction shows a 1:4 molar ratio of 4,4'-difluorobiphenyl to ***C15***, much greater than the 1:1 molar ratio expected. The increased molar ratio observed could either indicate that some 4,4'-diflourobiphenyl was removed during the reaction workup or that the initial formation of ***C15*** by ligand exchange somehow facilitates the formation of more ***C15***. This is as yet unexplained and requires further investigation.

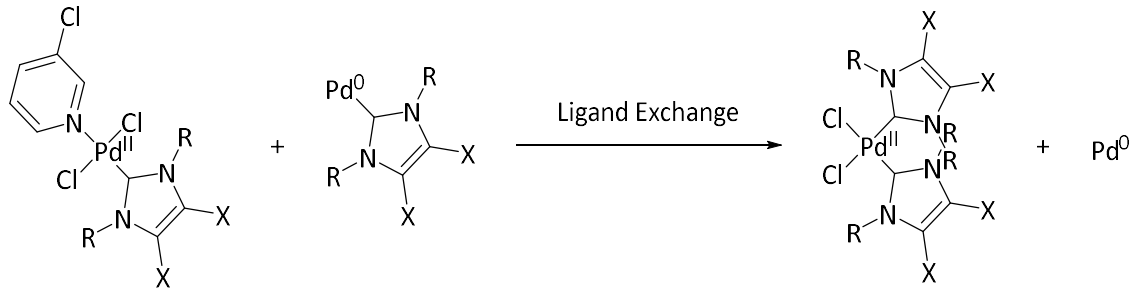

Scheme 5.3 – Proposed ligand exchange reaction to explain the formation of a bis-NHC-Pd(II) complex, ***C15****, from a Pd(II)-NHC and Pd(0)-NHC complexes.*

Assuming the formation of the *cis*-NHC complex does proceed as outlined (Scheme 5.3), it would be reasonable to infer that this mechanism may also be present in the full catalytic reaction, where both a Pd(II)-NHC species and Pd(0)-NHC species may be present simultaneously. As discussed previously (Chapter 4.4) the bulky Pd-NHC complexes are assumed to be unable to undergo this ligand exchange to form either a *cis*- or *trans*- Pd-NHC_2 complex due to steric clashes between the NHC ligands.[5] With application of the previously proposed mechanistic rationale for the selectivity of Pd-NHC complexes in the reaction of interest (Chapter 4.4.2), it would be expected that ***C15***, following activation by palladium reduction, would be 2-Ar selective in the catalytic reaction. It is expected, however, that 2-Ar formation is primarily due to a Pd-NHC with an N-bound pyridine, as in Neufeldt's rationale.[5]

5.1.3 Catalytic Cycle Progression of Non-Bulky Pd-NHC complexes - 1:2:1 Study

The addition of 2,4-dibromopyridine to the stoichiometric reactions was also investigated. It has already been established that the reduction of the precatalyst occurs with *p*-fluorophenylboronic acid, however, the generated Pd(0) species is not stable and rapidly undergoes speciation to form palladium black. Inclusion of the 2,4-dibromopyridine would facilitate the first step of the catalytic cycle, *i.e*. oxidative addition. This may allow the palladium to occupy a more stable Pd(II) state and prevent rapid deactivation. Again, the reaction was performed under standard reaction conditions (Scheme 5.4).

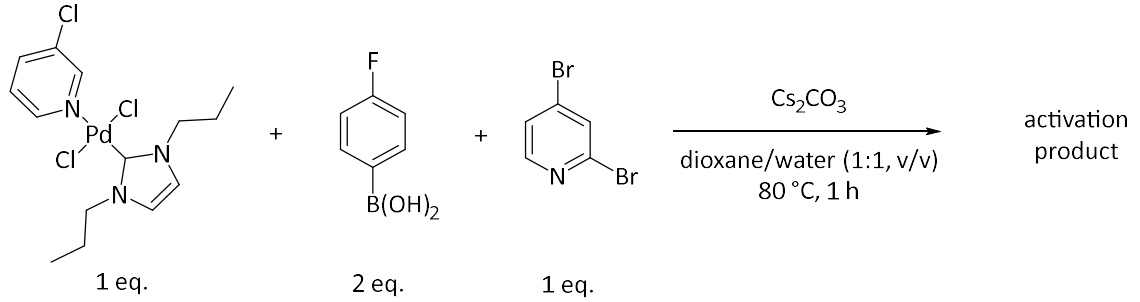

Scheme 5.4 – 1:2:1 reaction between ***C4****, p-fluorophenylboronic acid and 2,4-dibromopyridine to determine the activation route and identify any activation products. Standard catalytic reaction conditions were used.*

Visual observation of the reaction mixture indicated that the catalyst was indeed performing differently to the other stoichiometric reactions, as there were no palladium black deposits and the reaction mixture remained yellow in colour for the duration of the reaction (

Figure 5.8).

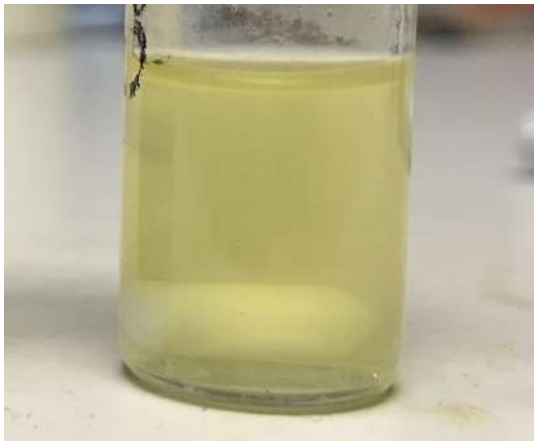

Figure 5.8 – Photograph of the reaction mixture outlined in Scheme 5.4. No palladium black generation has occurred.

The ^{1}H NMR spectrum following the reaction was significantly different to the previous reactions. Firstly, there was no significant shift in the 3-chloropyridine signals that would indicate ligand dissociation. All ^{1}H NMR signals associated with the parent complex were present in triplicate (Figure 5.9). Similar behaviour was observed during the synthesis of the Pd-NHC complexes when using imidazolium bromide ligand precursors, forming mixed halide complexes with triplicate ^{1}H NMR signals (Chapter 2.4). The homocoupled species, 4,4'-difluorobiphenyl (Figure 5.5), is also observed in the ^{1}H NMR spectrum suggesting that ***C4*** had undergone activation though. However, the relative integrations of the complex peaks and 4,4'-difluorobiphenyl indicate that only a small amount of the complex had undergone the activation reaction (approximately 20%).

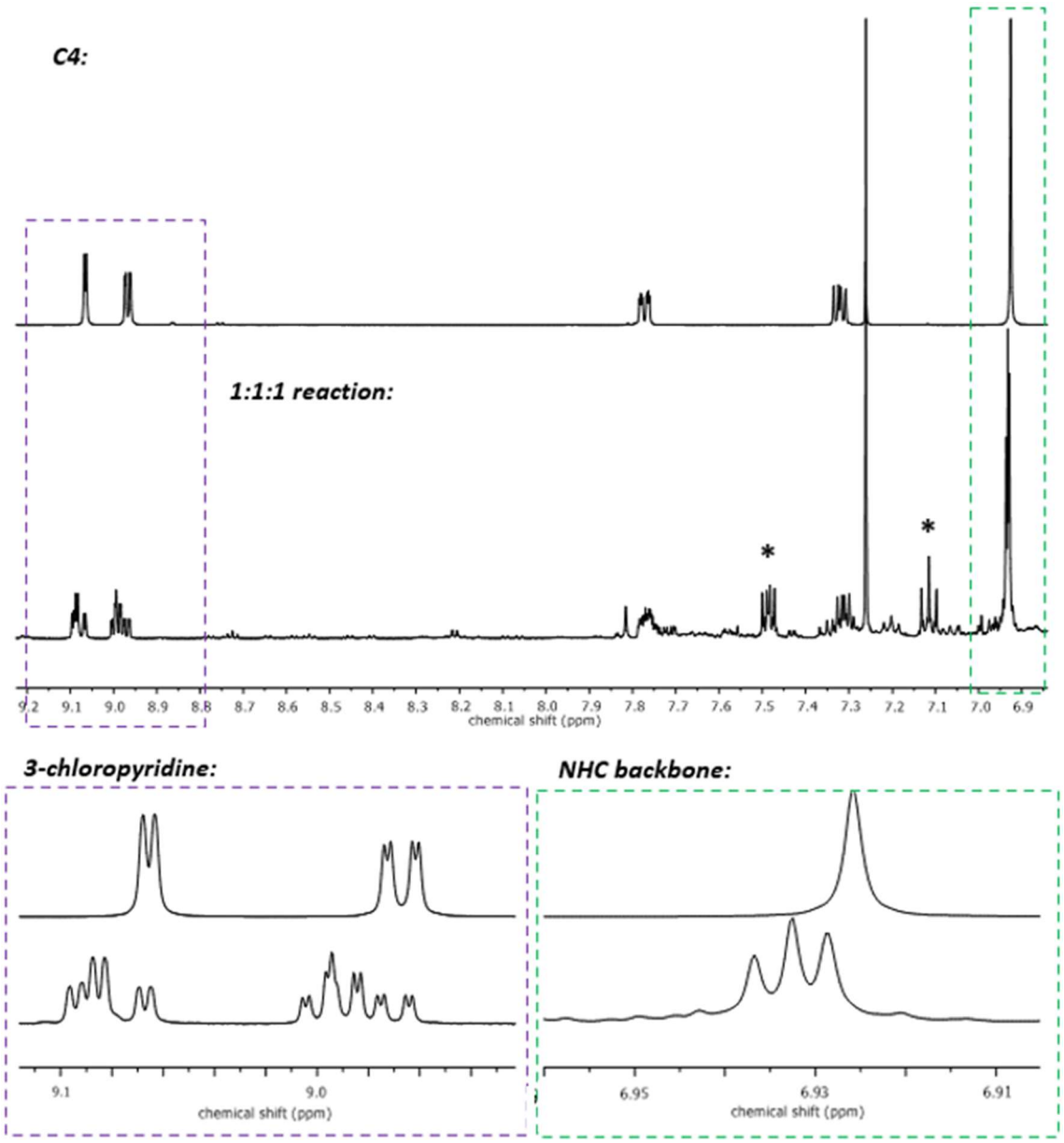

*Figure 5.9 – (top) Stacked ^{1}H NMR spectrum (500 MHz, chloroform-d) of **C4** and the reaction mixture outlined in Scheme 5.4, showing the appearance of two unknown species with similar chemical shifts to **C4**. (bottom) Zoomed in regions of the stacked spectra to show significant peaks more clearly. *4,4'-Difluorobiphenyl*

There are no extra signals indicating coordination of a pyridinyl ligand in the NMR spectrum for this reaction indicating the oxidative addition products were not isolated. The limited amount of activated complex generated in this reaction may have promoted the main catalytic reaction and exhausted the remaining boronic acid preventing the full activation of ***C4***. The remaining quantity of ***C4*** (approximately 80%) could then undergo halide exchange with bromide in solution to generate the mixed halide complex signals seen in the NMR spectrum. This assumes that the catalytic reaction is fast in comparison to complex activation. Indeed, a plethora of weak signals are seen in the aromatic region of the NMR spectra which may account for the generated products and any resting state catalytic species.

These stoichiometric studies using the non-bulky complex, ***C4***, have shown that the activation reaction proceeds through the accepted pathway and that the relative rate of activation may be slow in comparison to the main catalytic reaction. However, this difference in rates is not substantial enough to impart a noticeable induction period in the main catalytic reactions, as seen in the time course data previously discussed (Chapter 4.2). The stoichiometric studies have also shown that generation of unexpected palladium species can also occur and may be a possible side reaction in the main catalytic reaction.

5.2 Stoichiometric Reactions Studied Using HRMS

5.2.1 Catalytic Activation and Propagation of Bulky Pd-NHC Complexes

Stochiometric investigations were also conducted using the bulky complex, ***C7***. Analysis by NMR spectroscopy would be impractical for ***C7*** as the ligand environment is more complicated than ***C4***, so interpretation of the data would be significantly more challenging. Therefore, the bulky complex stoichiometric reactions were analysed by high-resolution mass spectrometry (HRMS) rather than NMR spectroscopy. HRMS is also much more sensitive than NMR spectrometry so very small amounts of species present in the reaction can be identified that may be unidentifiable in NMR spectrometry. However, it has been found that palladium complexes often fragment significantly when subjected to HRMS, for example, Figure 5.10 shows the HRMS from a single crystal of ***C7***. Despite being a crystalline sample and therefore expected to show only one distinct signal in HRMS, this sample gave a large array of fragmentation signals, most of which are unidentifiable. Some key peaks are identifiable, however, and show that the use of HRMS for the stoichiometric studies is valid.

Notably from this spectrum is a large peak associated with the NHC ligand (389.2957 AMU) despite being complexed to the palladium in the crystal (Figure 5.10). Observation of an NHC/imidazolium signal in the HRMS of the stoichiometric reactions therefore does not indicate that ligand dissociation has occurred in the reaction.

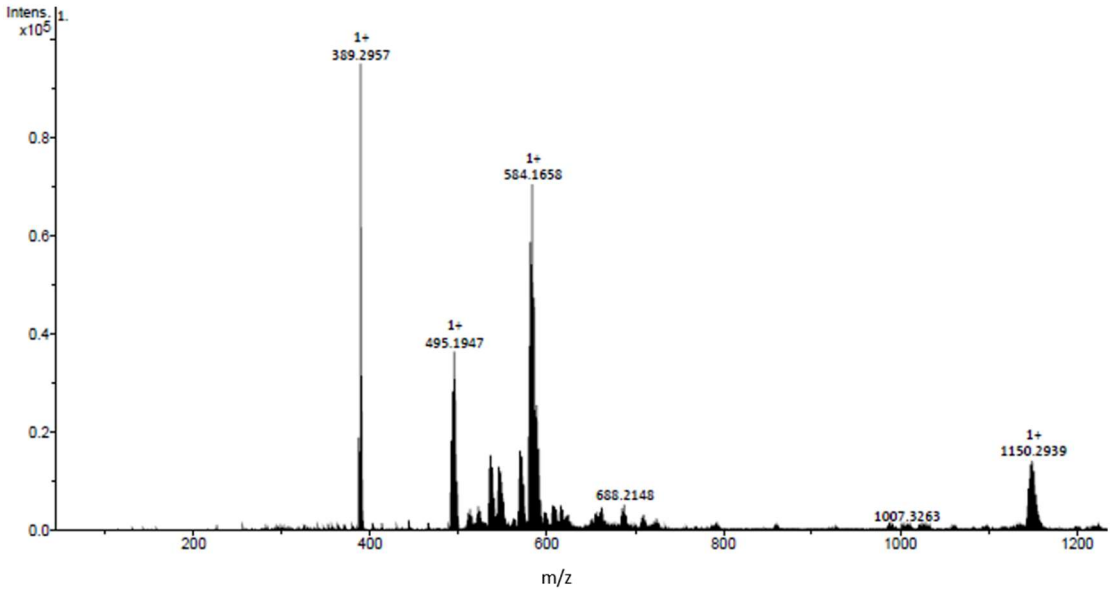

*Figure 5.10 – HRMS (ESI+) spectrum of crystalline **C7** using the same sample used for the SC-XRD data to show the extensive fragmentation of palladium complexes in HRMS. MeOH as HRMS solvent. [**C7**-Cl] – 643.1712 AMU is not seen in spectrum.*

The stoichiometric reaction with ***C7*** was conducted with two equivalents of *p*-fluorophenylboronic acid, to activate the precatalyst, and one equivalent of 2,4-dibromopyridine, to promote oxidative addition (Scheme 5.5).

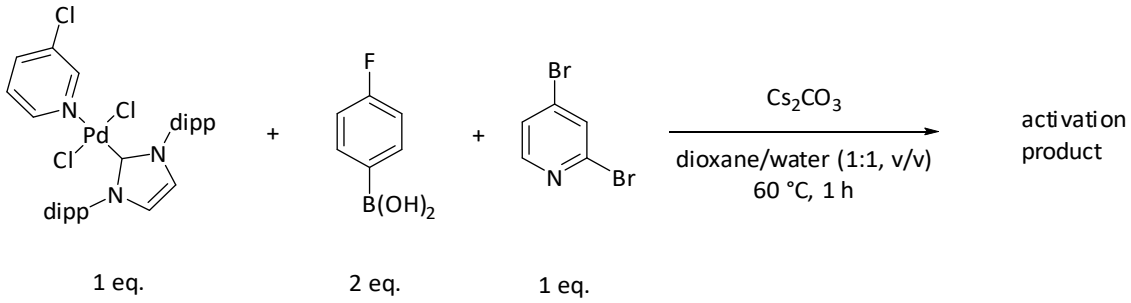

*Scheme 5.5 – 1:2:1 reaction between **C7**, p-fluorophenylboronic acid and 2,4-dibromopyridine respectively, to identify any reaction intermediates by HRMS analysis. Standard catalytic reaction conditions for **C7** were used.*

The mass spectrum following the stoichiometric reaction indicated the formation of several interesting species in the reaction (Figure 5.11). It is worth noting first that there is a significant peak associated with 2,4-Ar (268.0927 AMU). As with the previous stoichiometric study using ***C4***, the formation of this product was unexpected as the activation of the precatalyst should have exhausted all the *p*-fluorophenylboronic acid present in the reaction. Like ***C4*** then, it can be assumed that the activation rate of the precatalyst ***C7*** is relatively slow in comparison to the rate of the SMCC of 2,4-dibromopyridine and *p*-fluorophenylboronic acid. Therefore, despite being attempted as a stoichiometric reaction, these data represent more closely an 'early-stage' reaction sample, where the active catalytic species has formed and begun catalysis.

It is also worth noting the total absence of any mono-arylated products, once again indicating that the formation of 2,4-Ar is achieved *via* a concerted mechanism, offering further validation to the mechanistic rationale in Chapter 4.4.3, concerning the double oxidative addition of the substrate before transmetalation. There is a significant peak associated with the imidazolium ion corresponding to the NHC ligand (***I7***$^{+}$, 389.2962 AMU), the origin of which could be either attributed to unreacted ***C7*** or from any palladium species ligated with an NHC, as it has been shown that Pd-NHC complexes will readily fragment in HRMS (Figure 5.10).

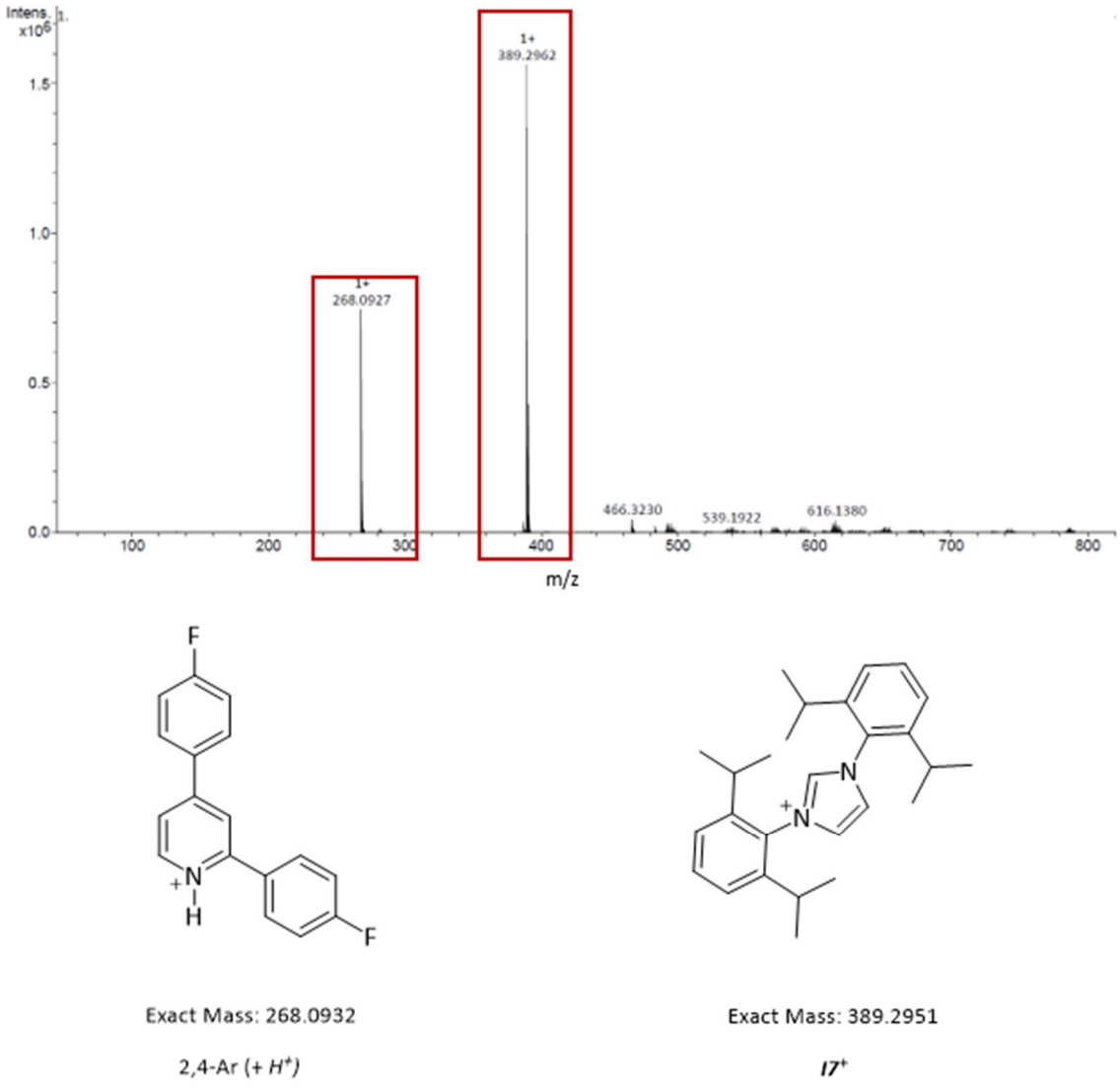

*Figure 5.11 – Full HRMS (ESI+) spectrum for the 1:2:1 reaction involving **C7** outlined in Scheme 5.5. The structures associated with 2,4-Ar + H^{+}: 268.0927 AMU and **I7**$^{+}$: 389.2951 AMU peaks are shown. MeOH as HRMS solvent.*

Closer examination of the lower intensity peaks between 450 and 750 AMU shows a large array of organic and palladium containing species (Figure 5.12), identified due to the characteristic isotope pattern. Unfortunately, only a few of the species could be identified. The identifiable

components are of reductively eliminated 2-arylated imidazolium ions, ***Ar-Imid1-3*** (466.3230, 483.3188 and 560.3460 AMU respectively) (Figure 5.12).

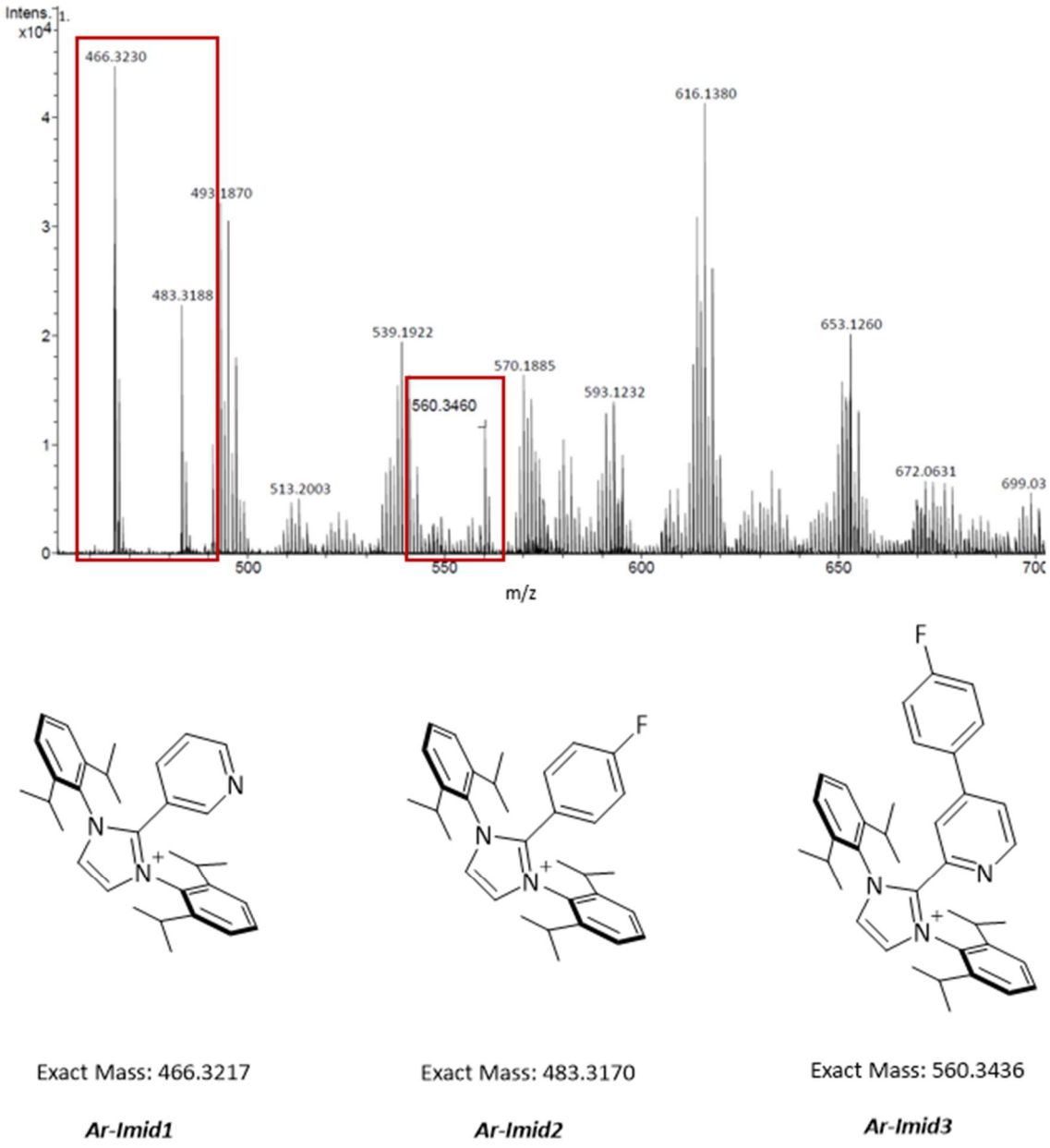

*Figure 5.12 – Zoomed in HRMS (ESI+) spectrum for the 1:2:1 reaction involving **C7** outlined in Scheme 5.5. The structures associated with **Ar-Imid1**: 466.3230 AMU, **Ar-Imid2**: 483.3188 AMU and **Ar-Imid3**: 560.3436 AMU peaks are shown. MeOH as HRMS solvent.*

Ar-Imid1 is assumed to have formed from the reductive elimination of the NHC and a complexed pyridine originating from the oxidative addition of 3-chloropyridine onto the palladium centre (Figure 5.13). This shows that the 3-chloropyridine ligand on PEPPSI complexes is not simply a spectator ligand and can undergo reaction. ***Ar-Imid2*** formed from the reductive elimination of the NHC and an aryl group presumably from the transmetalation of *p*-fluorophenylboronic acid onto palladium (Figure 5.13). Finally, ***Ar-Imid3*** formed from the reductive elimination of the NHC

and a ligated arylated pyridinyl. It is unclear for structure ***Ar-Imid3*** at which position the pyridinyl is arylated. The reductive elimination of 2-arylated imidazolium salts from palladium-NHC complexes is known in literature.[6]

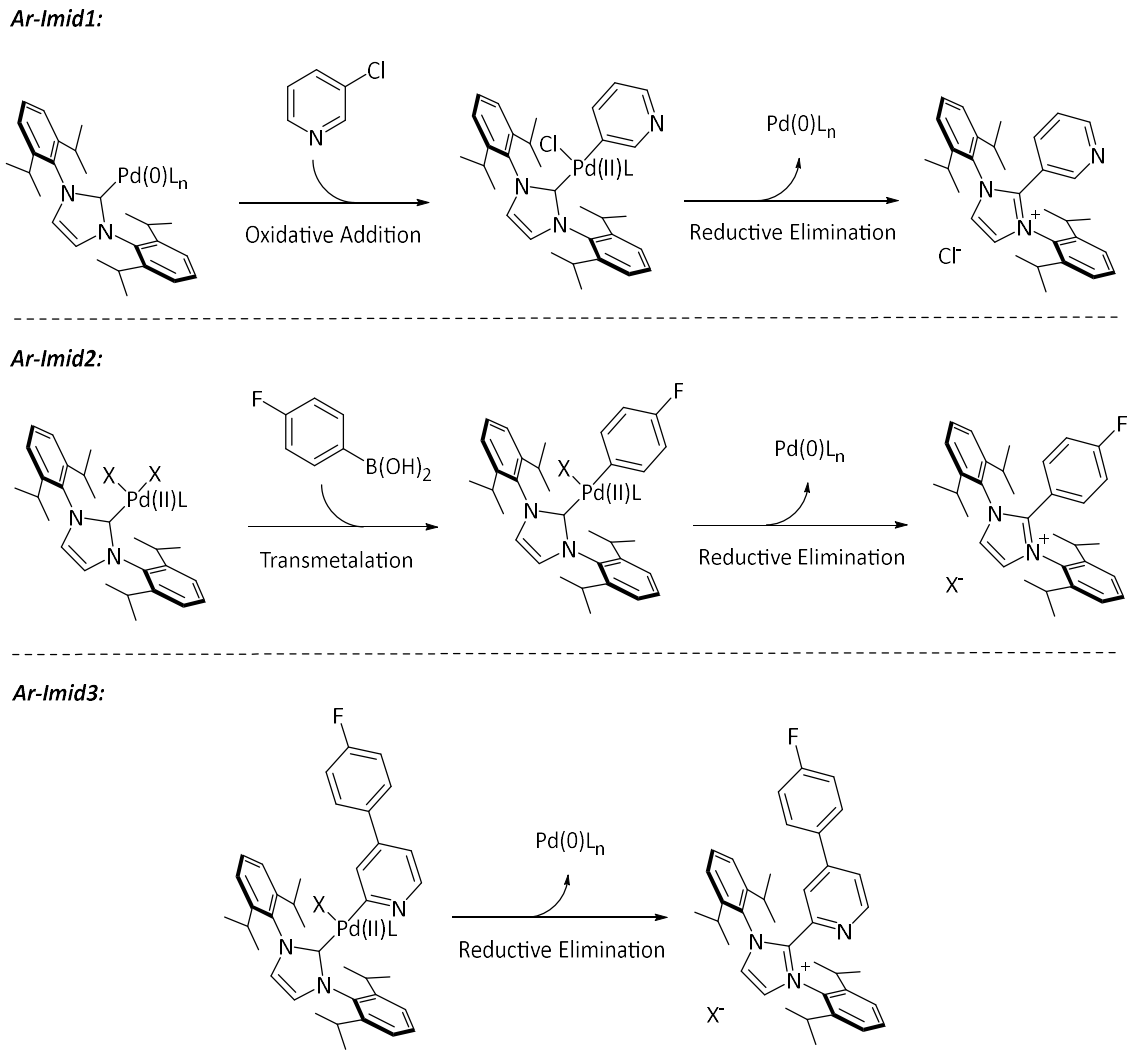

*Figure 5.13 - Possible routes for the formation of **Ar-Imid1**-**3**. Each route produces an arylated imidazolium ion and a Pd(0) species.*

These proposed routes to form the arylated imidazolium salts (***Ar-Imid1***-***3***) occur through removal of the NHC ligand from a Pd(II) species to form a Pd(0) species. Presumably this would alter the selectivity/activity of the palladium significantly, especially considering the direct 2,4-Ar selectivity in reactions with the bulky complexes which is NHC dependent (Chapter 4.1.1). Reductive elimination of an arylated imidazolium salt could be considered as a speciation pathway, or deactivation pathway if the generated Pd(0) fails to react further/agglomerates to form palladium black.

5.2.2 Mid- and Late-Stage Analysis of Bulky Pd-NHC Complexes

In a similar manner to the previous 'early stage' HRMS study, a reaction with ***C7*** as the precatalyst was sampled at later stages for analysis by HRMS to aid in identification of reaction intermediates. Samples were taken from a normal scale reaction (Scheme 5.6) rather than the previous study using stoichiometric amounts of the starting material with respect to the catalysis. This necessitated the processing of samples to remove the majority of the product, as the product signal(s) would have been too intense for analysis by HRMS at concentrations large enough to obtain meaningful data about any palladium species. The time course data (Chapter 4.2.2) was used to determine appropriate times to sample the reaction. The 'mid-reaction' sample was taken at 10 mins, just before half the maximum yield had been achieved, and an 'endpoint' sample at 6 hours to ensure the reaction had reached completion and any resting state intermediates could be identified.

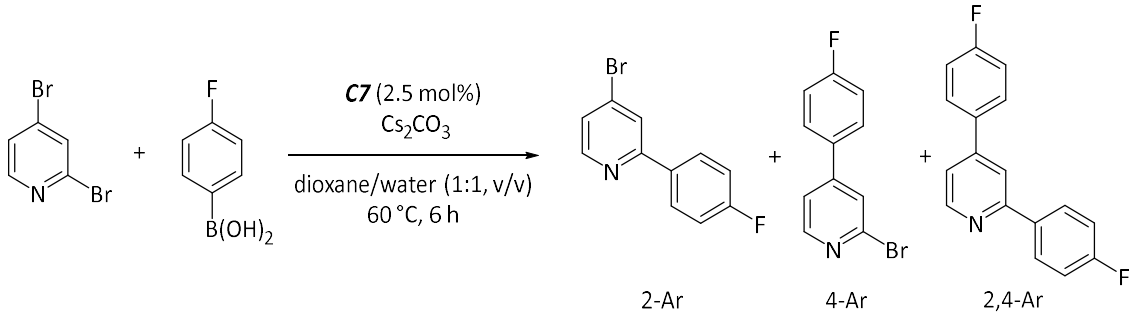

*Scheme 5.6 – Reaction between 2,4-dibromopyridine and p-fluorophenylboronic acid to yield 2-bromo-4-(p-fluorophenyl)pyridine (4-Ar), 2-(p-fluorophenyl)-4-bromo-pyridine (2-Ar) and 2,4-bis(p-fluorophenyl)pyridine (2,4-Ar) with **C7** as the precatalyst. HRMS samples taken at 10 mins (mid-point) and 6 hours.*

The 10-mins sample spectra (Figure 5.14) showed residual 2,4-Ar, not removed by the treatment of the sample prior to analysis, along with a signal associated with the imidazolium ion corresponding to the NHC ligand (***I7***$^+$) the presence of which has been discussed previously. There is a significant peak for reductively eliminated aryl imidazolium salt, ***Ar-Imid2***, however, it is present in a much greater relative intensity than observed previously (Figure 5.13). This could suggest that the reductive elimination of palladium bound *p*-fluorophenyl and the NHC ligand to form the arylated imidazolium (***Ar-Imid2***) is a major catalyst speciation pathway for the active palladium species.

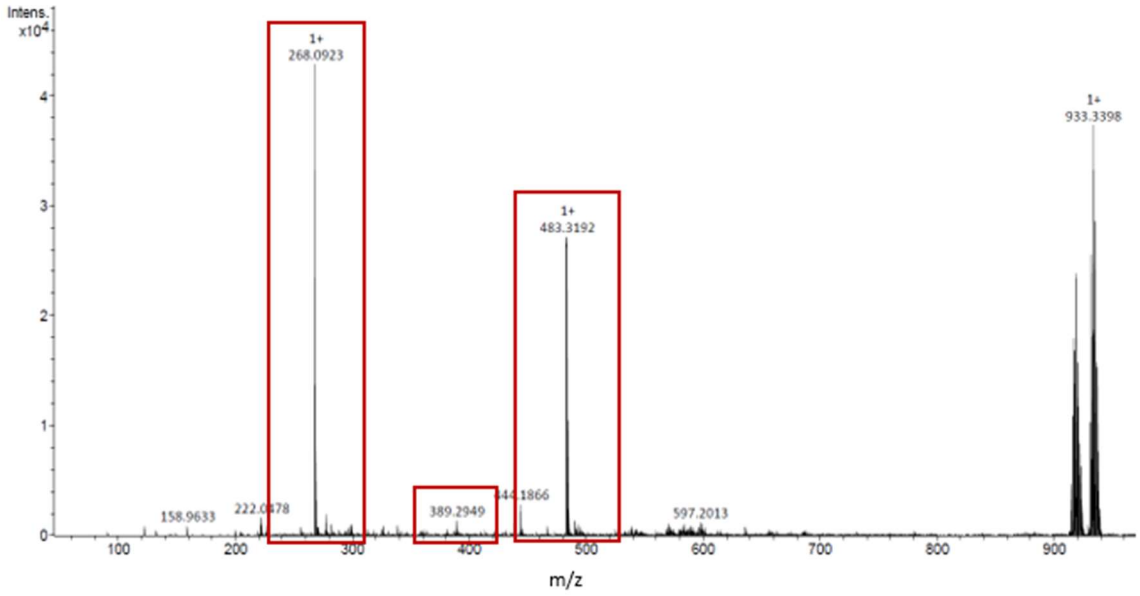

*Figure 5.14 – Full HRMS (ESI+) spectrum for the 10-mins sample of the reaction using **C7** as the precatalyst, as outlined in Scheme 5.6. The structures associated with 2,4-Ar + H^+: 268.0923 AMU, **I7**$^+$: 389.2949 AMU and **Ar-Imid2:** 483.3170 AMU peaks are shown. MeOH as HRMS solvent.*

The most significant species observed from the 'mid-reaction' sample spectra are of two (or more) palladium species featuring both pyridine and pyridinyl ligands (***Pd*$_{MS}$*1*$_{a\text{-}f}$** and ***Pd*$_{MS}$*2*$_{a\text{-}b}$**, Figure 5.15). The first signal (917.2216 AMU) could refer to any of six similar palladium-NHC structures ***Pd*$_{MS}$*1a-f***. ***Pd*$_{MS}$*1*$_a$** and ***Pd*$_{MS}$*1*$_b$** both feature a nitrogen bound 2,4-Ar and either a 2-bromo pyridine-4-yl or 4-bromo pyridine-2-yl ligand respectively. ***Pd*$_{MS}$*1*$_c$** and ***Pd*$_{MS}$*1*$_d$** feature a nitrogen bound 2-bromo-4-arylpyridine and either 2-arylpyridine-4-yl or 4-arylpyridine-2-yl respectively, and ***Pd*$_{MS}$*1*$_e$** and ***Pd*$_{MS}$*1*$_f$** bind the same but with a nitrogen bound 2-aryl-4-bromopyridine instead. The second signal (933.3398 AMU) could refer to two complexes ***Pd*$_{MS}$*2*$_a$** and ***Pd*$_{MS}$*2*$_b$**, both featuring a nitrogen bound 2,4-Ar and either 2-arylpyridine-4-yl or 4-arylpyridine-2-yl respectively.

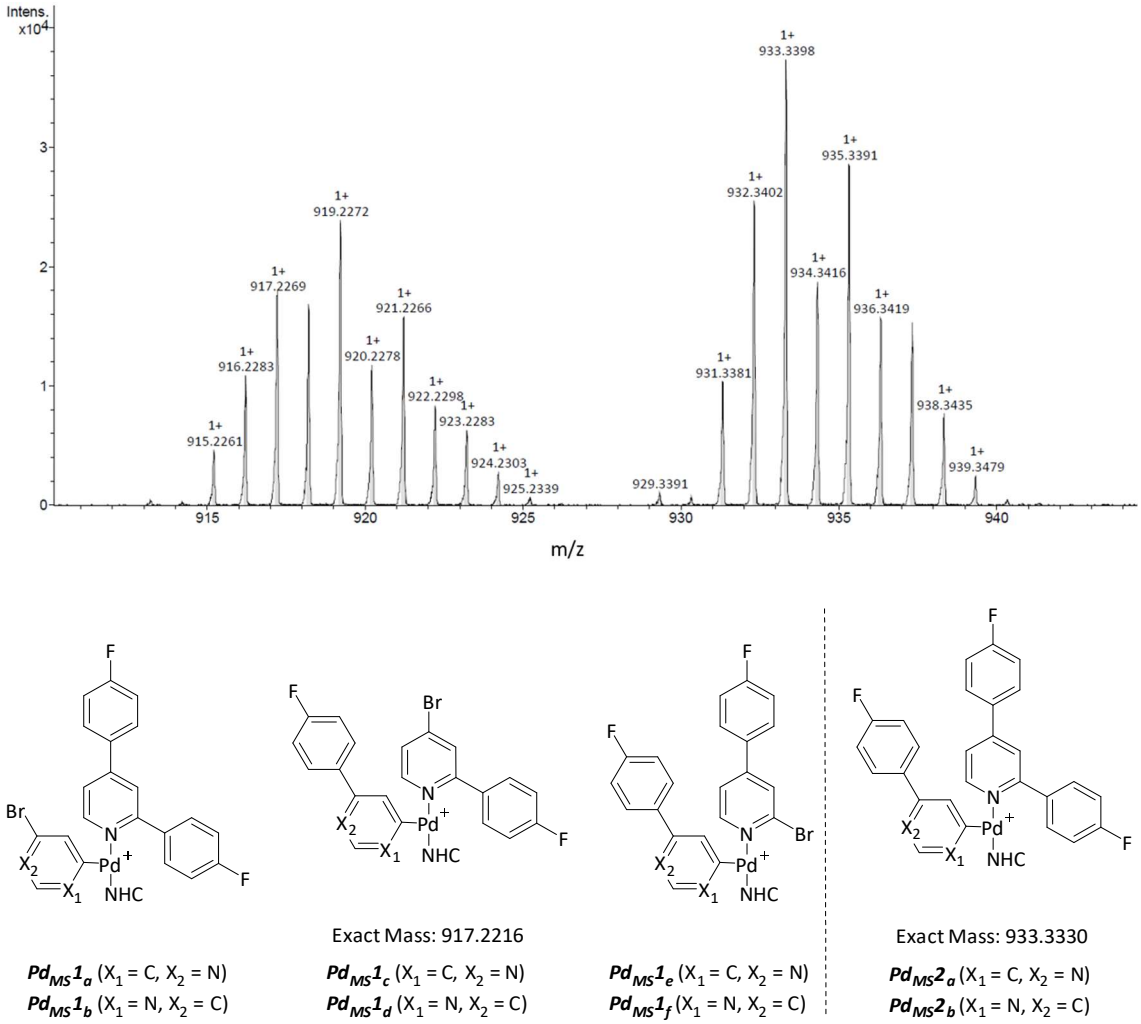

*Figure 5.15 – Zoomed in HRMS (ESI+) spectrum for the mid-point sample of the reaction using **C7** as the precatalyst, as outlined in Scheme 5.6, to show palladium intermediate signals **$Pd_{MS}1_{a-f}$**: 917.2216 AMU and **$Pd_{MS}2_{a-b}$** 933.3398 AMU. MeOH as HRMS solvent.*

All of the palladium species ***$Pd_{MS}1_{a-f}$*** and ***$Pd_{MS}2_{a-b}$*** are 3-coordinate due to the removal of a ligand, presumably by fragmentation, during HRMS as only positively charged ions are observed. The identity of any fourth ligand is unknown. Single crystal growth was attempted to obtain empirical structural data from these palladium species, by means of SC-XRD, but all attempts were unsuccessful.

Though the absolute structure of the species related to these signals is ambiguous, they do show some important information about the catalysis. All previous data has indicated that the active species for the catalysis has an NHC ligand bound; this data indicates structures with NHC ligands and bound pyridinyl ligands, which would be expected following oxidative addition of a bromopyridine. It is then reasonable to assume that one or more of the structures shown (Figure 5.15) could have originated from the fragmentation of one or multiple active catalytic species.

This is further evidenced when considering the data from the end point HRMS analysis of the catalytic reaction (Figure 5.16) whereby the two 'active species' signals had dissipated. This would be expected for signals associated with active species as lack of propagation due to exhaustion of starting materials would likely promote deactivation pathways. This is coupled with an increase in intensity of the arylated imidazolium ion peak, ***Ar-Imid2*** and ***Ar-Imid3***, assumed to be linked to catalyst speciation/deactivation.

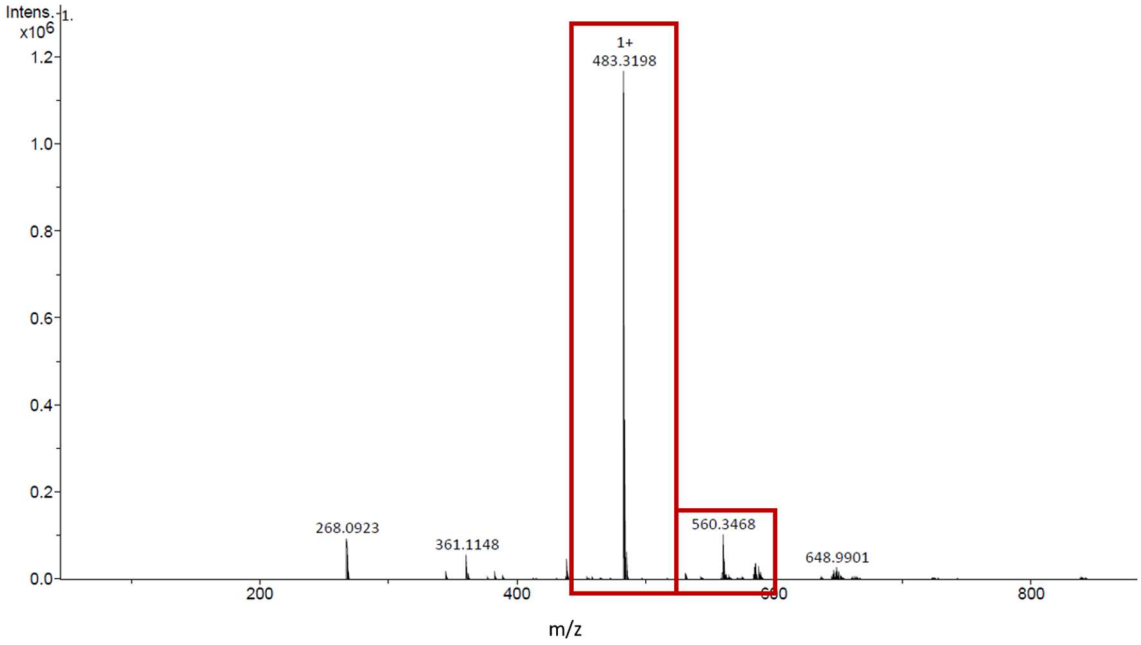

*Figure 5.16 – Full HRMS (ESI+) spectrum for the end-point sample of the reaction using **C7** as the precatalyst, as outlined in Scheme 5.6. The structures associated with 483.3170 and 560.3468 are shown. MeOH was used as the HRMS solvent.*

With reference to the proposed mechanistic rationale (Chapter 4.4) it is thought that oxidative addition of the 4-Br bond of 2,4-dibromopyridine occurs through a Pd-NHC active species (***PdL***) and that oxidative addition of the 2-Br occurs through a Pd-NHC-pyridine active species (***PdL_2***).

The observation of a pyridine coordinated to palladium following oxidative addition could either indicate that 2-Br oxidative addition has occurred or that 4-Br oxidative addition has occurred followed by coordination of pyridine to stabilise the resulting palladium species. It therefore remains ambiguous if $\boldsymbol{Pd_{MS}1_{a\text{-}f}}$ and $\boldsymbol{Pd_{MS}2_{a\text{-}b}}$ formed as a result of oxidative addition of the 2-Br or 4-Br bond in 2,4-dibromopyridine.

5.3 Investigation of 2,4-Ar Formation from Pre-Arylated Substrates

As discussed previously, the formation of 2,4-Ar was thought to form concertedly in the SMCC of 2,4-dibromopyridine and *p*-fluorophenylboronic acid. Though good evidence supports this rationale, kinetic analysis of time course data suggests that the formation of 2,4-Ar through consumption of the mono-arylated products (2-Ar and 4-Ar) may also occur and, therefore, was also investigated. The formation of 2,4-Ar was monitored over time from either 2-Ar or 4-Ar using the bulky and non-bulky complexes. These experiments would give data on the relative rates associated with the coupling at each halide position on the pyridine ring and infer how 2,4-Ar would form in the reaction by consumption of the mono-arylated pyridines. The data indicates that a completely different mechanism was operating for each of the mono-arylated pyridines when forming 2,4-Ar with both the bulky and non-bulky Pd-NHC complexes.

5.3.1 2,4-Ar Formation Using a Bulky Pd-NHC Complex

When using the bulky complex, ***C7***, in the reaction between 4-Ar and *p*-fluorophenylboronic acid (Scheme 5.7), the formation of 2,4-Ar over time shows a typical reaction profile (Figure 5.17). The product initially forms quickly then slows over time, to reach a maximum product yield of 93% at ~240 mins. This is the expected reaction profile where rate of reaction slows as reagent concentrations in solution wane and catalyst deactivation pathways reduce the overall catalytic activity. The reaction mixture showed no visible palladium deposits (Figure 5.18).

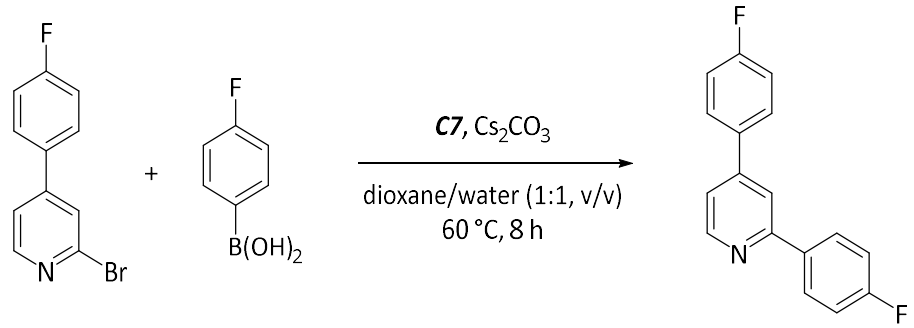

*Scheme 5.7 – SMCC of 2-bromo-4-(p-fluorophenyl)pyridine (4-Ar) and p-fluorophenylboronic acid in dioxane and water (1:1) at 60 °C with **C7** as the precatalyst.*

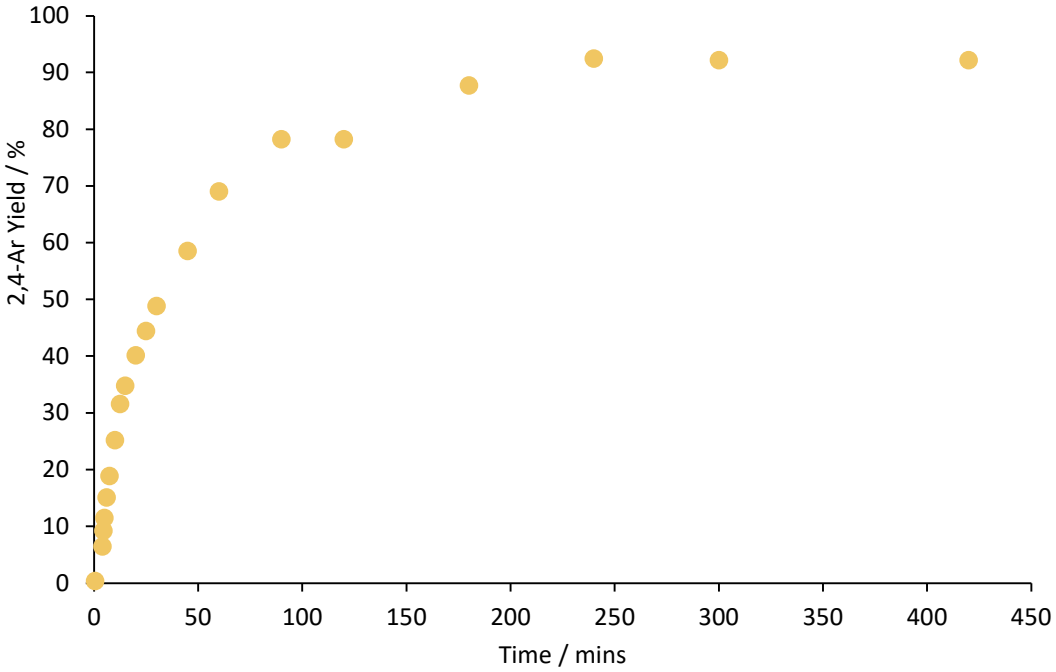

*Figure 5.17 – Time course data showing product yield of 2,4-Ar for the reaction between 2-bromo-4-(p-fluorophenyl)pyridine (4-Ar) and p-fluorophenylboronic acid in dioxane and water (1:1) at 60 °C with **C7** as the precatalyst. Product yields are determined by ^{19}F NMR spectroscopy with respect to FDMB internal standard. Error bars represent standard error.*

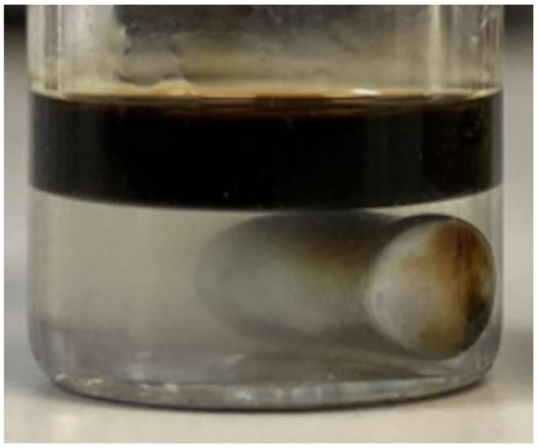

Figure 5.18 – Photograph of the reaction vessel following the reaction outlined in Scheme 5.7, with no palladium black deposits visible.

The reaction profile was significantly different when using 2-Ar with the same complex, ***C7*** (Scheme 5.8 and Figure 5.19). Most apparent from this plot is the significantly faster formation of 2,4-Ar, where an almost 10-fold increase is observed. There was also a small induction period (~ 3 mins) where product formation is relatively slow before the rate of reaction then increases rapidly. Additionally, significant black deposits were observed in the reaction mixture following the reaction (Figure 5.20), suggesting that a considerable amount of the palladium in the reaction had been reduced to Pd(0) and precipitated as palladium black.

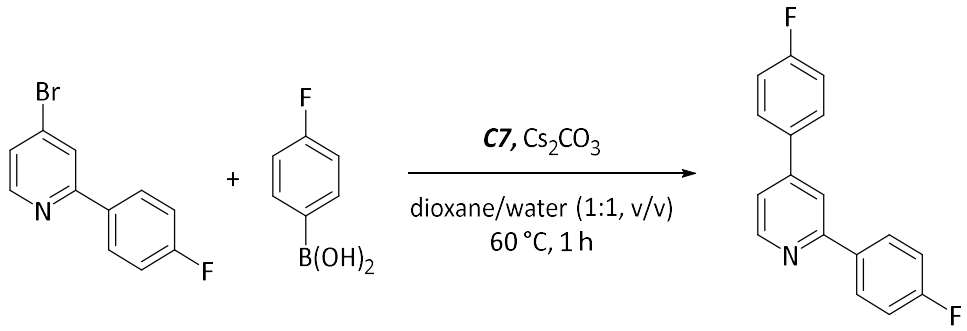

*Scheme 5.8 – SMCC of 2-(p-fluorophenyl)-4-bromo-pyridine (2-Ar) and p-fluorophenylboronic acid in dioxane and water (1:1) at 60 °C with **C7** as the precatalyst.*

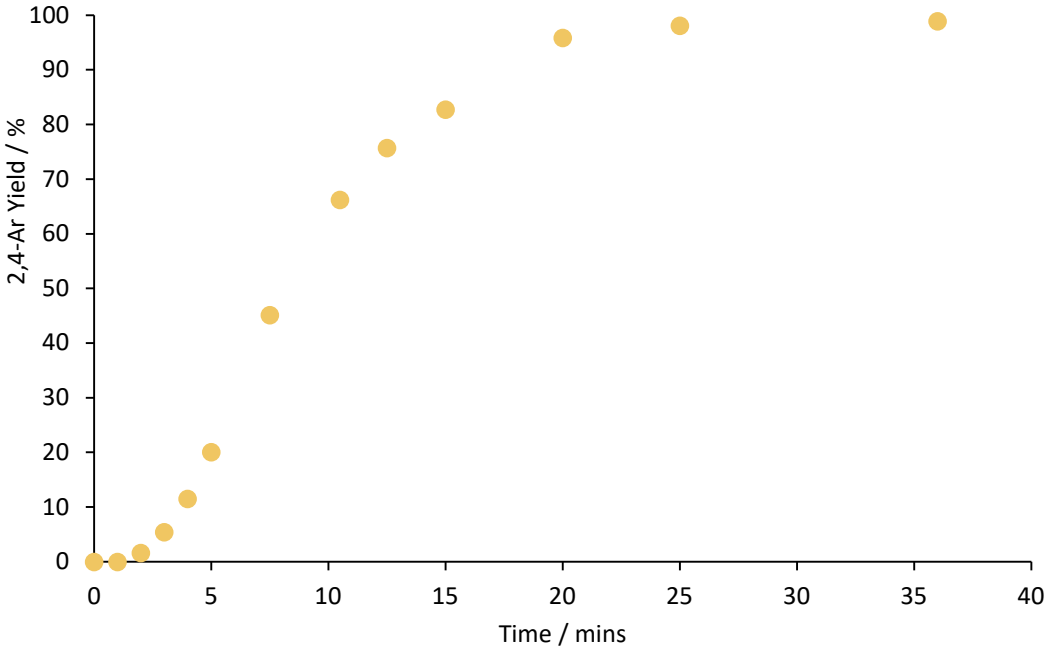

*Figure 5.19 – Time course data showing product yield of 2,4-Ar for the reaction between 2-(p-fluorophenyl)-4-bromo-pyridine (2-Ar) and p-fluorophenylboronic acid in dioxane and water (1:1) at 60 °C with **C7** as the precatalyst. Product yields are determined by ^{19}F NMR spectroscopy with respect to FDMB internal standard. Error bars represent standard error.*

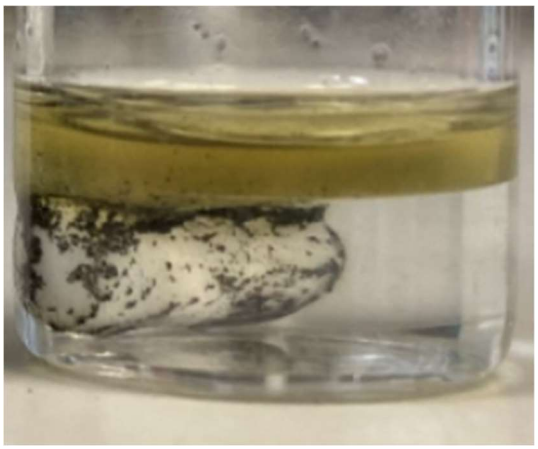

Figure 5.20 – Photograph of the reaction vessel following the reaction outlined in Scheme 5.8, with palladium black deposits present.

5.3.2 2,4-Ar Formation Using a Non-Bulky Pd-NHC Complex

The reaction profiles when using either 2-Ar or 4-Ar and the non-bulky complex, ***C14***, show analogous reactivity to the bulky complex with some minimal differences. The reaction between 4-Ar and phenylboronic acid with the non-bulky complex shows incomplete reactivity (Scheme 5.9 and Figure 5.21). This is not entirely unexpected as the non-bulky complexes showed much lower activity in comparison to the bulky complexes in the initial screen reactions. The reaction profile, however, is similar to the bulky complex in that the formation of 2,4-Ar proceeds quickly initially then decays to reach a maximum after some time. Again, similarly to the bulky complex, following this reaction, no black deposits were observed.

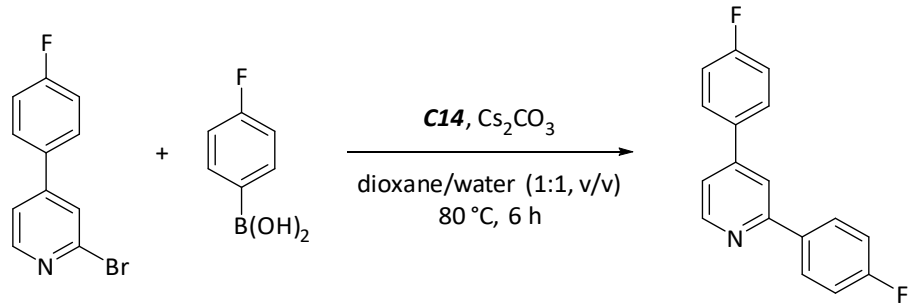

*Scheme 5.9 – SMCC of 2-bromo-4-(p-fluorophenyl)pyridine (4-Ar) and p-fluorophenylboronic acid in dioxane and water (1:1) at 80 °C with **C14** as the precatalyst.*

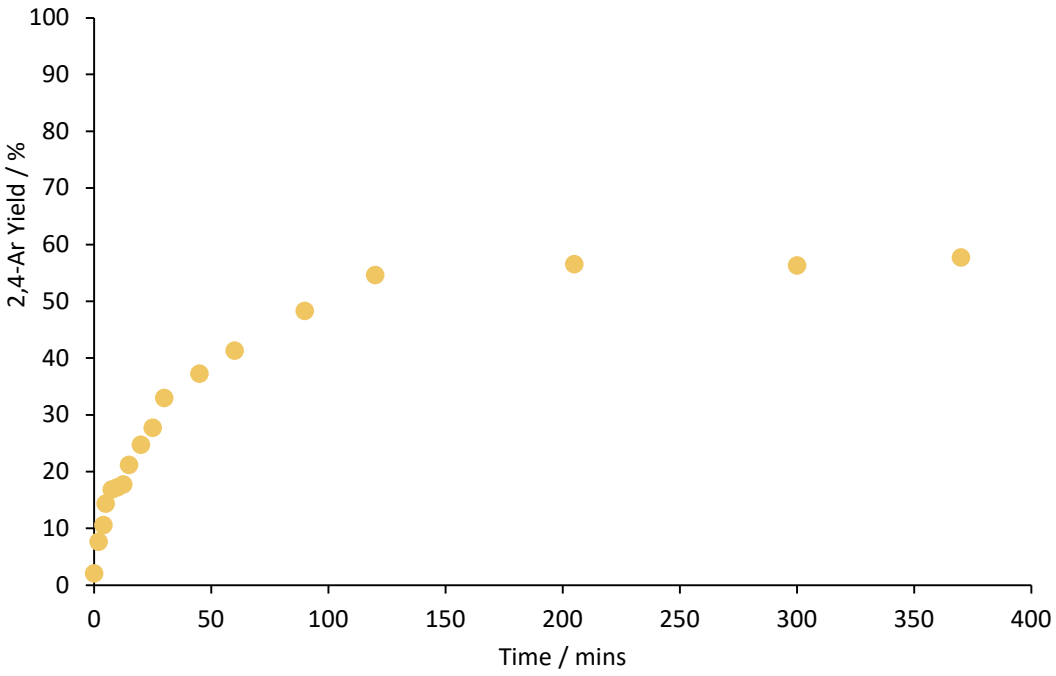

*Figure 5.21 – Time course data showing product yield of 2,4-Ar for the reaction between 2-bromo-4-(p-fluorophenyl)pyridine (4-Ar) and p-fluorophenylboronic acid in dioxane and water (1:1) at 80 °C with **C14** as the precatalyst. Product yields are determined by ^{19}F NMR spectroscopy with respect to FDMB internal standard. Error bars represent standard error.*

The reaction of 2-Ar using the non-bulky complex was once again much faster than for 4-Ar and the initiation period is observed (Scheme 5.10 and Figure 5.22). The activity of the complex with this starting material seems to be significantly higher than the bulky complex as the reaction reached completion in just 5 mins as opposed to the 30 mins with the bulky complex. This suggests that the non-bulky NHC ligand facilitates faster formation of the active species than the bulky NHC ligand. Again, the short initiation period at the start of the reaction was observed, as well as the presence of palladium deposits in the reaction mixture.

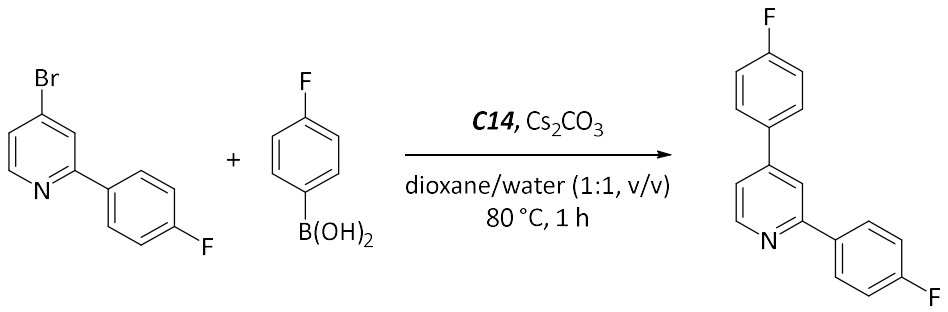

*Scheme 5.10 – SMCC of 2-(p-fluorophenyl)-4-bromo-pyridine (2-Ar) and p-fluorophenylboronic acid in dioxane and water (1:1) at 80 °C with **C14** as the precatalyst.*

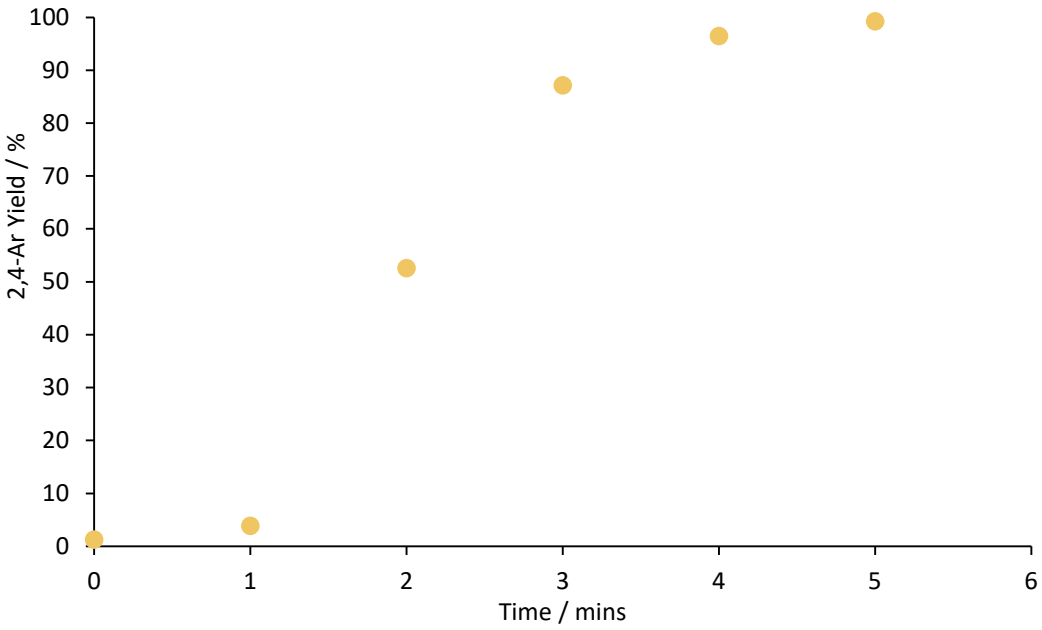

*Figure 5.22 – Time course data showing product yield of 2,4-Ar for the reaction between 2-(p-fluorophenyl)-4-bromo-pyridine (2-Ar) and p-fluorophenylboronic acid in dioxane and water (1:1) at 80 °C with **C14** as the precatalyst. Product yields are determined by ^{19}F NMR spectroscopy with respect to FDMB internal standard. Error bars represent standard error.*

5.3.3 Temperature Dependence of 2,4-Ar Formation from 2-Ar

The catalytic reaction using the bulky and non-bulky complexes as the precatalysts with 2-Ar as the starting material could both generate the same (or similar) active species, and the differences in rate between them may be due to the temperature at which each reaction was conducted being different. The non-bulky complex was used at 80 °C and showed a much faster reaction rate compared to the bulky complex which was examined at 60 °C. Considering that all previous data shows the bulky complex to have greater catalytic activity, the temperature dependence on active species generation may be the origin of this disparity. To test this, the non-bulky complex was used in the cross-coupling reaction with 2-Ar at a lowered temperature of 60 °C (Scheme 5.11).

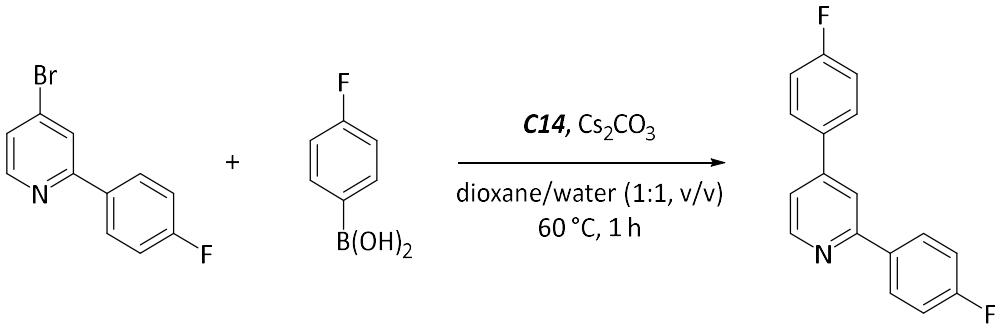

*Scheme 5.11 – SMCC of 2-(p-fluorophenyl)-4-bromo-pyridine (2-Ar) and p-fluorophenylboronic acid in dioxane and water (1:1) at 60 °C with **C14** as the precatalyst.*

The rate of reaction with the non-bulky complex, ***C14***, at 60 °C was much slower compared to that at 80 °C and the reaction profile is significantly different to the bulky complex, ***C7***, at 60 °C (Figure 5.23). The induction period and initial reaction rate is seemingly faster when using ***C14***, achieving a product yield of 25% in 5 mins, compared to that of ***C7*** with 18% in the same time period. However, the reaction with ***C14*** only reaches a maximum yield of 53%, significantly lower than ***C7*** which reached full conversion. This is more indicative of the behaviour of the non-bulky complex in the normal catalytic reaction, whereby the catalyst fully deactivates part way through the reaction. This does not eliminate the possibility of ***C7*** and ***C14*** having the same active species but does show that the formation of the active species happens at different rates depending on the parent precatalyst ligand structure, and the stabilisation of this active species may be ligand dependant. The reaction with the complex bearing the non-bulky ligand, ***C14***, appears to require a quick turnover (*i.e*. higher temperature) to prevent it from deactivating, whilst ***C7*** may have a more stable resting state.

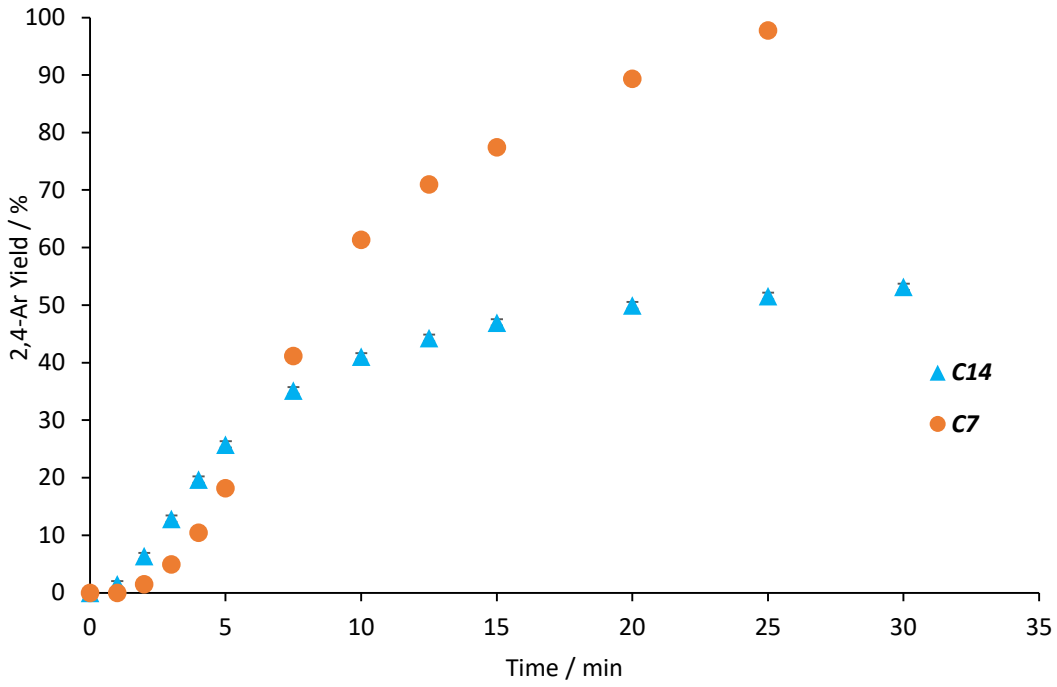

*Figure 5.23 – Time course data showing product yield of 2,4-Ar for the reaction between 2-(p-fluorophenyl)-4-bromo-pyridine (2-Ar) and p-fluorophenylboronic acid in dioxane and water (1:1) at 60 °C with **C7** and **C14** as the precatalyst. Product yields are determined by ^{19}F NMR spectroscopy with respect to FDMB internal standard. Error bars represent standard error.*

5.3.4 Mechanistic Rationale for 2,4-Ar Formation from Pre-Arylated Substrates

Slight differences in the rate of 2,4-Ar formation would be expected when using either 2-Ar or 4-Ar as the aryl halide coupling partner, due to the small differences in bond dissociation energies of the relative C-Br bonds. Indeed SC-XRD data for 2-Ar and 4-Ar show that the C-Br bond lengths are not significantly different (Figure 5.24, Table 5.2). Therefore, it is expected that other factors are strongly affecting the reaction.

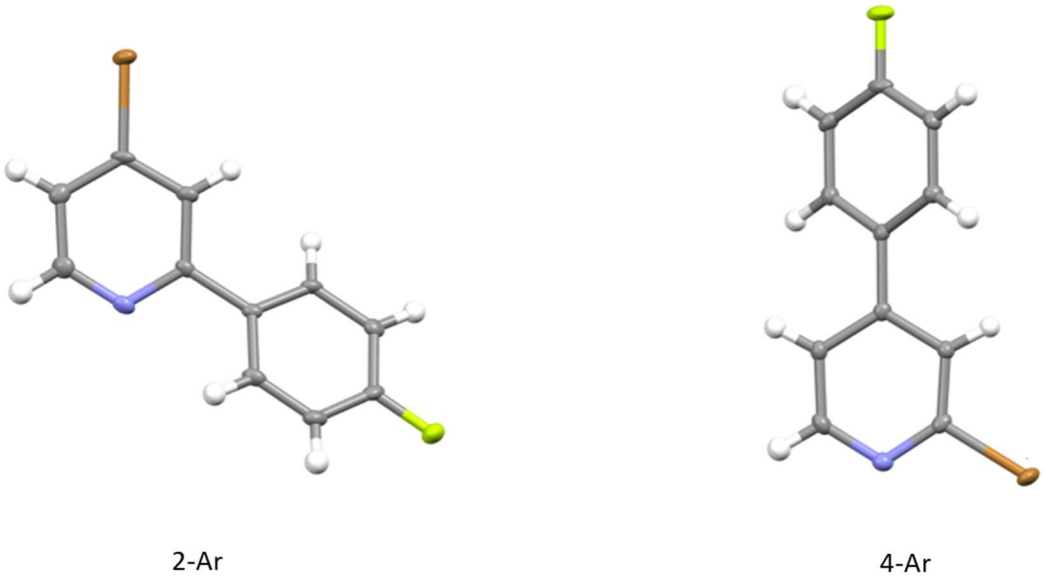

Figure 5.24 – SC-XRD structures of 2-Ar and 4-Ar with C-Br bond lengths shown. Thermal ellipsoids are at 50% probability level.

Table 5.2 – Showing the C-Br and C-C_{Ar} bond distances for 2-Ar and 4-Ar, as determined by SC-XRD.

Compound	C–Br distance / Å	C–C_{Ar} distance / Å
2-Ar	1.892 (5)	1.481 (5)
4-Ar	1.915 (3)	1.475 (5)

Assuming the initial stages of the reaction take place with a homogeneous catalyst system then the structures of the relative oxidative addition products of 2-Ar and 4-Ar with Pd(0)-NHC may give insight into the large differences in reactivity. The expected general structures of the oxidative addition products, ***Pd_{OA}2*** and ***Pd_{OA}4***, only differ in one way, the position of the pyridine nitrogen relative to the palladium centre (Figure 5.25). The ligand (L) on ***Pd_{OA}2*** and ***Pd_{OA}4*** represents a substituted pyridine, either coordinated before the oxidative additions or after to stabilise the structure.

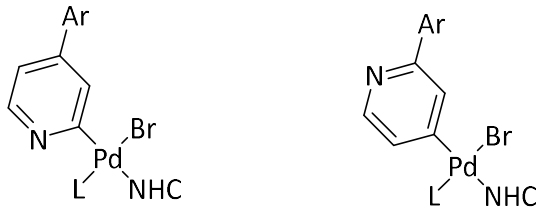

$Pd_{OA}2$ $Pd_{OA}4$

Figure 5.25 – Structures of ***$Pd_{OA}2$*** *(left) and* ***$Pd_{OA}4$*** *(right), corresponding to the expected oxidative addition products of 2-bromo-4-(p-fluorophenyl)pyridine (4-Ar) and 2-(p-fluorophenyl)-4-bromo-pyridine (2-Ar) respectively with a Pd(0)-NHC catalyst. L is a coordinating ligand, likely a substituted pyridine.*

Since the catalysis proceeds more slowly with 4-Ar starting material and there are no palladium deposits, there could a stabilisation mechanism preventing reduction to Pd black whilst also slowing the reaction. Figure 5.26 shows the structure of the proposed stabilised intermediate, ***$Pd_{cycle}2$*** formed from 4-Ar intermediate ***$Pd_{OA}2$***. The nitrogen atom of the pyridine ring is positioned such that it can form a dative bond with a second palladium species of similar architecture to form the palladacycle ***$Pd_{cycle}2$***. The structure of this palladacycle is known in the literature though featuring different ancillary ligands and pyridine substituents.[7-11] The palladium atoms in ***$Pd_{cycle}2$*** are buried within the large steric environment arising from the ligands, thus the palladacycle would be more protected against deactivation. Direct synthesis of ***$Pd_{cycle}2$*** was attempted to gauge the catalytic potential of this species, however, it has not been isolated to date.

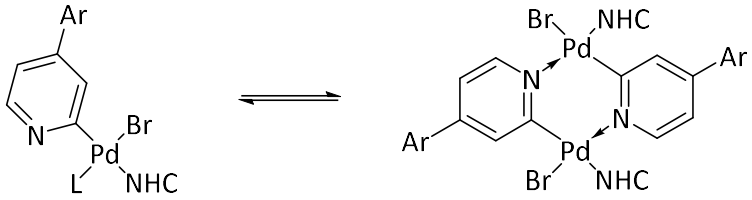

$Pd_{OA}2$ $Pd_{cycle}2$

Figure 5.26 – The equilibrium between ***$Pd_{OA}2$*** *(the oxidative addition product of 2-bromo-4-(p-fluorophenyl)pyridine (4-Ar) with a Pd(0)-NHC catalyst) and* ***$Pd_{cycle}2$*** *(the proposed palladacycle structure acting as a stabilisation mode for the active catalyst).*

Relating this to the standard reactions of 2,4-dibromopyridine and *p*-fluorophenylboronic acid, black deposits are not observed which could indicate that the proposed palladacycle formation could also occur. Since the proposed palladacycle structure can only form from Pd-NHC oxidative addition of the 2-Br bond of 2,4-dibromopyridine, its formation may act as a palladium sink and

hinder the formation of 2-Ar and therefore partially account for the low yield of 2-Ar with the Pd-NHC complexes in the standard reactions.

The mechanism for the formation of 2,4-Ar from 4-Ar would likely closely resemble a standard SMCC mechanism with the addition of the palladium sink arising from the formation of ***Pd$_{cycle}$2*** (Figure 5.27).

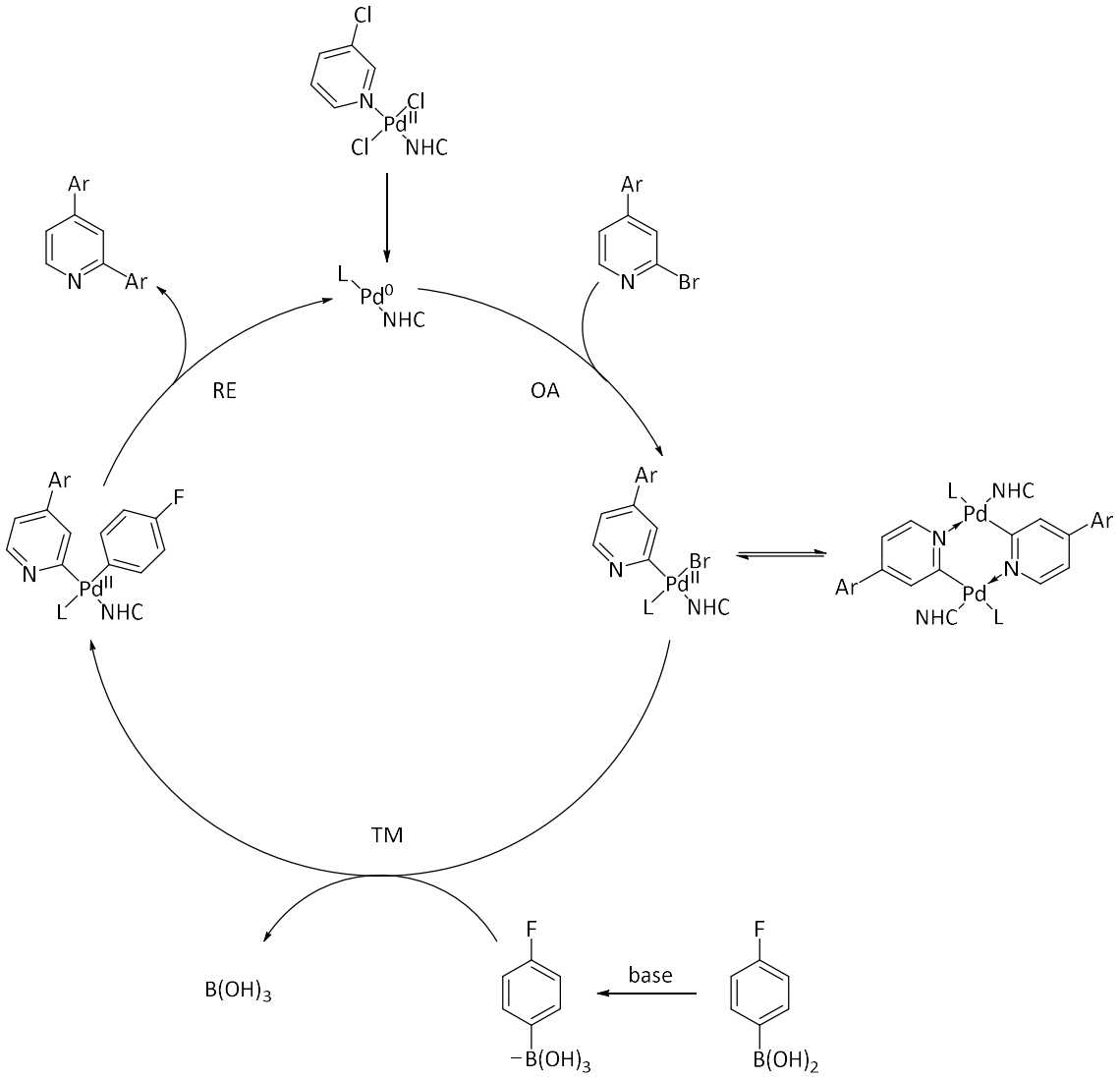

Figure 5.27 – The proposed catalytic cycle for the SMCC of 2-bromo-4-(p-fluorophenyl)pyridine (4-Ar) and p-fluorophenylboronic acid in the presence of base.

The pyridinyl nitrogen in ***Pd$_{OA}$4*** (Figure 5.25) is not positioned to be able to form the palladacycle motif so the proposed stabilisation mode is not accessible. Aggregation pathways are therefore more readily accessible to ***Pd$_{OA}$4*** and could facilitate the formation of higher-order palladium species in the reaction with 2-Ar, likely accounting for the observed palladium deposits.

Palladium black formation would usually be assumed a deactivation pathway for a given active palladium species, however, the reaction profiles when this is observed show an increased

activity (Figure 5.19 and Figure 5.22). It is hypothesised that during the speciation of the intermediate ***Pd$_{OA}$4*** to palladium black, a highly active high-order palladium species is formed. This short-lived high-order palladium species would then perform the catalysis rapidly before further speciation and deactivation can fully occur (Figure 5.28). The formation of this active species would explain the initiation period of the reaction profiles outlined earlier. The NHC ligand sterics may have some effect on the rate of speciation as the non-bulky NHC complex showed a marked increase in rate, suggesting that the speciation occurs more quickly. It is unlikely that the catalysis occurs solely by this outlined pathway and some amount of 2,4-Ar is formed by the standard mononuclear homogeneous mechanism. This hypothesis is shown mechanistically in Figure 5.28.

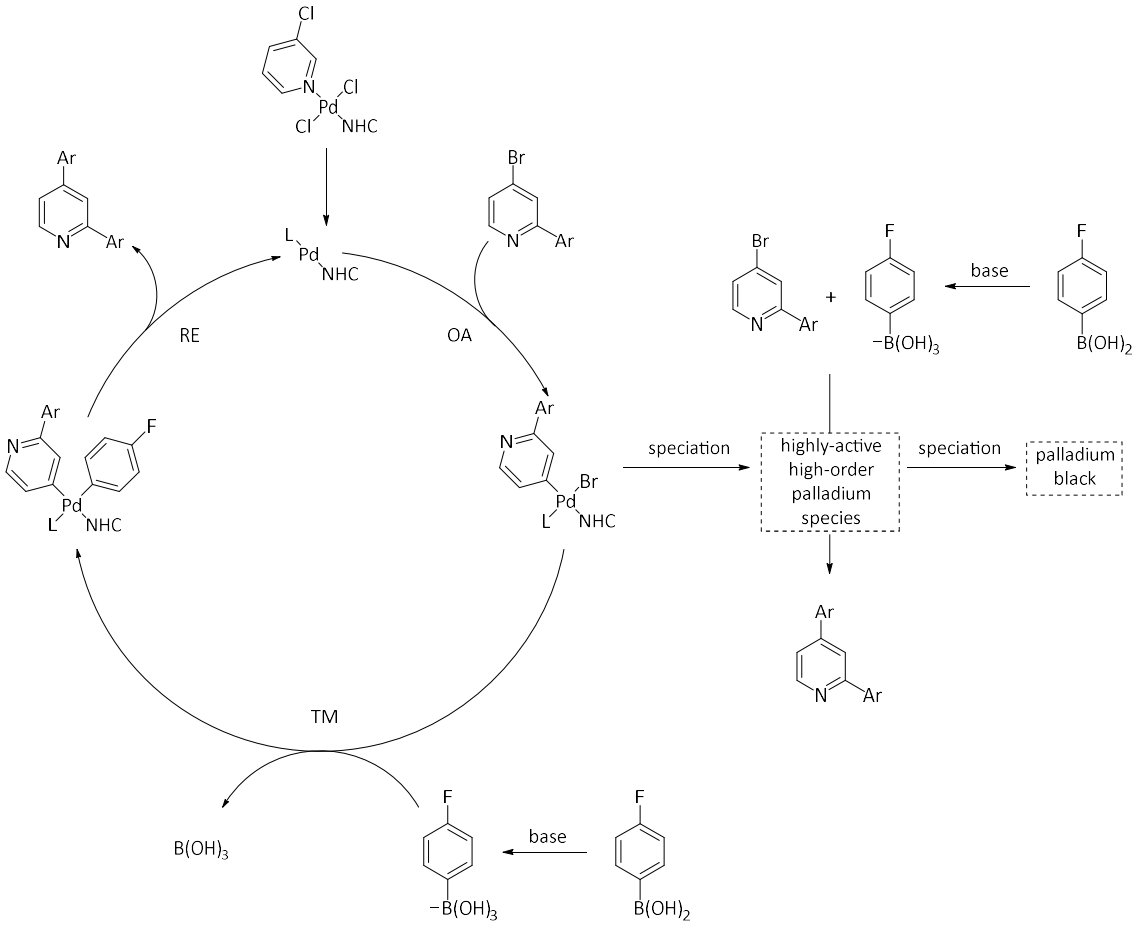

Figure 5.28 – The proposed catalytic cycle for the SMCC of 2-(p-fluorophenyl)-4-bromo-pyridine (2-Ar) and p-fluorophenylboronic acid in the presence of base.

It is unlikely that the proposed mechanism for the formation of 2,4-Ar from 2-Ar, through a high-order palladium species, is in operation during the standard catalytic reactions with 2,4-dibromopyridine. No visible black deposits were seen in the standard reactions and the reaction profiles when using 2,4-dibromopyridine and 2-Ar were significantly different to each other. Formation of 2,4-Ar from 4-Ar may occur during the standard reactions, as there were no

obvious factors in the 4-Ar starting material data to discount the involvement of this mechanism. However, since there was no observable consumption of 4-Ar in the formation of 2,4-Ar in the standard catalytic reactions, this mechanism may only account for the formation of a very small amount of 2,4-Ar. These investigations using 2-Ar and 4-Ar therefore further support the hypothesised concerted formation of 2,4-Ar (Chapter 4.4.3).

5.3.5 Kinetic Analysis of 2,4-Ar Formation from Pre-Arylated Substrates

The mechanistic rationale discussed above informed the models used to analyse the time course data using the Compunetics software. Firstly, a model was used to describe the reactivity of the bulky and non-bulky Pd-NHC complex when employing 4-Ar as the substrate, with terms relating to precatalyst activation, reaction propagation and catalyst deactivation (Table 5.3). This model resulted in a kinetic fit with excellent agreement to the experimental data for each complex (Figure 5.29). Comparison of the rate constants associated with each complex shows that the bulky complex is both more catalytically active in the reaction and deactivates at a slower rate. This observation was also seen when comparing ***C7*** and ***C14*** in the standard catalytic reaction and is to be expected with the larger steric environment provided by the bulky NHC ligand.

*Table 5.3 – Compunetics model terms, their descriptions and calculated rate constants (k) for kinetic fitting to experimental data collected for the SMCC reaction between 2-bromo-4-(p-fluorophenyl)pyridine (4-Ar) and p-fluorophenylboronic acid using **C7** or **C14** as the precatalyst. BA = p-fluorophenylboronic acid, precat = **C7** or **C14**, cat = active catalytic species and decat = deactivated catalyst.*

Model Term	Description	k value (***C7***)	k value (***C14***)
precat + 2BA → cat	Precatalyst activation	3.3 M^2min^{-1}	36.1 M^2min^{-1}
4-Ar + BA + cat → 2,4-Ar + cat	2,4-Ar formation	2.82 M^2min^{-1}	1.63 M^2min^{-1}
cat → decat	catalyst deactivation	0.00403 min^{-1}	0.0171 min^{-1}

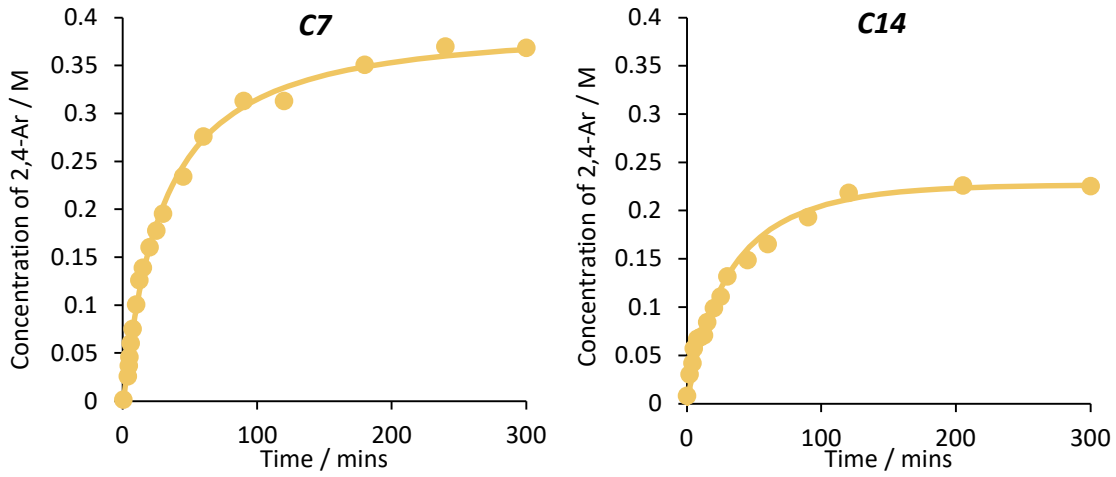

*Figure 5.29 – Time course data showing concentrations of 2,4-Ar for the reaction between 2-bromo-4-(p-fluorophenyl)pyridine (4-Ar) and p-fluorophenylboronic acid using **C7** (left) and **C14** (right) as the precatalyst. Error bars represent standard error. Kinetic fitting uses reaction model detailed in Table 5.3.*

Comparison of the rate constants associated with the model terms for each complex shows that the bulky complex is both more catalytically active in the reaction and deactivates at a slower rate. This observation was also seen when comparing ***C7*** and ***C14*** in the standard catalytic reaction and is to be expected with the larger steric environment provided by the bulky NHC ligand.

The model used to describe the reactivity of the bulky and non-bulky Pd-NHC complex when employing 2-Ar as the substrate is more complex than the 4-Ar substrate model, and includes extra terms to account for the rationale of catalyst speciation to higher order palladium species to catalyse the reaction (Table 5.4). Again, very good agreement is seen when this model is applied to the experimental data (Figure 5.30). Models not inclusive of a catalyst speciation term had a much poorer fit to the experimental data.

*Table 5.4 – Compunetics model terms, their descriptions and calculated rate constants (k) for kinetic fitting to experimental data collected for the SMCC reaction between 2--(p-fluorophenyl)-4-bromopyridine (2-Ar) and p-fluorophenylboronic acid using **C7** or **C14** as the precatalyst. BA = p-fluorophenylboronic acid, precat = **C7** or **C14**, cat1 and cat 2 = active catalytic species and decat = deactivated catalyst.*

Model Term	Description	k value (***C7***)	k value (***C14***)
precat + 2BA → cat 1	Precatalyst activation	0.409 M^2min^{-1}	1.808 M^2min^{-1}
2-Ar + BA + cat 1 → 2,4-Ar + cat 1	2,4-Ar formation (cat 1)	0 M^2min^{-1}	0 M^2min^{-1}
cat 1 → cat 2	Catalyst speciation	0.0859 min^{-1}	0.3899 min^{-1}
2-Ar + BA + cat 2 → 2,4-Ar + cat 2	2,4-Ar formation (cat 2)	118.4 M^2min^{-1}	511.6 M^2min^{-1}
cat 2 → decat	catalyst deactivation	0 min^{-1}	0 min^{-1}

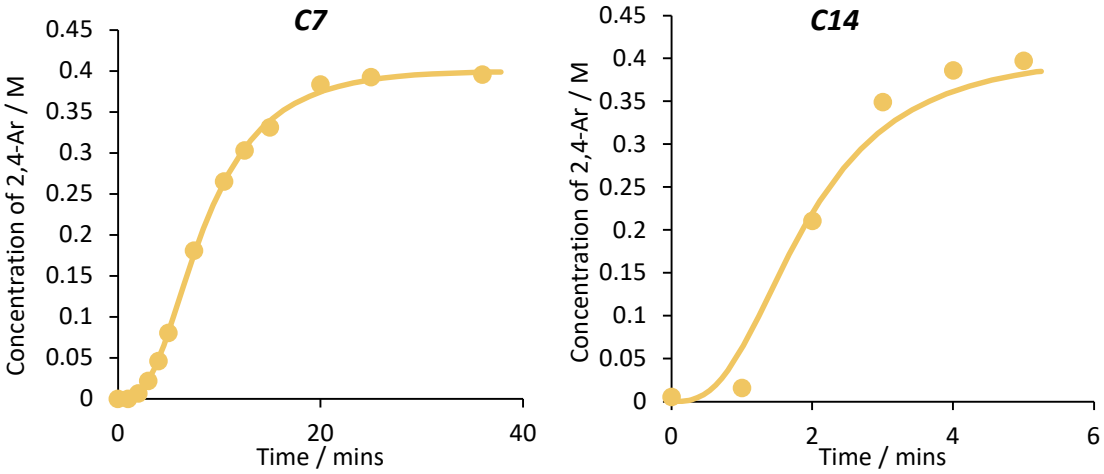

*Figure 5.30 – Time course data showing concentrations of 2,4-Ar for the reaction between 2--(p-fluorophenyl)-4-bromopyridine (2-Ar) and p-fluorophenylboronic acid using **C7** (left) and **C14** (right) as the precatalyst. Error bars represent standard error. Kinetic fitting uses reaction model detailed in Table 5.4.*

The rate constants associated with the model terms suggest that for both the bulky and non-bulky Pd-NHC complexes there is no catalytic activity associated with active palladium species formed from precatalyst activation. Instead, the reaction is catalysed by the product of catalyst speciation, in this case thought to be high-order palladium. The rate constant associated with the catalytic reaction with the second active catalytic species (high-order palladium) formed from ***C14*** is much larger than that of ***C7***, 511.6 M^2min^{-1} and 118.4 M^2min^{-1} respectively, which suggests that the active species may be different in each case. Assuming that a high-order palladium species is the catalytically active species, then the differences in rate constant may arise from either surface bound NHC ligand sterics or from the size of particle formed from each precatalyst. The kinetic model also suggests that there is no deactivation of the second active species in each reaction, however this may be due to the short time range of the reaction allowing for no appreciable catalyst deactivation to take place. These kinetic models therefore support the rationale outlined previously as to the mechanism for 2,4-Ar formation from either 2-Ar or 4-Ar.

5.4 4,4'-Bis(*p*-fluorophenyl)-2,2'-bipyridine Complexes

Two palladium complexes were identified serendipitously through treatment and analysis of the combined residues of several catalytic reaction mixtures used to investigate the cross-coupling reaction of 2,4-dibromopyridine and *p*-fluorophenylboronic acid. The reaction products, 2-Ar and 4-Ar, were separated from the residues and used in the previous investigation of 2,4-Ar formation (Chapter 5.3). Any 2,4-Ar was also removed. The remaining constituents were purified by column chromatography (DCM) and crystalised by slow vapour diffusion. The resulting crystals were analysed by SC-XRD and found to have interesting structures, ***C16*** and ***C17*** (Figure 5.31, Table 5.5). Both feature the homocoupled 4,4'-bis(*p*-fluorophenyl)-2,2'-bipyridine (4,4'-Ar-bipy). ***C16*** also features two bromide ligands and ***C17*** a bromide and a *p*-fluorophenyl ligand. Presumably, ***C17*** forms from the transmetalation of ***C16*** with *p*-fluorophenylboronic acid.

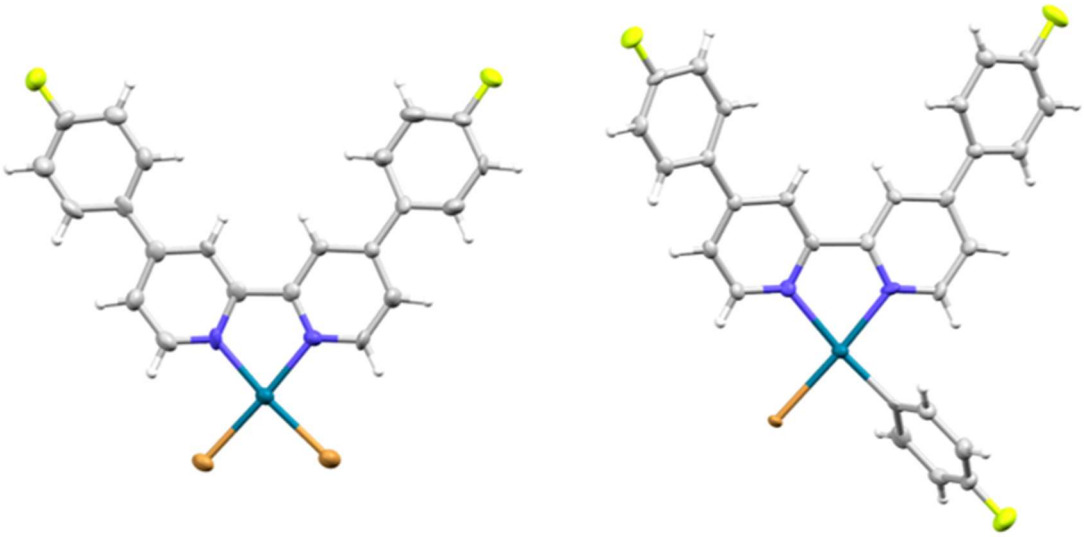

Figure 5.31 – *SC-XRD derived structures of* ***C16*** *and* ***C17*** *found through processing and crystallisation of collected catalysis waste mixtures. Thermal ellipsoids are at 50% probability level.*

Table 5.5 – Showing the Pd-N, Pd-Br and Pd-C_{Ar} bond distances and N-Pd-N bond angles for ***C16*** *and* ***C17****, determined by SC-XRD.*

Compound	Pd–N distance / Å	Pd–Br distance / Å	Pd–C distance / Å	N–Pd–N angle / deg
C16	2.044 (6)	2.426 (1)	-	80.2 (2)
	2.050 (6)	2.425 (1)	-	
C17	2.124 (5)	2.487 (1)	2.031 (7)	79.5 (2)
	2.075 (5)	-	-	

A possible route for the 4,4'-Ar-bipy ligand formation is two consecutive oxidative additions of a 2-bromopyridine (featuring either a bromo or aryl group at the 4-position) onto Pd(0), to form a Pd(IV) intermediate, which would then undergo reductive elimination of 4,4'-Ar-bipy (Scheme 5.12). Ligation of the 4,4'-Ar-bipy would be instantaneous due to the position of the nitrogen atoms following elimination. Chelating effects would prevent the dissociation of this ligand allowing the isolation of ***C16***, and the following transmetalation product, ***C17***, could be trapped and isolated too. It is unclear if this product forms exclusively from the double oxidative addition of 4-Ar, or if 2,4-dibromopyridine could be employed, making the 4,4'-dibromo-2,2'-bipyridyl which would then undergo SMCC in solution to form the observed product. The homo coupling of halo-pyridines with a Pd(IV) intermediate is known but the mechanism is not well discussed.[12, 13]

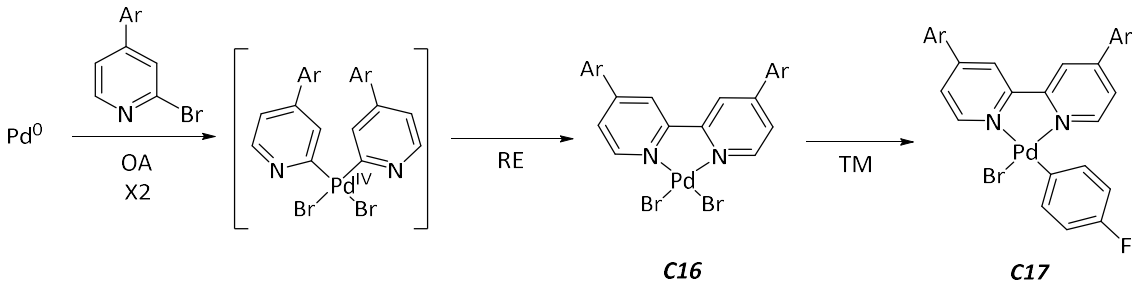

*Scheme 5.12 – Possible route for the formation of **C16** and **C17** through the double oxidative addition of 2-bromo-4-arylpyridine onto Pd(0) followed by reductive elimination (**C16**) and transmetalation with p-fluorophenylboronic acid (**C17**).*

The Pd(0) in the proposed route could originate either as the by-product of the reductive elimination of the 2-aryl imidazoliums (***Ar-Imid1-3***) discussed earlier in Chapter 5.2.1, or as the side product for the formation of the *cis*-NHC palladium complex (***C15***, Chapter 0). The formation of complexes ***C16*** and ***C17*** in solution is viable for both the bulky and non-bulky complexes as evidence shows that both can generate Pd(0). This side reaction would explain the apparent lack of palladium black deposits in the catalytic reactions as the Pd(0) would be consumed for this reaction. Complexes ***C16*** and ***C17*** could act as precatalysts for the cross-coupling reaction and would be interesting for further investigations.

5.5 Summary

The investigations discussed throughout this chapter, examining the activation, propagation and potential deactivation of the catalytic species, give additional evidence for the mechanistic rationale discussed in Chapter 4.4 and, more generally, highlight the complex nature of the catalyst system. The investigations of 2,4-Ar formation from the mono-arylated products in the reaction further support a concerted mechanism to 2,4-Ar formation as discussed in Chapter 4.4.3, as markedly different reactivity was seen in these investigations compared to that of the standard catalytic reaction.

The activation of the complexes has been shown to proceed as expected for Pd-NHC complexes and the importance of the pyridine coupling partner to prevent immediate palladium agglomeration was also demonstrated. Incomplete precatalyst activation has also been shown to generate ***C15***, a Pd-NHC_2 species, which opens further lines of investigation into ligand exchange in Pd-NHC catalyst systems, its propensity and the resultant effect on catalytic activity and product site-selectivity.

Identification of structures from HRMS show that reductive elimination of the NHC ligand from palladium can occur in this system and can generate free Pd(0) to undergo off-cycle or side reactions. Understanding these processes and how to impart control over them is crucial in

catalyst design, not only for this specific reaction but for all palladium catalysis. Similarly, the characterisation of structures accumulated in catalyst waste was shown to be a valuable methodology as unexpected, yet prevalent processes may be identified or inferred.

5.6 References

1. M. C. D'Alterio, E. Casals-Cruanas, N. V. Tzouras, G. Talarico, S. P. Nolan and A. Poater, *Chemistry (Easton)*, 2021, **27**, 13481-13493.
2. M. G. Organ, G. A. Chass, D. C. Fang, A. C. Hopkinson and C. Valente, *Synthesis-Stuttgart*, 2008, 2776-2797.
3. K.-T. Chan, Y.-H. Tsai, W.-S. Lin, J.-R. Wu, S.-J. Chen, F.-X. Liao, C.-H. Hu and H. M. Lee, *Organometallics*, 2009, **29**, 463-472.
4. C. F. Fu, C. C. Lee, Y. H. Liu, S. M. Peng, S. Warsink, C. J. Elsevier, J. T. Chen and S. T. Liu, *Inorg Chem*, 2010, **49**, 3011-3018.
5. J. P. Norman, N. G. Larson and S. R. Neufeldt, *ACS Catal.*, 2022, **12**, 8822-8828.
6. T. P. Nicholls;, J. R. Williams; and C. E. Willans, in *Adv. Organomet. Chem.*, 2021, vol. 75, ch. 6, pp. 245-329.
7. K. Nakatsu, K. Kinoshita, H. Kanda, K. Isobe, Y. Nakamura and S. Kawaguchi, *Chem. Lett.*, 1980, **9**, 913-914.
8. T. A. Anderson, R. J. Barton, B. E. Robertson and K. Venkatasubramanian, *Acta Crystallogr. Sect. C: Cryst. Struct. Commun.*, 1985, **41**, 1171-1173.
9. C. Sicre, J. L. Alonso-Gomez and M. M. Cid, *Tetrahedron*, 2006, **62**, 11063-11072.
10. C. Sicre, A. A. C. Braga, F. Maseras and M. M. Cid, *Tetrahedron*, 2008, **64**, 7437-7443.
11. K.-H. Yih and G.-H. Lee, *J. Chin. Chem. Soc.*, 2008, **55**, 109-114.
12. C. Z. Qi, X. D. Sun, C. Y. Lu, J. Z. Yang, Y. J. Du, H. J. Wu and X. M. Zhang, *J. Organomet. Chem.*, 2009, **694**, 2912-2916.
13. J. Nicasio-Collazo, K. Wrobel, K. Wrobel and O. Serrano, *New J. Chem.*, 2017, **41**, 8729-8733.

Chapter 6

Conclusions and Future Work

The aim of this body of work was to gain a deeper understanding of the site-selectivity in the Suzuki-Miyaura cross-coupling (SMCC) reaction of 2,4-dibromopyridine and arylboronic acid with Pd-NHC complexes as precatalysts. Whilst there is much more work to be done to completely understand this complicated system and the subtle nuances in operation, the studies conducted have enabled mechanistic proposals and the identification of proposed active species and possible deactivation routes. The importance of rigorously understanding palladium catalysis and site-selectivity cannot be understated, especially when considering the continued and significant reliance of palladium in industrially relevant processes.

Fourteen Pd-NHC complexes were successfully synthesised and characterised by ^{1}H and ^{13}C NMR spectroscopy, HRMS, and in some cases single-crystal X-ray diffractometry. These complexes featured NHC ligands with differing steric and electronic properties, to assess any structure activity relationships of the complexes when used as precatalysts in the SMCC reaction of 2,4-dibromopyridine and *p*-fluorophenylboronic acid. Mixing of halides on the palladium complexes was discovered to be an issue when utilising imidazolium bromide salts which was overcome by utilisation of imidazolium salt ligand precursors with a non-coordinating hexafluorophosphate counterion.

A catalytic protocol, including sampling and workup, was optimised to generate valid and accurate catalytic data, before being applied in the site-selectivity studies. A quantitative ^{19}F NMR spectroscopy method was used for the analysis of product yields with the use of an internal standard. The reaction workup procedure and analysis method was validated by replication of literature data on the site-selectivity for this SMCC reaction with a different palladium catalyst system.[1]

The use of ^{19}F NMR spectroscopy proved to be a valuable tool in expediting data analysis without compromising accuracy, as typically the ^{19}F NMR spectra were cleaner and less effected by signal overlapping than the ^{1}H NMR spectra. However, reaction analysis by means of gas chromatography (GC) or high-performance liquid chromatography (HPLC) would be an improvement over ^{1}H and ^{19}F NMR spectroscopic analysis and should be considered for future investigations. With the appropriate calibration, the product yields could be determined accurately and require a much simpler reaction work-up. It was shown that the sample workup for NMR spectroscopic analysis limits the kinetic analysis available, as reagent concentrations are diminished during the workup. The ability to accurately measure reagent concentrations

over time opens avenues such as visual kinetic analysis, where reagent and catalyst rate orders can be determined easily.

Initial screening of the Pd-NHC complexes under the same conditions as the benchmark reaction resulted in a complete lack of activity. Individual parameters of the reaction conditions were varied systematically to identify the possible source of inactivity when using the Pd-NHC complexes. It was found that the reaction performance was somewhat influenced by temperature and the choice of base. Additionally, it was speculated that peroxides formed from the THF solvent negatively impacted the catalytic activity, a consideration that must be observed for future studies. Appropriate reaction conditions were determined through this process such that analysis of the Pd-NHC complexes catalytic activity could begin.

No trends in site-selectivity were identified with respect to the Pd-NHC ligand electronics. The NHC ligand sterics were shown to have some influence on site-selectivity whereby the very bulky NHC ligand complexes facilitated the almost exclusive formation of 2,4-Ar, and the non-bulky NHC complexes formed the mono-arylated products with selectivity for 4-Ar over 2-Ar. This behaviour was examined further by mapping the product formations over time for a bulky and a non-bulky NHC complex. It became apparent that 2,4-Ar formed through a concerted mechanism as there was no depletion of the mono-arylated products corresponding with an increasing 2,4-Ar yield with both complexes.

The nature of the catalyst system was determined to be homogeneous based on results from the mercury drop tests and PVPy poisoning reactions. Further evidence could be gathered through use of the three-phase test and mid reaction filtration test to conclusively prove this. Catalyst speciation has been shown to play a major role in this SMCC reaction with a different catalyst system so it is not unreasonable to assume that some speciation can occur with Pd-NHC complexes in this reaction.[1, 2] Investigating site-selectivity within this reaction when using higher order Pd species with NHCs would be valuable and give interesting evidence on how catalyst speciation over time may influence site-selectivity similar to Pd-NHC catalyst systems. This is a relatively unexplored area of palladium catalysis and further research would be beneficial in predicting alterations to catalyst activity over time.

The effect of the catalyst loading was also explored during these investigations. It was shown that the catalyst loading influenced the activity of the non-bulky complexes. An unexplained outcome was obtained when using one of the non-bulky complexes where an increased catalyst loading (expected to promote catalyst deactivation) changed the selectivity of the complex, reducing the yield of only one of the products, 2,4-Ar. Further work is needed to understand this fully, possibly through the analysis of time course data over a range of catalyst loadings. This in

combination with HRMS to identify possible changes to the active species could build a more complete picture of the catalyst action and deactivation.

Work by Neufeldt and co-workers proved to be valuable in proposing a mechanistic rationale for the site-selectivity of the Pd-NHC complexes.[3-5] It was proposed that the active species generated from the Pd-NHC precatalysts interact preferentially at the 4-Br position of 2,4-dibromopyridine, analogously to Neufeldt's 2,4-dichloropyridine system. This would account for the selectivity of 4-Ar over 2-Ar with the Pd-NHC complexes.

2,4-Ar formation was also proposed to occur by a concerted mechanism (Figure 4.24). This rationale is based upon the relative rates of transmetalation versus oxidative addition from an oxidative addition intermediate. The sterics of the NHC ligand were shown to potentially influence these relative rates and therefore dictate the selectivity of the complexes for the mono-arylated products or the di-arylated product. Examination of the alternative sequential mechanism of 2,4-Ar formation by reaction of 2-Ar or 4-Ar with arylboronic acid indicated that this mechanism was not responsible for 2,4-Ar formation in the standard catalytic reaction. DFT calculations would likely give a good indication of the validity of this rationale. This hypothesis could also be tested through analysis of Pd-NHC complexes featuring asymmetrical *N*-substituents (Figure 6.1).

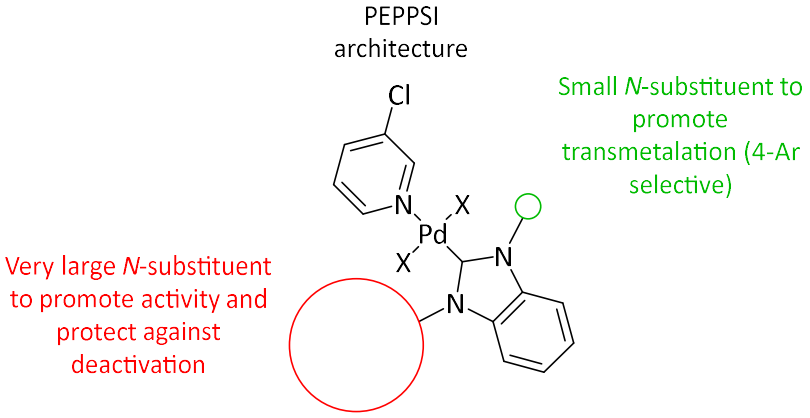

Figure 6.1 – General structure of possible precatalyst for 4-Ar selectivity in SMCC of 2,4-dibromopyridine and p-fluorophenyl boronic acid. A small N-substituent promotes transmetalation and therefore 4-Ar selectivity, whilst a large N-substituent aids in preventing catalyst deactivation.

More detailed analyses of certain aspects of the catalytic reaction were also conducted. The activation of the complexes was probed and it was found that activation proceeded through the expected aryl boronic acid homocoupling pathway, and under certain conditions side reactions were found to from unexpected *cis*-Pd-NHC_2 structures. The implications of this were not explored fully, however considering Neufeldt's work, the generation of a Pd-NHC_2 species in the catalytic reaction may have an effect on the overall site-selectivity.[3-5] A natural progression of

this work would be the examination of Pd-NHC_2 complexes and their selectivity in the reaction of interest. Going further still, investigation of strong and weak chelating effects on site-selectivity may also prove valuable in catalyst design for tailored reaction performance and improvement of catalyst lifetime.

Analysis of catalytic reaction mixtures with HRMS showed the formation of reductively eliminated arylimidazolium salts during the reaction. This is thought to be a possible deactivation pathway for the active catalytic species where Pd(0) generated from this reductive elimination may undergo speciation or side reactions to form catalytically inactive palladium. The potential active species for the catalytic reaction when using a bulky Pd-NHC complex was also identified by HRMS. Despite not being able to determine the absolute structure of this species, it was shown that an NHC ligand, an oxidatively added pyridinyl and a coordinating product pyridine were all bound to palladium. All of the data collected from the HRMS studies agreed with the proposed mechanism for both the formation of the mono-arylated products and the concerted formation of 2,4-Ar.

Finally, interesting and unexpected palladium structures were discovered when processing the catalyst waste from a series of reactions. Apparent homocoupling of substituted pyridine species had occurred to form a 4,4'arylated-2-bispyridine ligand in the catalytic reactions. The pathway towards this ligand formation in solution was discussed which linked back to Pd(0) generation from arylimidazolium reductive elimination from palladium, and Pd-NHC_2 generation. The serendipitous identification of this unusual complex appropriately highlights the inherently complex nature of palladium catalysis and the need for deeper understanding to impart better control in important processes.

There is a long way to go before this catalytic system may be understood completely but this is vital for the application of homogeneous palladium catalysis going forward in order to limit consumption of this valuable and finite resource.

6.1 References

1. N. W. J. Scott, M. J. Ford, N. Jeddi, A. Eyles, L. Simon, A. C. Whitwood, T. Tanner, C. E. Willans and I. J. S. Fairlamb, *J. Am. Chem. Soc.*, 2021, **143**, 9682-9693.
2. N. W. J. Scott, M. J. Ford, C. Schotes, R. R. Parker, A. C. Whitwood and I. J. S. Fairlamb, *Chem. Sci.*, 2019, **10**, 7898-7906.
3. J. P. Norman, N. G. Larson, E. D. Entz and S. R. Neufeldt, *J. Org. Chem.*, 2022, **87**, 7414-7421.
4. J. P. Norman, N. G. Larson and S. R. Neufeldt, *ACS Catal.*, 2022, **12**, 8822-8828.
5. J. P. Norman and S. R. Neufeldt, *ACS Catal.*, 2022, **12**, 12014-12026.

Chapter 7

Proof of Concept Studies for Future Research on SMCC Using Pd-NHC Complexes: Imidazolium Palladate Salts, Nanoparticles and Chelating NHC Ligands

This chapter covers work conducted during the course of the investigations into the site-selectivity of the SMCC reaction of 2,4-dibromopyridine and *p*-fluorophenylboronic acid that marginally diverges from the main narrative but relates to aspects of the future work described in Chapter 6. This initial future work, therefore, explores further aspects of the catalytic reaction and demonstrates the direction further investigations may take.

7.1 Imidazolium and NHC Ligand Stabilised Palladium Nanoparticles

The work previously discussed indicates that the SMCC reaction of 2,4-dibromopyridine and *p*-fluorophenylboronic acid with Pd-NHC precatalysts proceeds through a homogeneous route. However, with Fairlamb's seminal work on palladium speciation and the involvement of higher order palladium species in related catalytic reactions, the involvement of palladium nanoparticles in this reaction cannot be overlooked when gathering a full understanding of the catalyst system.[1, 2] Foundational work to identify the effects of palladium nanoparticle involvement in the catalytic reaction was therefore conducted as a starting point for further investigations.

Palladium nanoparticles stabilised either by surface bound NHC ligands or through electronic stabilisation of imidazolium ions appropriately relate to the SMCC reaction of interest with Pd-NHC precatalysts, as they are assumed to be the most likely to form during palladium speciation in this reaction. The synthesis of these palladium nanoparticles and investigation of their corresponding catalytic activity and site-selectivity would enable an inferred understanding of their influence in the standard catalytic reaction. Imidazolium palladate salts (IPSs) are reported as both NHC stabilised and imidazolium ion stabilised palladium nanoparticle precursors, and as such were used here (Figure 7.1).[3]

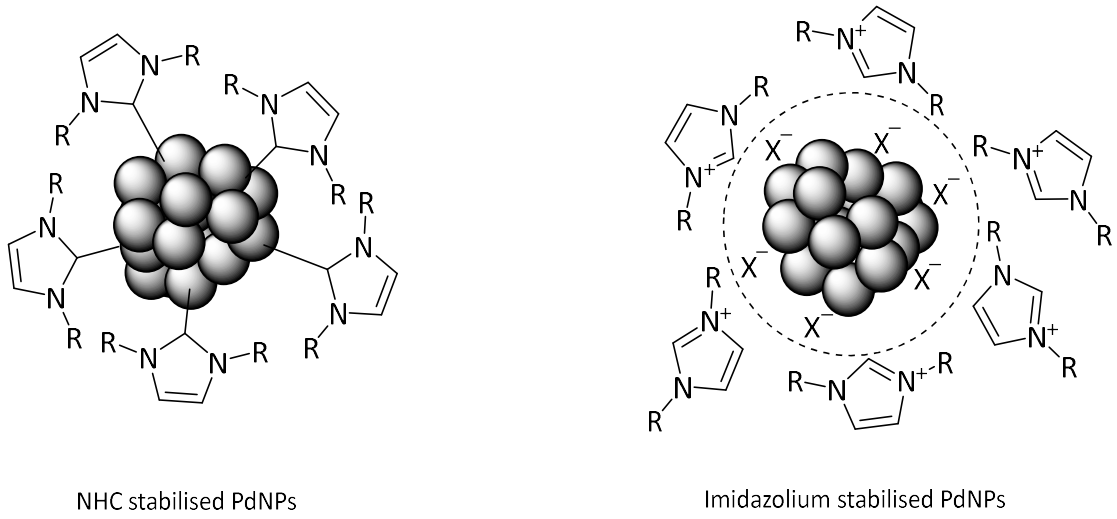

Figure 7.1 – Illustration of the structure of NHC and imidazolium stabilised palladium nanoparticles (X = halide). Adapted from Beer.[3]

A small library of imidazolium palladate salts was formed from a selection of the imidazolium salts used previously as NHC ligand precursors. The bulky imidazolium salts ***I7*** and ***I8*** featuring a chloride counterion were used to make the ***IPS7*** and ***IPS8*** respectively. The non-bulky imidazolium salts with bromide or chloride counterions, ***I4***, ***I5***, ***I6*** and ***I12***, were used to make ***IPS4***-***IPS6*** and ***IPS12*** respectively. The palladium nanoparticles formed from these imidazolium salts may offer insight into a structure activity relationship.

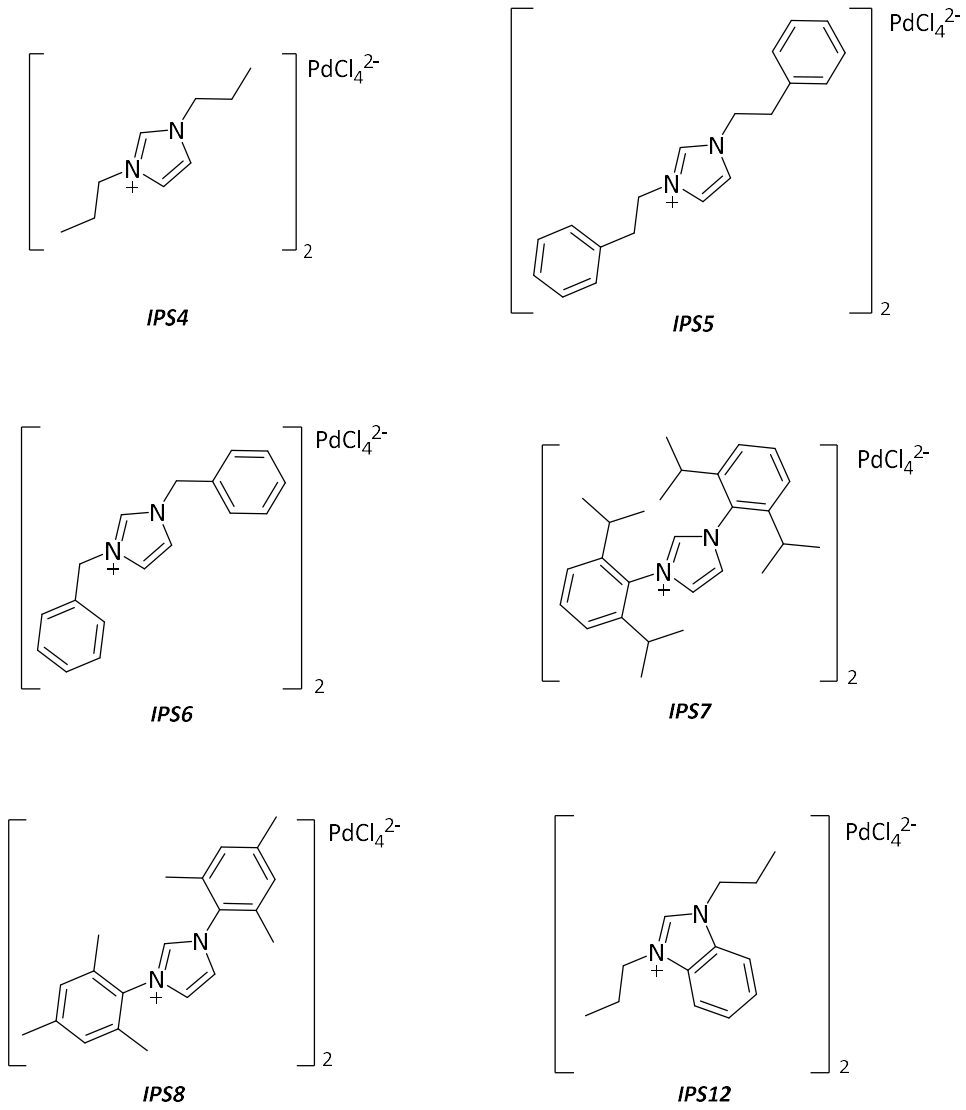

*Figure 7.2 – Imidazolium palladate salts **IPS4**–**IPS8** and **IPS12** to be used as precatalysts of NHC and imidazolium stabilised palladium nanoparticles.*

7.1.1 Palladium Nanoparticle Precursor Synthesis

The synthetic method used for imidazolium palladate salts was outlined by Beer and co-workers.[3] The imidazolium salts, with either a bromide or chloride counterion, were subjected to a counterion exchange with Na_2PdCl_4 at the solvent interface of chloroform and water (Scheme 7.1). When utilising this methodology, the dark red colour of the Na_2PdCl_4 aqueous solution would dissipate as the counterion exchange occurred, and the IPS would form in the organic phase. Any salt (NaBr or NaCl) by-products would reside in the aqueous phase. Separation of the organic phase and subsequent solvent removal resulted in clean isolation of the IPS with little purification needed. Na_2PdCl_4 was used in excess to ensure full reaction of the imidazolium salt.

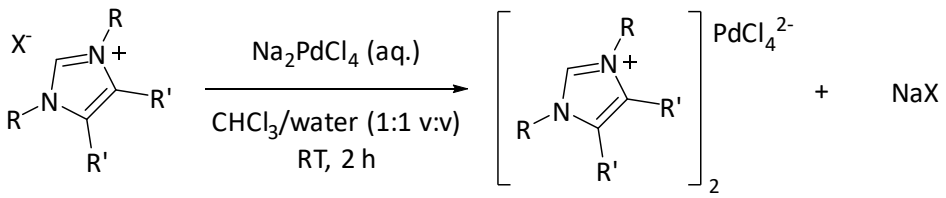

R = propyl, benzyl, 2-phenylethyl, Mes or Dipp
R' = H or (benzimidazole)
X = Cl or Br

Scheme 7.1 – General reaction scheme for the formation of imidazolium palladate salts (IPSs) through counterion exchange in chloroform and water. Adapted method by Beer and co-workers.[3]

The successful synthesis of ***IPS4***-***IPS8*** and ***IPS12*** was indicated by a shift in the ^{1}H NMR spectroscopy signals associated with the C2-proton and backbone protons compared with the parent imidazolium salt (Figure 7.3), with the exception of ***IPS5*** where only the C2-proton shift was observed as no backbone protons are present. Shifts in the corresponding carbon signals were also seen in ^{13}C NMR spectra. Mass spectrometry was also used to identify the imidazolium ion.

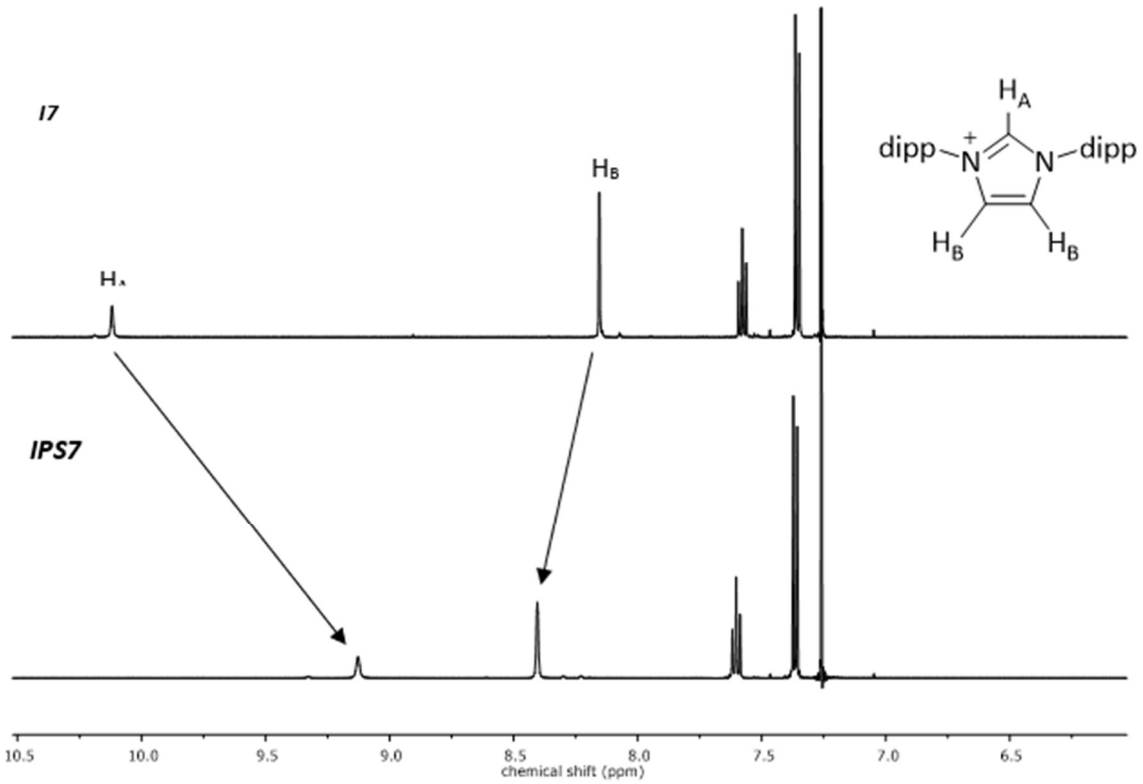

*Figure 7.3 – ^{1}H NMR spectrum (chloroform-d, 500 MHz) of **I7** (top) and IPS7 (bottom) to show the shift in key signals, namely the **C2** (H_A) and backbone (H_B) protons on the heterocycle.*

SC-XRD was also performed on IPS samples where single crystals could be obtained through slow vapour diffusion. The crystal structure of ***IPS7*** shows the presence of two imidazolium ions together with the $PdCl_4^{2-}$ counterion (Figure 7.4).

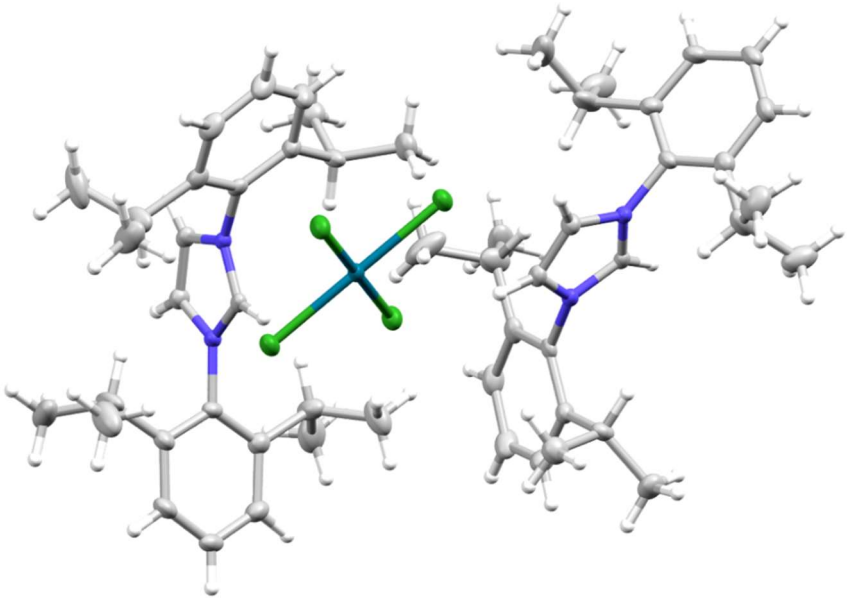

*Figure 7.4 – SC-XRD derived structure of **IPS7** showing two imidazolium ions and a single $PdCl_4^{2-}$ ion. Thermal ellipsoids are at 50% probability level.*

The SC-XRD data did highlight an issue with the synthesis regarding the palladium containing the counterion. The crystal structure of ***IPS8***, for example, showed that when using the imidazolium chloride salts for the conversion into the corresponding IPS, a mixture of $PdCl_4^{2-}$ and $Pd_2Cl_6^{2-}$ counterions may occur (Figure 7.5). It was assumed that the $Pd_2Cl_6^{2-}$ counterion formed spontaneously in the reaction as part of an equilibrium between Na_2PdCl_4 and $Na_2Pd_2Cl_6$. Addition of NaCl might push the equilibrium position to shift and increase the relative amount of Na_2PdCl_4. This was attempted for the repeated synthesis of ***IPS8*** with the addition of NaCl to the reaction mixture but was not successful in facilitating the generation of the $PdCl_4^{2-}$ counterion product, as evidenced by SC-XRD.

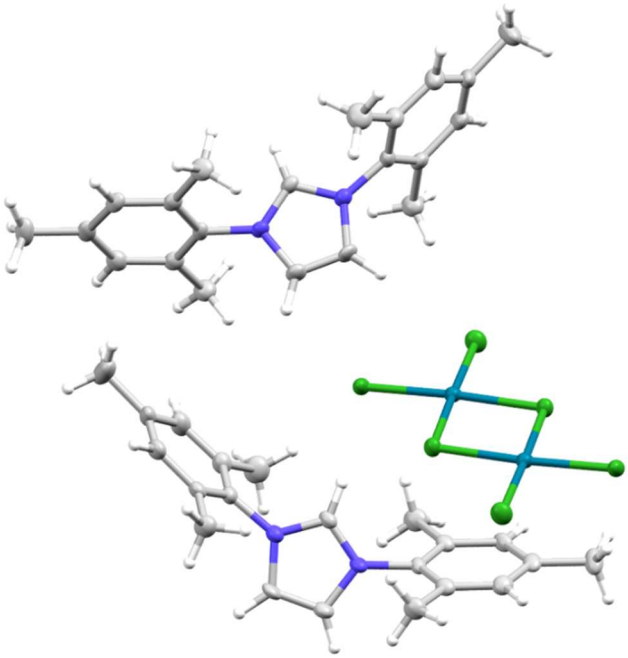

*Figure 7.5 – SC-XRD derived structure of **IPS8** showing the $Pd_2Cl_6^{2-}$ counterion. Thermal ellipsoids are at 50% probability level.*

A different issue was apparent when starting from the imidazolium salts with bromide counterions. It was observed from the crystal structure of ***IPS6*** that a change of the $PdCl_4^{2-}$ counterion to $PdBr_4^{2-}$ had occurred (Figure 7.6). The mixing of halides in the reaction could be overcome by the initial change of counterion of the imidazolium salt from Br^- to Cl^-. The mixing of halides, however, would not present an issue for nanoparticle synthesis.

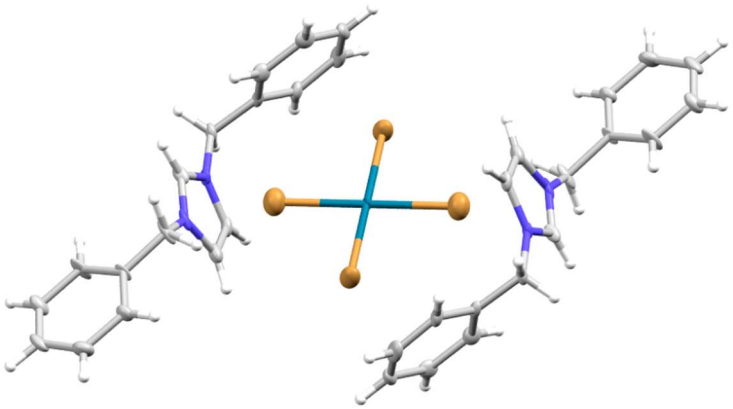

*Figure 7.6 – SC-XRD derived structure of **IPS6**, showing the $PdBr_4^{2-}$ counterion. Thermal ellipsoids are at 50% probability level.*

7.1.2 Catalytic Viability of Imidazolium Palladate Salts

Before using the imidazolium palladate salts to synthesise palladium nanoparticles, their catalytic viability was investigated in the reaction between 2,4-dibromopyridine and *p*-fluorophenylboronic acid, as nanoparticles may be formed in situ. Only ***IPS7*** and ***IPS8*** were used as precatalysts as halide mixing on the palladate counterion is absent and therefore does not introduce added variability in the data. As with the previous catalytic studies the precatalysts were used at an assumed loading of 2.5 mol%, though it is noted that the presence of the $Pd_2Cl_6^{2-}$ would skew this loading marginally. The product yields were measured quantitatively by ^1H and ^{19}F NMR spectroscopy. ***IPS7*** and ***IPS8*** were both screened using the standard reaction conditions (Scheme 4.1). For comparison the product yields of Na_2PdCl_4 and the Pd-NHC complexes relating to ***IPS7*** and ***IPS8***, ***C7*** and ***C8*** respectively are also shown (Figure 7.7). Structures of ***C7*** and ***C8*** are included for reference (Figure 1.8).

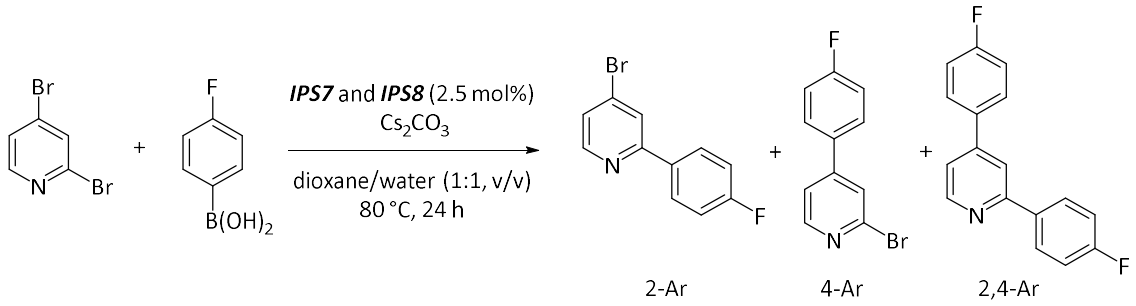

*Scheme 7.2 – Screening reaction between 2,4-dibromopyridine and p-fluorophenylboronic acid to yield 2-bromo-4-(p-fluorophenyl)pyridine (4-Ar), 2-(p-fluorophenyl)-4-bromo-pyridine (2-Ar) and 2,4-bis(p-fluorophenyl)pyridine (2,4-Ar) using standard conditions with **IPS7** and **IPS8** as precatalysts.*

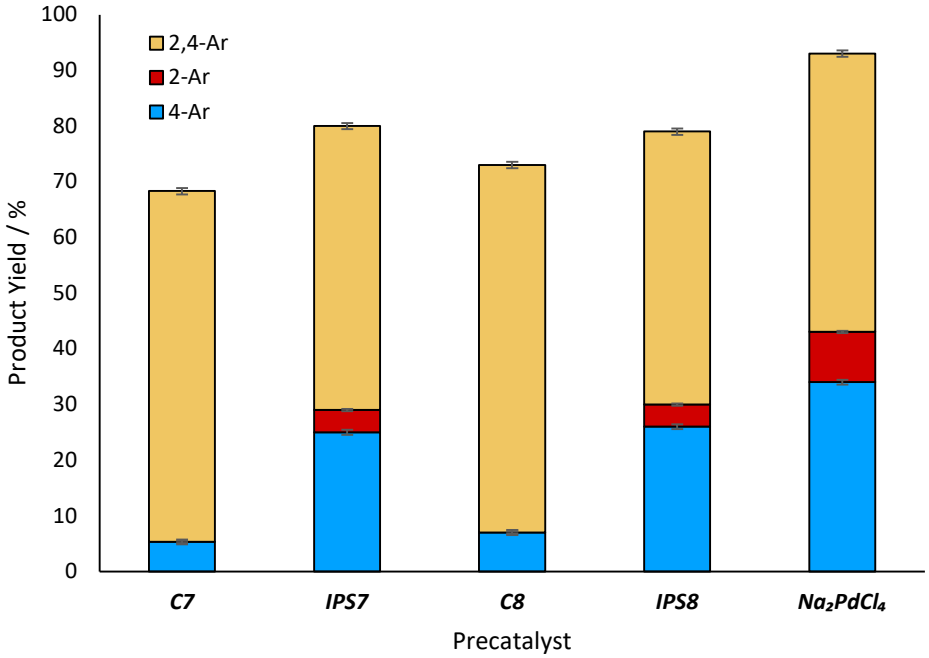

*Figure 7.7 – Product yields of 2-Ar, 4-Ar and 2,4-Ar for the reaction of 2,4-dibromopyridine and p-fluorophenylboronic acid using **IPS7** and **IPS8** as precatalysts under conditions shown in Scheme 4.1. Product yields are determined by ^{19}F NMR spectroscopy with respect to FDMB internal standard. Product yields for **C7**, **C8** and Na_2PdCl_4 are also shown for comparison. Error bars represent standard error.*

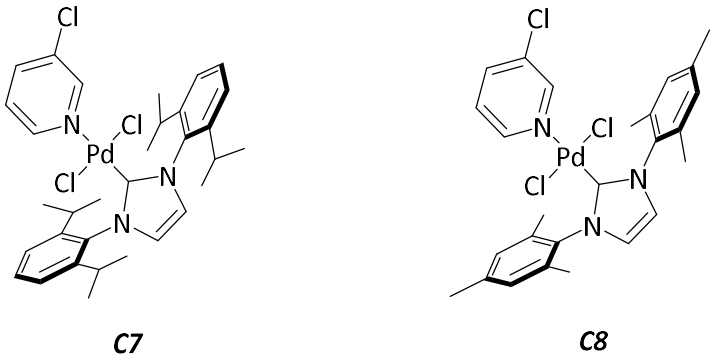

*Figure 7.8 – Structures of Pd-NHC complexes **C7** and **C8** for reference.*

The reaction outcome for both ***IPS7*** and ***IPS8*** are almost identical and are selective for 4-Ar over 2-Ar. There is a large amount of 2,4-Ar seen in each case also, resulting in 2,4-Ar being the major product. Comparison to the related Pd-NHC complexes, ***C7*** and ***C8***, show that ***IPS7*** and ***IPS8*** do react differently. As discussed previously (Chapter 4.1.1 and Chapter 5.2.2) this is likely due to the NHC ligand in the Pd-NHC complexes remaining attached during the catalysis thus influencing the product selectivity, and the lack of NHC ligand in ***IPS7*** and ***IPS8*** being unable to do so. Alternatively, the *in-situ* generation of both homogeneous Pd-NHC, accounting for high 2,4-Ar selectivity, and Pd-NPs stabilised by either imidazolium ions or NHC ligands, forming 4-Ar preferentially, may occur in the reaction and the result in the observed selectivity.[1] The catalytic product yields when utilising ***IPS7*** and ***IPS8*** do differ slightly from Na_2PdCl_4 where the latter

shows increased activity, which suggests that there may be some influence on the reaction outcome due to the presence of the imidazolium ion.

Currently, without further investigation into the active species generated by the imidazolium palladate salts, it is unclear what involvement the imidazolium may have in the catalysis. The screening of other IPSs under these conditions would give some further insight, as a structure activity relationship of the imidazolium ions of different IPSs may become apparent, which would indicate that the imidazolium does have an effect on activity and site-selectivity of an IPS. Indeed, closely related unpublished work within the group showed a different reaction outcome when using an IPS with a C2-arylated benzimidazolium ion (***Ar-IPS***, Figure 7.9) to the data collected for ***IPS7*** and ***IPS8*** (Figure 7.10). This could be due to the change in imidazolium structure, or the activity may have been influenced by the blocking of the C2-position, thus preventing NHC formation. The inclusion of iodide ions from ***Ar-IPS*** into the reaction mixture may also have an impact on selectivity. As such the study of catalysis using imidazolium palladate salts remains and open and interesting line of investigation.

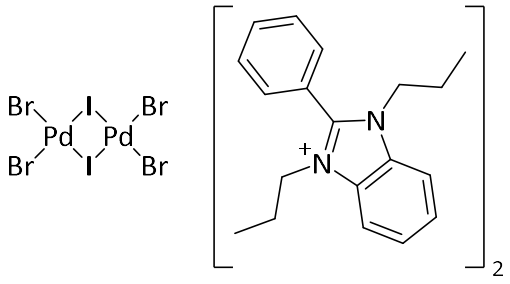

Ar-IPS

Figure 7.9 – Structure of the C2 arylated imidazolium palladate salt, ***Ar-IPS****, used for a related study in the group.*

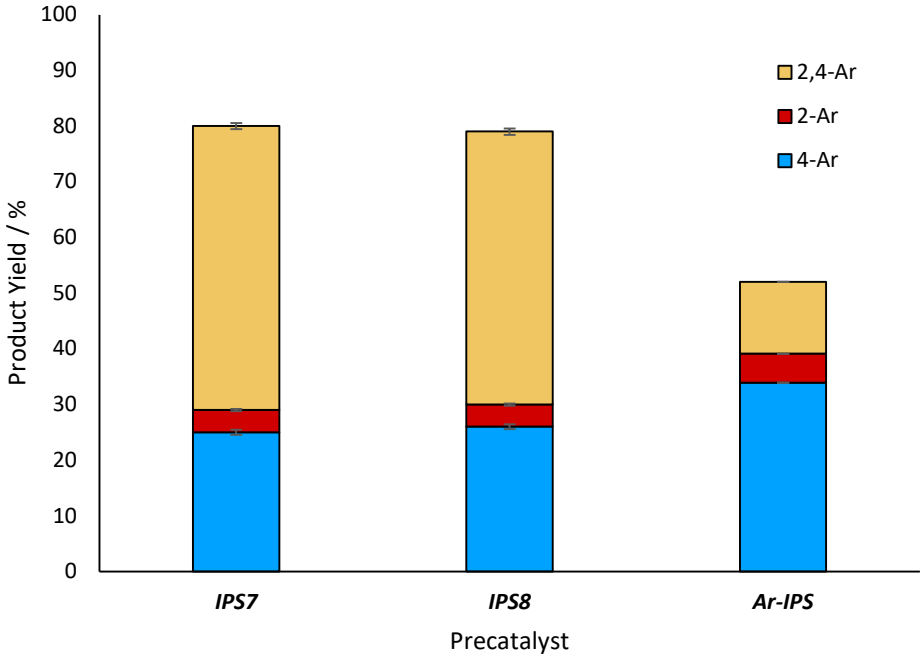

*Figure 7.10 – Product yields of 2-Ar, 4-Ar and 2,4-Ar for the reaction of 2,4-dibromopyridine and p-fluorophenylboronic acid using **IPS7**, **IPS8** and **Ar-IPS** as precatalysts under conditions shown in Scheme 4.1. Product yields are determined by ^{19}F NMR spectroscopy with respect to FDMB internal standard. Error bars represent standard error.*

7.1.3 Imidazolium and NHC Ligand Stabilised Palladium Nanoparticle Synthesis

The synthesis of palladium nanoparticles either stabilised by NHC ligands or imidazolium ions is described by Beer and co-workers.[3] For NHC stabilised palladium nanoparticles, deprotonation of the imidazolium ion in an IPS by a strong base to form the free carbene is followed by reduction of the palladate IPS counterion with sodium borohydride to yield the product (Route 1, Figure 7.11). For imidazolium stabilised palladium nanoparticles, the IPS palladium is reduced directly with sodium borohydride and the imidazolium ions in solutions form a bilayer around the nanoparticles, offering stabilisation (Route 2, Figure 7.11). Both methods are reported to produce stable palladium nanoparticles with a mean diameter of 2.7 and 1.8 nm respectively when using an IPS with *n*-hexyl *N*-substituents as the nanoparticle precursor.[3]

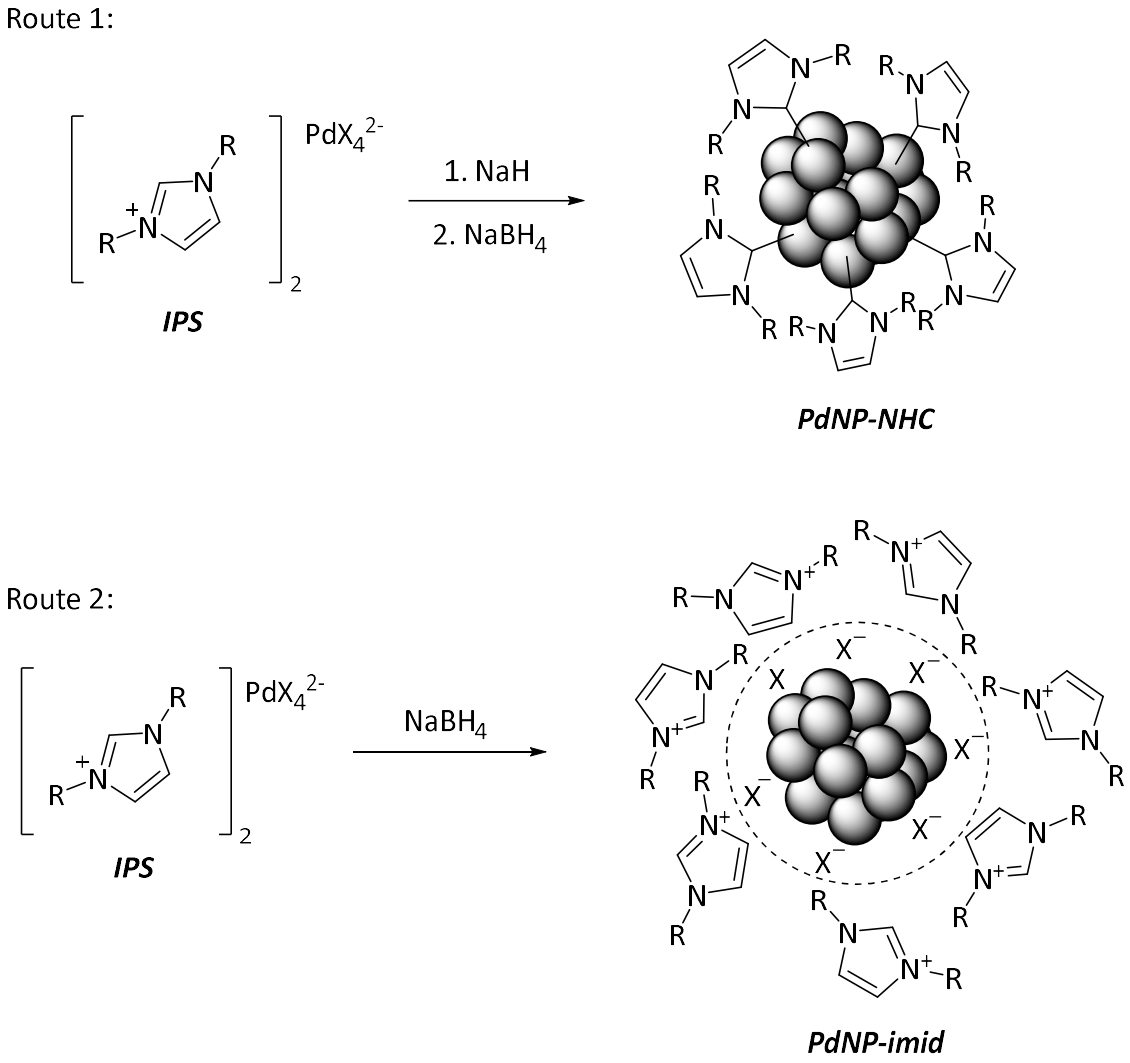

Figure 7.11 – Route 1: Synthetic pathway to make NHC stabilised palladium nanoparticles. Route 2: Synthetic pathway to make imidazolium salt stabilised palladium nanoparticles. Reported by Beer.[3]

The synthesis of NHC stabilised palladium nanoparticles was initially applied to ***IPS5*** (Scheme 7.3). The *N*-substituents on ***IPS5*** have the longest chain length of ***IPS4***-***IPS8*** and ***IPS12*** so therefore act as the best analogue to the imidazolium palladate salt used by Beer and co-workers, featuring *n*-hexyl *N*-substituents. During the first stage of the reaction the initial dark red solution of ***IPS5*** underwent a slight colour change to paler red. Following sodium borohydride addition, the solution went black and black deposits were seen on the side of the reaction vessel.

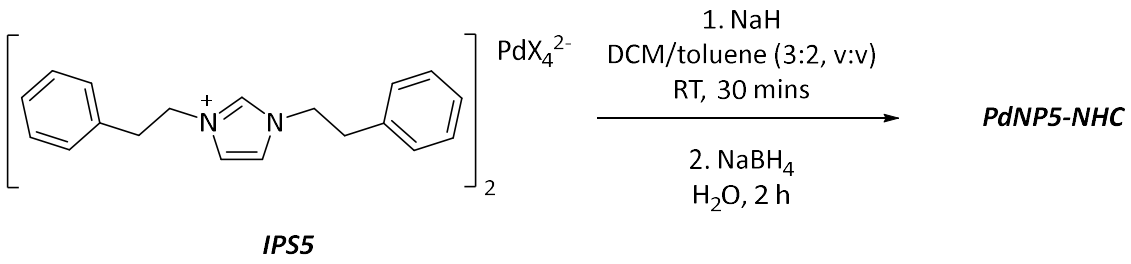

*Scheme 7.3 – Synthesis of NHC-stabilised palladium nanoparticles, **PdNP5-NHC**, from **IPS5**. Conditions and procedure adapted from Beer.[3]*

Characterisation of the reaction product by ^{1}H and ^{13}C NMR spectroscopy was attempted however the 'product' did not dissolve in any suitable NMR solvent. A small sample (5 mg) of the black residue was directly screened in the catalytic reaction of interest, however no catalytic activity was observed. This suggests that palladium black had formed instead of stable NHC furnished palladium nanoparticles and therefore this reaction was determined to have failed.

It was assumed that the most likely cause for this reaction failure was the structure of the NHC ligands not affording sufficient protection to any generated nanoparticles and thus palladium black would form through palladium agglomeration. Therefore, instead of persevering with the remaining nanoparticle precursors, ***IPS4***, ***IPS6***-***IPS8*** and ***IPS12***, the IPS reported by Beer and co-workers, with *n*-hexyl *N*-substituents (***IPS15***), was used since stable nanoparticles had been successfully formed which could be screened in the catalytic reaction of interest. ***IPS15*** was synthesised analogously to ***IPS4***-***IPS8*** and ***IPS12***, through counterion exchange of the corresponding imidazolium salt, ***I15*** (Scheme 7.4). Successful formation of ***IPS15*** was confirmed though ^{1}H and ^{13}C NMR spectroscopy and mass spectrometry.

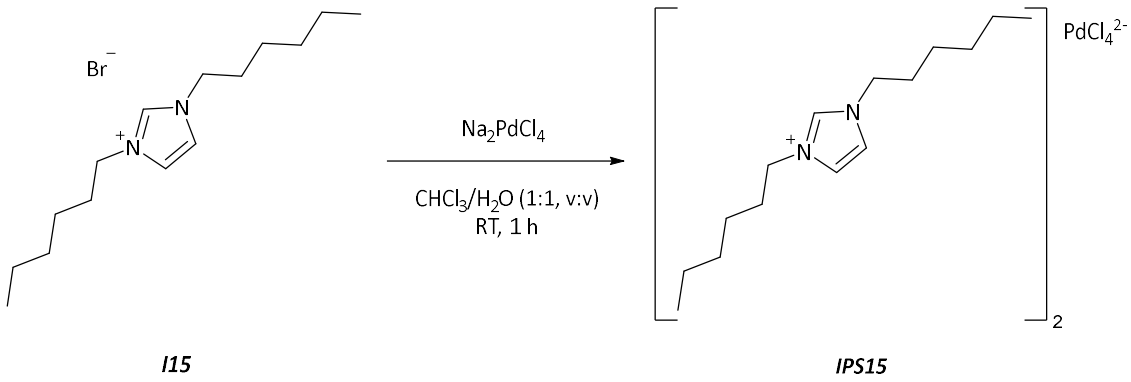

*Scheme 7.4 – Synthesis of **IPS15** through counterion exchange of **I15** using Na_2PdCl_4. Adapted method from Beer.[3]*

The two methods for imidazolium and NHC stabilised palladium nanoparticle synthesis were then applied to ***IPS15***. When attempting the synthesis of NHC stabilised palladium nanoparticles, ***PdNP15-NHC*** with ***IPS15*** (Scheme 7.5), a distinct colour change from dark red to yellow was observed upon base addition, which is indicative of free NHC formation in solution. Slow

addition of the reducing agent then facilitated another colour change of the reaction solution to black. Beer reports the product appearance as a black oil, which matched the appearance of the product isolated from this reaction.

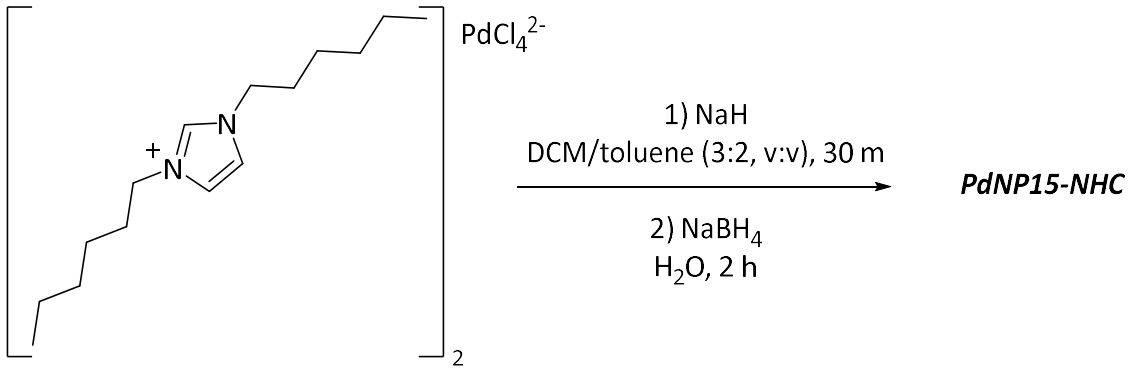

*Scheme 7.5 – Synthesis of NHC-stabilised palladium nanoparticles, **PdNP15-NHC**, from **IPS15**. Conditions and procedure adapted from Beer.*

The product was analysed by ^{1}H and ^{13}C NMR spectroscopy. The spectra in both instances are complicated and indicate a mixture of species in the sample. Comparison of the ^{13}C NMR spectra of the product to that of ***IPS15*** and the corresponding imidazolium salt, ***I15***, show the appearance of multiple signals in the region associated with the heterocycle carbons (Figure 7.12). The signals associated with ***IPS15*** have disappeared which suggests full reduction of the $PdCl_4^{2-}$ counterion to Pd(0). There are broad signals at shifts corresponding to ***I15***, which indicates that there may be some stabilisation of palladium nanoparticles by imidazolium salts (Figure 7.12), despite the target product being NHC stabilised nanoparticles. The ^{1}H NMR also shows broad signals associated with ***I15***.

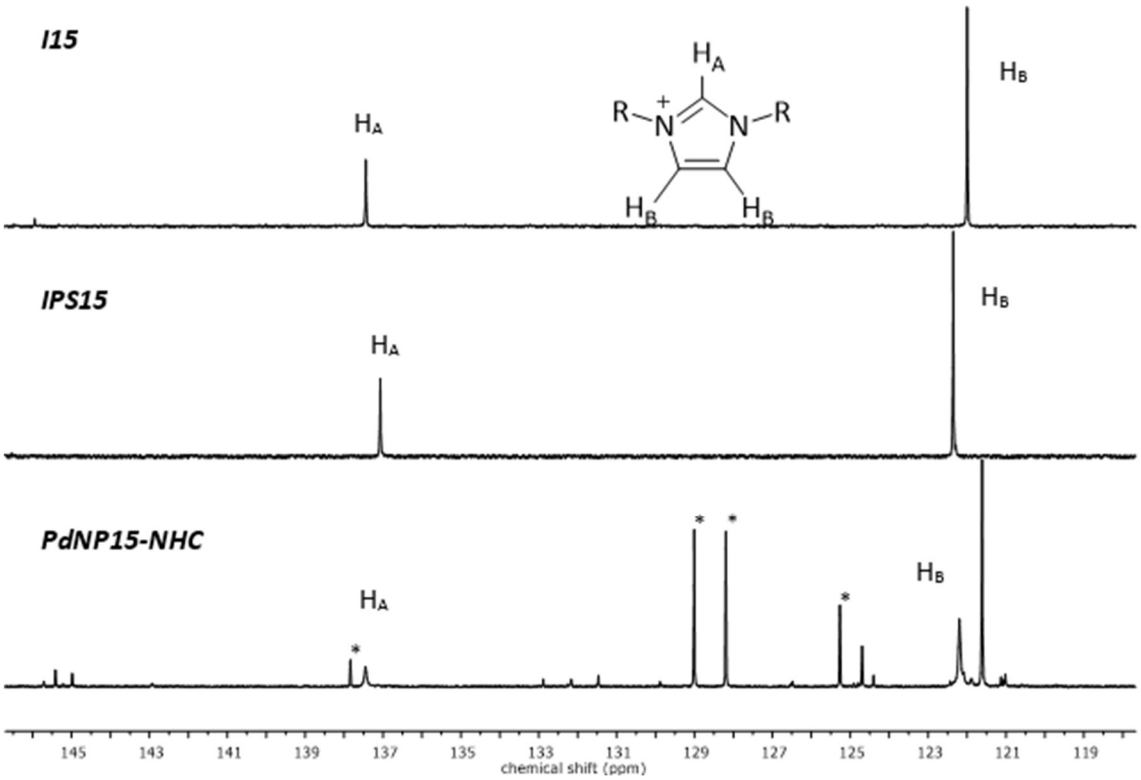

*Figure 7.12 – Stacked ^{13}C NMR spectra (chloroform-d, 500 MHz) of **I15** (top), **IPS15** (middle) and **PdNP7-NHC** (bottom) showing the appearance of multiple signals when forming **PdNP15-NHC** and the broadening of signals relating to **I15**. *Toluene peaks have been marked for clarity.*

In both the ^{1}H and ^{13}C NMR spectra, however, there were signals that indicated NHC ligand had formed during this reaction. In the ^{1}H NMR spectrum for example there are signals associated with protons on the imidazolium backbone and *N*-substituents but no corresponding C2 proton, which is characteristic of NHC formation. Likewise, the ^{13}C NMR spectrum shows backbone and *N*-substituent carbons and a very broad weak signal at 161 ppm which may correspond to a carbon bound to palladium nanoparticles (Figure 7.13). Broad signals with similar chemical shifts have been reported in successfully synthesised NHC bound palladium nanoparticles.[4]

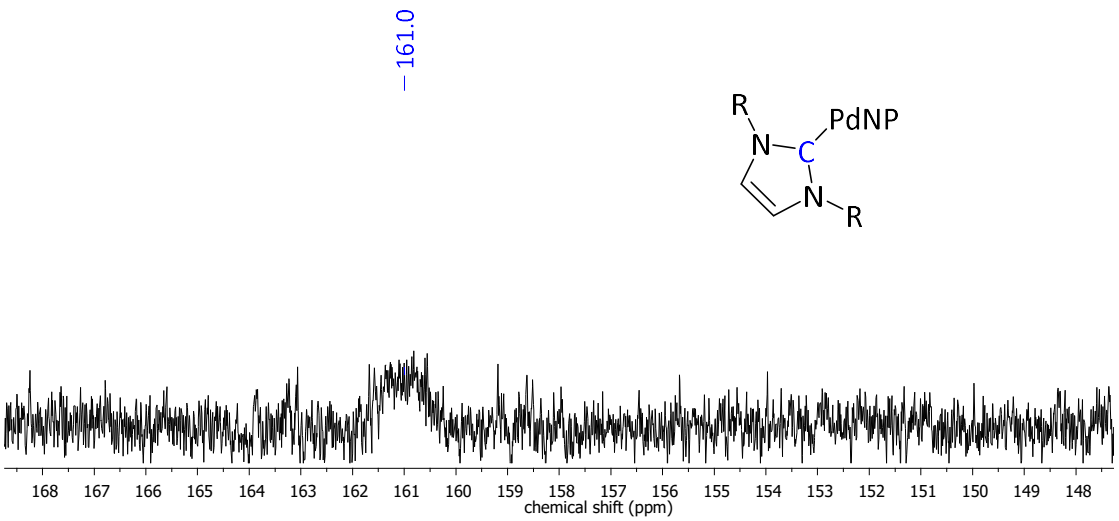

*Figure 7.13 – Zoomed in ^{13}C NMR spectra (chloroform-d, 500 MHz) of **PdNP15-NHC** showing a broad signal at 161 ppm, indicating NHC binding to palladium nanoparticles.*

Unfortunately, Beer does not report NMR spectroscopic data for the imidazolium or NHC stabilised nanoparticles. With this limited data it was determined that a mixture of imidazolium and NHC stabilised nanoparticles had formed in this reaction. Further analysis of the product by transmission electron microscopy (TEM) and energy-dispersive X-ray (EDX) spectroscopy would give more conclusive data for the success of nanoparticle synthesis and offer size data on any formed nanoparticles.

IPS7 was also used in the synthesis of imidazolium stabilised palladium nanoparticles, ***PdNP15-imid*** (Scheme 7.6). As before, a colour change from red to black was observed in the reaction solution and a black oil was isolated as the product, again matching the product appearance reported by Beer.[3] However, when the product was dissolved/dispersed in $CDCl_3$ for ^{1}H and ^{13}C NMR spectroscopic analysis the dissolved species quickly agglomerated and precipitated from solution. The corresponding NMR spectra showed no species in solution. This indicates that the product formed from this reaction was less stable than the ***PdNP15-NHC*** product in $CDCl_3$. Despite this, both ***PdNP15-NHC*** and ***PdNP15-imid*** were taken forward to assess their catalytic viability.

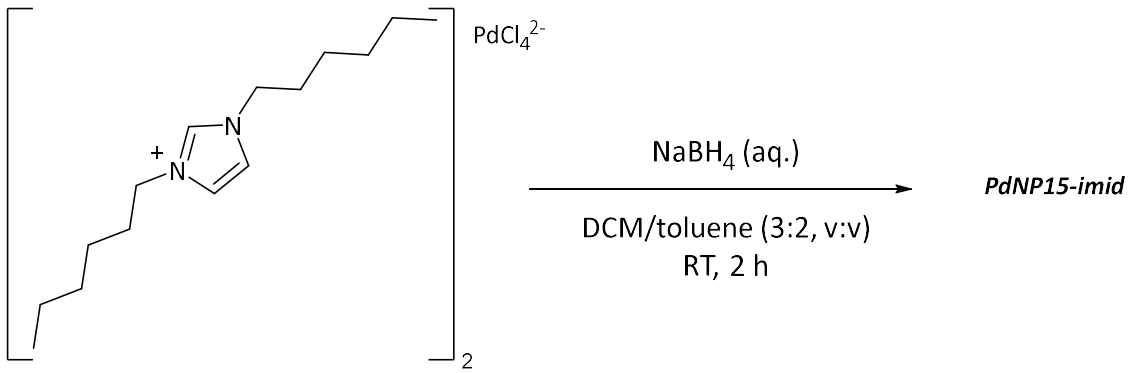

*Scheme 7.6 – Synthesis of NHC-stabilised palladium nanoparticles, **PdNP15-imid**, from **IPS15**. Conditions and procedure adapted from Beer.[3]*

7.1.4 Catalysis using Imidazolium Salt and NHC Ligand Stabilised Palladium Nanoparticles

PdNP15-NHC and ***PdNP15-imid*** were screened in the SMCC reaction between 2,4-dibromopyridine and *p*-fluorophenylboronic acid (Scheme 7.7). Samples were taken at 24 h reaction time and product yields were measured using ^{19}F NMR spectroscopy (Figure 7.14). Catalytic activity was seen for both nanoparticulate samples with ***PdNP15-NHC*** showing greater activity, though it is noted that ***PdNP15-NHC*** was assumed to be a mix of both imidazolium and NHC stabilised nanoparticles.

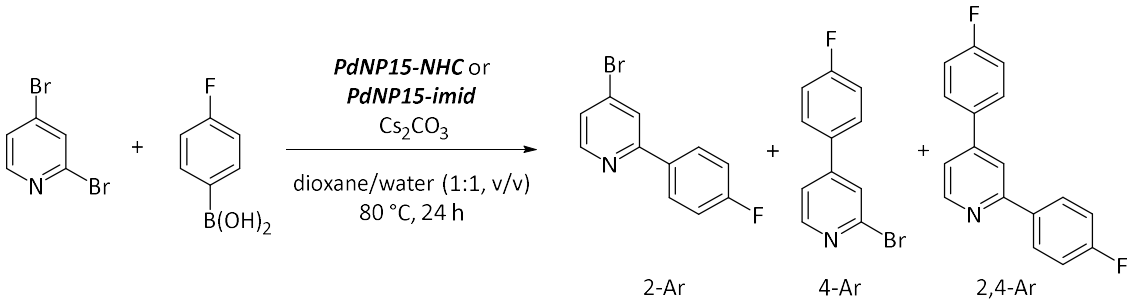

*Scheme 7.7 – Screening reaction between 2,4-dibromopyridine and p-fluorophenylboronic acid to yield 2-bromo-4-(p-fluorophenyl)pyridine (4-Ar), 2-(p-fluorophenyl)-4-bromo-pyridine (2-Ar) and 2,4-bis(p-fluorophenyl)pyridine (2,4-Ar) with **PdNP15-NHC** and **PdNP15-imid** as catalysts.*

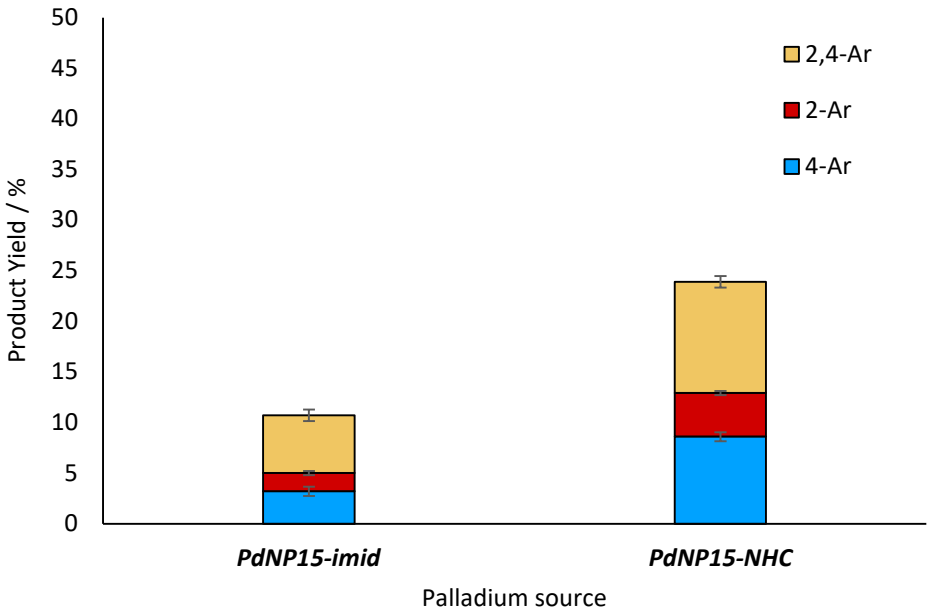

*Figure 7.14 – Product yields of 2-Ar, 4-Ar and 2,4-Ar for the reaction of 2,4-dibromopyridine and p-fluorophenylboronic acid using **PdNP15-NHC** and **PdNP15-imid** as catalysts under conditions shown in Scheme 7.7. Product yields are determined by ^{19}F NMR spectroscopy with respect to FDMB internal standard. Error bars represent standard error.*

Interestingly, similar abnormal site-selectivity for 4-Ar was seen with both nanoparticulate catalysts with respect to the non-bulky Pd-NHC complexes reported previously (Chapter 4.1). ***PdNP15-NHC*** and ***PdNP15-imid*** show similar product ratios but ***PdNP15-NHC*** is more active than ***PdNP15-imid***. This may be due to discrepancies in catalyst loadings.

This preliminary work conducted on imidazolium and NHC stabilised palladium nanoparticles and the associated challenges encountered here offer a firm basis for continued research. It has been shown that the suspected nanoparticulate catalysts ***PdNP15-NHC*** and ***PdNP15-imid*** are catalytically active in the SMCC reaction of interest and, more importantly, display the abnormal site-selectivity for 4-Ar. Continued research following on from this would require absolute characterisation of the imidazolium and NHC stabilised nanoparticles. Once achieved, the nanoparticles could be subjected to more rigorous investigations into their catalytic activity and rationale for their product site-selectivity. This would appropriately supplement the main body of this work and ultimately progress the aim of gaining a complete understanding of the nature and roll of palladium species in the SMCC reaction of interest, and extension to palladium catalysis in general.

7.2 Investigation of Pd-NHC_2 Complexes and chelating NHC ligands

A small library of six Pd-NHC complexes, ***C18***–***C23*** (Figure 2.10), previously synthesised in the group, were used to assess certain aspects of the precatalyst structure on catalytic activity and site-selectivity not previously investigated in this study. This included NHC *N*-substituent chelation, multiple NHC ligands and asymmetrical NHC ligand structures. Complexes ***C18***–***C20*** feature two NHC ligands with pyridyl containing *N*-substituents capable of chelation to the palladium centre. Similarly, ***C22*** has a single NHC ligand that is capable of chelation to the metal centre through the pyridyl *N*-substituent. ***C21*** also features two NHC ligands however with allyl *N*-substituents. The bis-NHC complexes, ***C18***–***C21***, and the chelating NHC complex ***C22*** may give valuable data on the current mechanistic rationale for the site-selectivity in the SMCC reaction of interest, as it is thought that PdL_2 active catalytic species would be 2-Ar selective (Chapter 4.4.2). ***C19***, ***C20***, ***C22*** and ***C23*** all feature asymmetrical NHCs with ***C23*** having one very bulky mesityl and one non-bulky allyl *N*-substituent. Comparison of the catalytic outcomes from these complexes, when used as precatalysts, allows for inferences to be made about how each structural element of the NHC ligand, or complex architecture, may affect the catalytic reaction individually. This, therefore, would serve as a basis for further investigations into any of the structural elements studied.

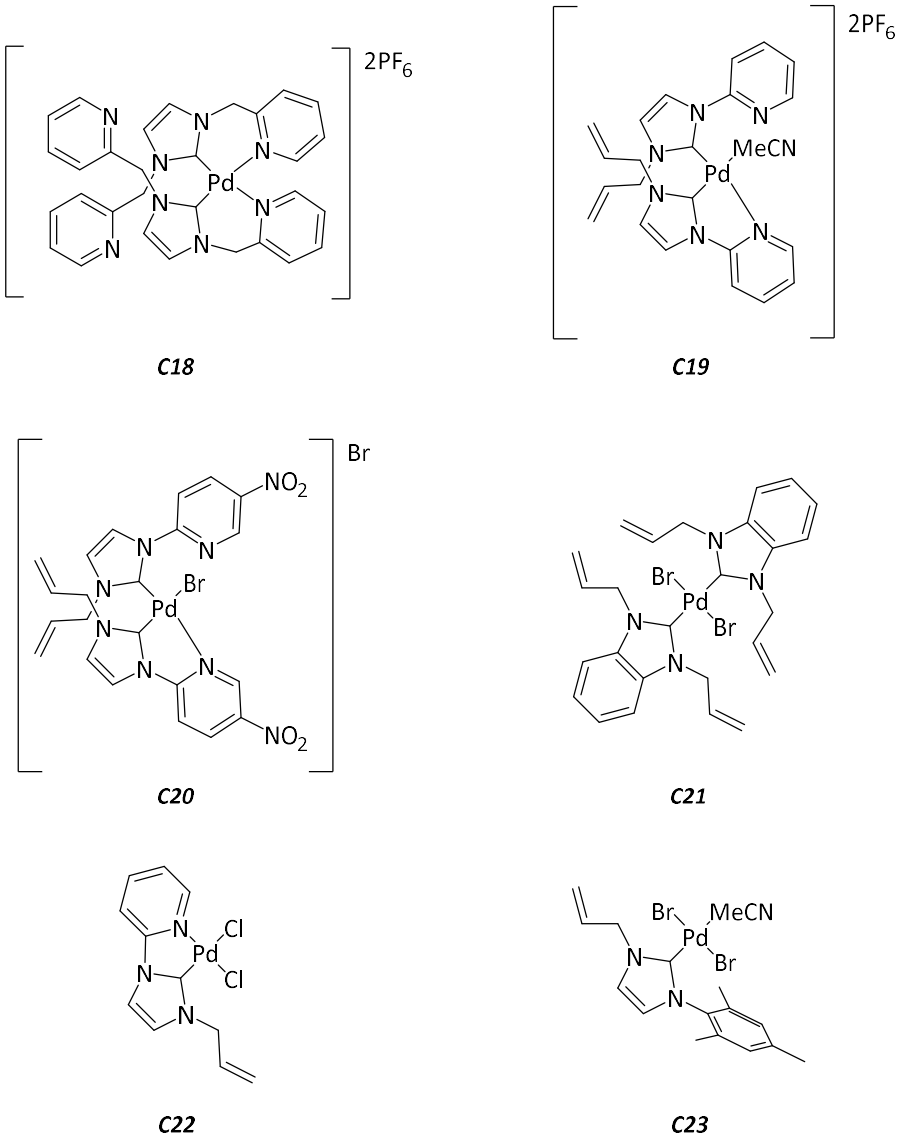

C18 *C19* *C20* *C21* *C22* *C23*

*Figure 7.15 – Structures of various Pd-NHC complexes (**C18-C23**) previously synthesised within the Willans group.*

Prior to the usage of ***C18***–***C23*** as precatalysts in the reaction of interest, their purity was assessed by ^{1}H and ^{13}C NMR spectroscopy and in all cases were found to be clean without need for further purification. The complexes were then screened in the SMCC of 2,4-dibromopyridine and *p*-fluorophenylboronic acid under standard reaction conditions (Scheme 7.8). Each complex was used at a catalyst loading of 2.5 mol%. Multiple samples were taken over time such that a reaction profile could be generated for each individual complex.

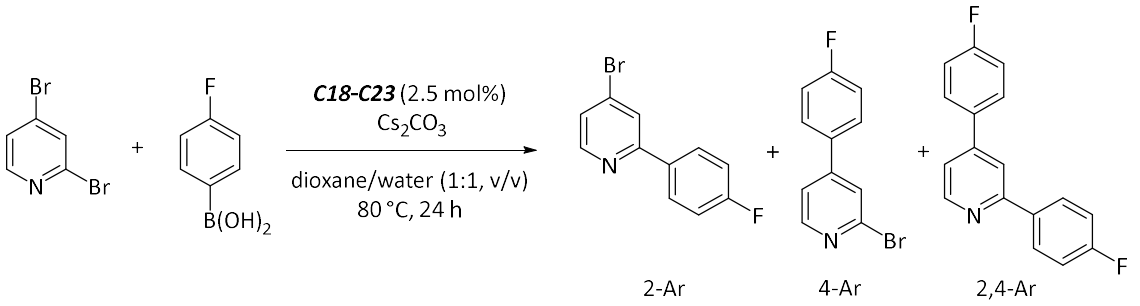

*Scheme 7.8 – Screening reaction between 2,4-dibromopyridine and p-fluorophenylboronic acid to yield 2-bromo-4-(p-fluorophenyl)pyridine (4-Ar), 2-(p-fluorophenyl)-4-bromo-pyridine (2-Ar) and 2,4-bis(p-fluorophenyl)pyridine (2,4-Ar) with **C18–C23** as precatalysts.*

When ***C18*** and ***C19*** were used as precatalysts in the reaction, there was no catalytic activity seen over the entire course of the reaction. This is not unexpected as both ***C18*** and ***C19*** do not feature any halide ligands, or any other ligands typically able to undergo transmetalation. Without the ability for transmetaltion to occur, the complex cannot activate through the accepted activation pathway for Pd-NHC complexes (Scheme 7.9). It is likely that these complexes remain unchanged during the course of the reaction.

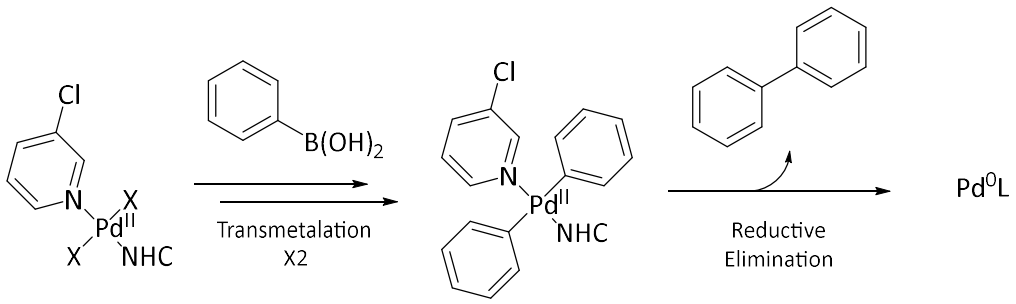

Scheme 7.9 – Generally accepted activation route for PEPPSI precatalysts: Two successive transmetalation reactions followed by reductive elimination to form the catalytically active Pd(0) species.

The structure of complex ***C20*** is similar to ***C19***, however it contains halide ligands and therefore was expected to undergo precatalyst activation. Indeed, there was a small amount of activity seen in the catalytic reaction, however the overall product yield of the reaction was only 5% (Figure 7.16). Kinetic modelling was conducted for ***C20*** and the best fitting model was found to be the same as for the bulky and non-bulky complexes, ***C7*** and ***C14***, discussed realier (Chapter 4.2). However, due to the relatively large error resulting from low product yields, the rate constants associated with the model terms of product formation are not significantly different and therefore will not be quoted. Despite the low activity of the complex, there were interesting features shown in the reaction profile.

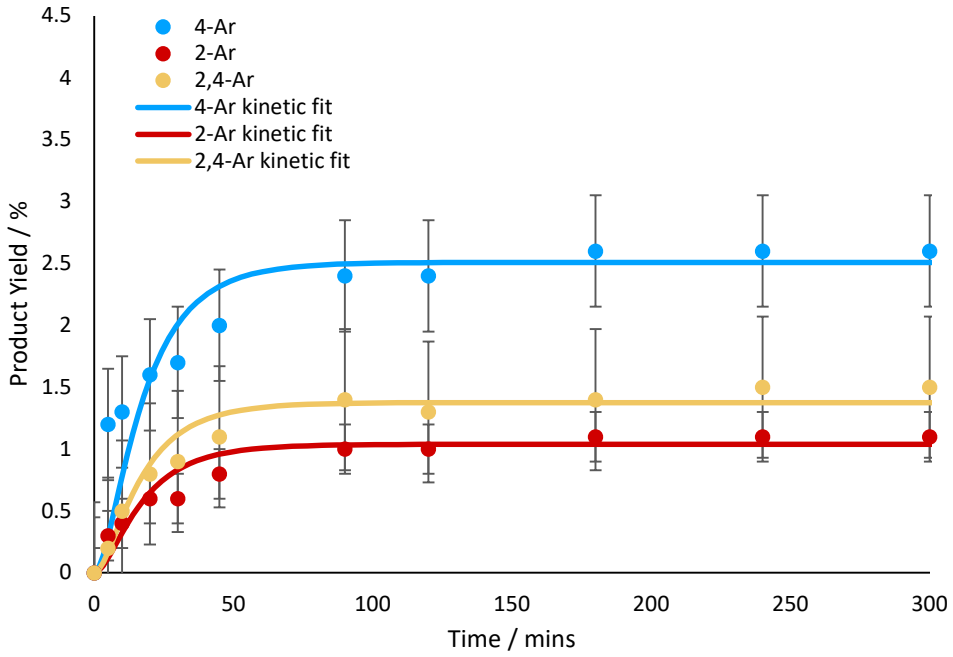

*Figure 7.16 – Time-course data showing product yields of 2-Ar, 4-Ar and 2,4-Ar for the reaction of 2,4-dibromopyridine and p-fluorophenylboronic acid using **C20** as the precatalyst under standard conditions. Product yields are determined by ^{19}F NMR spectroscopy with respect to FDMB internal standard. Error bars represent standard error.*

The product selectivity of ***C20*** for 4-Ar over 2-Ar and 2,4-Ar is unexpected. The theorised site-selectivity rationale for this reaction explained earlier (Chapter 4.4.1), and that of Neufeldt and co-workers, would suggest that a PdL_2 system selects for 2-Ar.[5-7] Assuming this rationale is correct and both NHC ligands of ***C20*** remain bound to the complex during and following precatalyst activation, then this complex would adopt a PdL_2 active species structure and thus select for 2-Ar. As these results show 4-Ar selectivity then more investigations to appropriately explore PdL_2 systems in much more detail are required. If, however, it is assumed that ***C20*** does not fully activate in the reaction and the catalytic activity originates from residual $PdBr_2$ left over from the synthesis of ***C20***, this would account for the low overall catalytic yield and 4-Ar site-selectivity observed.

Alternatively, activation of the complex may not take place through the expected pathway (Scheme 7.9), but through reductive elimination of either a C2-halogenated or arylated imidazolium salt to form a Pd-NHC active species (Figure 7.17). The active species formed from this activation is expected to have the site-selectivity observed. Reductive elimination of both C2-halogenated or arylated imidazolium salts from palladium are known.[8]

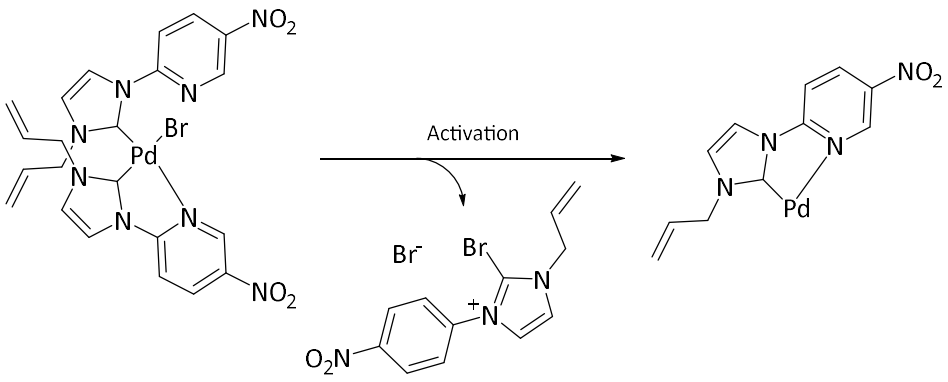

*Figure 7.17 – Possible activation of **C20** (and other Pd-NHC$_2$ complexes) through reductive elimination of an C2-hallogenated imidazolium ion to produce catalytically active Pd(0)-NHC.*

Interestingly, the formation of all three catalytic products seen when using ***C20*** follow a very similar shaped profile, which is unlike the previously collected time course data for the non-bulky Pd-NHC complex ***C14*** where 2,4-Ar continued after the mono-arylated products had reached a maximum yield (Chapter 4.2.1). This could indicate a different mechanism between the mono- and bis-NHC palladium complexes when forming 2,4-Ar, or again indicate that a different palladium source is facilitating catalysis, such as residual $PdBr_2$.

Similar features were present in the reaction profile when using ***C21*** as the precatalyst, namely low overall reaction yield, 4-Ar selectivity and similar reaction profiles for all three products (Figure 7.18). This suggests that both ***C20*** and ***C21*** behave similarly in the reaction. The activation of ***C21*** by the accepted pathway may not be viable due to the *trans*-NHC ligands blocking reductive elimination of biphenyl, whereas the activation of the complex by reductive elimination of a C2-halogenated or arylated imidazolium salt is viable. The NHC ligand would be *cis* to either the halide ligand or, following transmetalation, an aryl ligand and therefore could undergo reductive elimination. The rate constant for activation from kinetic modelling is 22.5 M^2min^{-1} for ***C21***, which is of comparable size to the activation for the other Pd-NHC complexes examined and suggests that, if present, this alternate mechanism for catalyst activation is of a similar rate to the expected activation route for similar mono-ligated Pd-NHC complexes. Again, the same kinetic model used for ***C7*** and ***C14*** was employed here to the achieve optimal kinetic fit, however, the rate constants generated suggest that 2,4-Ar is almost exclusively formed through the consumption of 4-Ar (12.7 M^2min^{-1}) rather than through a concerted mechanism (3.8 $x10^{-6}$ M^4min^{-1}). This may be due, in part, to the very limited yield of of 2,4-Ar when using ***C21*** as the precatalyst.

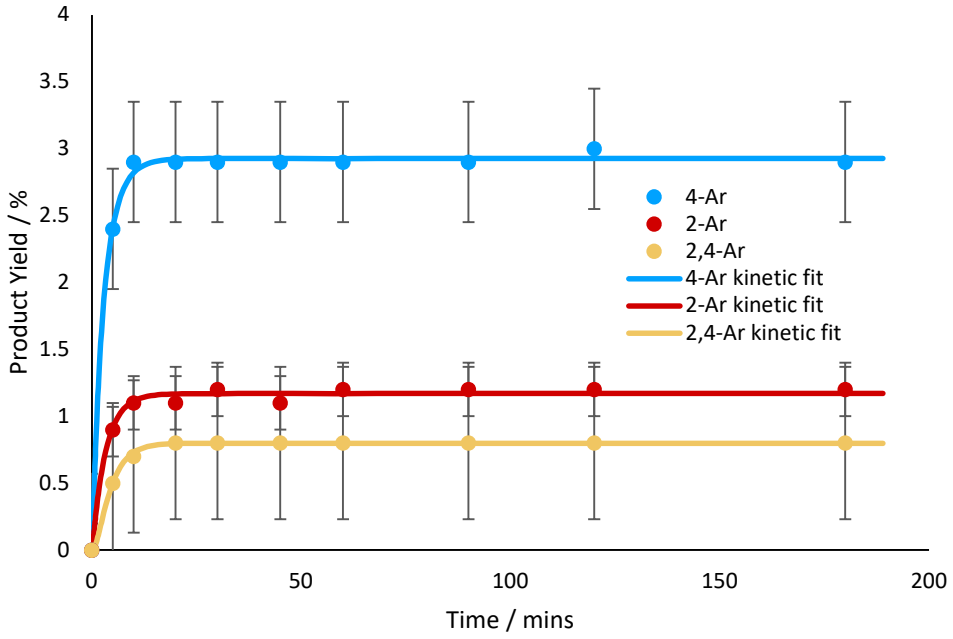

*Figure 7.18 – Time-course data showing Product yields of 2-Ar, 4-Ar and 2,4-Ar for the reaction of 2,4-dibromopyridine and p-fluorophenylboronic acid using **C21** as the precatalyst under standard conditions. Product yields are determined by ^{19}F NMR spectroscopy with respect to FDMB internal standard. Error bars represent standard error.*

The reaction profile of ***C21*** also shows an abrupt end to the catalytic activity after 10 mins reaction time, this is associated with a reasonably large kinetic model rate coeficiant for catalyst deactivation of 0.305 min^{-1}. This behaviour could be due to an interaction of the allyl *N*-substituents and palladium centre rendering the catalyst inactive. The Willans group reports upon C(sp^2)-H activation of distal protons appended to similar NHC ligands on palladium complexes.[9] the formation of a palladacycle through this mechanism may result in complete deactivation of the active catalytic species (Figure 7.19).

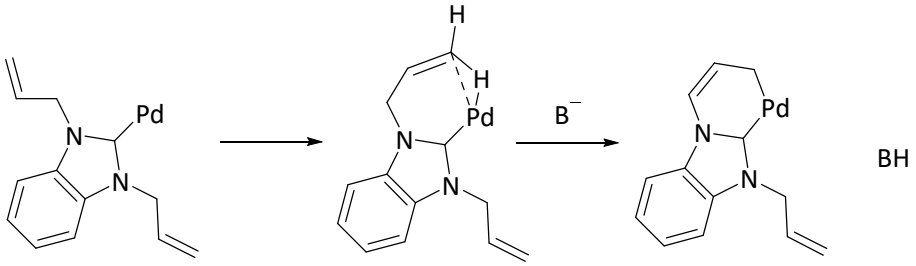

*Figure 7.19 – Possible C-H activation of an allyl N-substituent of the NHC ligand on **C21** in the presence of a base, to form a palladacyclic species which may be catalytically inactive.*

A similar abrupt stop in catalytic activity at 10 mins reaction time is also seen when using ***C23*** as the precatalyst (Figure 7.20) which, like ***C21***, features an allyl *N*-substituent on the NHC ligand. A similar value for the catalyst deactivation rate coefficient is also seen, 0.239 min^{-1} showing these processes may be analogous. This phenomenon is only observed for the Pd-NHC

complexes featuring allyl *N*-substituents and no other coordinating *N*-substituent *i.e.* ***C20***, with a pyridine and allyl *N*-substituent, did not have the abrupt end in activity. This is yet unexplained and may present an interesting line of research for future investigations.

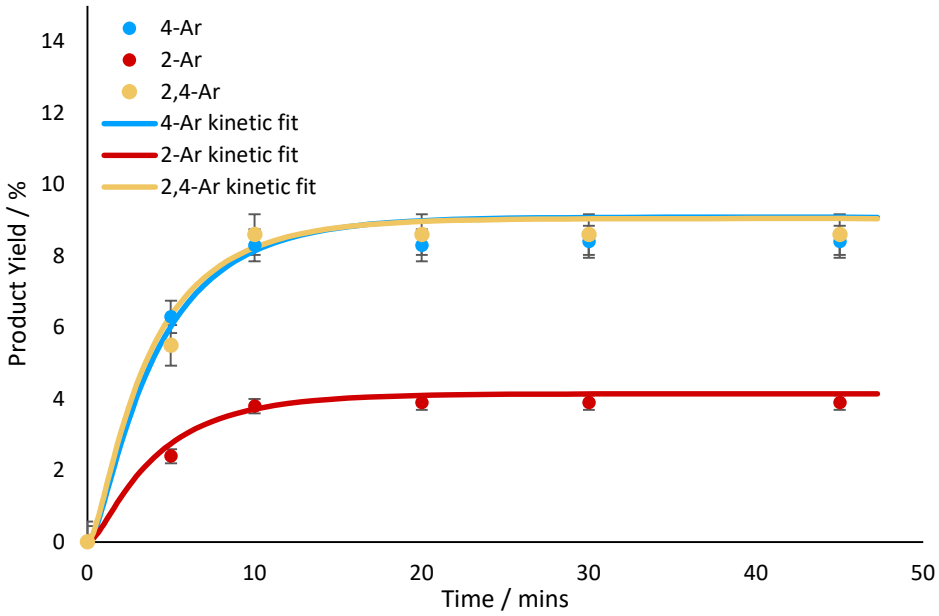

*Figure 7.20 – Time-course data showing Product yields of 2-Ar, 4-Ar and 2,4-Ar for the reaction of 2,4-dibromopyridine and p-fluorophenylboronic acid using **C23** as the precatalyst under standard conditions. Product yields are determined by ^{19}F NMR spectroscopy with respect to FDMB internal standard. Error bars represent standard error.*

Interestingly, the rection profile when using ***C23*** shows a marked increase in the monoarylated product yields with respect to 2,4-Ar when compared to the bulky Pd-NHC complex ***C8***, which displayed almost exclusive selectivity for 2,4-Ar when screened under identical conditions. The main difference between the two complexes is that ***C8*** features two symmetrical very bulky NHC *N*-substituents, whereas ***C23*** features a very bulky and a non-bulky NHC *N*-substituent (Figure 7.21). This asymmetry in the ligand structure is likely the main cause for the difference in reaction outcome.

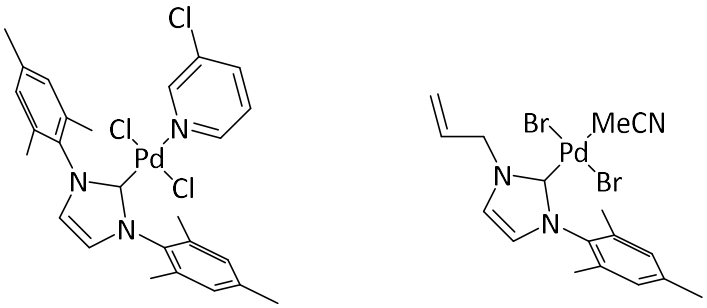

C8 ***C23***

*Figure 7.21 – Structures of **C8** and **C23** to show the difference in NHC structure.*

The reaction outcome with ***C23*** may support the concerted formation of 2,4-Ar. Transmetalation on ***C23*** during the catalytic cycle is expected to be more facile with the relaxed steric bulk, compared to ***C8***, corresponding with a reduced selectivity for 2,4-Ar, as is observed (Figure 7.20). Synthesis and screening of an analogous complex to ***C23***, where the allyl group is replaced by an inert group to prevent loss of catalytic activity would be the natural next step in this particular line of investigation (Figure 6.1).

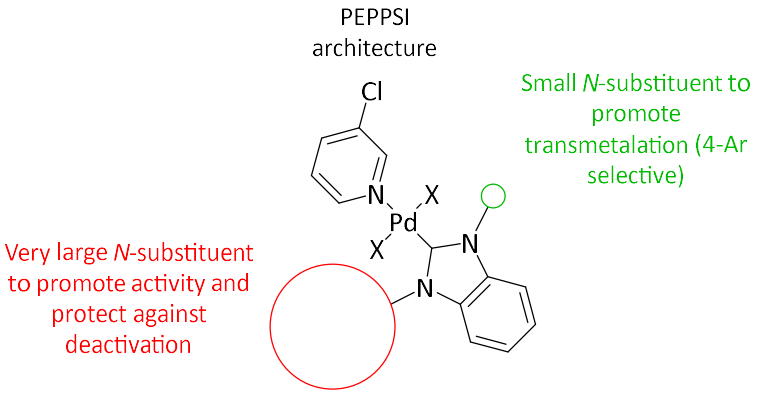

Figure 7.22 – General structure of a potentially efficient catalyst for 4-Ar selectivity in SMCC of 2,4-dibromopyridine and p-fluorophenyl boronic acid, a small N-substituent promotes transmetalation and therefore 4-Ar selectivity, and a large N-substituent aids in preventing catalyst deactivation.

Finally, the reaction profile for ***C22*** shows two distinct regions of product formation (Figure 7.23). The first at 0-100 mins reaction time strongly mirrors that of the non-bulky complex ***C14*** (Chapter 4.2.1), whereby the two mono-arylated products initially form quickly, and before 45 mins 4-Ar was the major product, which then plateaued in yield, whereas 2,4-Ar formed more slowly but then surpassed 4-Ar to become the major product. The second region, from 100 mins onwards, shows that catalytic activity is seemingly restored and the yield of the three products increased further. The yield of 2-Ar in this region increased from 3% to 9% whereas 4-Ar only increased marginally from 6% to 8%. This could indicate that, in the second region, 2-Ar is selected for over 4-Ar. However, when considering the sharp increase in 2,4-Ar yield from 7% to 21%, it may be more likely that some of 4-Ar was consumed in the formation of 2,4-Ar. If the rate of 4-Ar formation is greater than its consumption, then an overall increase in the yield of 4-Ar would be observed as it is here. Unfortunately, due to the limitations of input variables into the Compunetics software, no input model could provide a suitable kinetic fit to this data.

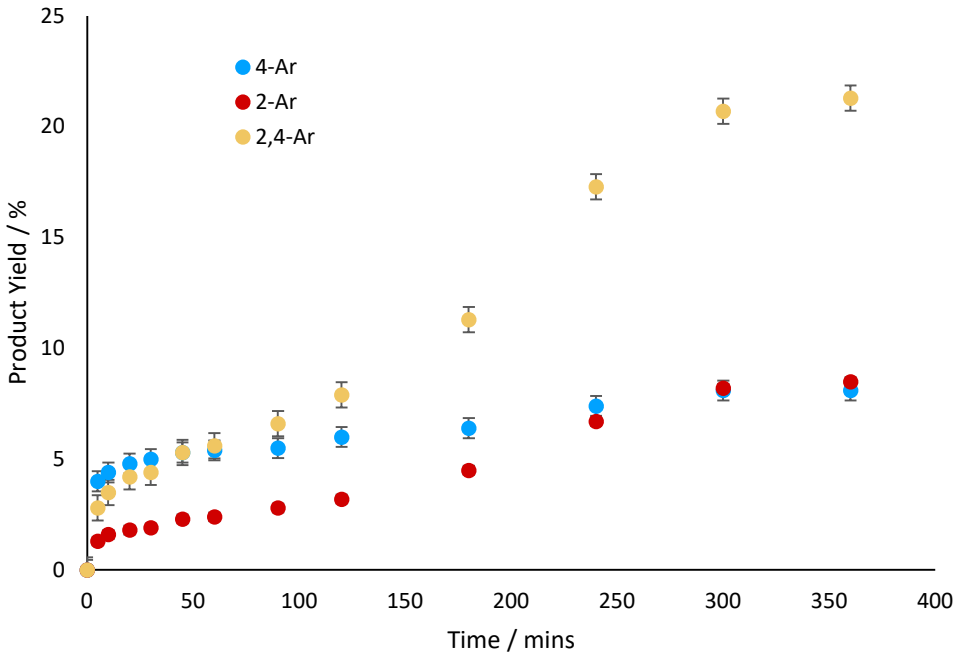

*Figure 7.23 – Time-course data showing Product yields of 2-Ar, 4-Ar and 2,4-Ar for the reaction of 2,4-dibromopyridine and p-fluorophenylboronic acid using **C22** as the precatalyst. Product yields are determined by ^{19}F NMR spectroscopy with respect to FDMB internal standard. Error bars represent standard error.*

This profile is thought to show catalyst speciation in action, whereby the first region of product formation is due to the expected Pd-NHC active catalytic species which becomes deactivated over time, then undergoes speciation to form a more active catalytic species responsible for the second region of product formation (Figure 7.24). This may be the first reported instance where palladium catalyst speciation is clearly visible in a reaction profile. If so, then ***C22*** may be a model catalyst to investigate speciation in this reaction from Pd-NHC catalysts. Identification and tracking of the active species formed during this reaction may be key in understanding how speciation takes place from Pd-NHC catalysts and methods for its prevention or manipulation may be tested.

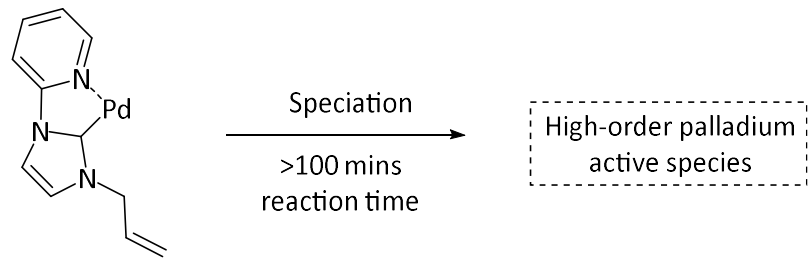

C22

*Figure 7.24 – Proposed speciation of **C22** to account for catalyst deactivation (<100 mins reaction time) and reactivation (>100 mins reaction time) seen in the reaction profile.*

7.3 Summary

This section of work, whilst broadening the scope of the main investigation, also highlights that there is still a significant amount of work to be conducted on Pd-NHC complexes as SMCC catalysts. It was shown here that imidazolium palladate salts present an interesting line of investigation as, similar to Pd-NHC complexes, a structure activity relationship may be present with relation to the imidazolium ion structure, though is not explored. The active species formed from IPSs may be heterogeneous in nature and relate to the proposed structure of imidazolium stabilised PdNPs. Imidazolium and NHC stabilised PdNPs have been shown to exhibit catalytic activity in the reaction of interest; further studies into how nanoparticle size may affect their selectivity is an interesting line of investigation and would build a picture of how the selectivity may change during speciation. More specialist and robust approaches to nanoparticle characterisation must be employed when pursuing this line of investigation, such as TEM and EDX spectroscopy.

The effect of several structural elements of Pd-NHC and Pd-NHC_2 complexes were explored in the catalytic reaction of interest, and it was found that activation requires the presence of at least one halide ligand. It is proposed that the activation of Pd-NHC_2 complexes may be achieved through the reductive elimination of C2-halogenated or arylated imidazolium ions from palladium, however this may be studied in more detail to assess its viability by DFT methodologies. The combination of allyl and pyridyl *N*-substituents on an NHC ligand was found to be problematic, whereby catalyst activity would abruptly halt after a short time. The mechanism for this phenomenon and its scope with other NHC ligands should be explored more completely in order to effectively prevent it as a catalyst deactivation pathway.

It has also been shown that the replacement of a single bulky *N*-substituent of an NHC ligand with a non-bulky *N*-substituent can modify the site-selectivity of the corresponding Pd-NHC complex significantly. This is an important area of further work considering it directly relates to the hypothesis of 2,4-Ar formation in the reaction of interest with Pd-NHC catalysts. It is thought that gaining a deeper understanding of this in particular will aid significantly in achieving the goal of smarter catalyst design.

Finally, the apparent first instance of clear catalyst speciation during a reaction was shown for ***C22***. This may be a crucial finding as it offers the possibility of directly investigating catalyst speciation in a single reaction where a switch from homogeneous to higher-order palladium active species may be present. Strengthening this link in knowledge would be extremely beneficial for catalyst design and understanding of palladium catalysis in general. This chapter

therefore has achieved the goal of highlighting further avenues of investigation of Pd-NHC catalysis and informing the direction they may begin from.

7.4 References

1. N. W. J. Scott, M. J. Ford, N. Jeddi, A. Eyles, L. Simon, A. C. Whitwood, T. Tanner, C. E. Willans and I. J. S. Fairlamb, *J. Am. Chem. Soc.*, 2021, **143**, 9682-9693.
2. N. W. J. Scott, M. J. Ford, C. Schotes, R. R. Parker, A. C. Whitwood and I. J. S. Fairlamb, *Chem. Sci.*, 2019, **10**, 7898-7906.
3. C. J. Serpell, J. Cookson, A. L. Thompson, C. M. Brown and P. D. Beer, *Dalton Trans.*, 2013, **42**, 1385-1393.
4. C. A. Smith, M. R. Narouz, P. A. Lummis, I. Singh, A. Nazemi, C. H. Li and C. M. Crudden, *Chem. Rev.*, 2019, **119**, 4986-5056.
5. J. P. Norman, N. G. Larson, E. D. Entz and S. R. Neufeldt, *J. Org. Chem.*, 2022, **87**, 7414-7421.
6. J. P. Norman, N. G. Larson and S. R. Neufeldt, *ACS Catal.*, 2022, **12**, 8822-8828.
7. J. P. Norman and S. R. Neufeldt, *ACS Catal.*, 2022, **12**, 12014-12026.
8. T. P. Nicholls;, J. R. Williams; and C. E. Willans, in *Adv. Organomet. Chem.*, 2021, vol. 75, ch. 6, pp. 245-329.
9. M. R. Chapman, C. M. Pask, A. Ariafard and C. E. Willans, *Chem. Commun.*, 2015, **51**, 5513-5515.

Chapter 8

Experimental

8.1 General Considerations

Where stated, manipulations were performed under an atmosphere of dry nitrogen or argon, by means of standard Schlenk line or glovebox techniques. Anhydrous solvents were dried by passing over activated alumina to remove water, copper catalyst to remove oxygen, and molecular sieves to remove any remaining water, with the Dow-Grubbs solvent system. DCM and THF were freeze-pump-thaw degassed, while other solvents were degassed by purging with argon. All chemicals were purchased from Sigma Aldrich, Alfa Aesar, Apollo scientific or Fluorochem and unless otherwise stated, used without further purification.

NMR spectra were recorded on a JEOL ECA600ii, Bruker AV4 NEO 500 (C/H dual cryoprobe), Bruker AV4 NEO 500 (4-channel), Bruker AV3HD 400 or a Bruker DPX300 spectrometer. ^{1}H NMR and ^{13}C{^{1}H} chemical shifts were referenced against residual solvent peaks. ^{19}F chemical shifts were referenced to the internal standard. Assignment of ^{1}H and ^{13}C{^{1}H} NMR spectra was aided by 2D ^{1}H^{13}C HMQC, and ^{13}C{^{1}H} DEPT 135 where relevant. Mass spectra were collected on a Bruker Daltonics (micro TOF) instrument operating in the electrospray mode.

8.2 NHC Ligand Precursors

8.2.1 4,5-Dimethylimidazole

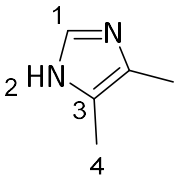

Paraformaldehyde (2.28 g, 76 mmol) was added to a solution of ammonium sulphate (20.0 g, 150 mmol) in water (38 mL) and the solution was stirred for 15 mins. 2,3-butadione (6.50 g, 76 mmol) was then added and the reaction mixture was heated to 100 °C for 1 h. The reaction mixture was then cooled and made alkaline using a saturated solution of sodium hydroxide in water (20 mL). The solution was extracted into ethyl acetate (3 x 50 mL). The organic layers were combined, dried over magnesium sulphate and the solvent removed under reduced pressure. The residue was dissolved in a minimal amount of ethyl acetate and diethyl ether was added to form precipitate which was filtered and dried under reduced pressure to deliver the product as an off-white solid (2.14 g, 22 mmol, 30%). ^{1}H NMR (500 MHz, chloroform-d) δ 8.56 (s (br), 1H, *H2*), 7.45 (s, 1H, *H1*), 2.17 (s, 6H, *H4*) ppm. ^{13}C{^{1}H} NMR (126 MHz, chloroform-d) δ 132.15 (*C1*), 126.51 (*C3*), 10.64 (*C4*) ppm. HRMS (ESI+), *m/z*: 97.0758 $[M+H]^{+}$ (calc: 97.0761).

8.2.2 1,3-Dipropyl-4,5-dimethylimidazolium hexafluorophosphate (*I1$_{PF6}$*)

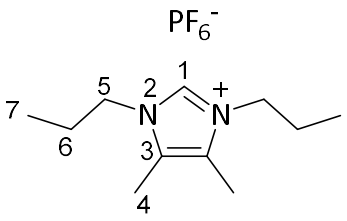

Sodium hydroxide (0.24 g, 6.0 mmol) was added to a solution of 4,5-dimethylimidazole (0.49 g, 5.0 mmol) in acetonitrile (10 mL) and stirred at room temperature for 30 mins. 1-bromopropane (1.3 mL, 15 mmol) was then added and the reaction heated to 80 °C for 16 h. The reaction mixture was cooled and filtered. The solvent was removed under reduced pressure to yield a dark brown oil, which was dissolved in water (10 mL). Ammonium hexafluorophosphate (0.75 g, 5.0 mmol) was added and the mixture stirred at room temperature for 15 mins. A white precipitate formed which was filtered and washed with water and diethyl ether and dried under reduced pressure yielding the product as an off-white solid (865 mg, 2.65 mmol, 53%). ^{1}H NMR (400 MHz, chloroform-d) δ 9.03 (s, 1H, *H1*), 4.04 (t, J = 7.2 Hz, 4H, *H5*), 2.16 (s, 6H, *H4*), 1.81 – 1.68 (m, 4H, *H6*), 0.87 (t, J = 7.4 Hz, 6H, *H7*) ppm. ^{13}C{^{1}H} NMR (101 MHz, chloroform-d) δ 135.55 (*C1*), 126.22 (*C3*), 48.45 (*C5*), 23.11 (*C6*), 10.62 (*C4*), 8.47 (*C7*) ppm. HRMS (ESI+), *m/z*: 181.1696 [M- PF_6]$^{+}$ (calc: 181.1699).

8.2.3 1,3-Bis(2-phenylethyl)-3,4-dimethylimidazolium hexafluorophosphate (*I2$_{PF6}$*)

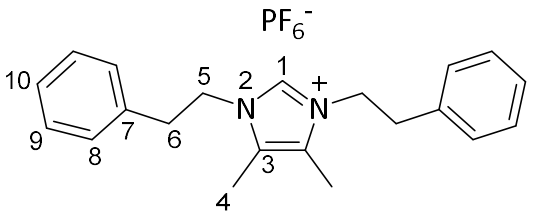

Sodium hydroxide (0.24 g, 6.0 mmol) was added to a solution of 4,5-dimethylimidazole (0.49 g, 5.0 mmol) in acetonitrile (10 mL) under inert conditions and the solution was stirred at room temperature for 30 mins. 2-Ethylbromo benzene (2.0 mL, 2.75 g, 15 mmol) was then added and the reaction heated to 80 °C for 16 h. The reaction was cooled, filtered and the solvent was removed under reduced pressure to yield a pale brown oil, which was dissolved in water (10 mL). Ammonium hexafluorophosphate (0.75 g, 5.0 mmol) was added and the mixture stirred at room temperature for 15 mins. A white precipitate formed which was filtered, washed with water and diethyl ether then dried under reduced pressure yielding the product as an off-white solid (1.38 g, 3.1 mmol, 62%). ^{1}H NMR (400 MHz, DMSO-d6) δ 8.83 (s, 1H, *H1*), 7.29 (dq, J = 13.8, 7.0 Hz, 6H, *H8+10*), 7.16 (d, J = 7.4 Hz, 4H, *H9*), 4.30 (t, J = 7.2 Hz, 4H, *H5*), 3.00 (t, J = 7.2 Hz, 4H, *H6*), 2.06 (s, 6H, *H4*) ppm. ^{13}C NMR (101 MHz, DMSO-d6) δ 137.27 (*C1*), 134.92 (*C7*), 129.30 (*C9*), 129.09 (*C8*), 127.44 (*C10*), 126.87 (*C3*), 47.85 (*C5*), 35.70 (*C6*), 8.01 (*C4*) ppm. HRMS (ESI+), *m/z*: 305.2025 [M- PF_6]$^{+}$ (calc: 305.2012).

8.2.4 1,3-Dibenzyl-3,4-dimethylimidazolium hexafluorophosphate (*I3$_{PF6}$*)

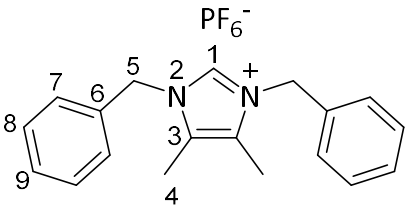

Sodium hydroxide (0.24 g, 6.0 mmol) was added to a solution of 4,5-dimethylimidazole (0.49 g, 5.0 mmol) in acetonitrile (10 mL) under inert conditions and the solution was stirred at room temperature for 30 mins. Benzyl bromide (1.8 mL, 15.0 mmol) was then added and the reaction heated to 80 °C for 16 h. The reaction was cooled, filtered and the solvent was removed under reduced pressure to yield a pale brown oil, which was dissolved in water (10 mL). Ammonium hexafluorophosphate (0.75 g, 5.0 mmol) was added and the mixture stirred at room temperature for 15 mins. A white precipitate formed which was filtered, washed with water and diethyl ether then dried under reduced pressure yielding the product as an off-white solid (1.02 g, 2.4 mmol, 48%). ^{1}H NMR (501 MHz, DMSO-d6) δ 9.24 (s, 1H, *H1*), 7.47 – 7.37 (m, 6H, *H7+9*), 7.34 – 7.29 (m, 4H, *H8*), 5.42 (s, 4H, *H5*), 2.12 (s, 6H, *H4*) ppm. ^{13}C{^{1}H} NMR (126 MHz, DMSO-d6) δ 135.34 (*C1*), 134.23 (*C6*), 129.10 (*C8*), 128.57 (*C7*), 127.72 (*C9*), 127.20 (*C3*), 49.68 (*C5*), 8.08 (*C4*) ppm. HRMS (ESI+), *m/z*: 277.1702 [M-PF6-]$^{+}$ (calc: 277.1705).

8.2.5 1,3-Dipropylimidazolium chloride (*I4*)

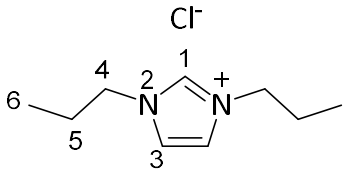

Paraformaldehyde (1.50 g, 50 mmol) was added slowly to a solution of *n*-propylamine (4.2 mL, 51 mmol) in toluene (50 mL) with intense stirring. The reaction mixture was then stirred for 30 mins before cooling to 0 °C. Another equivalent of *n*-propylamine (4.2 mL, 51 mmol) was added dropwise and the reaction mixture was allowed to stir for a further 10 mins at 0 °C. This was followed by dropwise addition of HCl (4 M in dioxane, 13 mL, 52 mmol). The reaction mixture was left to warm to room temperature and glyoxal (40% in H_2O, 8 mL, 50 mmol) was added and the mixture stirred for 16 h. The solvent was removed under reduced pressure and the residue washed with diethyl ether (3 × 10 mL) to deliver the product as a brown oil (4.58 g, 38.8 mmol, 77%). ^{1}H NMR (400 MHz, chloroform-d) δ 10.53 (s, 1H, *H1*), 7.43 (d, J = 1.3 Hz, 2H, *H3*), 4.31 (t, J = 7.3 Hz, 4H, *H4*), 2.00 – 1.87 (m, 4H, *H5*), 0.95 (t, J = 7.4 Hz, 6H, *H6*) ppm. ^{13}C{^{1}H} NMR (126 MHz, chloroform-d) δ 137.0 (*C1*), 122.2(*C3*), 51.3 (*C4*), 23.5 (*C5*), 10.6 (*C6*) ppm. LCMS, m/z: 153.14 [M-Cl]$^{+}$ (calc: 153.1386).

8.2.6 1,3-Bis(2-phenylethyl)imidazolium bromide (*I5$_{Br}$*)

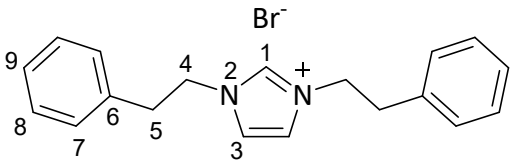

Imidazole (0.85 g, 12.5 mmol) was dissolved in toluene (10 mL) and stirred at 0 °C. Sodium hydride (60% suspension in mineral oil, 0.31 g, 13 mmol) was added in small portions followed by stirring at 0 °C for 30 mins. 2-bromoethylbenzene (7.4 mL, 9.25 g, 51 mmol) was added dropwise and the solution stirred for a further 30 mins. The reaction mixture was then heated to 110 °C for 26 h. The resulting slurry was cooled, filtered and the solvent removed under reduced pressure to deliver a dark orange oil which was treated with diethyl ether (20 mL) to deliver the product as a pale brown solid (2.13 g, 5.9 mmol, 48%). ^{1}H NMR (400 MHz, chloroform-d) δ 10.05 (s, 1H, *H1*), 7.24 – 7.12 (m, 6H, *H7+9*), 7.06 (ddd, J = 16.5, 9.6, 7.0 Hz, 4H, *H8*), 6.95 (d, J = 1.6 Hz, 2H, *H3*), 4.50 (t, J = 7.0 Hz, 4H, *H4*), 3.11 (t, J = 7.0 Hz, 4H, *H5*) ppm. ^{13}C{^{1}H} NMR (126 MHz, chloroform-d) δ 137.3 (*C1*), 135.9 (*C6*), 129.2 (*C8*), 128.2 (*C7*), 127.5 (*C9*), 121.8 (*C3*), 51.3 (*C4*), 36.6 (*C5*) ppm. LCMS, m/z: 277.18 [M-Br]$^{+}$ (calc: 277.1699).

8.2.7 1,3-Bis(2-phenylethyl)imidazolium hexafluorophosphate (*I5$_{PF6}$*)

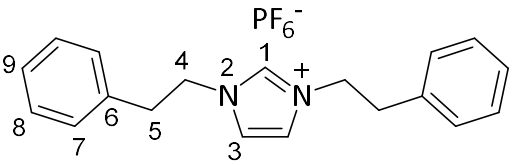

1,3-Bis(2-phenylethyl)-imidazolium bromide (1.00 g, 28 mmol) was dissolved in methanol/water (1:1) (5 mL). A saturated solution of ammonium hexafluorophosphate (1.00 g, 61 mmol) in methanol/water (1:1) was added dropwise. The solution was then stirred for 1 hour, filtered and the residue washed with diethyl ether (10 mL) to deliver the product as an off-white solid (0.99 g, 22 mmol, 79%). ^{1}H NMR (400 MHz, DMSO-d6) δ 8.99 (s, 1H, *H1*), 7.66 (s, 2H, *H3*), 7.27 (dq, J = 14.2, 7.1 Hz, 6H, *H7+9*), 7.14 (d, J = 7.2 Hz, 4H, *H8*), 4.40 (t, J = 7.2 Hz, 4H, *H4*), 3.07 (t, J = 7.2 Hz, 4H, *H5*) ppm. ^{13}C{^{1}H} NMR (101 MHz, DMSO-d6) δ 136.7 (*C1*), 135.8 (*C6*), 128.6 (*C8*), 126.8 (*C7*), 122.4 (*C9*), 49.8 (*C4*), 35.4 (*C5*) ppm. LCMS, m/z: 277.18 [M-PF$_6$]$^{+}$ (calc: 277.1619).

8.2.8 1,3-Dibenzylimidazolium bromide (*I6$_{Br}$*)

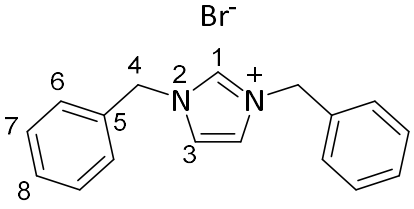

A solution of imidazole (1.50 g, 22 mmol) in THF (100 mL) was cooled to 0 °C. Sodium hydride (60% suspension in mineral oil, 0.90 g, 23 mmol) was added in small portions and the solution stirred for 1 h at 0 °C. Benzyl bromide (5.3 mL, 44 mmol) was added dropwise and the solution was stirred for a further 30 mins at 0 °C then warmed to room temperature and stirred for 16 h. The resulting pale-yellow slurry was then filtered, and the filtrate concentrated under reduced

pressure to deliver the product as a pale-yellow solid (4.13 g, 12 mmol, 56%). ^{1}H NMR (400 MHz, chloroform-d) δ 10.78 (s, 1H, *H1*), 7.52 – 7.32 (m, 10H, *H6-8*), 7.24 (s, 2H, *H3*), 5.57 (s, 4H, *H4*) ppm. ^{13}C{^{1}H} NMR (126 MHz, chloroform-d) δ 136.7 (*C1*), 132.9 (*C5*), 129.5 (*C7*), 129.4 (*C6*), 129.0 (*C8*), 122.1 (*C3*), 53.3 (*C4*) ppm. LCMS, m/z: 249.06 [M-Br]$^{+}$ (calc: 249.1386).

8.2.9 1,3-Dibenzylimidazolium hexafluorophosphate (*I6$_{PF6}$*)

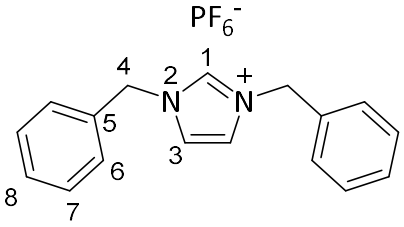

1,3-Bis(2-phenylmethyl)-imidazolium bromide (1.00 g, 30 mmol) was dissolved in methanol/water (1:1) (5 mL). A saturated solution of ammonium hexafluorophosphate (1.00 g, 61 mmol) in methanol/water (1:1) was added dropwise. The solution was then stirred for 1 hour, filtered and washed with diethyl ether (10 mL) to deliver the product as an off white solid (1.00 g, 24 mmol, 84%). ^{1}H NMR (400 MHz, chloroform-d) δ 10.64 (s, 1H, *H1*), 7.48 – 7.25 (m, 10H, *H6-8*), 7.33 (s, 2H, *H3*), 5.51 (s, 4H, *H4*) ppm. ^{13}C{^{1}H} NMR (126 MHz, chloroform-d) δ 136.4 (*C1*), 133.0 (*C5*), 129.6 (*C7*), 129.6 (*C6*), 129.0 (*C8*), 122.2 (*C3*), 53.5 (*C4*) ppm. LCMS, m/z: 249.07 [M-PF$_6$]$^{+}$ (calc: 249.1386).

8.2.10 *N*,*N*-Diisopropylphenyl-1,4-diaza-1,3-butadiene

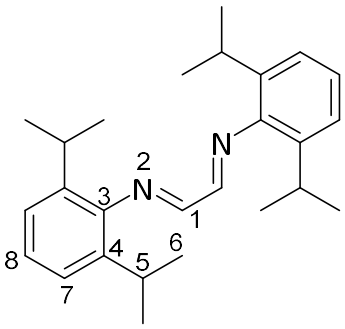

Glyoxal (40% in H_2O, 1.5 mL, 15 mmol) was added to a solution of 2,6-diisopropylaniline (5.3 mL, 28 mmol) in ethanol (40 mL) with constant stirring. Formic acid (3 drops) was then added and the solution was stirred for 16 h. The resulting yellow slurry was filtered and the solid washed with ethanol (20 mL), methanol (20 mL) and dried under vacuum to deliver the product as a pale-yellow solid (1.40 g, 3.7 mmol, 26%). ^{1}H NMR (400 MHz, chloroform-d) δ 8.11 (s, 2H, *H1*), 7.22 – 7.13 (m, 6H, *H7+8*), 3.01 – 2.88 (m, 4H, *H5*), 1.22 (d, J = 6.9 Hz, 24H, *H6*) ppm. ^{13}C{^{1}H} NMR (101 MHz, chloroform-d) δ 163.2 (*C1*), 148.1 (*C3*), 136.8 (*C4*), 125.2 (*C7*), 123.3 (*C8*), 28.1 (*C5*), 23.5 (*C6*) ppm. LCMS, m/z: 377.49 [M+H]$^{+}$ (calc: 377.2951).

8.2.11 1,3-Bis(diisopropylphenyl)imidazolium chloride (*I7*)

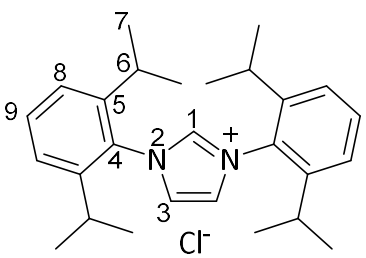

A solution of *N*,*N*-diisopropylphenyl-1,4-diaza-1,3-butadiene (1.40 g, 3.7 mmol) and paraformaldehyde (0.10 g, 4.5 mmol) in anhydrous toluene (50 mL) was heated to 100 °C with stirring for 30 mins. The reaction mixture was cooled to 40 °C and HCl (4 M in dioxane, 1 mL, 4 mmol) added dropwise with vigorous stirring. The reaction mixture was then heated to 70 °C and stirred for 16 h to produce a dark

brown solution which was filtered and washed with diethyl ether and ethyl acetate until washings ran clear. The grey solid was then recrystallized from methanol and diethyl ether to deliver the product as a grey powder (0.19 g, 0.44 mmol, 12%). ^{1}H NMR (400 MHz, chloroform-d) δ 9.98 (s, 1H, *H1*), 8.16 (s, 2H, *H3*), 7.60 (t, J = 7.8 Hz, 2H, *H9*), 7.38 (d, J = 7.8 Hz, 4H, *H8*), 2.48 (dt, J = 13.6, 6.8 Hz, 4H, *H6*), 1.30 (dd, J = 18.9, 6.8 Hz, 24H, *H7*) ppm. ^{13}C{^{1}H} NMR (126 MHz, chloroform-d) δ 145.0 (*C1*), 138.5 (*C5*), 132.2 (*C4*), 129.8 (*C8*), 126.8 (*C9*), 124.7 (*C3*), 24.7 (*C6*), 23.7 (*C7*) ppm. LCMS, m/z: 389.51 $[M\text{-}Cl]^{+}$ (calc: 389.2951).

8.2.12 *N,N*-Dimesityl-1,4-diaza-1,3-butadiene

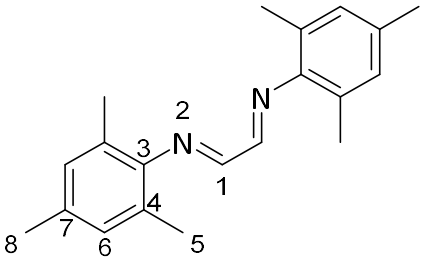

Glyoxal (40% in H_2O, 2.1 mL, 18 mmol) was added to a solution of 2,4,6-trimethylaniline (5 mL, 36 mmol) in ethanol (40 mL) with constant stirring. Formic acid (5 drops) was then added and the solution stirred for 24 h. The resulting yellow slurry was filtered and the solid washed with ethanol (20 mL) and methanol (20 mL), then dried to deliver the product as a bright yellow solid (4.00 g, 14 mmol, 76 %). ^{1}H NMR (400 MHz, chloroform-d) δ 8.10 (d, 2H, *H1*), 6.91 (d, 4H, *H6*), 2.29 (s, 6H, *H8*), 2.16 (s, 12H, *H5*) ppm. ^{13}C{^{1}H} NMR (101 MHz, chloroform-d) δ 163.6 (*C1*), 147.5 (*C3*), 134.4 (*C4*), 129.1 (*C6*), 126.7 (*C7*), 20.9 (*C5*), 18.4 (*C8*) ppm. LCMS, m/z: 293.27 $[M+H]^{+}$ (calc: 293.2012).

8.2.13 1,3-Bis(mesityl)imidazolium chloride (*I8*)

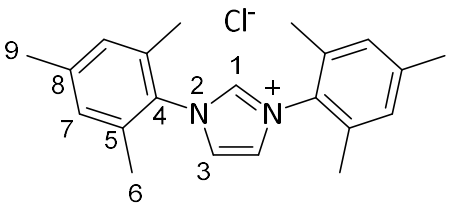

A solution of *N*,*N*-dimesityl-1,4-diaza-1,3-butadiene (3.50 g, 12 mmol) and paraformaldehyde (0.40 g, 13 mmol) in anhydrous toluene (100 mL) was heated to 100 °C with stirring for 30 mins. The reaction mixture was then cooled to 40 °C and HCl (4 M in dioxane, 3.3 mL, 13 mmol) added dropwise. The reaction mixture was then heated to 70 °C for 16 h, yielding a pink slurry which was filtered and washed with ethyl acetate (20 mL) and diethyl ether (20 mL). The pink solid was recrystallized from methanol and diethyl ether to deliver the product as an off-white solid (0.21 g, 0.6 mmol, 5 %). ^{1}H NMR (501 MHz, chloroform-d) δ 10.86 (s, 1H, *H1*), 7.60 (d, J = 1.4 Hz, 2H, *H3*), 7.03 (s, 4H, *H7*), 2.34 (s, 6H, *H9*), 2.18 (s, 12H, *H6*) ppm. ^{13}C{^{1}H} NMR (126 MHz, chloroform-d) δ 141.5 (*C1*), 139.9 (*C4*), 134.2 (*C5*), 130.7 (*C8*), 130.0 (*C7*), 124.4(*C3*), 21.2 (*C6*), 17.7 (*C9*) ppm. LCMS, m/z: 305.30 $[M\text{-}Cl]^{+}$ (calc: 305.2012).

8.2.14 1,3-Dipropyl-3,4-dichloroimidazolium hexafluorophosphate (*I9$_{PF6}$*)

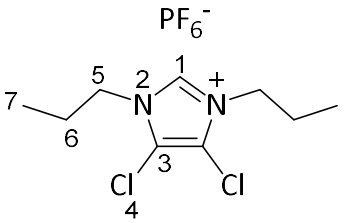

Sodium hydroxide (0.15 g, 4.0 mmol) was added to a solution of 3,4-dichloroimidazole (0.54 g, 4.0 mmol) in acetonitrile (20 mL) under inert conditions and stirred at room temperature for 30 mins. 1-bromopropane (1.1 mL, 12 mmol) was then added and the reaction heated to 80 °C for 16 h. The reaction mixture was cooled, filtered and the solvent removed under reduced pressure to yield an off white solid. The solid was dissolved in water (10 mL), ammonium hexafluorophosphate (0.61 g, 4 mmol) added and the mixture stirred at room temperature for 15 mins. A white precipitate formed which was filtered and washed with water and diethyl ether then dried under reduced pressure delivering the product as an off-white solid (0.48 g, 1.3 mmol, 33%). ^{1}H NMR (500 MHz, DMSO-d6) δ 9.48 (s, 1H, *H1*), 4.17 (t, J = 7.6, 4H, *H5*), 1.82 – 1.80 (m, 4H, *H6*), 0.92 (t, J = 7.4, 6H, *H7*) ppm. ^{13}C{^{1}H} NMR (126 MHz, DMSO-d6) δ 136.56 (*C1*), 119.04 (*C3*), 50.35 (*C5*), 22.15 (*C6*), 10.80 (*C7*) ppm. HRMS (ESI+), *m/z*: 221.0614 [M- PF_6]$^{+}$ (calc: 221.0607).

8.2.15 1,3-Bis(2-phenylethyl)-3,4-dichloroimidazolium hexafluorophosphate (*I10$_{PF6}$*)

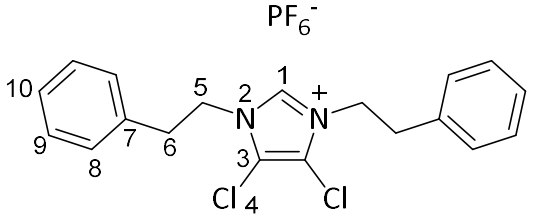

Sodium hydroxide (0.12 g, 3.0 mmol) was added to a solution of 3,4-dichloroimidazole (0.27 g, 2.0 mmol) in acetonitrile (20 mL) under inert conditions and stirred at room temperature for 30 mins. 2-Ethylbromo benzene (1.10 g, 0.8 mL, 6.0 mmol) was then added and the reaction heated to 80 °C for 72 h. Upon cooling the solution was filtered and the solvent removed under reduced pressure to yield a white solid. The solid was dissolved in water (5 mL), ammonium hexafluorophosphate (0.28 g, 1.7 mmol) added and the mixture stirred at room temperature for 15 mins. A white precipitate formed which was filtered, washed with water and diethyl ether then dried under reduced pressure delivering the product as an off-white solid (0.41 g, 0.84 mmol, 42%). ^{1}H NMR (500 MHz, DMSO-d6) δ 9.38 (s, 1H, *H1*), 7.32 – 7.30 (m, 6H, *H8+10*), 7.19 – 7.17 (m, 4H, *H9*), 4.47 (t, J = 7.2 Hz, 4H, *H5*), 3.08 (t, J = 7.2 Hz, 4H, *H6*) ppm. ^{13}C{^{1}H} NMR (126 MHz, DMSO-d6) δ 136.23 (*C1*), 136.05 (*C7*), 128.12 (*C9*), 128.80 (*C8*), 127.21 (*C10*), 118.63 (*C3*), 49.40 (*C5*), 34.60 (*C6*) ppm. HRMS (ESI+), *m/z*: 347.0913 [M-PF_6]$^{+}$ (calc: 345.0920).

8.2.16 1,3-Diphenyl-4,5-dichloroidazolium hexafluorophosphate (*I11$_{PF6}$*)

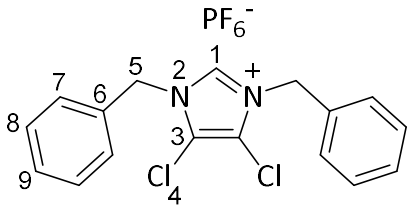

Sodium hydroxide (0.12 g, 3.0 mmol) was added a solution of 3,4-dichloroimidazole (0.27 g, 2.0 mmol) in acetonitrile (20 mL) under inert conditions stirred at room temperature for 30 mins. Benzyl bromide (1.40 g, 1.0 mL, 4.0 mmol) was then added and the reaction heated to 80 °C for 72 h. Upon cooling colourless crystals formed from solution which were filtered and re-dissolved in hot acetonitrile (20 mL). The hot solution was filtered and the solvent was removed under reduced pressure to yield a white crystalline solid. The solid was dissolved in water (5 mL), ammonium hexafluorophosphate (0.16 g, 1.0 mmol) added and the mixture stirred at room temperature for 15 mins. A white precipitate formed which was filtered and washed with water and diethyl ether (20 mL) then dried under reduced pressure delivering the product as an off-white solid (0.12 g, 0.47 mmol, 24%). ^{1}H NMR (500 MHz, DMSO-d6) δ 9.57 (s, 1H, *H1*), 7.45 – 7.32 (m, 10H, *H7-9*), 5.50 (s, 4H, *H5*) ppm. ^{13}C{^{1}H} NMR (126 MHz, DMSO-d6) δ 137.13 (*C1*), 133.14 (*C6*), 129.53 (*C8*), 129.44 (*C7*), 128.77 (*C9*), 119.72 (*C3*), 52.04 (*C5*) ppm. HRMS (ESI+), *m/z*: 317.0602 [M- PF_6]$^{+}$ (calc: 317.0607).

8.2.17 1,3-Dipropylbenzimidazolium hexafluorophosphate (*I12$_{PF6}$*)

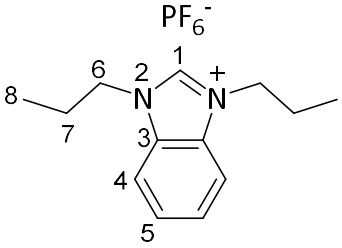

Sodium hydroxide (0.16 g, 4.2 mmol) was added to a solution of benzimidazole (0.5 g, 4.2 mmol) in MeCN (8 mL) and stirred at room temperature under inert conditions for 30 mins. bromopropane (1.15 mL, 13 mmol) was then added and the reaction mixture heated to 80 °C for 72 h. The solution was then cooled, filtered and removed under reduced pressure yielding a dark orange oil which slowly crystalised over 16 h. The orange residue was dissolved in water (5 mL), ammonium hexafluorophosphate (0.32 g, 2.0 mmol) added and the mixture stirred at room temperature for 15 mins. A white precipitate formed which was filtered and washed with water then dried under reduced pressure delivering the product as an off-white solid (0.67 g, 1.8 mmol, 43%). ^{1}H NMR (500 MHz, DMSO-d6) δ 9.79 (s, 1H, *H1*), 8.12 (dd, J = 6.2, 3.1 Hz, 2H, *H5*), 7.71 (dd, J = 6.3, 3.1 Hz, 2H, *H4*), 4.47 (t, J = 7.1 Hz, 4H, *H6*), 1.99 – 1.89 (m, 4H, *H7*), 0.93 (t, J = 7.4 Hz, 6H, *H8*) ppm. ^{13}C{^{1}H} NMR (126 MHz, DMSO-d6) δ 142.11 (*C1*), 131.18 (*C3*), 126.56 (*C5*), 113.73 (*C4*), 48.11 (*C6*), 22.01 (*C7*), 10.68 (*C8*) ppm. HRMS (ESI+), *m/z*: 203.1567 [M-PF_6]$^{+}$ (calc: 203.1543).

8.2.18 1,3-Bis(2-phenylethyl)benzimidazolium hexafluorophosphate (*I13$_{PF6}$*)

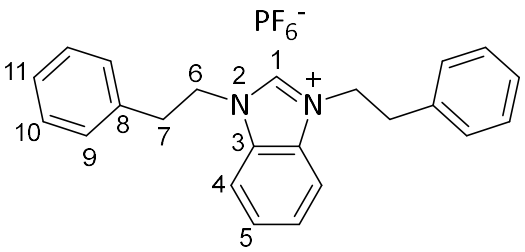

Sodium hydroxide (0.33 g, 8.4 mmol) was added to a solution of benzimidazole (1.00 g, 8.4 mmol) in MeCN (15 mL) under inert conditions and stirred at room temperature for 30 mins. (2-Ethylbromo)benzene (2.30 g, 1.6 mL, 12 mmol) was added and the reaction mixture heated to 80 °C for 16 h. The solution was then cooled, filtered and the solvent removed under reduced pressure. The resulting oil was suspended in toluene (80 mL), (2-ethylbromo)benzene (2.30 g, 1.6 mL, 12 mmol) added and the reaction mixture heated to 100 °C for 24 h. An insoluble oil was formed which was isolated and washed with toluene (3 x 10 mL) and diethyl ether (3 x 10 mL). The oil was dissolved in water/methanol (9:1, 5 mL) and ammonium hexafluorophosphate (1.60 g, 10 mmol) was added and stirred at room temperature for 15 mins. A white precipitate formed which was filtered and washed with water (20 mL) then dried under reduced pressure delivering the product as a white solid (2.10 g, 4.5 mmol, 54%). ^{1}H NMR (400 MHz, DMSO-d6) δ 9.73 (s, 1H, *H1*), 8.10 – 8.03 (m, 2H, *H4*), 7.73 – 7.67 (m, 2H, *H5*), 7.39 – 7.25 (m, 10H, *H9-11*), 4.83 (t, J = 7.3 Hz, 4H, *H6*), 3.27 (t, J = 7.3 Hz, 4H, *H7*) ppm. ^{13}C{^{1}H} NMR (101 MHz, DMSO-d6) δ 142.54 (*C1*), 137.29 (*C8*), 131.33 (*C3*), 129.24 (*C10*), 129.09 (*C9*), 128.94 (*C11*), 127.43 (*C5*), 126.98 (*C4*), 48.15 (*C6*), 33.27 (*C7*) ppm. HRMS (ESI+), *m/z*: 327.1859 [M-PF_6]$^{+}$ (calc: 327.1856).

8.2.19 1,3-Diphenylbenzimidazolium hexafluorophosphate (*I14$_{PF6}$*)

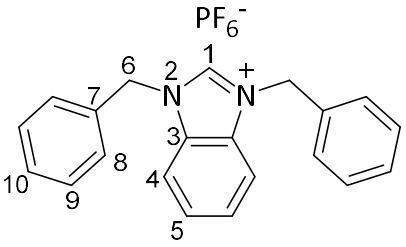

Sodium hydroxide (0.48 g, 12 mmol) was added solution of benzimidazole (1.40 g, 12 mmol) in MeCN (25 mL) under inert conditions and stirred at room temperature for 30 mins. Benzyl bromide (2.10 g, 1.4 mL, 12 mmol) was then added and the reaction mixture heated to 80 °C for 16 h. The solution was then cooled, filtered and the solvent removed under reduced pressure. The solid residue was suspended in toluene (80 mL), benzyl bromide (2.10 g, 1.4 mL, 12.3 mmol) added and the reaction mixture heated to 100 °C for 16 h. The resulting white precipitate was filtered, washed with toluene (3 x 10 mL), diethyl ether (3 x 10 mL), and dried under reduced pressure. The solid was dissolved in water/methanol (9:1, 10 mL), ammonium hexafluorophosphate (2.40 g, 15 mmol) added and the mixture stirred at room temperature for 15 mins. A white precipitate formed which was filtered and washed with water (20 mL) delivering the product as a white solid (3.90 g, 8.9 mmol, 75%). ^{1}H NMR (501 MHz, DMSO-d6) δ 10.03 (s, 1H, *H1*), 7.99 – 7.94 (m, 2H, *H4*), 7.66 – 7.61 (m, 2H, *H5*), 7.54 – 7.50 (m, 4H, *H9*), 7.46

– 7.37 (m, 6H, *H8+10*), 5.79 (s, 4H, *H6*) ppm. $^{13}C\{^{1}H\}$ NMR (126 MHz, DMSO-d6) δ 143.18 (*C1*), 134.41 (*C7*), 131.57 (*C3*), 129.51 (*C9*), 129.25 (*C8*), 128.77 (*C10*), 127.30 (*C5*), 114.50 (*C4*), 50.51 (*C6*) ppm. HRMS (ESI+), *m/z*: 299.1564 $[M\text{-}PF_6]^+$ (calc: 299.1543).

8.2.20 1,3-Dihexylimidazolium bromide (*I15*)

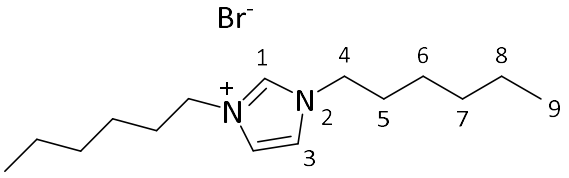

A solution of imidazole (2.00 g, 30 mmol) in toluene (50 mL) was cooled to 0 °C. Sodium hydride (60% suspension in mineral oil, 1.50 g, 35 mmol) was added in portions and the solution was stirred for 1 h at 0 °C. 1-Bromohexane (16.5 mL, 118 mmol) was added dropwise and the solution stirred for a further 30 mins at 0 °C then heated to reflux at 110 °C for 16 h. The resulting amber solution was cooled and concentrated under reduced pressure to yield an orange yellow oil (6.20 g, 20 mmol, 67%). ^{1}H NMR (501 MHz, chloroform-d) δ 10.61 (s, 1H, *H1*), 7.43 (d, *J* = 1.8 Hz, 2H, *H3*), 4.34 (t, *J* = 7.2 Hz, 4H, *H4*), 1.94 – 1.82 (m, 4H, *H5*), 1.36 – 1.20 (m, 12H, *H6-8*), 0.90 – 0.79 (m, 6H, *H9*) ppm. ^{13}C NMR (126 MHz, chloroform-d) δ 137.44 (*C1*), 122.00 (*C3*), 50.18 (*C4*), 31.16 (*C5*), 30.36 (*C6*), 25.96 (*C7*), 22.46 (*C8*), 14.00 (*C9*) ppm. HRMS (ESI+), *m/z*: 237.2329 $[M\text{-}Br]^+$ (calc: 237.2325).

8.3 General Synthesis of Pd-NHC Complexes

NHC precursor (0.56 mmol), $PdCl_2$ (100 mg, 0.56 mmol) and potassium carbonate (386 mg, 2.5 mmol) were suspended in degassed anhydrous 3-chloropyridine (6 mL) and heated to 80 °C for 16 h. The reaction solvent was then removed through short-path distillation. DCM was added to the residues and the mixture passed over a short silica plug (5 cm) and washed with DCM until the eluent ran clear. The solvents were removed under reduced pressure and the residue was triturated in hexane (20 mL) with sonication for 15 mins or for 16 h without sonication. The suspension was then filtered to deliver the product as a fine yellow/orange solid:

8.3.1 C1

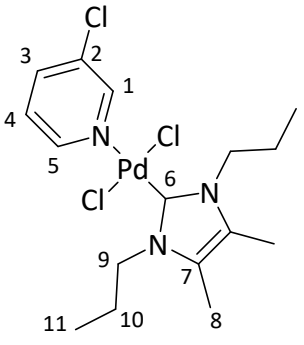

NHC precursor: 1,3-Dipropyl-4,5-dimethylimidazolium hexafluorophosphate. ***C1*** yielded as an orange solid (128 mg, 0.27 mmol, 49%). ^{1}H NMR (501 MHz, chloroform-d) δ 9.07 – 9.06 (m, 1H, *H1*), 8.97 (dd, *J* = 5.5, 1.4 Hz, 1H, *H5*), 7.77 (ddd, *J* = 8.2, 2.4, 1.4 Hz, 1H, *H3*), 7.32 (ddd, *J* = 8.2, 5.5, 0.5 Hz, 1H, *H4*), 4.42 – 4.37 (m, 4H, H9), 2.13 – 2.06 (m, 10H, *H10+8*), 1.08 (t, *J* = 7.4 Hz, 6H, *H11*) ppm. $^{13}C\{^{1}H\}$ NMR (126 MHz, chloroform-d) δ 150.44 (*C1*), 149.37 (*C5*), 142.76 (*C6*), 138.08 (*C4*), 132.74 (*C2*), 126.79 (*C7*), 124.93 (*C3*), 49.96 (*C9*), 24.07 (*C10*), 11.68 (*C8*), 9.23

(*C11*) ppm. HRMS (ESI+), *m/z*: 181.1707 $[imid]^+$ (calc: 181.1705), 285.0581 $[M\text{-}py\text{-}2Cl]^+$ (calc: 286.0661).

8.3.2 C2

NHC precursor: 1,3-Bis(2-phenylethyl)-3,4-dimethylimidazolium hexafluorophosphate. ***C2*** yielded as a yellow solid (56 mg, 0.09 mmol, 17%). ^{1}H NMR (500 MHz, chloroform-d) δ 9.12 (d, J = 2.3 Hz, 1H, *H1*), 9.02 (dd, J = 5.5, 1.1 Hz, 1H, *H5*), 7.80 (dd, J = 5.5, 4.5 Hz, 1H, *H3*), 7.36 (dd, J = 8.2, 5.5 Hz, 1H, *H4*), 7.33 – 7.19 (m, 10H, *H12-14*), 4.69 (t, J = 7.5 Hz, 4H, *H9*), 3.53 (t, J = 7.5 Hz, 4H, *H10*), 1.67 (s, 6H, *H8*) ppm. $^{13}C\{^1H\}$ NMR (126 MHz, chloroform-d) δ 150.37 (*C1*), 149.28 (*C5*), 141.78 (*C6*), 138.48 (*C4*), 132.66 (*C2*), 129.61 (*C12*), 129.22 (*C14*), 128.59 (*C11*), 126.68 (*C13*), 126.33 (*C7*), 124.93 (*C3*), 49.58 (*C9*), 36.86 (*C10*), 8.56 (*C8*) ppm. HRMS (ESI+), *m/z*: 304.1920 $[imid]^+$ (calc: 304.1939), 409.0902 $[M\text{-}py\text{-}2Cl]^+$ (calc: 410.0974).

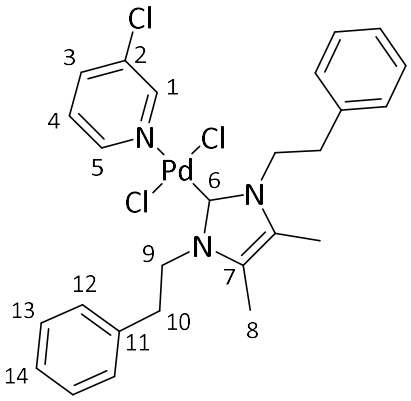

8.3.3 C3

NHC precursor: 1,3-Diphenyl-4,5-dimethylidazolium hexafluorophosphate. ***C3*** yielded as a pale-yellow solid (202 mg, 0.36 mmol, 64%). ^{1}H NMR (501 MHz, chloroform-d) δ 8.92 (d, *J* = 2.0 Hz, 1H, *H1*), 8.82 (dd, *J* = 5.5, 1.4 Hz, 1H, *H5*), 7.65 (ddd, *J* = 8.2, 2.0, 1.4 Hz, 1H, *H3*), 7.42 (dd, *J* = 8.0, 1.4 Hz, 1H, *H4*), 7.33 – 7.25 (m, 10H, *H11-13*), 5.84 (s, 4H, *H9*), 1.80 (s, 6H, *H8*) ppm. $^{13}C\{^1H\}$ NMR (126 MHz, chloroform-d) δ 150.36 (*C1*), 149.30 (*C5*), 137.94 (*C4*), 135.84 (*C*), 132.50 (*C2*), 129.30 (*C6*), 128.82 (*C11*), 127.88 (*C13*), 127.62 (*C11*), 127.47 (*C3*), 124.70 (*C7*), 52.82 (*C9*), 9.41 (*C8*) ppm. HRMS (ESI+), *m/z*: 277.1701 $[imid]^+$ (calc: 277.1705), 381.0585 $[M\text{-}py\text{-}2Cl]^+$ (calc: 382.0661).

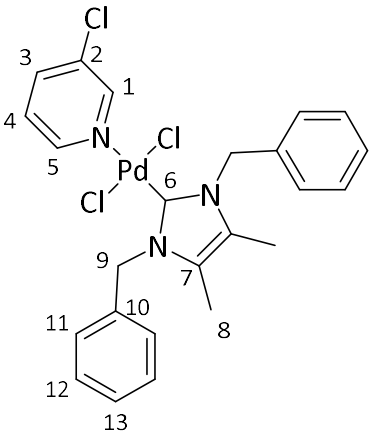

8.3.4 C4

NHC precursor: 1,3-Dipropylimidazolium chloride. ***C4*** yielded as a yellow solid (101 mg, 0.22 mmol, 41%). ^{1}H NMR (501 MHz, chloroform-d) δ 9.07 (d, *J* = 2.3 Hz, 1H, *H1*), 8.97 (dd, *J* = 5.5, 0.9 Hz, 1H, *H5*), 7.79 – 7.75 (m, 1H, *H3*), 7.32 (dt, *J* = 10.0, 5.0 Hz, 1H, *H4*), 6.93 (s, 2H, *H7*), 4.56 – 4.45 (m, 4H, *H8*), 2.16 – 2.07 (m, 4H, *H9*), 1.06 (t, *J* = 7.4 Hz, 6H, *H10*) ppm. ^{13}C{^{1}H} NMR (126 MHz, chloroform-d) δ 150.4 (*C1*), 149.3 (*C5*), 146.6 (*C6*), 138.1 (*C4*), 132.7 (*C2*), 124.9 (*C3*), 121.7 (*C7*), 52.8 (*C8*), 24.0 (*C9*), 11.4 (*C10*) ppm. HRMS (ESI+), *m/z*: 408.0049 $[M\text{-}Cl]^+$ (calc: 407.0147), 151.1236 $[imid]^+$ (calc: 153.1392), 257.0236 $[M\text{-}py\text{-}2Cl]^+$ (calc: 259.0427).

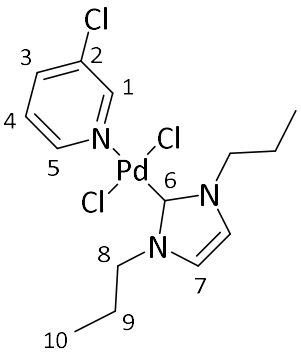

8.3.5 C5

NHC precursor: 1,3-Bis(2-phenylethyl)imidazolium hexafluorophosphate. ***C5*** yielded as a pale-yellow solid (255 mg, 0.45 mmol, 81%). ^{1}H NMR (501 MHz, chloroform-d) δ 9.11 (d, J = 2.3 Hz, 1H, *H1*), 9.02 (dd, J = 5.5, 1.3 Hz, 1H, *H5*), 7.81 (ddd, J = 8.2, 2.3, 1.3 Hz, 1H, *H3*), 7.36 (ddd, J = 8.2, 5.5, 1.3 Hz, 1H, *H4*), 7.31 –7.22 (m, 10H, *H11-13*), 6.30 (s, 2H, *H7*), 4.78 (t, J = 7.2 Hz, 4H, *H8*), 3.47 (t, J = 7.2 Hz, 4H, *H9*) ppm. ^{13}C{^{1}H} NMR (126 MHz, chloroform-d) δ 150.50 (*C1*), 149.43 (*C5*), 147.10 (*C6*), 138.27 (*C4*), 138.11 (*C10*), 132.86 (*C2*), 129.29 (*C11*), 128.79 (*C13*), 126.88 (*C12*), 125.07 (*C3*), 122.06 (*C7*), 52.76 (*C8*), 36.95 (*C9*) ppm. HRMS (ESI+), m/z: 382.0659 $[M\text{-}py\text{-}2Cl]^+$ (calc: 383.0740), 275.1542 $[imid]^+$ (calc: 277.1705).

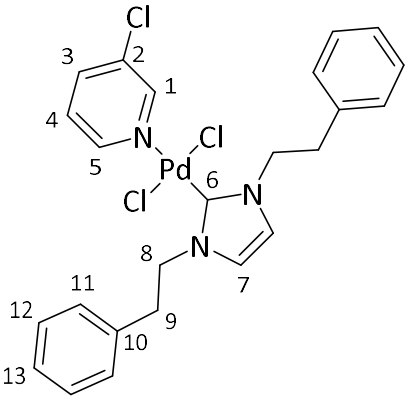

8.3.6 C6

NHC precursor: 1,3-Dibenzylimidazolium hexafluorophosphate. ***C6*** yielded as an orange solid (205 mg, 0.38 mmol, 68%). ^{1}H NMR (400 MHz, chloroform-d) δ 9.06 (d, *J* = 2.3 Hz, 1H, *H1*), 8.96 (dd, *J* = 5.5, 1.3 Hz, 1H, *H5*), 7.77 (ddd, *J* = 8.2, 2.2, 1.3 Hz, 1H, *H3*), 7.53 – 7.49 (m, 4H, *H11*), 7.42 – 7.30 (m, 7H, *H4+10+12*), 6.71 (s, 2H, *H7*), 5.85 (s, 4H, *H8*) ppm. ^{13}C{^{1}H} NMR (101 MHz, chloroform-d) δ 150.48 (*C1*), 149.39 (*C5*), 148.76 (*C3*), 138.23 (*C4*), 135.34 (*C9*), 132.78 (*C2*), 129.12 (*C10*), 128.71 (*C12*), 124.98 (*C3*), 121.99 (*C11*), 55.00 (*C8*) ppm. HRMS (ESI+), m/z: 353.0274 $[M\text{-}py\text{-}2Cl]^+$ (calc: 355.0247), 249.1388 $[imid]^+$ (calc: 249.1392).

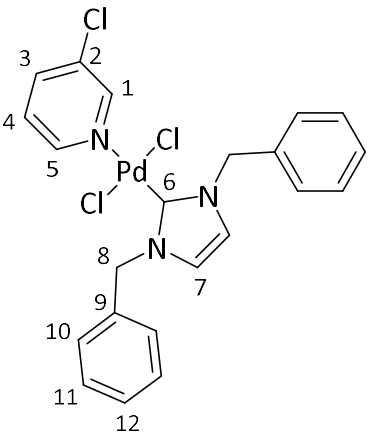

8.3.7 C7

NHC precursor: 1,3-Bis(diisopropylphenyl)imidazolium chloride. ***C7*** yielded as a pale-yellow solid (200 mg, 0.29 mmol, 53%). ^{1}H NMR (400 MHz, chloroform-d) δ 8.60 (d, *J* = 2.3 Hz, 1H, H1), 8.52 (dd, *J* = 5.5, 1.3 Hz, 1H, *H5*), 7.55 (ddd, *J* = 8.2, 2.3, 1.4 Hz, 1H, *H3*), 7.52 – 7.47 (m, 2H, *H11*), 7.35 (d, *J* = 7.7 Hz, 4H, *H10*), 7.14 (s, 2H, *H7*), 7.07 (dd, *J* = 8.2, 5.6 Hz, 1H, *H4*), 3.23 – 3.06 (m, 4H, *H12*), 1.48 (d, *J* = 6.6 Hz, 12H, *H13*), 1.12 (d, *J* = 6.9 Hz, 12H, *H13*) ppm. ^{13}C{^{1}H} NMR (126 MHz, chloroform-d) δ 153.5 (*C1*), 150.6 (*C8*), 149.5 (*C5*), 146.7 (*C6*), 137.5 (*C4*), 135.1 (*C8*), 132.1 (*C2*), 130.4 (*C11*), 125.2 (*C10*), 124.4 (*C7*), 124.2 (*C3*), 26.4 (*C12*), 23.3 (*C13*) ppm. HRMS (ESI+), *m/z*: 387.2789 [imid]$^{+}$ (calc: 389.2957), 493.1835 [M-py-2Cl]$^{+}$ (calc: 495.1992).

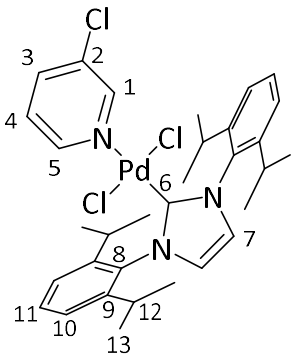

8.3.8 C8

NHC precursor: 1,3-Bis(mesityl)imidazolium chloride. ***C8*** yielded as a pale-yellow solid (169 mg, 0.29 mmol, 51%). ^{1}H NMR (501 MHz, chloroform-d) δ 8.59 (d, *J* = 2.3 Hz, 1H, *H1*), 8.50 (dd, *J* = 5.5, 1.0 Hz, 1H, *H5*), 7.56 (ddd, *J* = 8.2, 1.0, 1.4 Hz, 1H, *H3*), 7.21 – 7.18 (m, 1H, *H4*), 7.07 (s, 2H, *H7*) 7.06 (s, 4H, *H10*), 2.38 (s, 6H, *H12*), 2.35 (s, 12H, *H13*) ppm. ^{13}C{^{1}H} NMR (126 MHz, chloroform-d) δ 151.2 (*C8*), 150.4 (*C1*), 149.5 (*C5*), 148.6 (*C6*), 147.2 (*C9*), 139.2 (*C4*), 137.4 (*C11*), 131.9 (*C2*), 129.2 (*C10*), 124.3 (*C3*), 124.2 (*C7*) , 21.2 (*C13*), 19.1 (*C12*) ppm. HRMS (ESI+), *m/z*: 303.1856 [imid]$^{+}$ (calc: 305.2018), 409.0895 [M-py-2Cl]$^{+}$ (calc: 411.1053).

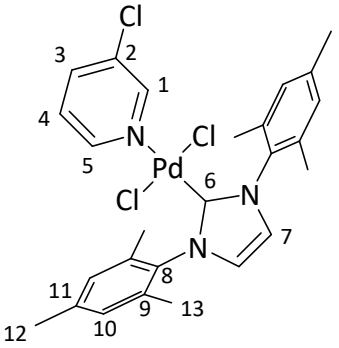

8.3.9 C9

NHC precursor: 1,3-Dipropyl-4,5-dichloroimidazolium hexafluorophosphate. ***C9*** yielded as a yellow solid (202 mg, 0.40 mmol, 71%). ^{1}H NMR (501 MHz, chloroform-d) δ 9.02 (s, 1H, *H1*), 8.93 (d, *J* = 5.2 Hz, 1H, *H5*), 7.80 (d, *J* = 7.8 Hz, 1H, *H3*), 7.34 (dd, *J* = 7.8, 5.2 Hz, 1H, *H4*), 4.57 – 4.51 (m, 4H, *H8*), 2.21 – 2.12 (m, 4H, *H9*), 1.10 (t, *J* = 7.3 Hz, 6H, *H10*) ppm. ^{13}C{^{1}H} NMR (126 MHz, chloroform-d) δ 150.45 (*C1*), 149.38 (*C5*), 148.58 (*C6*), 138.41 (*C4*), 132.88 (*C2*), 125.08 (*C3*), 117.48 (*C7*), 51.74 (*C8*), 23.49 (*C9*), 11.41 (*C10*) ppm. HRMS (ESI+), m/z: 326.9471 [M-py-2Cl]$^{+}$ (calc: 326.9647).

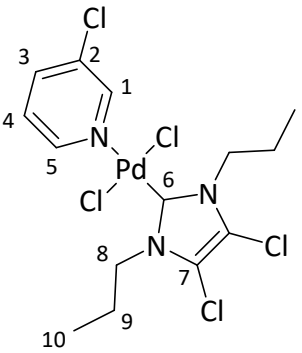

8.3.10 C10

NHC precursor: 1,3-Bis(2-phenylethyl)-4,5-dichloroimidazolium hexafluorophosphate. ***C10*** yielded as an orange solid (204 mg, 0.32 mmol, 57%). ^{1}H NMR (501 MHz, chloroform-d) δ 9.07 (d, *J* = 2.1 Hz, 1H, *H1*), 8.97 (d, *J* = 4.9 Hz, 1H, *H5*), 7.83 (d, *J* = 8.2 Hz, 1H, *H3*), 7.41 – 7.29 (m, 11H, *H4+11-13*), 4.87 – 4.81 (m, 4H, *H8*), 3.54 – 3.48 (m, 4H, *H9*) ppm. ^{13}C{^{1}H} NMR (126 MHz, chloroform-d) δ 150.49 (*C1*), 149.73 (*C10*), 149.40 (*C5*), 138.52 (*C4*), 137.39 (*C6*), 133.01 (*C2*), 129.23 (*C11*), 128.88 (*C13*), 127.14 (*C12*), 125.24 (*C3*), 117.62 (*C7*), 51.38 (*C8*), 36.28 (*C9*) ppm. HRMS (ESI+), m/z: 450.9789 $[M\text{-py-}2Cl]^{+}$ (calc: 450.9960), 345.0912 $[imid]^{+}$ (calc: 345.0925).

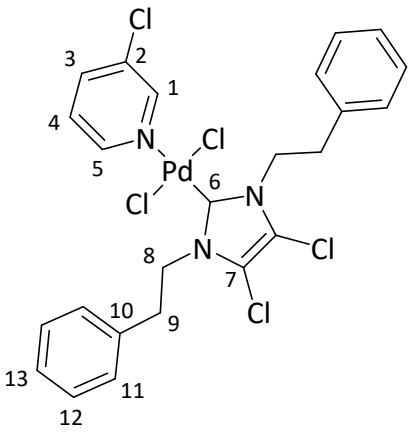

8.3.11 C11

NHC precursor: 1,3-Diphenyl-4,5-dichloroidazolium hexafluorophosphate. ***C11*** yielded as a pale-yellow solid (96 mg, 0.16 mmol, 29%). ^{1}H NMR (500 MHz, chloroform-d) δ 8.91 (d, *J* = 2.3 Hz, 1H, *H1*), 8.82 (dd, *J* = 5.5, 1.3 Hz, 1H, *H5*), 7.76 (ddd, *J* = 8.2, 2.3, 1.3 Hz, 1H, *H3*), 7.44 – 7.33 (m, 11H, *H10-12*), 7.30 (dd, *J* = 8.2, 5.5 Hz, 1H, *H4*), 5.92 (s, 4H, *H8*) ppm.^{13}C{^{1}H} NMR (126 MHz, chloroform-d) δ 150.48 (*C1*), 149.68 (*C9*), 149.48 (*C5*), 138.46 (*C4*), 136.75 (*C6*), 132.91 (*C2*), 129.27 (*C10*), 128.89 (*C12*), 127.18 (*C11*), 126.02 (*C3*), 118.72 (*C7*), 51.74 (*C8*) ppm. HRMS (ESI+), m/z: 421.9559 $[M\text{-py-}2Cl]^{+}$ (calc: 422.9697), 317.0598 $[imid]^{+}$ (calc: 317.0612).

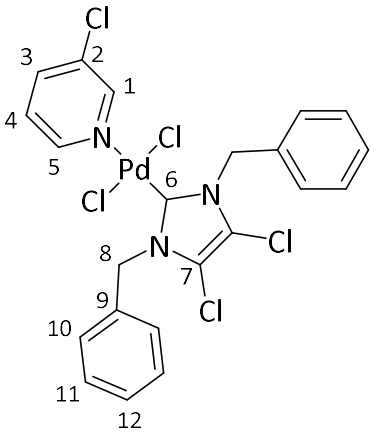

8.3.12 C12

NHC precursor: 1,3-Dipropylbenzimidazolium hexafluorophosphate. ***C12*** yielded as a yellow solid (192 mg, 0.39 mmol, 70%). ^{1}H NMR (501 MHz, chloroform-d) δ 9.12 – 9.10 (m, 1H, *H1*), 9.01 (dd, *J* = 5.5, 1.3 Hz, 1H, *H5*), 7.82 – 7.79 (m, 1H, *H3*), 7.44 – 7.39 (m, 2H, *H12*), 7.36 (ddd, *J* = 8.2, 5.5, 0.6 Hz, 1H, *H4*), 7.31 – 7.26 (m, 2H, *H13*), 4.84 – 4.78 (m, 4H, *H9*), 2.30 – 2.21 (m, 4H, *H10*), 1.14 (t, *J* = 7.4 Hz, 6H, *H11*) ppm. ^{13}C{^{1}H} NMR (126 MHz, chloroform-d) δ 161.04 (*C6*), 150.43 (*C1*), 149.35 (*C5*), 138.32 (*C4*), 134.64 (*C13*), 132.88 (*C2*), 125.07 (*C12*), 123.23 (*C3*), 110.62

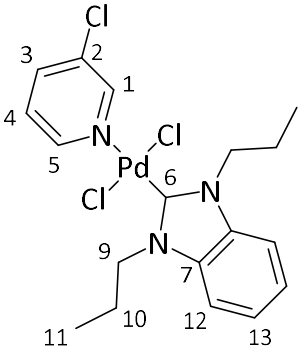

(*C7*), 50.29 (*C9*), 23.18 (*C10*), 11.87 (*C11*) ppm. HRMS (ESI+), m/z: 305.0281 $[M\text{-py-}2Cl]^+$ (calc: 309.0583), 201.1477 $[imid]^+$ (calc: 203.1548).

8.3.13 C13

NHC precursor: 1,3-Bis(2-phenylethyl)benzimidazolium hexafluorophosphate. ***C13*** yielded as a pale-yellow solid (185 mg, 0.30 mmol, 54%). ^1H NMR (500 MHz, chloroform-d) δ 9.15 (d, *J* = 2.3 Hz, 1H, *H1*), 9.06 (dd, *J* = 5.5, 1.1 Hz, 1H, *H5*), 7.86 – 7.82 (m, 1H, *H3*), 7.41 (dd, *J* = 8.2, 5.5 Hz, 1H, *H4*), 7.30 – 7.19 (m, 10H, *H13-15*), 7.11 – 7.07 (m, 2H, *H8*), 7.06 – 7.02 (m, 2H, *H9*), 5.07 – 5.11 (m, 4H, *H10*), 3.62 – 3.57 (m, 4H, *H11*) ppm. $^{13}C\{^1H\}$ NMR (126 MHz, chloroform-d) δ 162.86 (*C6*), 150.49 (*C1*), 149.39 (*C5*), 138.44 (*C12*), 138.37 (*C4*), 134.40 (*C2*), 129.20 (*C13*), 128.84 (*C15*), 126.94 (*C14*), 125.21 (*C3*), 123.08 (*C8*), 110.30 (*C7*), 50.14 (*C10*), 36.17 (*C11*) ppm. HRMS (ESI+), *m/z*: 327.1851 $[imid]^+$ (calc: 327.1861), 431.0741 $[M\text{-py-}2Cl]^+$ (calc: 432.0818).

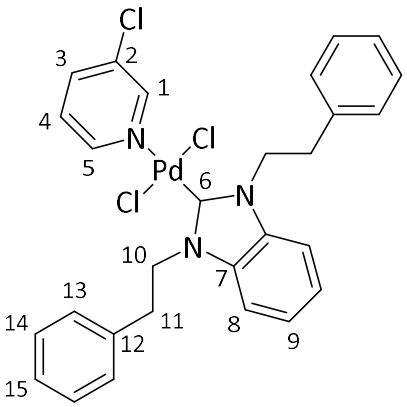

8.3.14 C14

NHC precursor: 1,3-Bisphenylbenzimidazolium hexafluorophosphate. ***C14*** yielded as a pale-yellow solid (186 mg, 0.32 mmol, 57%). ^1H NMR (501 MHz, chloroform-d) δ 9.05 (d, *J* = 2.3 Hz, 1H, *H1*), 8.95 (dd, *J* = 5.5, 1.2 Hz, 1H, *H5*), 7.79 – 7.76 (m, 1H, *H3*), 7.79 – 7.64 (m, 4H, *H8+9*), 7.41 – 7.30 (m, 7H, *H4+12+14*), 7.14 – 7.07 (m, 4H, *H13*), 6.24 (s, 4H, *H10*) ppm. $^{13}C\{^1H\}$ NMR (126 MHz, chloroform-d) δ 163.47 (*C6*), 150.35 (*C1*), 149.26 (*C5*), 138.20 (*C4*), 134.97 (*C11*), 134.55 (*C2*), 128.95 (*C12*), 128.29 (*C14*), 128.06 (*C9*), 127.99 (*C13*), 124.89 (*C3*), 123.40 (*C8*), 111.50 (*C7*), 53.24 (*C10*) ppm. HRMS (ESI+), m/z: 403.0443 $[M\text{-py-}2Cl]^+$ (calc: 405.0583), 297.1381 $[imid]^+$ (calc: 299.1548).

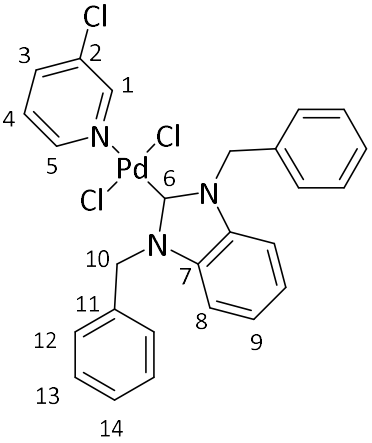

8.4 General Synthesis of Imidazolium Palladate Salts

Imidazolium salt precursor (1.0 mmol) was dissolved in chloroform (5 mL). A second solution of Na_2PdCl_4 (145 mg, 0.5 mmol) in water (5 mL) was prepared. The two solutions were then mixed vigorously for 2 hours, during which the dark red colour transferred from the aqueous to the organic layer. The organic layer was separated, dried with $MgSO_4$ and concentrated to dryness under a reduced pressure to yield the product as a dark red oily residue or solid.

8.4.1 1,3-Diphenyl-4,5-dichloroidazolium tetrachloropalladate (*IPS4*)

Imidazolium salt precursor: ***I4***. ***IPS4*** yielded as a red/brown solid (41 mg, 0.058 mmol, 12%). ^{1}H NMR (500 MHz, chloroform-d) δ 9.83 (s, 1H, *H1*), 7.39 (d, J = 1.5 Hz, 2H, *H3*), 4.53 – 4.46 (m, 4H, *H4*), 2.12 – 2.00 (m, 4H, *H5*), 1.06 (t, J = 7.4 Hz, 6H, *H6*) ppm. ^{13}C{^{1}H} NMR (126 MHz, chloroform-d) δ 138.3 (*C1*), 122.0(*C3*), 51.2 (*C4*), 23.8 (*C5*), 10.4 (*C6*) ppm. HRMS, m/z: 153.1386 $[M\text{-}PdCl_4]^+$ (calc: 153.1386).

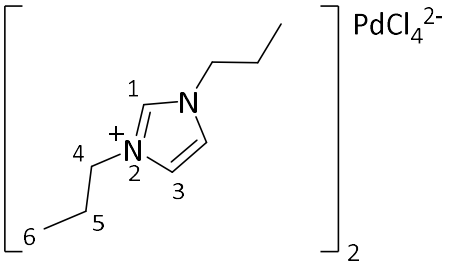

8.4.2 1,3-Bis(2-phenylethyl)imidazolium tetrachloropalladate (*IPS5*)

Imidazolium salt precursor: ***I5 IPS5*** yielded as a red/brown waxy solid (340 mg, 0.42 mmol, 85%). ^{1}H NMR (400 MHz, chloroform-d) δ 10.22 (s, 1H, *H1*), 7.30 – 7.12 (m, 10H, *H7-9*), 6.85 (s, 2H, *H3*), 4.72 (t, J = 6.9 Hz, 4H, *H4*), 3.22 (t, J = 6.9 Hz, 4H, *H5*) ppm. ^{13}C{^{1}H} NMR (101 MHz, chloroform-d) δ 137.6 (*C1*), 135.8 (*C6*), 129.1 (*C7*), 129.0 (*C7*), 128.7 (*C9*), 128.1 (*C8*), 127.8 (*C8*), 121.9 (*C3*), 51.3 (*C4*), 35.3 (*C5*) ppm. HRMS (ESI+), *m/z*: 277.1703 $[M\text{-}PdCl_4]^+$ (calc: 277.1699).

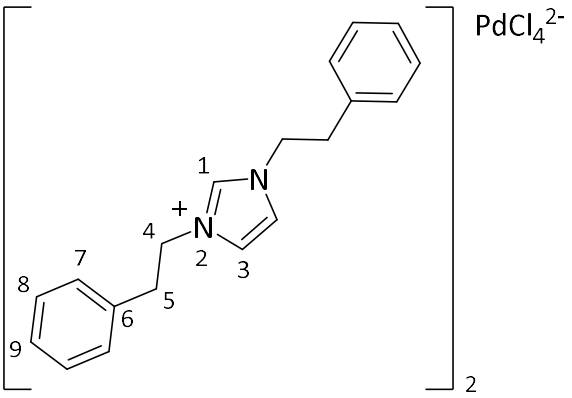

8.4.3 1,3-Dibenzylimidazolium tetrachloropalladate (*IPS6*)

Imidazolium salt precursor: ***I6***. ***IPS6*** yielded as a red oily residue (140 mg, 0.18 mmol, 36%). ^{1}H NMR (501 MHz, chloroform-d) δ 10.49 (s, 1H, *H1*), 7.52 – 7.48 (m, 4H, *H7*), 7.41 – 7.37 (m, 6H, *H6+8*), 7.11 (s, 2H, *H3*), 5.74 (s, 4H, *H4*) ppm. ^{13}C{^{1}H} NMR (126 MHz, chloroform-d) δ 138.50 (*C1*), 132.90 (*C5*), 129.47 (*C6*), 129.43 (*C8*), 128.24 (*C7*), 121.69 (*C3*), 54.31 (*C4*) ppm. HRMS (ESI+), *m/z*: 249.1381 [M-$PdCl_4$]$^{+}$ (calc: 249.1386).

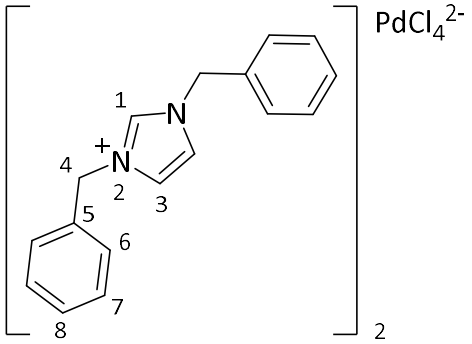

8.4.4 1,3-Bis(diisopropylphenyl)imidazolium tetrachloropalladate (*IPS7*)

Imidazolium salt precursor: ***I7***. ***IPS7*** yielded as a red/brown oily residue (232 mg, 0.32 mmol, 64%). ^{1}H NMR (501 MHz, chloroform-d) δ 9.13 (s, 1H, *H1*), 8.40 (s, 2H, *H3*), 7.63 – 7.58 (m, 2H, *H9*), 7.39 – 7.34 (m, 4H, *H8*), 2.56 – 2.49 (m, 4H, *H6*), 1.33 (d, J = 6.9 Hz, 12H, *H7*), 1.22 (d, J = 6.9 Hz, 12H, *H7*) ppm. ^{13}C{^{1}H} NMR (126 MHz, chloroform-d) δ 145.35 (*C1*), 132.40 (*C4*), 130.04 (*C5*), 128.34 (*C9*), 127.84 (*C8*), 124.96 (*C3*), 24.93 (*C6*), 24.13 (*C7*) ppm. HRMS (ESI+), *m/z*: 389.2954 [M-$PdCl_4$]$^{+}$ (calc: 389.2951).

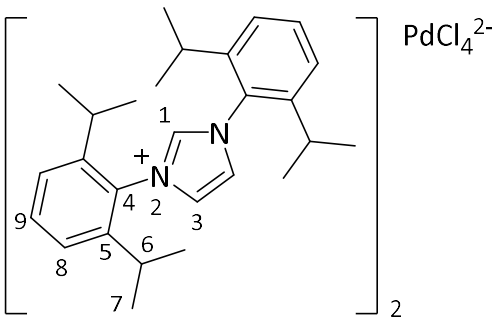

8.4.5 1,3-Bis(mesityl)imidazolium tetrachloropalladate (*IPS8*)

Imidazolium salt precursor: ***I8****.* ***IPS8*** yielded as a red/brown oily residue (312 mg, 0.36 mmol, 72%). ^{1}H NMR (501 MHz, chloroform-d) δ 10.18 (s, 1H, *H1*), 7.68 (d, J = 8.0 Hz, 2H, *H3*), 7.09 (s, 4H, *H7*), 2.38 (s, 6H, *H9*), 2.20 (s, 12H, *H6*) ppm. ^{13}C{^{1}H} NMR (126 MHz, chloroform-d) δ 141.74 (*C1*), 139.19 (*C4*), 134.36 (*C5*), 130.75 (*C8*), 130.29 (*C7*), 124.74 (*C3*), 21.45 (*C6*), 17.92 (*C9*) ppm. HRMS (ESI+), *m/z*: 305.2009 [M-$PdCl_4$]$^{+}$ (calc: 305.2012).

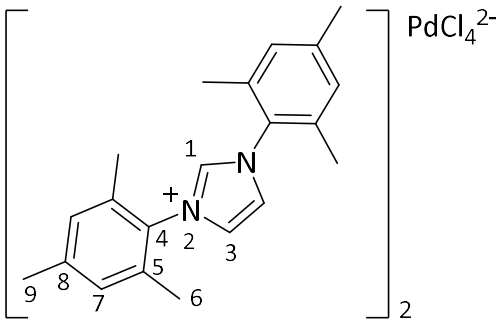

8.4.6 1,3-Diphenylbenzimidazolium tetrachloropalladate (*IPS12*)

Imidazolium salt precursor: ***I12****.* ***IPS12*** yielded as a red/brown solid (115 mg, 0.17 mmol, 35%). ^{1}H NMR (501 MHz, chloroform-d) δ 10.41 (s, 1H, *H1*), 7.84 – 7.79 (m, 2H, *H5*), 7.75 – 7.70 (m, 2H, *H4*), 4.87 – 4.82 (m, 4H, *H6*), 2.22 (dt, J = 14.7, 7.4 Hz, 4H, *H7*), 1.13 (t, J = 7.4 Hz, 6H, *H8*) ppm. ^{13}C NMR (126 MHz, chloroform-d) δ 144.42 (*C1*), 138.47 (*C3*), 127.64 (*C5*), 113.68 (*C4*), 49.99 (*C6*), 23.23 (*C7*), 11.42 (*C8*). HRMS (ESI+), *m/z*: 203.1549 [M-$PdCl_4$]$^{+}$ (calc: 203.1543).

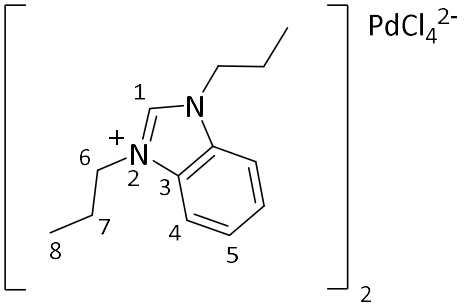

8.4.7 1,3-Dihexylimidazolium tetrachloropalladate (*IPS15*)

Imidazolium salt precursor: ***I15****.* ***IPS15*** yielded as a red/brown oil (296 mg, 0.41 mmol, 82%). ^{1}H NMR (501 MHz, chloroform-d) δ 10.17 (s, 1H), 7.49 (d, J = 1.2 Hz, 2H), 4.54 (t, J = 7.4 Hz, 4H), 2.03 – 1.85 (m, 4H), 1.45 – 1.18 (m, 12H), 0.85 (t, J = 7.0 Hz, 6H) ppm. ^{13}C NMR (126 MHz, chloroform-d) δ 137.07 (*C1*), 122.36 (*C3*), 50.69 (*C4*), 31.28 (*C5*), 30.51 (*C6*), 26.08 (*C7*), 22.55 (*C8*), 14.09 (*C9*) ppm. HRMS (ESI+), *m/z*: 237.2327 [M-$PdCl_4$]$^{+}$ (calc: 237.2325).

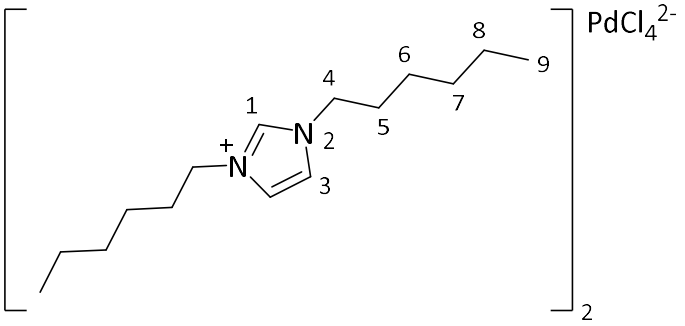

8.5 Imidazolium and NHC Ligand Stabilised Palladium Nanoparticles Synthesis

8.5.1 PdNP7-NHC

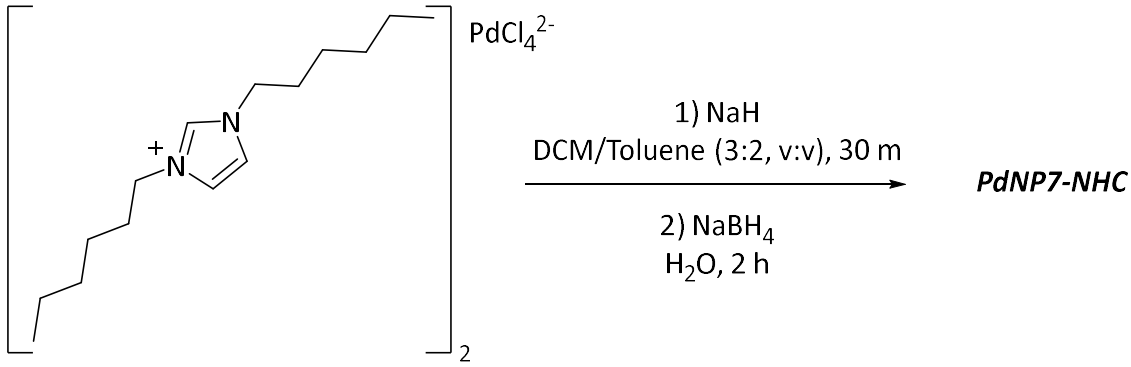

Sodium hydride (60% in mineral oil) (30 mg, 0.75 mmol) was added to an ampoule under an inert atmosphere. Dry DCM and toluene (3:2 v:v, 30 mL) were added and the suspension stirred at 0 °C for 5 mins. ***IPS7*** (362 mg, 0.50 mmol) in dry DCM (6 mL) was then added to the sodium hydride suspension and stirred for 30 mins, where the colour changed from red to yellow. A solution of $NaBH_4$ (25 mg, 2.5 mmol) in water (3 mL) was prepared and added dropwise to the reaction mixture with vigorous stirring. The reaction mixture changed colour from yellow to black upon addition of the $NaBH_4$ solution. The reaction was stirred for 2 hours then washed with water (3 x 10 mL), filtered and concentrated to dryness under reduced pressure to yield a black oily residue.

8.5.2 PdNP7-imid

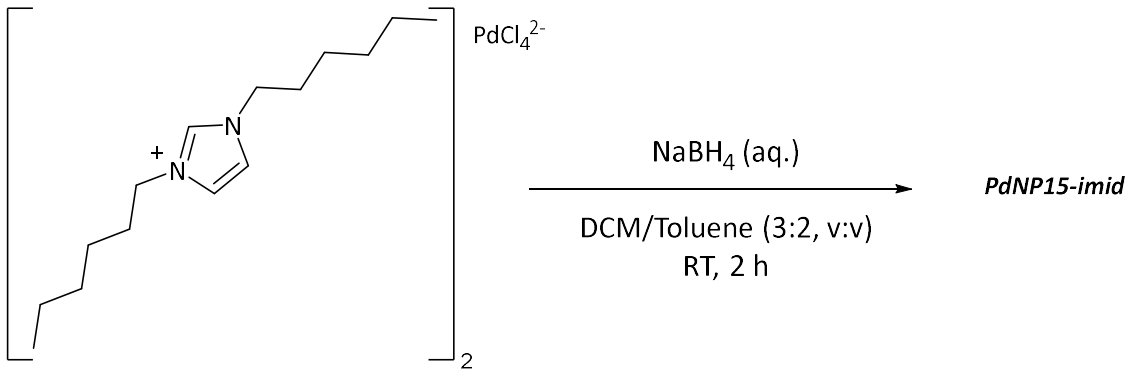

IPS7 (232 mg 0.32 mmol) was dissolved in dry DCM and toluene (3:2 v:v, 16 mL) and stirred under and inert atmosphere. A solution of $NaBH_4$ (60 mg, 1.6 mmol) in water (2 mL) was prepared and added dropwise to the reaction mixture with vigorous stirring. The reaction mixture changed colour from red/brown to black upon addition of the $NaBH_4$ solution. The reaction was stirred for 2 hours then washed with water (3 x 10 mL), filtered and concentrated to dryness under reduced pressure to yield a black residue.

8.6 General Catalytic Protocols

THF was collected from Grubbs solvent purification system. 1,4-Dioxane/water mix was degassed with argon. All reagents were used as supplied, without further purification other than *p*-fluorophenylboronic acid which was recrystallised prior to use. chloroform-d NMR solvent was dried and de-acidified using $CaCO_3$ and activated 3 Å molecular sieves. Celite® was oven dried prior to use. "Reaction vial" corresponds to a 7 mL soda-lime glass vial with a silicone septum lid. An IKA® C-MAG HS7 stirrer hotplate equipped with external temperature probe and aluminium heating block was used for all catalytic reactions, stirring set to 3.

8.6.1 Initial Conditions

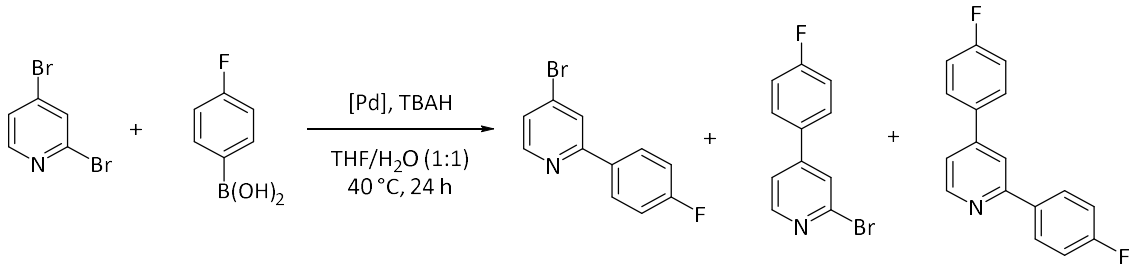

In an ampule, a solution of tetrabutylammonium hydroxide in water (1 M) was prepared and degassed with argon over an hour. This will be known as 'the base stock'.

An oven-dried vial (*Vial 1*) equipped with a silicone sceptre and magnetic follower was charged with catalyst (0.025 mmol), evacuated and backfilled with argon. Dry, degassed THF (1.25 mL) was added *via* syringe and the vial was heated to 40 °C with stirring. A second oven-dried vial (*Vial 2*) equipped with a silicone sceptre and magnetic follower was charged with 2,4-dibromopyridine (237 mg, 1.00 mmol) and *p*-fluorophenylboronic acid (168 mg, 1.20 mmol) and subsequently evacuated and backfilled with argon. After 30 mins of stirring, the contents of *Vial 1* was transferred into *Vial 2 via* syringe and the resulting mixture was allowed to stir for 5 mins in order to thermally equilibrate at 40 °C. 2.5 mL of the pre-heated base stock was then added *via* syringe to *Vial 2* to commence the reaction (t_0). 1-Fluoro-3,5-dimethoxybenzene (133 µL, 1.00 mmol, *NMR standard*) was added at the start of the reaction.

8.6.2 Standard (Pd-NHC Precatalyst Refined) Conditions

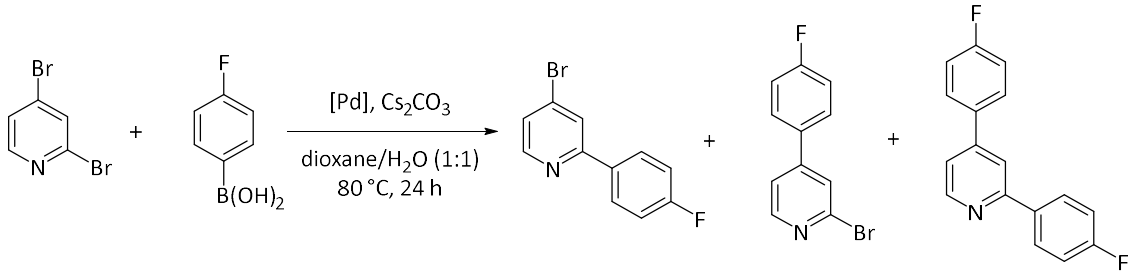

In an ampule, 1,4-dioxane (5 mL) and water (5 mL) were combined and degassed with argon over 1 h. An oven-dried vial (*Vial 1*) equipped with a silicone sceptre and magnetic follower was charged with catalyst (0.025 mmol), 2,4-dibromopyridine (237 mg, 1.00 mmol), *p*-fluorophenylboronic acid (168 mg, 1.20 mmol) and caesium carbonate (650 mg, 2.00 mmol) then subsequently evacuated and backfilled with argon. Dioxane/water (2.5 mL) was then added *via* syringe and heated at 80 °C, commencing the reaction (t_0). 1-Fluoro-3,5-dimethoxybenzene (133 µL, 1.0 mmol, *NMR standard*) was added at the start of the reaction.

8.6.3 Sampling of Catalytic Reactions

Reaction samples (100 µL), taken using a 500 µL syringe were rapidly quenched by dissolution in CH_2Cl_2 (1.0 mL) then filtered through a pipette fitted with a celite plug (*ca.* 1 cm depth). The filtrate was concentrated under reduced pressure and the residue was dissolved in chloroform-d (0.5 mL) for analysis through ^{1}H and ^{19}F NMR spectroscopy.

8.6.4 Time Course and Poisoning Reactions

8.6.4.1 General Procedure for Time Course Reactions (*C7* and *C14*)

A reaction vial equipped with a magnetic follower was charged with catalyst (0.025 mmol), *p*-fluorophenylboronic acid (167 mg, 1.20 mmol), 2,4-dibromopyridine (263 mg, 1.00 mmol) and caesium carbonate (650 mg, 2.00 mmol), then was evacuated and backfilled with argon (x 3). Degassed 1,4-dioxane and water (1:1, 2.5 mL) preheated to reaction temperature (***C7***-60 °C and ***C14***-80 °C) was then added to the reaction vial, followed by 1-fluoro-3,5-dimethoxybenzene (133 µL, 156 mg, 1.00 mmol). The vial was maintained at reaction temperature and stirred constantly for 7 hours. Samples (100 µL) were then taken at t = 0, 1, 2, 3, 4, 5, 7.5, 10, 12.5, 15, 20, 25, 30, 45, 60, 90, 120, 180, 240, 300, 360 and 420 mins. Each sample was diluted in DCM (2.0 mL) then passed over a Celite® plug (~1 cm). The solvent was removed under reduced pressure and the residue dissolved in chloroform-d and analysed using ^{1}H and ^{19}F NMR spectroscopy.

8.6.4.2 General Procedure for Time Course Reactions (*C16* - *C21*)

A reaction vial equipped with a magnetic follower was charged with catalyst (0.025 mmol), *p*-fluorophenylboronic acid (167 mg, 1.2 mmol), 2,4-dibromopyridine (263 mg, 1.00 mmol) and caesium carbonate (650 mg, 2.00 mmol), then was evacuated and backfilled with argon (x 3). Degassed 1,4-dioxane and water (1:1, 2.5 mL) preheated to reaction temperature (80 °C) was then added to the reaction vial, followed by 1-fluoro-3,5-dimethoxybenzene (133 µL, 156 mg, 1.00 mmol). The vial was maintained at reaction temperature and stirred constantly for 7 hours. Samples (100 µL) were then taken at t = 5, 10, 20, 30, 45, 60, 90, 120, 180, 240, 300 and 360 mins. Each sample was diluted in DCM (2 mL) then passed over a Celite® plug (~1 cm). The solvent was removed under reduced pressure and the residue dissolved in chloroform-d and analysed using ^{1}H and ^{19}F NMR spectroscopy.

8.6.4.3 General Procedure for Mercury Drop Tests

An ampoule equipped with a magnetic follower was charged with catalyst (0.05 mmol), *p*-fluorophenylboronic acid (334 mg, 2.40 mmol), 2,4-dibromopyridine (526 mg, 2.00 mmol) and caesium carbonate (1.30 g, 4.00 mmol), then was evacuated and backfilled with argon (x3). Degassed 1,4-dioxane and water (1:1, 5 mL) preheated to reaction temperature (***C7***-60 °C and ***C14***-80 °C) was added to the ampoule, followed by 1-fluoro-3,5-dimethoxybenzene (266 µL, 312 mg, 2.00 mmol). The vial was maintained at reaction temperature and stirred constantly for 7 hours. Mercury (0.1 mL) was added at 15 mins and 20 mins for ***C7*** and ***C14*** respectively. Samples of the reaction mixture (100 µL) were then taken at t = 0, 1, 2, 3, 4, 5, 7.5, 10, 12.5, 15, 20, 25, 30, 45, 60, 90, 120, 180 and 240 mins. Each sample was diluted in DCM (2.0 mL) then passed over a Celite® plug (~1 cm). The solvent was removed under reduced pressure and the residue dissolved in chloroform-d and analysed using ^{1}H and ^{19}F NMR spectroscopy.

8.6.4.4 General Procedure for PVPy Poisoning Reactions

A reaction vial equipped with a magnetic follower was charged with catalyst (0.025 mmol), *p*-fluorophenylboronic acid (167 mg, 1.20 mmol), 2,4-dibromopyridine (263 mg, 1.00 mmol) and caesium carbonate (650 mg, 2.00 mmol), then was evacuated and backfilled with argon (x 3). A second reaction vial was charged with PVPy (100 mg, 1.05 mmol, 40 eq.) and evacuated and backfilled with argon (x 3). Degassed 1,4-dioxane and water (1:1, 2.5 mL) preheated to reaction temperature (***C7***-60 °C and ***C14***-80 °C) was then added to the first reaction vial to commence the reaction. The reaction mixture was then transferred to the PVPy vial at 15 mins and 20 mins for ***C7*** and ***C14*** respectively *via* syringe. 1-Fluoro-3,5-dimethoxybenzene (266 µL, 312 mg, 2.00 mmol) was then added. The vial was maintained at reaction temperature and stirred constantly

for 7 hours. Samples of the reaction mixture (100 µL) were then taken at t = 0, 1, 2, 3, 4, 5, 7.5, 10, 12.5, 15, 20, 25, 30, 45, 60, 90, 120, 180 and 240 mins. Each sample was diluted in DCM (2.0 mL) then passed over a Celite® plug (~1 cm). The solvent was removed under reduced pressure and the residue dissolved in chloroform-d and analysed using ^{1}H and ^{19}F NMR spectroscopy.

8.6.5 Pre-Arylated Substrates in Catalysis

8.6.5.1 General Procedure for 2-Ar Starting Material

A reaction vial equipped with a magnetic follower was charged with catalyst (0.025 mmol), *p*-fluorophenylboronic acid (139 mg, 1.00 mmol), 2-(*p*-fluorophenyl)-4-bromo-pyridine (252 mg, 1.00 mmol) and caesium carbonate (650 mg, 2.00 mmol), then was evacuated and backfilled with argon (x 3). Degassed 1,4-dioxane and water (1:1, 2.5 mL) preheated to reaction temperature (***C7***-60 °C and ***C14***-80 °C) was added to the reaction vial, followed by 1-fluoro-3,5-dimethoxybenzene (133 µL, 156 mg, 1.00 mmol). The vial was maintained at reaction temperature and stirred constantly for 1 hour. Samples (100 µL) were taken at t = 0, 1, 2, 3, 4, 5, 7.5, 10, 12.5, 15, 20, 25, 30, 45 and 60 mins. Each sample was diluted in DCM (2.0 mL) then passed over a Celite® plug (~1 cm). The solvent was then removed under reduced pressure and the residue dissolved in chloroform-d and analysed using ^{1}H and ^{19}F NMR spectroscopy.

8.6.5.2 General Procedure for 4-Ar Starting Material

A reaction vial equipped with a magnetic follower was charged with catalyst (0.025 mmol), *p*-fluorophenylboronic acid (139 mg, 1.00 mmol), 2-bromo-4-(*p*-fluorophenyl)pyridine (252 mg, 1.00 mmol) and caesium carbonate (650 mg, 2.00 mmol), then was evacuated and backfilled with argon (x 3). Degassed 1,4-dioxane and water (1:1, 2.5 mL) preheated to reaction temperature (***C7***-60 °C and ***C14***-80 °C) was then added to the reaction vial, followed by 1-fluoro-3,5-dimethoxybenzene (133 µL, 156 mg, 1.00 mmol). The vial was maintained at reaction temperature and stirred constantly for 7 hours. Samples (100 µL) were then taken at t = 0, 1, 2, 3, 4, 5, 7.5, 10, 12.5, 15, 20, 25, 30, 45, 60, 90, 120, 180, 240, 300, 360 and 420 mins. Each sample was diluted in DCM (2.0 mL) then passed over a Celite® plug (~1 cm). The filtrate solvent was then removed under reduced pressure and the residue dissolved in chloroform-d and analysed using ^{1}H and ^{19}F NMR spectroscopy.

8.7 Stoichiometric Investigations

8.7.1 1:2 Study

A reaction vial equipped with a magnetic follower was charged with ***C4*** (11.0 mg, 0.025 mmol), *p*-fluorophenylboronic acid (8.4 mg, 0.05 mmol) and caesium carbonate (32.5 mg, 0.050 mmol), then was evacuated and backfilled with argon (x 3). Degassed 1,4-dioxane and water (1:1, 2.5 mL) was then added to the reaction vial. Immediately following solvent addition, the vial was heated to 80 °C and stirred constantly for 1 hour. The reaction mixture changed colour quickly from clear yellow to opaque black. After 1 hour, the reaction mixture was filtered over a Celite® plug (~2 cm) to remove black deposits and the filtrate extracted into chloroform-d. Analysis by ^{1}H and ^{19}F NMR spectroscopy was conducted.

8.7.2 1:1 Study

A reaction vial equipped with a magnetic follower was charged with ***C4*** (11.0 mg, 0.025 mmol), *p*-fluorophenylboronic acid (4.2 mg, 0.025 mmol) and caesium carbonate (32.5 mg, 0.050 mmol), then was evacuated and backfilled with argon (x 3). Degassed 1,4-dioxane and water (1:1, 2.5 mL) was added to the reaction vial. Immediately following solvent addition, the vial was heated to 80 °C and stirred constantly for 1 hour. The reaction mixture changed colour quickly from clear yellow to opaque black. After 1 hour, the reaction mixture was filtered over a Celite® plug (~2 cm) to remove black deposits and the filtrate extracted into chloroform-d. Analysis by ^{1}H and ^{19}F NMR spectroscopy was conducted. Slow evaporation of the NMR sample lead to formation of single crystals of ***C15*** which were analysed using SC-XRD and MS.

8.7.3 1:2:1 Study

A reaction vial equipped with a magnetic follower was charged with ***C4*** (11.0 mg, 0.025 mmol), *p*-fluorophenylboronic acid (8.4 mg, 0.05 mmol), 2,4-dibromopyridine (5.9 mg, 0.025 mmol) and caesium carbonate (32.5 mg, 0.050 mmol), then was evacuated and backfilled with argon (x 3). Degassed 1,4-dioxane and water (1:1, 2.5 mL) was added to the reaction vial. Immediately following solvent addition, the vial was heated to 80 °C and stirred constantly for 1 hour. After 1 hour, the reaction mixture was filtered over a Celite® plug (~2 cm) to remove any insoluble deposits and the filtrate extracted into chloroform-d. Analysis by ^{1}H and ^{19}F NMR spectroscopy was conducted.

8.7.4 Stoichiometric HRMS Studies

A reaction vial equipped with a magnetic follower was charged with ***C7*** (17.0 mg, 0.025 mmol), *p*-fluorophenylboronic acid (8.4 mg, 0.050 mmol), 2,4-dibromopyridine (5.9 mg, 0.025 mmol)

and caesium carbonate (32.5 mg, 0.050 mmol), then was evacuated and backfilled with argon (x 3). Degassed 1,4-dioxane and water (1:1, 2.5 mL) was added to the reaction vial. Immediately following solvent addition, the vial was heated to 60 °C and stirred. After 1 hour, the reaction mixture was filtered over a Celite® plug (~2 cm) and the solvent removed under reduced pressure. The resulting residue was triturated in hexane and methanol added for HRMS analysis.

8.7.5 Mid- and Late-Stage HRMS Studies

A reaction vial equipped with a magnetic follower was charged with ***C7*** (17.0 mg, 0.025 mmol), *p*-fluorophenylboronic acid (167.0 mg, 1.20 mmol), 2,4-dibromopyridine (263 mg, 1.00 mmol) and caesium carbonate (650.0 mg, 2.00 mmol), then was evacuated and backfilled with argon (x 3). Degassed 1,4-dioxane and water (1:1, 2.5 mL) was added to the reaction vial. Immediately following solvent addition, the vial was heated to 60 °C and stirred constantly for 6 hours. A 100 µL sample was taken at 20 mins and 6 hours, quenched in DCM (1 mL), filtered over a Celite® plug (~2 cm) and the solvent removed under reduced pressure. The resulting residue was triturated in hexane and methanol added for HRMS analysis.

8.8 X-ray data tables

X-Ray diffraction was performed on an Agilent SuperNova dual-source diffractometer with Atlas S2 CCD detector using MoKα (λ = 0.71073 Å). Crystals were mounted under oil and flash frozen to 100 K. Data was corrected for Lorentzian and polarization effects and absorption corrections were applied using multi-scan methods. The structures were solved on Olex2 using the ShelXT*62* structure solution program using Intrinsic Phasing and refined by full-matrix least squares on F*2* using the ShelXL refinement package. Unless otherwise specified, all nonhydrogen atoms were refined as anisotropic, and hydrogen positions were included at geometrically estimated positions. Organic compounds were grown by slow solvent evaporation of DCM, all palladium containing complexes and salts were grown by slow vapour diffusion of hexane into DCM.

Table 8.1 – X-ray crystallographic data table showing parameters for all structures displayed in this investigation.

	p-fluorophenylboronic acid	2-Ar	4-Ar	***C2***
Empirical formula	$C_{18}H_{12}B_3F_3O_3$	$C_{11}H_7BrFN$	$C_{11}H_7NFBr$	$C_{26}H_{28}Cl_3N_3Pd$
Formula weight	365.71	241.58	252.09	496.31
Temperature/K	100.02(10)	100.01(10)	100.01(10)	130.00(10)
Crystal system	monoclinic	monoclinic	orthorhombic	monoclinic
Space group	$P2_1/m$	$P2_1/c$	$P2_12_12_1$	$P2_1/c$
a/Å	3.8110(4)	11.5545(12)	7.1797(2)	13.6741(2)
b/Å	20.827(2)	7.2624(6)	11.1728(3)	14.1771(2)
c/Å	10.4003(14)	11.4365(11)	11.6118(3)	13.3594(2)
α/°	90	90	90	90
β/°	96.889(12)	106.609(11)	90	98.6650(10)
γ/°	90	90	90	90
Volume/Å^3	819.52(17)	919.64(16)	931.47(4)	2560.28(6)
Z	2	4	4	4
ρ_{calc}g/cm^3	1.482	1.745	1.798	1.596
μ/mm^{-1}	0.119	4.431	5.782	9.334
F(000)	372	475	496	1243
Crystal size/mm^3	0.058 × 0.069 × 0.388	0.212 × 0.071 × 0.053	0.218 × 0.054 × 0.049	0.059 × 0.078 × 0.221
Radiation	MoKα (λ = 0.71073)	MoKα (λ = 0.71073)	CuKα (λ = 1.54184)	CuKα (λ = 1.54184)
2Θ range for data collection/°	7.072 to 59.02	7.144 to 58.99	10.99 to 143.898	9.04 to 145.032
Index ranges	-3 ≤ h ≤ 5, -20 ≤ k ≤ 28, -13 ≤ l ≤ 11	-14 ≤ h ≤ 15, -7 ≤ k ≤ 9, -15 ≤ l ≤ 11	-7 ≤ h ≤ 8, -9 ≤ k ≤ 13, -13 ≤ l ≤ 14	-16 ≤ h ≤ 12, -17 ≤ k ≤ 15, -16 ≤ l ≤ 13
Reflections collected	3916	4576	2402	9228
Independent reflections	1968 [R_{int} = 0.0323, R_{sigma} = 0.0683]	2172 [R_{int} = 0.0439, R_{sigma} = 0.0785]	1591 [R_{int} = 0.0157, R_{sigma} = 0.0257]	4929 [R_{int} = 0.0346, R_{sigma} = 0.0398]
Data/restraints/parameters	1968/0/130	2172/0/127	1591/0/127	4929/0/291
Goodness-of-fit on F^2	1.073	0.831	1.09	1.051
Final R indexes [I>=2σ (I)]	R_1 = 0.0680, wR_2 = 0.1422	R_1 = 0.0459, wR_2 = 0.1191	R_1 = 0.0205, wR_2 = 0.0523	R_1 = 0.0603, wR_2 = 0.1503
Final R indexes [all data]	R_1 = 0.1250, wR_2 = 0.1757	R_1 = 0.0656, wR_2 = 0.1410	R_1 = 0.0215, wR_2 = 0.0532	R_1 = 0.0616, wR_2 = 0.1519
Largest diff. peak/hole/eÅ^{-3}	0.33/-0.30	0.62/-0.80	0.31/-0.33	1.79/-4.99
Flack parameter			-0.05(2)	

	C4	***C5***	***C6***	***C7***
Empirical formula	$C_{14}H_{20}Cl_3N_3Pd$	$C_{25}H_{24}Cl_6N_3Pd$	$C_{22}H_{20}Cl_3N_3Pd$	$C_{32}H_{40}Cl_3N_3Pd$
Formula weight	444.11	685.57	539.19	679.42
Temperature/K	130.00(10)	130.01(10)	130.01(10)	130.00(10)
Crystal system	triclinic	triclinic	monoclinic	monoclinic
Space group	P-1	P-1	$P2_1/n$	I2/a
a/Å	7.8275(4)	8.2224(3)	14.7926(6)	12.5287(3)
b/Å	8.8821(5)	15.3664(7)	8.8228(3)	15.7079(3)
c/Å	14.0201(7)	23.6471(10)	16.9302(5)	32.3825(8)
α/°	96.574(4)	79.836(4)	90	90
β/°	94.796(4)	80.428(3)	100.503(3)	96.047(2)
γ/°	114.096(5)	79.456(4)	90	90
Volume/$Å^3$	874.78(9)	2863.4(2)	2172.58(13)	6337.4(3)
Z	2	4	4	8
$\rho_{calc}g/cm^3$	1.577	1.59	1.293	1.424
μ/mm^{-1}	0.66	10.536	0.308	0.864
F(000)	427	1372	882	2800
Crystal size/mm^3	0.291 × 0.056 × 0.049	0.319 × 0.301 × 0.025	0.079 × 0.088 × 0.126	0.265 × 0.163 × 0.076
Radiation	MoKα (λ = 0.71073)	CuKα (λ = 1.54184)	MoKα (λ = 0.71073)	MoKα (λ = 0.71073)
2Θ range for data collection/°	6.844 to 59.184	7.522 to 144.994	6.734 to 59.192	6.76 to 59.382
Index ranges	-10 ≤ h ≤ 8, -12 ≤ k ≤ 12, -16 ≤ l ≤ 18	-10 ≤ h ≤ 9, -18 ≤ k ≤ 18, -21 ≤ l ≤ 29	-18 ≤ h ≤ 18, -12 ≤ k ≤ 10, -22 ≤ l ≤ 21	-17 ≤ h ≤ 11, -20 ≤ k ≤ 19, -44 ≤ l ≤ 44
Reflections collected	7581	23388	12695	17953
Independent reflections	4094 [R_{int} = 0.0334, R_{sigma} = 0.0599]	10582 [R_{int} = 0.0496, R_{sigma} = 0.0590]	5213 [R_{int} = 0.0310, R_{sigma} = 0.0435]	7589 [R_{int} = 0.0264, R_{sigma} = 0.0388]
Data/restraints/parameters	4094/0/192	10582/0/619	5213/0/262	7589/0/360
Goodness-of-fit on F^2	1.056	1.032	1.027	0.938
Final R indexes [I>=2σ (I)]	R_1 = 0.0361, wR_2 = 0.0658	R_1 = 0.0709, wR_2 = 0.1791	R_1 = 0.0406, wR_2 = 0.0814	R_1 = 0.0363, wR_2 = 0.1161
Final R indexes [all data]	R_1 = 0.0466, wR_2 = 0.0729	R_1 = 0.0779, wR_2 = 0.1862	R_1 = 0.0537, wR_2 = 0.0896	R_1 = 0.0439, wR_2 = 0.1264
Largest diff. peak/hole/ $eÅ^{-3}$	0.69/-0.76	2.28/-1.62	1.17/-0.94	1.49/-1.54

	C8	***C11***	***C13***	***C15***
Empirical formula	$C_{26}H_{28}Cl_3N_3Pd$	$C_{22}H_{18}Cl_5N_3Pd$	$C_{28}H_{26}Cl_3N_3Pd$	$C_{19}H_{33}Cl_5N_4Pd$
Formula weight	595.26	608.04	608.08	601.17
Temperature/K	130.01(10)	130.00(10)	130.00(10)	130.02(10)
Crystal system	monoclinic	orthorhombic	monoclinic	monoclinic
Space group	C2/c	$P2_12_12_1$	$P2_1/c$	$P2_1$
a/Å	32.8214(11)	10.8308(3)	13.9989(7)	7.5266(8)
b/Å	11.9546(4)	13.1495(5)	14.3956(5)	19.7835(14)
c/Å	15.3503(4)	16.8578(5)	13.6682(7)	9.4242(10)
α/°	90	90	90	90
β/°	94.975(3)	90	112.990(6)	110.851(12)
γ/°	90	90	90	90
Volume/Å^3	6000.3(3)	2400.88(13)	2535.7(2)	1311.4(2)
Z	8	4	4	2
ρ_{calc}g/cm^3	1.318	1.682	1.617	1.505
μ/mm^{-1}	0.903	1.345	1.071	1.23
F(000)	2416	1208	1248	601
Crystal size/mm^3	0.084 × 0.182 × 0.093	0.055 × 0.221 × 0.213	0.184 × 0.161 × 0.152	0.165 × 0.050 × 0.226
Radiation	MoKα (λ = 0.71073)	MoKα (λ = 0.71073)	MoKα (λ = 0.71073)	MoKα (λ = 0.71073)
2Θ range for data collection/°	6.816 to 59.214	3.928 to 59.008	6.63 to 59.278	4.626 to 59.04
Index ranges	-40 ≤ h ≤ 42, -13 ≤ k ≤ 16, -15 ≤ l ≤ 21	-14 ≤ h ≤ 14, -9 ≤ k ≤ 16, -22 ≤ l ≤ 23	-18 ≤ h ≤ 17, -19 ≤ k ≤ 16, -18 ≤ l ≤ 18	-9 ≤ h ≤ 9, -26 ≤ k ≤ 20, -9 ≤ l ≤ 12
Reflections collected	15362	9252	12894	6908
Independent reflections	7105 [R_{int} = 0.0486, R_{sigma} = 0.0656]	5213 [R_{int} = 0.0281, R_{sigma} = 0.0464]	5986 [R_{int} = 0.0267, R_{sigma} = 0.0443]	4751 [R_{int} = 0.0346, R_{sigma} = 0.0810]
Data/restraints/parameters	7105/0/304	5213/0/290	5986/0/316	4751/1/271
Goodness-of-fit on F^2	1.168	0.722	1.039	0.916
Final R indexes [I>=2σ (I)]	R_1 = 0.0490, wR_2 = 0.1637	R_1 = 0.0289, wR_2 = 0.0879	R_1 = 0.0345, wR_2 = 0.0768	R_1 = 0.0537, wR_2 = 0.1299
Final R indexes [all data]	R_1 = 0.0620, wR_2 = 0.1800	R_1 = 0.0317, wR_2 = 0.0934	R_1 = 0.0443, wR_2 = 0.0823	R_1 = 0.0707, wR_2 = 0.1447
Largest diff. peak/hole/ eÅ^{-3}	1.82/-0.94	0.37/-0.70	0.80/-0.69	1.31/-0.76
Flack parameter		0.28(2)		

	C16	***C17***	***IPS7***	***IPS8***
Empirical formula	$C_{22}H_{13}Br_2F_2N_2Pd$	$C_{28}H_{18}BrF_3N_2Pd$	$C_{54}H_{74}Cl_4N_4Pd$	$C_{21}H_{25}Cl_3N_2Pd$
Formula weight	609.56	625.75	1027.37	518.18
Temperature/K	100.00(10)	100.00(10)	100 (0)	130.00(10)
Crystal system	triclinic	triclinic	monoclinic	monoclinic
Space group	P-1	P-1	$P2_1/n$	$P2_1/n$
a/Å	7.0957(7)	9.7496(8)	12.01430(10)	10.5067(5)
b/Å	13.5771(12)	10.1583(7)	14.16260(10)	16.4897(7)
c/Å	14.1273(16)	12.8036(9)	16.61960(10)	13.1793(7)
α/°	67.736(9)	70.464(6)	90	90
β/°	89.360(9)	75.400(7)	109.7650(10)	105.847(6)
γ/°	80.239(8)	87.580(6)	90	90
Volume/$Å^3$	1239.2(2)	1155.24(16)	2661.29(4)	2196.56(19)
Z	2	2	2	4
$\rho_{calc}g/cm^3$	1.634	1.799	1.282	1.567
μ/mm^{-1}	3.997	2.577	0.584	1.218
F(000)	586	616	1080	1048
Crystal size/mm^3	0.183 × 0.110 × 0.071	0.409 × 0.166 × 0.134	0.183 × 0.480 × 0.084	0.127 × 0.312 × 0.191
Radiation	MoKα (λ = 0.71073)	MoKα (λ = 0.71073)	synchrotron (λ = 0.6889)	MoKα (λ = 0.71073)
2Θ range for data collection/°	6.778 to 58.938	4.26 to 59.31	3.55 to 50.44	6.886 to 58.938
Index ranges	-8 ≤ h ≤ 9, -13 ≤ k ≤ 17, -19 ≤ l ≤ 19	-13 ≤ h ≤ 11, -14 ≤ k ≤ 13, -15 ≤ l ≤ 16	-14 ≤ h ≤ 14, -16 ≤ k ≤ 15, -17 ≤ l ≤ 18	-14 ≤ h ≤ 13, -16 ≤ k ≤ 22, -12 ≤ l ≤ 18
Reflections collected	10241	10793	11179	12123
Independent reflections	5715 [R_{int} = 0.0394, R_{sigma} = 0.1002]	5453 [R_{int} = 0.0410, R_{sigma} = 0.0780]	3999 [R_{int} = 0.0266, R_{sigma} = 0.0301]	5199 [R_{int} = 0.0346, R_{sigma} = 0.0552]
Data/restraints/parameters	5715/0/262	5453/0/316	3999/0/294	5199/0/250
Goodness-of-fit on F^2	1.01	1.062	1.081	1.062
Final R indexes [I>=2σ (I)]	R_1 = 0.0689, wR_2 = 0.1519	R_1 = 0.0592, wR_2 = 0.1295	R_1 = 0.0256, wR_2 = 0.0645	R_1 = 0.0414, wR_2 = 0.0844
Final R indexes [all data]	R_1 = 0.1203, wR_2 = 0.1732	R_1 = 0.0842, wR_2 = 0.1436	R_1 = 0.0275, wR_2 = 0.0654	R_1 = 0.0582, wR_2 = 0.0952
Largest diff. peak/hole/ $eÅ^{-3}$	1.49/-1.14	2.00/-1.46	0.48/-0.35	0.86/-0.75

	IPS6
Empirical formula	$C_{34}H_{34}Br_4N_4Pd$
Formula weight	924.69
Temperature/K	130.01(10)
Crystal system	monoclinic
Space group	$P2_1/n$
a/Å	12.1542(9)
b/Å	8.6476(5)
c/Å	16.5726(12)
α/°	90
β/°	107.274(8)
γ/°	90
Volume/Å^3	1663.3(2)
Z	2
ρ_{calc}g/cm^3	1.846
μ/mm^{-1}	5.393
F(000)	904
Crystal size/mm^3	0.353 × 0.065 × 0.084
Radiation	MoKα (λ = 0.71073)
2Θ range for data collection/°	6.98 to 58.888
Index ranges	-16 ≤ h ≤ 11, -8 ≤ k ≤ 11, -21 ≤ l ≤ 22
Reflections collected	10529
Independent reflections	3932 [R_{int} = 0.0391, R_{sigma} = 0.0576]
Data/restraints/parameters	3932/0/196
Goodness-of-fit on F^2	1.843
Final R indexes [I>=2σ (I)]	R_1 = 0.0858, wR_2 = 0.2623
Final R indexes [all data]	R_1 = 0.1082, wR_2 = 0.2762
Largest diff. peak/hole/ eÅ^{-3}	4.54/-3.10